Assessing particle deposition in a representative *in vitro* model of the rat respiratory tract

Dissertation zur Erlangung des naturwissenschaftlichen Doktorgrades der Julius-Maximilians-Universität Würzburg

vorgelegt von

Arabe Ahmed

aus Baghdad, Iraq

Würzburg 2014

zur Erlangung

des naturwissenschaftlichen Doktorgrades

der Julius – Maximilians – Universität Würzburg

Eingereicht bei der Fakultät für Chemie und Pharmazie am

_____

Gutachter der schriftlichen Arbeit

1. Gutachter: _____

2. Gutachter: _____

Prüfer des öffentlichen Promotionskolloquiums

1. Prüfer: _____

2. Prüfer: _____

3. Prüfer: _____

Datum des öffentlichen Promotionskolloquiums

_____

Doktorurkunde ausgehändigt am

_____

Publications

Sections of this thesis have already been published in the following form:

1. Poster presentation entitled: Characterisation of Nose-only Exposure system for Rodents. Journal of Aerosol Medicine and Pulmonary Drug Delivery. December 2010.

2. Ahmed A, Prime D, Burnell PKP & Hogger P (2012): Development of an in vitro model to assess deposition of aerosol particles in a representative replica of the rat's respiratory tract. J Aerosol Med Pulm Drug Deliv 25, 169-178.

Acknowledgments

This thesis was carried out at GlaxoSmithKline research facilities in the UK, mainly at the Ware and Stevenage sites during the period 2007-2013.

I would like to express my warmest gratitude and sincerest thanks to my supervisors, Prof. Dr. Petra Högger, Würzburg University, and Dr David Prime, GSK Inhaled Product Department, Ware, for their patience, guidance and wealth of knowledge which allowed me to grow as a person and as a scientist.

I owe a tremendous debt of gratitude to the late Dr. Pat Burnell, GSK Inhaled Product Department, who was my industrial supervisor at the start of this project. She supported, encouraged and pushed me to pursue this research. Her enthusiasm and passion for scientific knowledge was truly infectious and she will always remain my role model and inspiration in science.

Thank you to my friends at GSK who encouraged me, as well as those people who took the time to train me in the various techniques I needed in order to do the work. In particular, I would like to thank Graham Paul, Kay Rush and Paul Giffen as well as the whole staff of the Safety Assessment department for giving me the opportunity to use the rat model as part of their *in vivo* rat experiments. I am also grateful to the staff of the Drug Metabolism and Pharmacokinetic division, particularly Richard Snell and Doug Ball at GSK Ware and Stevenage respectively, for analysing the *in vivo* rat lung samples. Thanks also to Dr Nia Stevens for her valuable guidance and assistance in the analysis of the three-dimensional CAD images of the rat model, upon which the in vitro rat model was constructed.

My deepest gratitude belongs to my dear mother and family, especially my beloved wife Lubaba and two daughters Sara and Sofia, for their loving support and patience during this work.

Finally, I am grateful to GlaxoSmithKline who sponsored the project.

A. Introduction

1 General Introduction

There is a significant challenge in the pharmaceutical development of inhaled drugs in trying to relate pre-clinical data on safety and effective doses to human situations for healthy volunteers and patient studies (Forbes et al, 2011) .The preclinical and safety data can be highly variable within and between species, leading to challenges in interpretation. In turn, this results in the need to develop a significant number of dose strengths for clinical use (Schlesinger, 1985).

A significant contributory factor to this situation is the assumption underlying rodent inhalation exposure studies, which is that 10% of the delivered dose is deposited in the animal lung, regardless of the lung geometry and particle size distribution of the dose (Forbes et al, 2011). This is not likely to be true, as animal studies, particularly nose-only exposure studies, have shown extensive nasal airway deposition due to filtration by extra-thoracic structures in the nose and mouth. In addition, it is well known from *in vitro* and *in vivo* studies that only a small fraction of the drug product is deposited in the lungs (Raabe et al, 1988).

Not unexpectedly, responses vary in different species, which may not be accountable to exposure/mass data. Based on the same assumption, clinical doses are usually predicted from animal models. In cases where this provides unexpected responses, it is difficult to determine whether this is due to molecule, particle physiochemical attributes or regional lung deposition.

A review of current pre-clinical dosing methods to study the deposition and fate of inhaled drug molecules indicated that the high levels of variability when dosing animals may be attributed to a poor understanding of the airway morphology of the test species and the associated impact of the particle size distribution of the delivered dose on regional lung distribution (Phalen et al, 2008). Thus, there is a need for a more explicit method to assess regional dose deposition, aiding in the interpretation of safety and efficacy data.

One technique that has shown a great deal of promise in quantifying lung deposition is gamma scintigraphy (Newman, 2000). The quantified dose may be considered as a measure of local bioavailability and a surrogate measure for the clinical response. However, the main draw back with this technique is its lack of sensitivity, as it is required to provide the necessary information in preclinical and clinical situations.

Mechanisms of deposition in lungs have been studied by others and are well understood. Work by Usmani *et al.* (Usmani et al, 2003) and Zanen *et al.* (Zanen et al, 1996) have shown that

particle size and regional deposition in mild to moderate asthmatics who inhaled mono-sized $ß_2$ agonists had a significant effect on efficacy. In both studies, the very finest particles (1.5 µm) did not provide the best bronchodilation; instead, this was provided by the larger sizes (Mitchell and Authors, 2008).

It was hypothesised that this was due to better regional targeting of $ß_2$-receptors using the larger sized $ß_2$-agonists (Mitchell and Authors, 2008). Despite the $ß_2$-receptors' density being the highest in the alveolar region, smooth airway muscles are most prominent in the conducting airways. Thus, for effective bronchodilation, $ß_2$-agonists should preferentially be targeted in this region (Usmani et al, 2005). In addition, Usmani *et al.* showed that equivalent efficacy was obtained from significantly lower inhaled doses of the targeted drug of the 'correct' size compared to the marketed products.

However, there are significant difficulties in relating regional lung deposition profiles for these mono-sized particles with those used in inhaled products, where there may be up to four orders of magnitude in particle sizes within the blend. Therefore, a better understanding of drug deposition in the lungs should enable the design of specifically targeted inhalation therapies to their sites of optimum activity, whilst minimising their systemic effects and associated side effects.

This section will review the current knowledge with regards to inhalation drug therapy, with particular emphasis on pre-clinical aerosol exposure studies and the extrapolation of data from pre-clinical species to human subjects. First, the deposition of inhaled particles within human subjects and pre-clinical animal species will be discussed. The factors affecting aerosol deposition, such as particle characteristics, breathing conditions and lung morphology will be explored.

Second, the review will cover the currently applied method to study aerosol drug deposition in both human and animal species and the various techniques used to characterise the aerosol output from these studies. In addition, the techniques used to assess biological responses to inhaled aerosol therapy will be reviewed.

1.1 Deposition of particles in the lung

The deposition of aerosol particles in the lung is a highly complex process and is dependent on multiple factors. In general, these factors may be divided into three main groups: the aerodynamic properties of the aerosol, the airflow conditions encountered by the particles, and the anatomy of the lung. Furthermore, the interaction between these three factors must be considered in order to fully understand the implications for drug delivery.

1.1.1 Aerosol particle characteristics

Particle size is the single most important factor affecting the deposition of aerosol particles in the lung (Telko and Hickey, 2005). The main factors that contribute to the aerodynamic properties of aerosol particles have been described in Stokes' Law. This law describes the frictional forces (also called drag forces) exerted on small particles in a continuous viscous fluid (Hinds, 1999).

Stokes' force can be expressed in the following equation, derived by solving the Stokes flow limit of the Navier-Stokes equation as described in Equation 1:

$$Fd = \frac{\pi \mu V d}{Cc} \qquad \textbf{Equation 1}$$

Where:

- Fd is the frictional force (N)
- μ is the viscosity of the air (Pa)
- V is the particle's velocity (m/s)
- d is the particle diameter (μm)
- Cc is the Cunningham slip correction factor

Understanding the influence of these factors on particle behaviour in the air can be used to aid the deposition of particles in the human lung. For example, the higher the Stokes' force, the more likely the particle to deposit by impaction mechanism.

An important assumption underlying Stokes' Law is that the velocity of the carrier gas is zero (Hinds, 1999). This is true for particles greater than 10 μm in size. However, for particles less than 10 μm, a correction factor known as the Cunningham Slip correction factor should be

applied. In addition, this factor needs to be applied when determining the particle terminal velocity, V_{TS}, as described in Equation 2 (Crowder et al, 2002):

$$V_{TS}= \frac{\rho_p d_p^2 g c_c}{18\mu}$$ **Equation 2**

Where:

- ρ_p is the particle density
- d_p is the particle diameter (µm)
- g is the gravitational constant

The importance of this factor can be clearly demonstrated for particles less than one micron. For a 0.001 µm particle with a Cunningham correction factor of 228, the terminal velocity increases by a multiplication factor of 228 when this factor is utilised. Therefore, the slip correction must be taken into account for particles of less than one micron size, as it contributes significantly to its size distribution and, by inference, its pharmaceutical effect (Crowder et al, 2002). However, in general, particles less than 0.5 µm will be exhaled from the lungs without deposition (Schmid et al, 2008).

Another important factor to consider is the particle density as it is used to calculate the aerodynamic diameter for aerosol particles. This is defined as the diameter of a unit density sphere that has the same settling velocity as the particle in question (Mitchell and Nagel, 2003). The aerodynamic diameter is considered to be the most appropriate measure of aerosol particle size because it relates to particle dynamic behaviour.

The Mass Median Aerodynamic Diameter (MMAD), d_{ae}, can be calculated using Equation 3:

$$d_{\mathrm{ae}} = \sqrt{\rho_{\mathrm{p}}}\mathrm{d}_{\mathrm{g}} \qquad \textbf{Equation 3}$$

Where:

- ρ_p is the particle density
- d_g is the particle diameter

This equation shows that, for a given aerodynamic diameter, it may be possible to target the same diameter by decreasing the density of the particle whilst increasing its geometric diameter. For example, in a study by Batycky *et al.*, porous particles of density less than 1 g/cm^3 and a geometric diameter greater than 10 µm were successfully produced with an MMAD of less than 5 µm, thus achieving an aerodynamic diameter in the respirable range (Batycky et al, 1999).

These particles showed a higher distal lung deposition due to increasing deposition in the peripheral regions in preference to the extrathoracic regions. This finding may, in the future, enable the targeting of distal lung diseases such cystic fibrosis and bronchitis. Shape plays an important role in the airway deposition of particles. The vast majority of medicinal aerosol particles can be considered as fibres, characterised by a rod-like appearance (Sturm and Hofmann, 2009). For non-spherical particles, a shape factor must be included in equations 1 and 2, as this will also impact the aerodynamic properties of the particles.

The aerodynamic properties of individual fibres may be determined in terms of their length (L) and diameter (D) and aspect ratio (L/D). An important feature to note is that the aerodynamic diameter D_{ae} is independent of the length, being proportional to $(L)^{1/6}$, (Harris and Fraser, 1976). Thus, fibres are ideally suited to delivering large masses of material to the lungs without adversely affecting their aerodynamic diameter.

This effect of fibres was demonstrated in a study by Chan and Gonda, who developed elongated crystals of cromoglycic acid (Chan and Gonda, 1989). These particles had an average diameter of 2 µm and aspect ratio of 10, resulting in a MMAD of 0.7 µm. This resulted in deeper lung deposition and more efficacious therapeutic effect.

Thus, from Equation 1 and Equation 2, it becomes obvious that the importance of slip, density and shape on the deposition of particles in the human lung and, without corrections for these factors, the calculation of the aerodynamic particle size would be inaccurate.

For the particle size range we are interested in, namely 1-10 µm, it is widely accepted that the main mechanisms affecting aerosol transport and deposition in the lung include inertial impaction, gravitational sedimentation, and Brownian diffusion and, to a lesser extent, interception and electrostatic precipitation (Schmid et al, 2008). The relationship between the deposition mechanisms to particle size is summarised in Figure 1. Aerosol characteristic parameters such as particle slip, shape and density affect particle deposition by contributing at least to one of these three mechanisms.

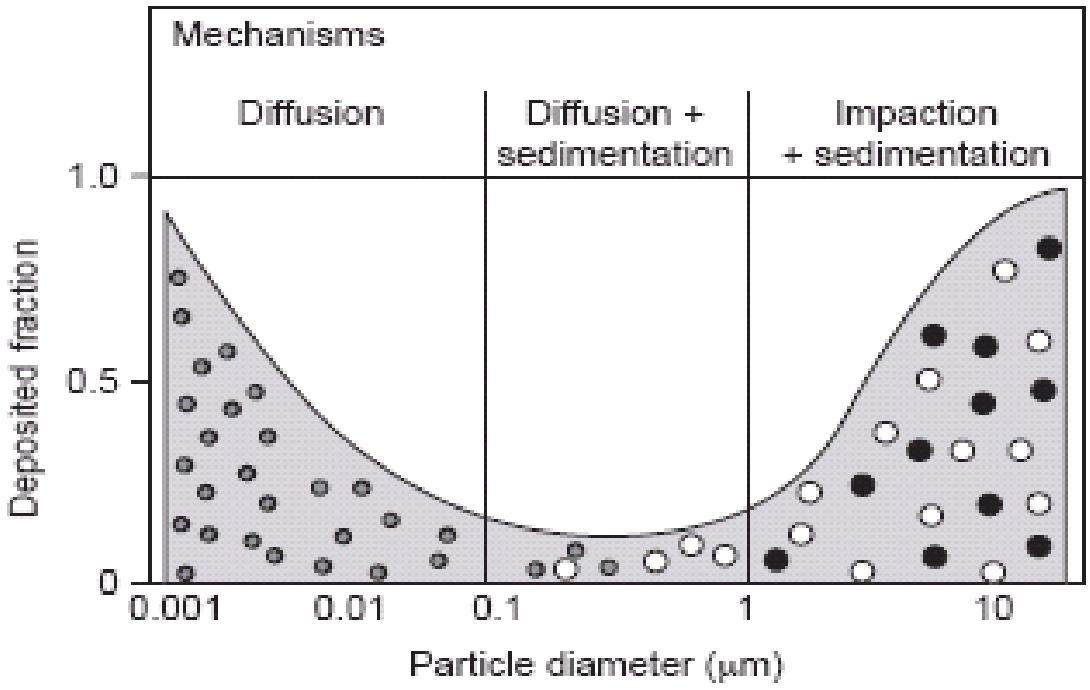

Figure 1: Schematic overview of particle deposition in the respiratory system for unit density spheres. The typical deposition values for an adult during quiet mouth breathing are given as a function of the inhaled particle diameter. The dominant deposition mechanisms are indicated. From Schulz (Schulz, 1998). Reproduced by permission of Elsevier Limited.

Inertial impaction occurs as aerosol particles suspended in the gas stream have a tendency to travel along in a forward motion, due its momentum, which is the product of its mass and velocity. However, when the gas stream encounters an obstacle or a bend, the suspended particles, rather than change direction with the airstream, tend to impact to a surface in the particles' original path. The likelihood of impaction depends on the momentum of the particle in question. Factors such as particle velocity, diameter and density all contribute to increased deposition by impaction. This mechanism of deposition is most prevalent in the nose and throat regions of the respiratory tract and affects particles greater than 5 µm in size (Darquenne, 2012).

In sedimentation, as particles travel through air, gravitational forces and air resistance eventually overcome their buoyancy. The result is that the particles settle on a surface of the lung. This type of deposition is most common in the lower airways for particles, which escape the capture by impaction. The displacement of particles by gravitational transport increases with time and with particle diameter and density. This deposition mechanism is most effective for particles in the range of 1-8 µm. However, this mechanism is not considered an important factor when the aerodynamic diameter of the particle is less than 0.5 µm (Hinds, 1999).

Diffusion occurs when random collisions with air molecules cause a particle to come in contact with a surface. Diffusion is the most important mechanism for deposition in the small airways and alveoli (Schulz, 1998). Deposition due to interception is the mechanism by which particles are intercepted by the airway wall because of their shape and size. This mechanism mainly affects elongated particles such as needle-shaped fibres (Crowder et al, 2002).

In addition, deposition by electrostatic precipitation may occur. This is caused by the attraction of charged particles to an oppositely charged surface and plays a small role in the overall deposition of most aerosols (Ali et al, 2008). Furthermore, deposition within the lung is not uniform, even when highly uniform monosised particles are used. Areas of relatively high deposition, known as "hot spots", are likely to occur at the bifurcation points, where the main airway splits into two smaller daughter airways. High concentrations of compounds are likely to be found in these regions (Phalen et al, 2008).

1.1.2 The airflow conditions

Another important factor affecting the site of aerosol deposition in the respiratory tract is the inhalation mode. This, in turn, is dependent on a number of parameters which characterise the inhalation model: the volume of inhaled air, the inhalation flow rate, the breath-holding period after inhalation and the volume of the lungs at the start of inhalation (Timsina et al, 1994).

In the extrathoracic region, for a given flow rate and particle size, variation in inhalation volume has a negligible effect on the fraction of particle deposited. This is because deposition in this region is governed in the main by inertial impaction, as flow velocities in this region are relatively high and the residence time of particles is short (Swift and Proctor, 1988). A study carried out by Svartengren *et al.* (Svartengren et al, 1996) showed it was possible to reduce the fraction of particle deposition in the extrathoracic region and target the tracheobronchial region by using a very low inspiratory flow rate. This effect was particularly pronounced for large particles.

The effects of ventilation parameters variation on tracheobronchial deposition were studied using an empirical model developed by Rudolf *et al.* (Rudolf et al, 1990). This study showed that changes in tidal volume did not have a significant impact on deposition levels, whereas a reduction in breathing frequency for different tidal volumes resulted in significantly higher deposition levels. As the predominant deposition mechanisms acting in this region are inertial impaction and gravitational sedimentation, lowering the breathing frequency leads to a substantial increase in the residence time of particles in the conducting airways and greater deposition levels due to sedimentation.

For the alveolar region, both tidal volume and breathing frequency play an important role. Deposition in this region is governed by Brownian motion and sedimentation, and both are dependent on residence time; thus, any factor which increases this time, such as reduction in breathing frequency, will result in higher deposition levels (Schulz, 1998).

1.2 Respiratory Tract Anatomy

1.2.1 Human respiratory tract

The lungs are located in the thoracic cavity and are surrounded by the rib cage and diaphragm (see Figure 2). There are three lobes on the right side of the chest and two on the left side, allowing the accommodation of the heart within the thoracic cavity. In the right lung, the main bronchus divides into the upper and lower lobe branches, while the latter gives off a branch to the middle lobe. In the left lung, the main bronchus divides into the upper and lower branches (D.Behera, 2010). Further branching takes place in the bronchi until bronchioles are formed. These are known as airways and further divide until the terminal bronchiole is reached, which connects with alveoli. These alveoli are termed respiratory bronchioles.

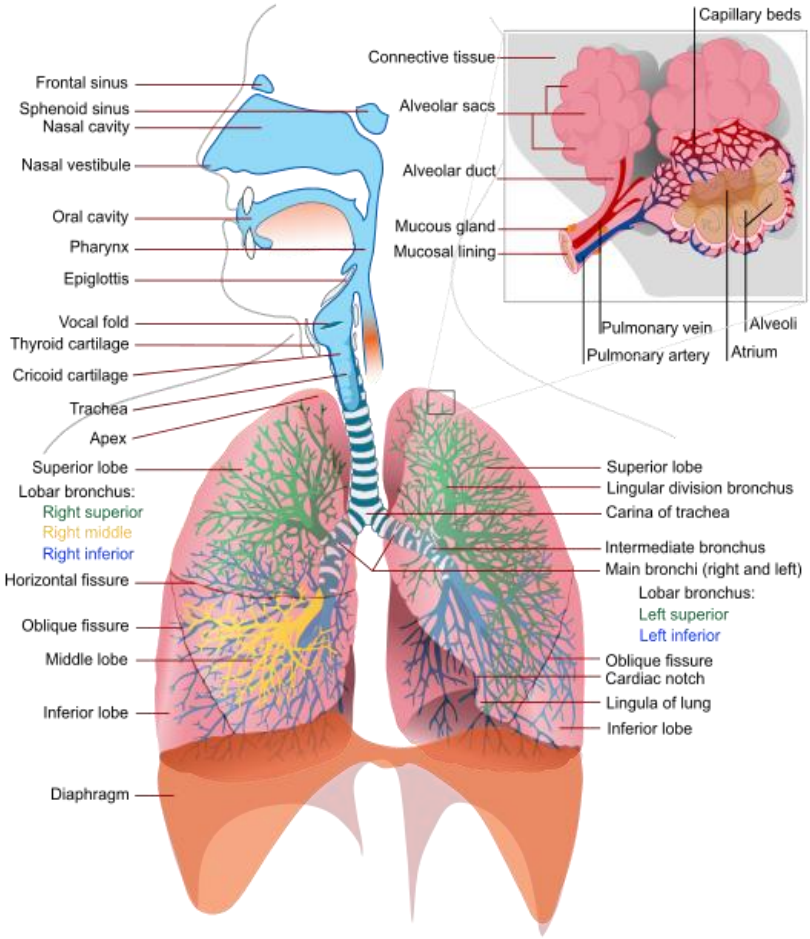

Figure 2: Diagram of the human lung. Retrieved from Wikimedia. 11 January 2014

The airways undergo 23 generations until they reach the alveolar sacs. The surface area of the lungs increases from the trachea, estimated to be 2.5 m^2, to the alveolar sacs at up to 102 m^2 during inspiration (Weibel, 1963). With the increase in surface area, the thickness of the airway walls becomes increasingly thinner as the alveoli are neared (see Figure 3).

The tracheobronchial region consisting of trachea, bronchi, and bronchioles airways are surrounded by smooth muscle. They are lined with specialised cells, some of which produce mucus while others are ciliated. Together, they form an escalator (mucociliary escalator) that carries mucus, which also contains macrophages, cell debris and deposited inhaled material, upward to maintain the sterility and general cleanliness of the lung (Green et al, 1977).

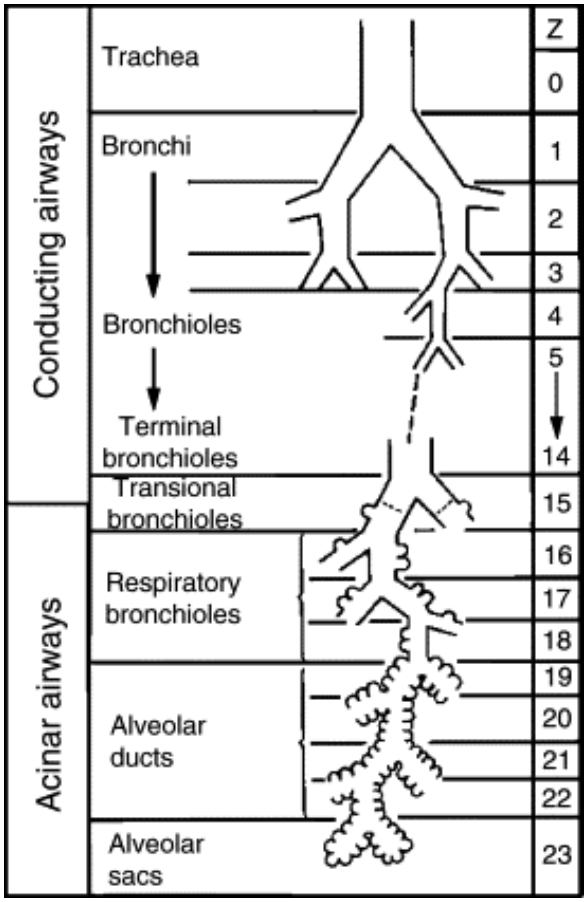

Figure 3: Model of human airway system assigned to generations of symmetric branching from trachea (generation 0) to acinar airways (generations 15–23), ending in alveolar sacs. Modified from Lee (Lee et al, 2009). Reproduced by permission of Springer Limited.

Considerable research has been undertaken to understand the anatomical structures of the human respiratory tract and how they affect aerosol particles deposition. Physical models of the human respiratory tract have been constructed based on a lost wax technique and, more recently, from magnetic resonance imaging (MRI). However, many of the model data generated were based on geometries of healthy adults, while the impact of age, gender, and disease state and their effects on respiratory tract anatomy remain potential avenues for future research (Byron et al, 2010).

Several models of the human respiratory tract have been proposed, but three are widely used, particularly in inhalation toxicology (Phalen, 1984). These models tend to divide the respiratory tract into three main regions: (i) the extrathoracic (ET) region, extending from the mouth and nose to and including the larynx, (ii) the tracheobronchial tree (TB), from the trachea to terminal bronchioles and (iii) the pulmonary (P) region, containing the respiratory bronchioles to the terminal alveolar sacs. These components have been grouped into larger regions or compartments for simplification and for mathematical modelling purposes.

The models are as follows: Task Groups of International Commission on Radiological Protection, the International Standard Organisation (ISO), and the American Conference of Governmental Industrial Hygienist (ACGIH). These are summarised in Table 1.

Table 1: Compartmental models of the human respiratory systems

Region	Anatomical Structures included	Task group region	ISO region	ACGIH region
1	Nose, mouth, nasophyarynx, oropharynx, laryngopharynx and larynx	Nasophyarynx	Extrathoracic (ET)	Head airways region
2	Trachea, bronchi, bronchioles (to terminal bronchioles)	Tracheo-bronchial	Tracheo-bronchial (TB)	Tracheo-bronchial region
3	Respiratory bronchioles, alveolar ducts, alveolar sacs, alveoli	Pulmonary (P)	Alveolar	Gas exchange region

Region 1 structure and function: This region begins at the anterior nares and ends at the larynx. Inhaled air is conditioned with respect to temperature and humidity, and there is an active mucociliary system for the removal of foreign solid particles. Large particles greater than 5 µm are mainly deposited in this region, as their inertial properties cause impaction in the oral and nasal passages of the airways. In addition, very fine particles (< 0.1 µm in diameter) are removed from the nose via diffusion due to the large surface area of the turbinates.

Region 2 structure and function: This region begins below the larynx and includes the trachea and bronchial airways, down to the terminal bronchioles. The mechanism of inertial impaction at airway bifurcation dominates, although other mechanisms such as sedimentation, Brownian diffusion and interception also play an important role in the deposition of inhaled particles. This region is ciliated and equipped with mucus-secreting elements. Thus, in healthy, non-smoking adults the clearance of most of the deposited particles occurs within 24 hours by way of mucociliary escalator to the throat for swallowing. Another important characteristic of this region is that particles depositing here are distributed differently depending on their size, with smaller particles depositing more distally in comparison with larger particles.

Region 3 structure and function: This region includes respiratory bronchioles, alveolar ducts, alveolar sacs and alveoli, and areas where gaseous exchange occurs. Aerosol particles deposit in this region mainly via Brownian diffusion and/or interception and must successfully negotiate the first two regions.

The alveolar surface lining the alveolar is composed of surfactants, mainly phospholipids. These are surface active materials, which reduce the work of breathing by lowering surface tensions, thereby stabilising alveoli and preventing their collapse. Clearance from this region is thought to be due to a combination of several mechanisms, including direct passage of particles in the blood, transfer to the lymphatic system and dissolution of soluble particles and subsequent absorption into the systemic circulation.

Some authors have criticised the three-region model as too simplistic and assume that deposition in each region is uniform and that this may lead to inaccurate estimation of risk, with associated effects on the health of individuals. The model was based largely on the pioneering work of Ewald Weibel (Weibel, 1963) and was derived from measurements of cast made from the excised lung of a deceased young male.

In the Weibel model, the lung is divided into two major zones, namely the conducting and respiratory zones. The conducting zone starts with the trachea (generation 0). This subdivides into two main bronchia which, in turn, further subdivide into smaller bronchi. These bronchi further subdivide to form smaller and smaller airway generations, the bronchioles. The conducting zone ends with the terminal bronchioles (generation 16). The main function of the airways in the conducting zone is to allow for air movement in and out of the lungs during each breath (see Figure 3).

Following the conducting zone, the respiratory zone starts at the respiratory bronchioles (generation17) level and continues to subdivide until the alveolar sacs (generation 23) are reached. It is in this region that gas exchange occurs.

This model makes a number of assumptions. Firstly, it assumes the branching structure to be dichotomous. Secondly, it assumes the branching structure to comprise of 23 generations. In reality, however, the lung is asymmetric and this model overestimates the number of airway generations. In addition, there is no separation of the regions between the terminal bronchioles and alveolar ducts and sacs. This region is also characterised by the presence of structures that have both conducting and gas exchange properties (Hofmann, 2011).

1.2.2 Rat respiratory tract

The rat is perhaps the most commonly used laboratory species in aerosol studies as it has anatomical structures similar to human, although significant differences exist between the two species.

Probably the most significant difference occurs in the upper respiratory tract. Humans have a relatively simple nasal anatomy, with few shelf-like nasal turbinates and a small olfactory region. This is in stark contrast to rats, which have complex internal nasal structures with a large olfactory apparatus. In addition, rats, in common with other rodents, are obligate nose breathers (Schlesinger, 1985). The major implication of this difference is that the probability of getting inhaled particles greater than 5 µm through the nasal passage is very small.

In addition, ultra-fine particles (<0.1 µm in diameter) are effectively filtered from the nose via diffusion mechanism. This is because the surface area of the nasal turbinates is large in comparison to its cross-sectional area, and is in close proximity to the inhaled air (Miller, 2000).

The inhaled air then arrives in the tracheobronchial region, where some of it is captured and some is distributed to the alveoli. In humans, the branching of the airways is dichotomous. This is probably related to having a relatively spherical chest cavity and symmetric branching being the most efficient way to fill such a space. In rats, the airway branching tends to be monopodial, which is believed to be a more efficient way of filling elongated chest cavities and removing heat from the blood (Parent, 1992).

In rats, the terminal bronchioles can be reached anywhere from 7 to 32 branching whereas, in humans, the airways require anything from 9 to 22 branching to reach a terminal bronchiole (Mercer et al, 1994). A schematic representation of the rat respiratory tract is illustrated in Figure 4.

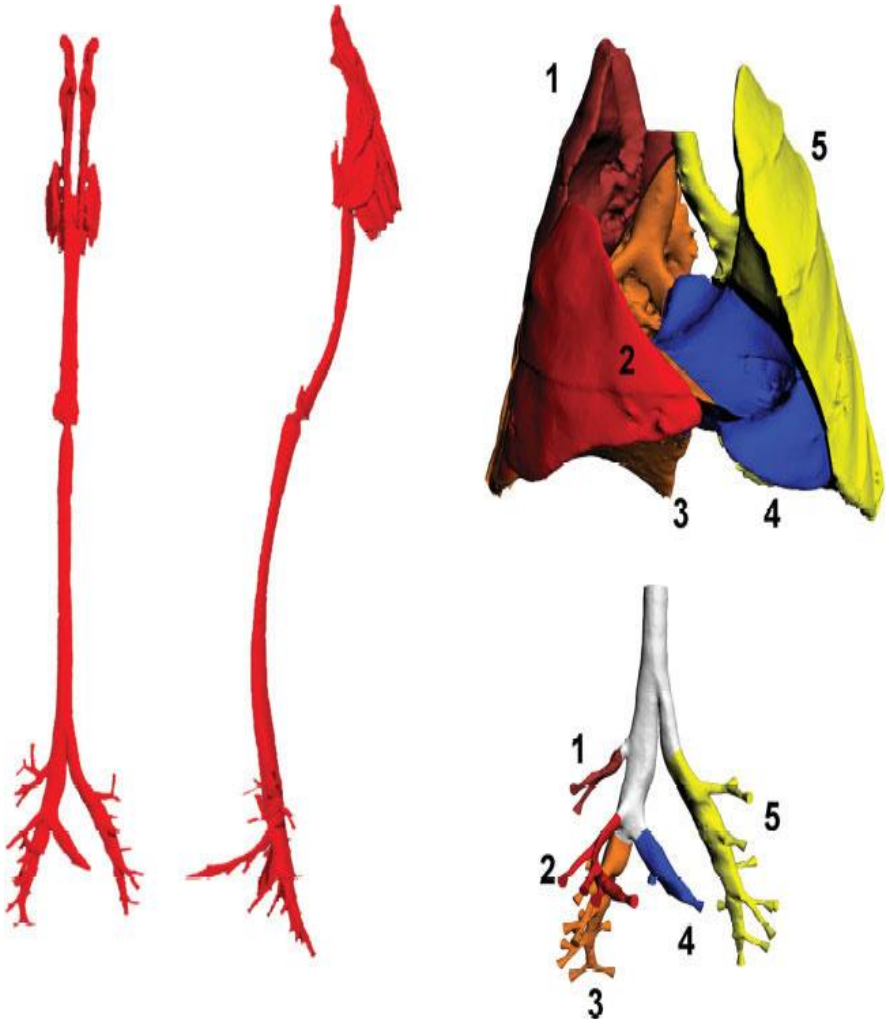

Figure 4: Mean rat model (left, ventral view), lobular segmentation (top right), and airways coloured by lobular pathway (bottom right). From De backer *et al.* (De Backer et al, 2009). Reproduced by permission of John Wiley and Sons.

Another significant difference in airway morphology between rats and humans is the absence of respiratory bronchioles in rats, and the sudden transition from ciliated tracheobronchial airway to alveolar ducts. This contrasts with humans, where the transition is more gradual. In addition, respiratory bronchioles are implicated in the suppression of alveolar clearance of insoluble particles. Rats, on the other hand, have much faster alveolar clearance of such particles, which may be due to the absence of respiratory bronchioles (Phalen et al, 2008).

Further down the respiratory airway, humans and rats differ with respect to the number and size distributions of alveoli. In general, there is a positive correlation between body size and alveolar size as well as total body surface area (Phalen et al, 2008). Work carried out by Stone *et al.*

demonstrated remarkable similarities in structure of the alveoli in mammals ranging over more than five orders of magnitude in body weight (Stone et al, 1992). The wall of the alveolar epithelium is covered with a layer of surfactant, composed mainly of phospholipids. Work carried out by Scarpelli *et al.* has shown close similarities in chemical composition of this layer between rats and humans (Scarpelli, 1998).

As airflow velocity reduces with each bifurcation of the airways, airflow in the alveolar region is low and essentially laminar. Consequently, diffusion is the primary mechanism by which particles of less than 0.5 µm are deposited in the alveolar region. For particles greater than 1.0 µm, sedimentation is the primary mechanism of deposition (Schmid et al, 2008).

Thus, it can be concluded that deposition of particles in the various locations within the respiratory tract is a highly complex process, dependent on many factors such as species-species respiratory tract anatomy, ventilation factors and particle-specific physical factors. For rats and humans, impaction is the primary mechanism of deposition in the ET region. In the TB region, both sedimentation and impaction play an important role, though to a different extent between rats and humans. In rats, both processes are important, whereas in humans impaction is the predominant mechanism. This can be attributed to differences in airway size and overall lung architecture.

1.3 Dosimetry in inhaled drug delivery

Accurate assessment of the inhaled dose is important in order to assess its safety and efficacy in biological subjects. Two equations are widely used in the design of clinical and non-clinical safety studies. The first is the Delivered Dose, Equation 4, which is defined as the amount of drug inhaled by the animal subject. The second is the Deposited Dose, Equation 5, which is defined as the actual amount of drug that is deposited in the lungs. These terms are recommended by the Association of Inhalation Toxicologist (Alexander et al, 2008).

A number of alternative terms are used to describe the Delivered Dose, for example total, inhaled, targeted and presented dose. Alternative terms for the Deposited Dose are the achieved or lung dose (Forbes et al, 2011). However, these various terms describing the same measure may lead to confusion, thus highlighting the need to harmonise the terminology used to describe these metrics.

$$\text{Delivered Dose (mg/kg)} = (\text{C x RMV x D x IF}) \div \text{BW} \qquad \textbf{Equation 4}$$

$$\text{Deposited Dose (mg/Kg)} = (\text{C x RMV x D x IF x DF}) \div \text{BW} \qquad \textbf{Equation 5}$$

Where:

- C: concentration of substance in air (mg L^{-1})
- RMV: respiratory minute volume (L min^{-1})
- D: duration of exposure (min)
- BW: body weight (kg)
- IF: inhalable fraction; the proportion by weight of particles that is inhalable by test species (IF is often assumed to be 100% if the test material has a Mass Median Aerodynamic Diameter (MMAD) less than 3-4 µm).
- DF: deposition fraction or the fraction of the Delivered Dose that is deposited in the lungs.

In addition to the multiplicity of terms used to describe the Delivered and Deposited Dose, a number of algorithms are used to determine the RMV values for non-clinical species (Bide et al, 2000).

However, the algorithm proposed by the Association of Inhalation Toxicologist (Alexander et al, 2008), namely Equation 6, is generally adopted by most investigators working in this field and is widely accepted for use in regulatory inhalation toxicology studies (Alexander et al, 2008). This algorithm was derived from RMV data collected from approximately 2000 individual observations across four species in ten separate laboratories.

$$RMV\ (L\ min^{-1}) = 0.608 \times BW\ (kg)^{0.852}$$ **Equation 6**

With respect to the Deposition Fraction (DF), the American Food and Drug Administration (FDA) Division of Pulmonary, Allergy and Rheumatology Products applied default values to calculate the Deposited Dose: 10% in rats, 25% in dogs and 100% in humans. These values are based primarily on publications by Wolff and Dorato and Snipes *et al.* (Snipes et al, 1989;Wolff and Dorato, 1993).

Wolff and Dorato compiled published data on pulmonary deposition of particles across species commonly used in non-clinical pharmaceutical testing. In addition, Snipes *et al.* performed a meta-analysis of data from different deposition studies (assuming particles within an MMAD of 2 µm) and calculated the average deposition for each species.

However, a major drawback of using the default values proposed by Wolff and Dorato and Snipes *et al*. for DF is that the particles studied in these investigations were insoluble particles such as plutonium, iron oxide and aluminium silicate. On the other hand, drug substances typically used for inhaled drug delivery have different physiochemical properties in the terms hygroscopicity, variable dissolution and transport rates. Thus, these differences may give rise to very different deposition profiles in the lung than predicted using insoluble particles (Forbes et al, 2011).

1.4 Methods to assess drug deposition in preclinical models

Numerous methods are available to measure the deposited dose and to verify the estimates outlined in the previous section. The two most widely used are: i) measurement of systemic exposures of the inhaled drug in terms of plasma area under the curve (AUC) by inhalation compared to intravenous dose and charcoal-block method, and ii) removal of the lung tissue immediately after drug administration and measurement of drug content in the lung tissue homogenate. The details, strengths and weaknesses of each method are described below.

1.4.1 Pharmacokinetic methods

Pharmacokinetic methods can be used to estimate the total deposited dose via the inhaled route. Two different methods, 30 min urinary excretion data and charcoal block, have been suggested (Chrystyn, 2001;Derendorf et al, 2001). These methods provide good evidence of dosing following inhalation, especially when the drug compound exhibits both high solubility and permeability.

The charcoal block method uses blockage of gastrointestinal absorption of the swallowed drug to estimate pulmonary bioavailability in relation to the total systemic bioavailability, determined by giving an intravenous dose as a reference administration. The method has been used for a range of drugs including terbutaline, formoterol, budesonide and beclomethasone dipropionate (Borgstrom and Nilsson, 1990).

Limitation of the charcoal block method means it cannot be used for inhaled drugs which exhibit significant systemic bioavailability and for drugs which are not adsorbed to a great extent to the activated charcoal (Derom et al, 2001). Furthermore, the method has a number of limitations, especially when applied to preclinical species. For rodents, inhaled compound bioavailability is influenced by both oral and nasal absorption. While oral absorption can be charcoal-blocked, nasal absorption cannot be blocked at present. The ability to block absorption would be very useful in order to fully understand inhaled bioavailability in non-clinical species (Forbes et al, 2011).

The 30 minute urinary excretion method (Hindle and Chrystyn, 1992) is based on the assumption that there is a delay in gastrointestinal absorption of swallowed drugs, and that the amount of drug swallowed in the first 30 minutes following inhalation is negligible. Therefore, the

drug present in the urine during this initial period must represent pulmonary absorption. This method has been used to determine the pulmonary bioavailability for a number of drugs such as salbutamol (Hindle and Chrystyn, 1992), as well as gentamicin (Al-Amoud et al, 2005), formoterol (Al-Amoud et al, 2005;Nadarassan et al, 2007), sodium cromoglicate (Nadarassan et al, 2007) and terbutaline (Abdelrahim et al, 2011).

A major limitation of pharmacokinetic methods is that they provide no information on the regional distribution of the inhaled drug in the lung (Scheuch et al, 2010). In addition, target non-clinical doses are often achieved by changing the combination of aerosol concentration and duration of exposure. However, different combinations of these parameters may lead to variable pharmacokinetics for the same deposited dose. In addition, the accumulation of dissolved drugs in the lung by any uptake mechanisms such as active transporters and lysosomal trapping cannot be assessed using this method (Forbes et al, 2011).

However, despite these limitations, pharmacokinetic methods provide essential information on the total bioavailability of inhaled drugs and their contribution to systemic side effects. In addition, in non-clinical species, PK methods provide proof of dosing and is a useful indication of clinical performance.

1.4.2 Lung homogenate method

A direct method of measuring the total deposited dose may be via the determination of drug concentration in lung homogenate. This method is used to measure the deposited doses of poorly soluble compounds for acute exposure, particularly for compounds where accumulation after chronic dosing is a concern (Forbes et al, 2011).

Typically, the method involves the removal of the lung and trachea from the rat immediately after exposure to the test material, or at a predetermined time interval during the exposure period, depending on the method protocol requirements. Samples are subsequently prepared for homogenisation. Thereafter, supernatant samples are taken for spectrophotometeric analysis (MacLoughlin et al, 2009). If knowledge of the regional distribution of the drug in the lung was desired, the lung may be dissected into a number of regions, e.g. trachea and bronchi, right lung, superior lobe, middle lobe and inferior lobe, left lung and upper, middle and lower sections (see Figure 5).

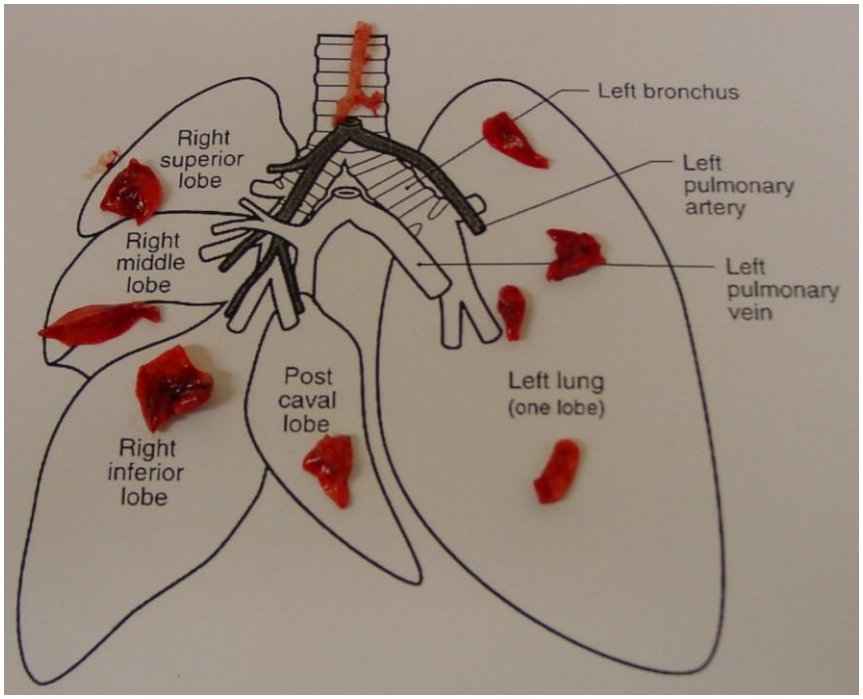

Figure 5: Rat lung regions used for estimating total and regional inhaled drug deposition using lung tissue homogenate assay technique. Reproduced with permission from GSK R&D Ware, UK

Limitations of this method include lack of detailed knowledge beyond gross definitions, such as tracheobronchial and pulmonary regions, regarding where the drug is deposited in the lung. In addition, measurements are affected by duration of exposure, which may need to be adjusted to achieve the desired deposited dose. However, as consequence, a large portion of the drug may already be absorbed into the systemic circulation by the time the lungs are excised for dose determination post exposure.

Furthermore, rapid absorption during the dosing and sampling period results in loss of drug from the lung, reducing the accuracy of the dose determination. Processing lung tissues for drug analysis involves homogenisation to complete destruction. This often involves the indiscriminate use of the whole lung tissue or various compartments thereof, with the data expressed as average drug concentration for the entire lung.

Due to the lack of precision and accuracy of the lung homogeniate analysis method, research has moved to the determination of the free drug concentration and correlating this with pharmacological activity, such as the levels of inflammatory markers (Forbes et al, 2011). Wu *et al.* used the equilibrium dialysis technique of lung tissue homogenates and rat plasma to

study the effects of different plasma and tissue binding of synthetic glucocorticoid upon their occupancy of glucocorticoid receptors (Wu et al, 2009). Following intravenously infused des-ciclesonide and budesonide, total drug concentrations in lung and plasma were reported to be comparable, whereas the free concentration of budesonide in both lung and plasma was seven-fold greater than the free concentrations of des-ciclesonide; the greater free concentration for budesonide correlated with the greater lung glucocorticoid receptor occupancy.

This work highlighted the importance of measuring free drug concentrations. However, the use of this technique is not standard practice in PK/PD investigations; indeed, the measurement of free drug fraction in tissue homogenates may actually lead to erroneous estimates of the true free concentration within the intact lung. For example, homogenisation of the lung tissue will release drugs into the solution that, in the intact lung, may remain undissolved, e.g. drug in suspension or dry powder dosage formulations.

Thus, while lung tissue can be easily collected in the non-clinical setting, there is very little published data on the use of lung tissue homogenates in PK/PD experimentation. Thus, many questions remain to be resolved as to which approach is best to further advance knowledge in this area.

1.5 Modelling of aerosol deposition in lungs

In an effort to better understand aerosol deposition in the lungs of humans and animal species used in non-clinical studies, a number of *in silico* and experimental *in vitro* deposition models have been developed (Rostami, 2009).

In silico models are based on airflow in the airways and particle physics. These models allow the effect of small changes, such as airway diameters or particle properties, on overall deposition to be assessed (Byron et al, 2010). The use of these models is becoming more prevalent as computational power and imaging techniques power increase.

Experimental models are useful for predicting deposition in the lung when the exposure conditions *in vivo* experiments are simulated. These models, once developed, may be regarded as quality-by-design tools that could be used to improve the performance of inhaled orally-inhaled drugs during the product development. In addition, they may be used to make accurate dose predictions and enable a better understanding of relationships among aerodynamic particle-size distribution, pharmacokinetics and local delivery of inhaled drugs (Byron et al, 2010).

In comparison with *in vivo* techniques, *in silico* and *in vitro* models are more economic and less complex to conduct. In addition, *in vivo* methods tend to show a high degree of variability due to the numerous biological factor differences between individual animals and human subjects (Cooper et al, 2012). However, significant challenges remain in validating these deposition models and demonstrating their capability to accurately model the airflow and particle dynamics of airborne particles. The strengths and limitations of each approach are discussed in this review.

1.5.1 *In Vitro* models

In vitro models based on plastic casts of the lung have been prepared by several groups using variations of a process sometimes referred to as the "lost wax technique". In addition to producing molds of a human lung, this technique has been applied in the preparation of molds for various animal species, such as rats, guinea pigs and sheep (Cohen and Briant, 1989;Cohen et al, 1993;McRobbie et al, 2003).

The basic procedure begins with air-drying the excised lung, held at an orientation that represents the normal state for the species, typically upright for human lungs. Once the lung tissue dries and becomes rigid, a dissolvable wax-like resin material is poured into the production mold; after the resin solidifies, the lung tissue is then dissolved away in a primary bath, leaving behind the resin cast. This is then transferred into a secondary bath and time is allowed for the resin to cure, revealing the external airway geometries. The final step involves dissolving the internal resin, leaving behind the airway wall shapes enclosing the airway shapes themselves (Annapragada and Mishchiy, 2007).

However, this method has a number of limitations, including being technically challenging to implement, difficult to change after production and suffering from distortions due to tissue shrinkage (Cheng et al, 1999). In addition, these lung casts do not represent the entire tracheobronchial tree due to incomplete filling of the original airway spaces by the resin. Furthermore, the entire process of producing these molds is destructive, meaning that every experiment conducted using the models is incapable of replication (Annapragada and Mishchiy, 2007).

To address this limitation, airway geometries can now be produced from images generated using magnetic resonance imaging (MRI) or computer topography (CT) data. Thereafter, physical airway models are constructed from polymer resins using rapid prototyping techniques. The developed casts can then be used in deposition experiments, in which the casts are held in a chamber that simulate the airflow pressures of the thoracic cavity. After deposition of the particles is complete, the cast is usually destructively sectioned and the particle content of each section is analysed by a wet chemical assay (McRobbie et al, 2003).

Studies using *in vitro* casts of human respiratory tract replicas have been used to assess regional lung deposition. Nasopharyngeal deposition of up to 90% was noted in nasal casts for particles below 1 µm (Cheng et al, 1995). This data correlated well with computational fluid

dynamic modelling, which used a combination of turbulent and laminar airflow conditions (Martonen et al, 2003). In addition, theoretical models also generally agree with data gathered from casts made from trachea-bronchial airways of cadavers (Zhou and Cheng, 2005).

These studies demonstrated the importance of particle size in influencing the site of deposition within the respiratory tract. For animal models, a number of groups have fabricated nasal molds for different rat species and conducted experiments comparing the deposition of aerosol material in these, as opposed to either direct *in vivo* measurement of deposition or against published deposition studies in preclinical species (Asgharain et al, 2003;Raabe et al, 1988).

Experimental studies of deposition in rat nasal airways have been performed for ultrafine particles (particles with an aerodynamic diameter < 0.1 µm) (Cheng et al, 1990) and particles with an aerodynamic diameter greater than 1 µm (Kelly et al, 2001). Comparison of ultrafine particle deposition efficiencies from *in vivo* and nasal molds showed good agreement between the deposition efficiencies from live animal and nasal molds over a range of flow rates and particle sizes. This indicates that studies using nasal molds may be suitable alternatives to *in vivo* studies for ultrafine particle deposition (Gerde et al, 1991;Martonen and Yang, 1993).

For larger particles, a study by Asgharian *et al.*, 2003 (Asgharain et al, 2003) comparing nasal deposition data derived from a F344 nasal mold airway with Long-Evans airways (*in vivo*) showed good agreement between deposition for particles with a diameter between 0.5 and 4 µm. The molds used in this investigation were life-size replicas of a post-mortem nasal airway of an approximately 220 g F344 male rat, comprised of the nares, nasal cavities pharynx and larynx. The casting procedures for fabricating the molds were described in Morgan *et al.* (Morgan et al, 1989).

Results from this study suggested that good estimates of nasal deposition can be obtained by using rat nasal molds as surrogates for their live counterparts in studies of the deposition of particles greater than 0.5 µm. There a number of limitations affecting *in vitro* models and their process of construction. First, whilst studies using replica molds have shown good reproducibility at a range of ventilation profiles and particle sizes, their most significant shortcoming is their inability to estimate regional particle deposition in the respiratory beyond the tracheobronchial region (Byron et al, 2010).

In the case of human models, radiation safety concerns have limited the usable imaging techniques such 3D computerised tomography (CT) to the upper five or six airway generations

of the respiratory tract. Thus, the human lung cast models have to be limited to the upper airways regions. Beyond generation 12, the airway diameters are too small to produce *in vitro* models for deposition studies, thus idealised shapes have to represent the alveoli (Alexander et al, 2008;Berg et al, 2010).

Second, *in vitro* models may not replicate exposure conditions found *in vivo*, leading to differing estimates of pulmonary deposition as opposed to the *in vivo* situation (Schroeter et al, 2012). Third, there is no agreement amongst researchers on what methods should be used to construct the respiratory tract model, with different groups using slightly different approaches to produce the models. Some groups construct the models from an analysis of imaging data, whereas others use geometries taken from well-documented cadaveric casts in the literature. The impact of the different approaches on deposition of aerosol particles is unknown (Byron et al, 2010).

In addition, the airway wall surface in these models is unlikely to have the same particle trapping properties as the real lung, where the surfactant layer results in a very effective particle trapping layer of hydrophobic particles. In contrast, particle bounce from the cast surface may lead to inaccurate deposition measurements (Annapragada and Mishchiy, 2007).

1.5.2 *In Silico* models

A number of computational models have been developed to estimate particle deposition in the respiratory tract for both human and preclinical species. The use of these models has become more widespread due to the increase in computing power, as well as improvements in resolution of the imaging technologies used to scan the respiratory airways (Hofmann, 2011). For all types of *in silico* models, four main types of information are needed as input data to the deposition model (see Figure 6). These are lung morphometry, respiratory physiology, particle properties and fluid dynamics (Asgharain et al, 2003;Rostami, 2009). A brief description of these four factors and how they affect *in silico* models follows:

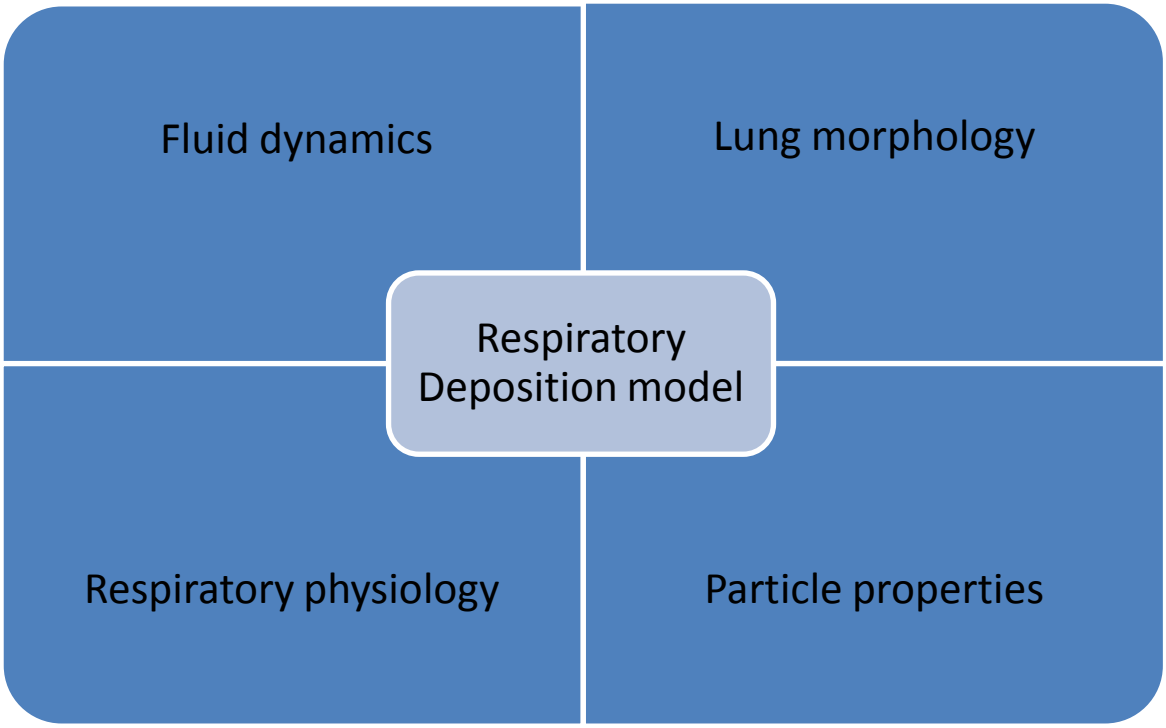

Figure 6: Four categories of input data required for computational airway deposition model development.

Lung morphometry: The size and dimensions of the airways strongly affect the deposition of particles in the lung. In addition, the number of airway generations increases, moving down from the upper to the lower airways, when the dimensions become smaller and this will strongly influence the mechanism by which airway deposition takes place. Furthermore, the lung volume expands during inhalation and contracts during exhalation resulting in altered geometry, especially in the lower respiratory tract (Rostami, 2009).

Respiratory physiology: The most important physiological factors affecting lung deposition are the breathing frequency f, i.e. the number of breaths per minute, and the tidal volume VT, which is the volume inhaled during a single breath. Both of these factors vary depending on the physical activity of a person (Hofmann, 2011). For example, an increase in the breathing rate can lead to greater deposition in the upper airways due to an enhanced deposition by impaction. Conversely, a reduction in the breathing rate will lead to enhanced lower airway deposition, as the residence time for particles is increased and enhanced deposition due to sedimentation will take place (Schulz, 1998). Additional breathing parameters for modelling purposes are the inspiration, expiration and breath-hold times (Hofmann, 2011).

Particle properties: The aerodynamic particle size distribution (APSD) of inhaled particles is known to strongly influence deposition in the respiratory tract. Large particles (> 6 µm) tend to deposit mainly in the upper airways via impaction mechanism. In contrast, smaller particles (< 2 µm) deposit mainly in the alveolar region (Usmani et al, 2005).

Fluid dynamics: Aerosol generation and lung deposition can be adversely affected as a function of either moisture uptake or hygroscopic growth. Hygroscopicity is defined as the intrinsic tendency of a material to take on moisture from its surroundings. Typical respiratory tract conditions are generally considered to be 99.5% relative humidity and 37ºC (Longest and Holbrook, 2012). As aerosol particles enter the lungs, they experience a high humidity environment and susceptible particles may be subject to hygroscopic growth, leading to an increase in particle dimensions, thus affecting lung deposition. Ferron *et al.* (Ferron et al, 2013) demonstrated a significant effect of hygroscopic growth in terms of increasing particle size for a range of common aerosol drugs and particles, such as Histamine dihydrochloride, Carbenicillin di sodium, and Atropine sulphate.

Computational models of aerosol lung deposition may be divided into two main groups: whole-lung models and local deposition models, commonly referred to as Computational Fluid Dynamic (CFD) models. Whole-lung models are based on idealised lung geometry and simplifying equations to estimate the total or regional deposition of particles in airways. Numerous versions of a whole-lung model are widely used for inhalation dosimetry assessment. Amongst these, the International Commission on Radiological Protection (ICRP) and multiple path dosimetry (MPPD) models are the most widely used (Hofmann, 2011;Rostami, 2009).

The ICRP model was first published in 1966 and later revised in 1994 (ICRP, 1994). The model was developed to estimate the radiation exposure of workers resulting from inhalation of radionuclide in nuclear power plants. In this model, the human lung is depicted as a series of compartments through which aerosol particles are inhaled and exhaled. In addition, each of the compartments is treated as a filter and deposition in each compartment is derived from experimental work. The model is able to assess deposition in the lung based on a number of inputs. These include: physical activity, gender, ethnic origin, body size, particle size in the range 0.005-100 µm, smoking and COPD lung conditions.

This model predicts nasopharyngeal deposition greater than 80% for very small (<1 nm) and large (> 5 µm) particles, with the least deposition of particles from 10 nm to 1 µm. Predicted alveolar deposition is almost the opposite, with a maximum deposition of approximately 20% for 1-2 µm particles and 50% deposition for particles between 10 and 100 nm. Predicted TB deposition is approximately 10% for particles from 10 nm to 10 µm. The main limitation of this model is that, due the simplifying assumptions, the site-specific deposition information provided is either unavailable or unreliable (Jarvis and Birchall, 1994).

In contrast with the ICRP model, the MPPD dosimetry model is more user-friendly and has been validated with some experimental data (Cassee et al, 2002;Kuehl et al, 2012). This model was developed by CIIT (Chemical Industry Institute of Toxicology, USA) in close collaboration with RIVM (National Institute for Public Health and the Environment, Bilthoven, The Netherlands). The MPPD model allows calculation of aerosol deposition fractions and exposure doses for humans and rats for particles ranging from ultrafine (0.01 µm) to coarse (> 2µm) sizes (Asgharian and Anjilvel, 1998). An updated version of the MPPD model was released in 2006 and the software is freely available for download online.

This model is based on a detailed description of the airway and lung geometry for humans and rats. Deposition within each region or airway is calculated using theoretically derived equations for the various deposition mechanisms, i.e. diffusion, sedimentation and impaction. Furthermore, the model allows the user to test a variety of inputs, such as lung geometry, breathing conditions and particle characteristics such as size, distribution and mass density.

As in the case of the ICRP model, the main limitation of this model is that the site of deposition is not well-described; that is, deposition is predicted in general regions such as the throat or trachea-bronchial airways. In addition, these models do not currently account for a number of

factors known to influence particle deposition such as changes in lung morphometry and fluid dynamic properties (Rostami, 2009).

In order to overcome some of the shortcomings of whole-based models, CFD models were developed to assess particle deposition in the lungs. In contrast, with whole-lung models, CFD simulations calculate the flow and aerosol physics based on first principles, i.e. the model outputs are solved mathematically, and are not based on assumptions from an empirical model and fitting parameters (Ferziger, 2002).

A primary strength of CFD models is that they provide a detailed description of the flow fields at millions of representative points and can predict deposition at a localised level (Longest and Holbrook, 2012). In addition, CFD has been used successfully to identify inertial impaction as the governing mechanism of deposition in the mouth-throat region of the respiratory tract (Zhang et al, 2006). Furthermore, CFD models represent a non-invasive technique to visualise the complex flow occurring in the respiratory tract and draw a map of regional drug deposition.

Other applications of CFD models have been to predict the deposition in animal species. In a study by Schroeter *et al.* (Schroeter et al, 2012), a computational model of the whole nasal tract of an adult Sprague-Dawley rat was developed. This model was then used to predict the regional deposition of particles in the size range from 1 nm to 10 µm. Inspiratory flow rates corresponding to 50, 100 and 200% of the estimated minute volumes during resting breathing. Predictions of total nasal deposition compared well with experimental data from literature when deposition fractions were plotted against Stokes numbers.

Furthermore, results showed deposition within the regional nasal fraction to be highly dependent on particle size and flow rate. However, despite the advances in this field due to increasing computing processes and imaging capabilities, most CFD-based lung models address deposition in the upper airway regions only (generation 5-6). This is primarily due to the lack of accurate morphometric data on the lower airways.

In addition, as deposition in the lower airway regions is believed to be mainly due to sedimentation processes and is not affected greatly by the flow conditions, huge computational power and time is required to model deposition accurately. Robinson *et al.* reported that different CFD software packages lacked agreement in particle deposition predictions (Robinson et al, 2008).

The type of model selected for simulation analysis, whether whole-lung or CFD, depends on the level of detail required. For example, in cases in which deposition is only required to be known in general regions, e.g. the nasal and lungs, then whole-lung models are often sufficient (Byron et al, 2010). If further details are required, for instance where the drug distributed within the lung, as in the case of drugs with a long duration of topical activity or compound administered for systemic effects, then CFD-models may be required (Longest and Holbrook, 2012).

In silico models are now used as design tools to improve respiratory aerosol delivery and to potentially target the site of deposition. Specifically, models are currently applied to: improving inhaler design, modify usage parameters for improved delivery, and assist in developing new methods to target the site of deposition within the respiratory airways (Byron et al, 2010).

In summary, *in silico* models of aerosol deposition are currently being applied to effectively improve the delivery of pharmaceutical aerosols and to target the site of aerosol deposition. Both whole-lung and CFD models have been used to develop new drug delivery approaches (Hindle and Longest, 2010). In general, model predictions are in moderate agreement with *in vitro* and *in vivo* data sets. In terms of model development, future work remains in the areas of improving particle modelling efficiencies and improved estimation of localised deposition predictions (Longest and Holbrook, 2012).

1.5.3 Validation of *in silico* lung deposition models

Validation of *in silico* lung models is very challenging due to the lack of consensus amongst experts in this field as to what the validation process would entail. Oldham reviewed the challenges in validation of *in silico* models used in human studies (Oldham, 2006). These included (1) defining what validation is, (2) defining appropriate experimental data for validation and (3) demonstrating the results are in agreement with the *in vivo* experimental data and that this agreement is not coincidental, i.e. resulting from statistical errors.

In order to fulfil these criteria, Oldham argued that a large data set covering populations other than healthy volunteers is required. This database should contain individuals suffering from chronic lung diseases such as chronic obstructive pulmonary disease (COPD) and bronchitis, as well as diverse population groups including children and the elderly. In addition, the effect of different inhaler types, i.e. pressurised metered dose inhalers and dry powder inhalers, on deposition in the lung should be considered for inclusion (Oldham, 2006).

For CFD-based models in depth comparison is required to eliminate the possibility of coincidental agreement with *in vivo* experimental data. However, sometimes it is impossible to compare the CFD data with *in vivo* data due to the lack of experimental measurements; for example, particle deposition has rarely been validated at the regional level because there were no direct methods to measure the regional drug deposition in terms of *in vivo* anatomical space. Therefore, the interpretation of the model predictions requires expertise in fluid mechanics, knowledge of past results, as well as a good understanding of the computer code use to generate the CFD model.

1.6 Imaging techniques

Imaging techniques can be used to evaluate drug deposition in the lung following inhaled delivery. These techniques provide information on the total amount of drug delivered to the whole lungs and the distribution of the drug within the airways. The imaging techniques most commonly used include two-dimensional (2D) techniques such as gamma scintigraphy, and three-dimensional techniques such as single photon emission computed tomography (SPECT) and positron emission tomography (PET) (Conway, 2012).

In the case of gamma scintigraphy, the main gamma radiation-emitting isotope used is 99mTechnetium (Wu et al, 2011), which can be incorporated into pulmonary formulations and used as a surrogate marker for the drug. This technique has proved to be a very useful tool for studying pulmonary delivery, allowing the assessment of the extent and pattern of lung deposition, e.g. central versus peripheral. However, a major drawback of this technique is that the 2D images obtained do not account for the three-dimensional nature of the lung tissue. Consequently, the drug deposition includes an overlay of structures of interest, namely alveoli, small and large airways (Lee et al, 2001).

With regards to three-dimensional techniques, SPECT involves the use of a rotating camera which is rotated through 360° and results in the reconstruction of a three-dimensional lung images. This allows for a more complete profile of the penetration of the drug through the lung compared to the two-dimensional techniques. In addition, regional deposition is more clearly defined and may be expressed in a number of ways, such as sections through the lungs (transverse, coronal and sagittal) or the amount of drug in different airway generations. However, SPECT is more technically demanding than gamma scintigraphy (Eberl et al, 2001).

A further advance in the field three-dimensional techniques is the use of PET techniques. This technique allows for the direct labelling of drug particles themselves by short, half-life radionuclide, e.g. carbon-11, Fluorine-18 (Annapragada and Mishchiy, 2007). Thus, the drug particles are processed in an identical manner to normal clinical material, and delivered by identical devices. A significant advantage of PET over SPECT is the dramatic increase in the single-to-noise ratio.

However, the choice of either PET or SPECT techniques is not straightforward and is dependent on a number of considerations, such as the level of resolution required, or radiation dose required to produce the images. Unfortunately, there is no head-to-head comparison of the

two techniques in the literature, which makes it difficult to make definitive statements about the superiority of one technique over the other.

Numerous examples of imaging applications to assess deposition in preclinical models have been published. Wu *et al.*, developed an aerosol delivery system coupled with the SPECT imaging technique to measure the pulmonary clearance rate as a measure of lung permeability. They used guinea pig models of chronic obstructive pulmonary disease (COPD) to determine its usefulness in studying pathogenesis of the condition (Wu et al, 2011).

Other applications include their use as tools to evaluate regional deposition patterns of pharmaceutical aerosols lungs of preclinical species. A study conducted by Kuehl *et al.* (Kuehl et al, 2012), evaluated aerosol deposition patterns as a function of particle size in rats and mice using a novel image analysis technique, known as the Onion model. This model was so called as the lung images are segmented in a pattern similar to an onion, with dark regions representing the central mass of the lung and different, lighter colours representing the outward segments of the lung.

In this study, mice and rats were exposed to radio-labelled polydisperse aerosols at 0.5, 1.0, 3.0 and 5.0 µm MMAD followed by SPECT/CT imaging for imaging analysis. Images were quantified for both total and regional deposition. The lung deposition fraction in both rats and mice was shown to increase with decreasing particle size. In addition, the Onion model suggested that the smaller particles resulted in increased peripheral deposition. In comparison to historical data set provided by Otto Raabe (Raabe et al, 1988), the 1.0, 3.0 and 5.0 µm particles resulted in similar lung deposition fractions for both mice and rats. However, the 0.5 µm lung deposition fraction was significantly different. This difference was attributed to different methodologies among the studies, such as the use of polydisperse particles in the onion study, whereas the historical data was generated using monodisperse aerosols.

1.7 Inhalation exposure studies

Inhalation studies using preclinical species are conducted for a variety of purposes including toxicity, pharmacokinetic and pharmacodynamic studies of airborne materials and inhaled therapies.

For toxicity studies, a number of investigations are required prior to the administration of inhaled drugs to humans in clinical trials. The development plans usually follow recommendations outlined in the relevant International Conference on Harmonisation (ICH) guidelines (Owen, 2013). Different endpoints may be used to determine the inhalation toxicity of airborne materials. For example, LC50 studies defined as the dose required to kill 50% of the animals exposed is used to determine the lethality of dose. Other studies may assess the carcinogenicity and safety pharmacology of inhaled drugs (Y.S.Cheng and O.R.Moss, 1989).

Pharmacokinetic studies are used to assess the amount of drug deposited, retained, distributed and metabolised. In addition, airway challenge studies, such as the acute lipopolysaccharide (LPS)-induced inflammation model in rats, can be used to assess the efficacy of inhaled anti-inflammatory drugs. This model utilises the recruitment of neutrophils into bronchial alveolar lavage fluid (BALF) as the efficacy endpoint (Chiang et al, 2010).

For all these studies, an exposure system must be specifically designed to provide a measurement of these endpoints. A fundamental requirement of any exposure system selected should be that it delivers a stable, well-characterised study atmosphere to the subjects under investigation for the specified duration of the experiment. Thus, the variability in the resulting lung burden would then be solely to biological factors and not location within the system. An additional but nonetheless important requirement should be to minimise the stress to subjects, to protect laboratory personnel from exposure to the test substances and to prevent or eliminate non-respiratory tract exposure of the study subjects (Griffis et al, 1981).

1.7.1 Design, Method and Characterisation of aerosol exposure systems

Numerous systems have been developed to expose animals to various test agents and provide a controlled environment for exposure. These systems can be classified into one of two broad categories: whole-body exposure chambers and nose or head-only chambers (Cheng, 1995).

In a whole-body exposure chamber, the test animals are able to move freely within the chamber and are exposed fully to the exposure atmosphere. These systems are most commonly employed for chronic exposure studies where daily exposure durations are 6 to 24 hours, and for dosing large number of laboratory animals. The main benefits of these systems are the ability to expose relatively large numbers of animals to exposure atmosphere and in a relatively stress-free environment. Drawbacks of this system include the high consumption of test materials due to the likely exposure of all surfaces of the animals to the test material (Cheng, 1995).

Furthermore, the instillation of sophisticated ventilation systems is often required in order to ensure the exposure atmosphere is continually cleaned of animal waste, microorganisms and ammonia. Therefore, in order to satisfy this requirement, most of these systems are operated on a dynamic flow basis where there is a continuous flow of air through the chambers (Wong, 2007).

Nose-only exposure systems are designed to expose the subjects to the test material whilst minimising skin and fur contamination. The test subject is typically confined in an inhalation tube such that only the nose or head is exposed to the test atmosphere (Wong, 2007). Early designs of this system consisted of test animals inhaling from a plenum containing the test atmosphere and exhaling back into the same plenum (Smith, 1981). The main disadvantage of this system was that animals placed downstream may inhale air that was exhaled from the upstream test animals. Therefore, if the airflow was too low, then it was highly likely that downstream test subjects would get a lower dose or a highly variable dose (Cannon et al, 1983).

This design fault has been mainly overcome by designing systems in which the test atmosphere flows directly toward the nose or head of each test animal. In addition, any exhaled air is removed directly from each dosing port by an exhaust airflow system. Consequently, all the test subjects are exposed to the same atmosphere.

A critical parameter which needs to be tightly controlled and closely monitored is the airflow through each port. The airflow to each port must exceed the minute ventilation rate of the animal; otherwise, the airflow may be insufficient to clear the exhaled atmosphere away from the animal. This will then result in the animal beginning to re-breath exhaled air, leading to a reduction in oxygen concentration, an increase in carbon dioxide concentration and a reduction in the dose of test atmosphere delivered to the test animals (Wong, 2007).

Various authors have recommended minimum airflow conditions to overcome this problem. Moss *et al.* recommended airflow of 2.5-4 times minute ventilation of animal in order minimise test material consumption whilst maintaining a concentration at 90% of the target (Moss et al, 2006). However, other investigators have proposed higher airflow multiples; for example, Phalen (2010) recommended airflow of 10 times minute ventilation to prevent re-breathing of exhaled air, especially if the animal becomes inactive (Phalen et al, 2010).

The advantages of nose-only exposure are considerable. Firstly, they totally eliminate the non-respiratory pathway of exposures. Secondly, they are very efficient with respect to the volumes of study material and throughput air that is required, resulting in more precise dosing to the test animals. The disadvantages of these systems are similar to whole-body exposure systems, plus the subject may become stressed due to restricted movements within the inhalation tubes. In addition, animals may attempt to turn around in the tube, suffocate, or suffer from possible heat build-up.

1.7.2 Generation of Aerosols

The generation of atmospheres containing particles of known size and concentration can be very challenging. Aerosols may be generated by condensation of vapours, dispersion of dry particles, or dispersion of solids in liquids. This section gives an overview of the most widely used techniques used to produce aerosols.

1.7.2.1 Liquid aerosol generation

Nebulisers are used to generate aerosol particles for inhalation studies from liquid solutions and suspensions. In this method, aerosol droplets are generated by pushing air under high pressure conditions through a nozzle, which induces liquid to flow into the airstream. The liquid is then broken up into a range of particle-size distribution of droplets (Le Brun et al, 2000).

There are two basic types of nebulisers: Jet and Ultrasonic nebulisers. The Jet nebuliser uses compressed air to flow at high velocity through a liquid medicine to turn it into an aerosol, which is then inhaled by the test subject. The main advantages of the Jet nebuliser are the relatively low operational cost in comparison with other aerosol generation systems, and its relative ease of use (Lange and Finlay, 2006).

Ultrasonic nebulisers operate on the principle of using sound waves to generate a vapour mist. In these types of nebulisers, an electronic oscillator generates a high frequency wave, which in turns vibrates a piezoelectric element with sufficient force to produce an aerosol liquid in the form of a vapour mist from the liquid reservoir containing the test material. The main advantages of this system include its low weight, thus making it a portable and almost silent aerosol generation; therefore, it reduces the noise discomfort for the test subject that has inhaled the aerosol generated from this machine. A drawback of this system is the excessive liquid waste (Amani et al, 2011). An example of this type of nebuliser currently on the market is the Omron NE-U22 nebuliser (Wakasugi et al, 2014).

The physical properties of the drug solution reported in the literature as affecting the particle size distribution and efficiency of aerosol delivery by nebulisation include viscosity, surface tension, temperature and concentration (Le Brun et al, 2000) . Newman *et al.* showed that jet nebulisers tend to produce a smaller particle size as the viscosity of the solution increases (Newman et al, 1987).

McCallion *et al.* investigated whether viscosity and surface tension of nebulised fluids influenced the aerosol's size and output characteristics from jet and ultrasonic nebulisers, as theoretical assumptions derived from empirical formulas (Le Brun et al, 2000) suggest that the median droplet diameter increases with increasing surface tension of the drug solution. Results from this study did confirm this trend; however, no clear relationship was established (McCallion et al, 1995).

An advantage of using the nebulisation method of delivery includes ease of preparation, especially in the case of drugs which are difficult to formulate as dry powder or pressurised liquid formulation (O'Callaghan and Barry, 1997). In addition, the nebulisation method is frequently used in initial proof-of-concept drug studies, where the efficacy and safety of drug molecules is screened prior to committing resources to developing a dry powder form of the drug (Schachtner W, 2011).

A disadvantage of using the nebulisation method is the high degree of variability exhibited for both droplet size and released dose between various nebuliser types. One study showed the particle size (MMAD) of six commonly used nebulisers of various types varied from < l.0 µm to >10 µm, with most in the range of 4-6 µm (Nerbrink et al, 1994). In addition, a study by Finlay *et al.* comparing 19 nebuliser types aerosolising Salbutamol sulphate showed a large degree of variation in the predicted lung dose between the devices (Finlay et al, 1998)

1.7.2.2 **Wright dust feeder**

The Wright dust feeder is the most widely used aerosol generator in inhalation toxicology studies. The generator operates by loading powder into a cup. This cup rotates slowly across a scraper plate, which removes irregular quantities of powder from the cup (see Figure 7). The airstream will then entrain the powder and carry it out of the generator and into the exposure chamber. This generator works best for non-cohesive powders that have a significant portion of the particle size distribution in the respirable range (Hinds, 1999).

The Wright dust feed unit generates powders in the particle size range of 0.2-10 µm. In addition, it can be operated at a flow rate in the range of 10-40 L/min. The output mass concentration is 10 g/m^3 while the output concentration only requires five minutes to stabilise (Wright, 1950). The main drawback with this generator is the fluctuation in the feed rate, resulting in poor replication in the aerosol concentration generated. This is due to the build-up of powder on the scraping plate before the airstream carries it away. This issue is partly overcome by connecting the generator to a large exposure chamber to diminish fluctuations (Raeburn et al, 1992).

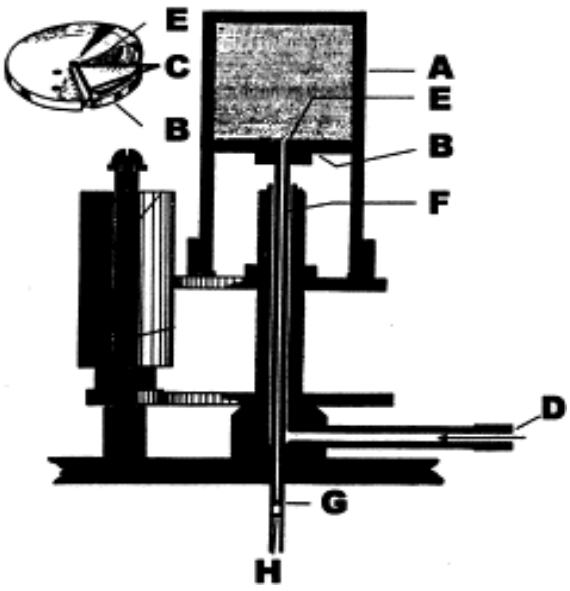

Figure 7: Schematic of the Wright dust feed used to evenly coat epithelium with tantalum powder aerosol. (A) Dust cylinder, (B) Scraper head shown in more detail in upper left-hand corner, (C) Groove, (D) Air inlet, (E) Hole in centre of scraper head, (F) Aerosol outlet tube, (G) Nozzle, and (H) Plate. Taken from B.M. Wright (Wright, 1950). Reproduced by permission of IOP Publishing Ltd.

1.7.2.3 **Fluidised bed aerosol generator (FBAG)**

This type of generator was initially developed for calibrating dust-measuring instruments such as optical counters and mass monitors (Marple et al, 1978). This method has been used to generate a variety of powders for both pharmaceutical and non-pharmaceutical applications, such as fibrous particles and polystyrene latex spheres (Byron et al, 1986;Yeh et al, 1987). The benefit of this type generation is its ability to produce a relatively stable aerosol concentration (Marple et al, 1978).

However, the time required to reach a steady state can take 2-3 hours, meaning a great deal of material can be wasted before reaching the desired aerosol concentration. In addition, the fluidised bed worked well for non-cohesive powders, but worked less well for more cohesive powders typical of micronised drug substances found in inhalation studies. Further details relating to the operation of this generator can be found in the Results and Discussion section (see 1.1, B. Results and Discussion).

1.7.2.4 **Rotating Brush**

Another method of dust generation uses the rotating brush method. In this technique, a rotating brush with high-velocity airflow of 150 m/sec is used to remove powder from a plug of powder that is slowly being pushed into the brush.

A particle size of up to 100 µm can be dispersed. Airflow rates required to operate this generator are specified from 10 to 50 L/min. Aerosol concentration up to 100g/m^3 can be obtained. A desirable characteristic of this generator is its ability to disperse cohesive powders. In addition, some authors have used this method to generate fibrous particles (Bernstein et al, 1994). However, the duration of operation is limited by the volume of powder plug and feed rate which, in turn, also affects the stability of aerosol concentration generated.

1.7.2.5 **Small-Scale Powder Disperser**

This type of generator uses the venturi effect to aspire particles from a rotating turntable. The venturi effect refers to the fluid pressure that results when an incompressible fluid flows through a constricted section of pipe, leading to a pressure drop that entrains the powder (Tang et al, 2008). As the constriction opens again, a turbulence flow is created that helps to break apart the powder. Commercial forms of this generator include the small-scale powder disperser (see Figure 8) developed jointly by TSI™ and the University of Minnesota Particle Technology Laboratory.

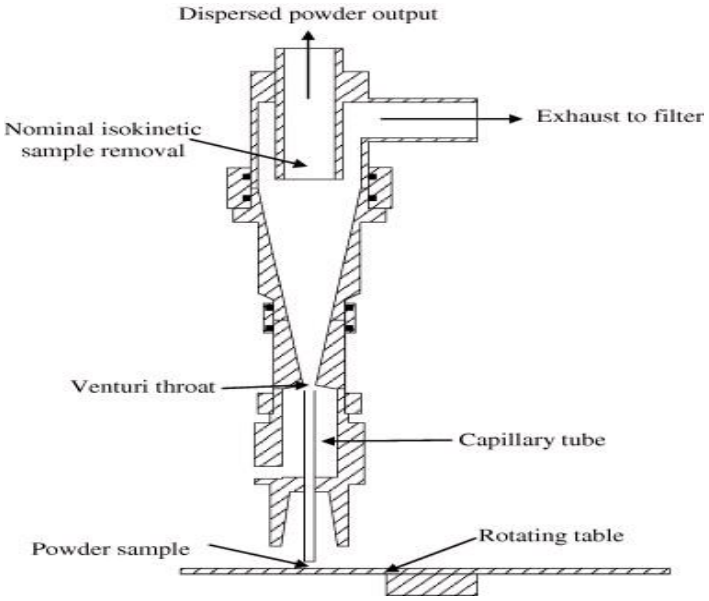

Figure 8: Small-scale powder disperser. Reproduced with permission from TSI product literature.

The main advantage of this type of generator is that it can produce aerosol powder using a limited quantity of test material. This is a very useful feature for pharmaceutical applications, where drug materials may be available in limited quantities for evaluation. In addition, the device is capable of deagglormating dry powder particles in the range of 0.5 to 50 µm. Limitations include a decrease in the dispersion efficiency as particle size increases. In addition, the device requires careful setup, as poor alignment of the connecting tubes will result in significant powder losses and a reduction in generation efficiency (Chen et al, 1995).

1.8 Exposure atmosphere characterisation

A critical objective in most aerosol inhalation studies is establishing a quantitative relationship between an observed biological response and a measured physical and chemical property of the test atmosphere. The most commonly measured proprieties are the mass concentration and median size distribution. Other particle properties that may be assessed include surface area, dissolution rate, shape and hygroscopicity of particles (Owen, 2013).

An important point to note is that any measurements undertaken to characterise the aerosol atmosphere must be taken in the "breathing zone". This is defined as volume or space from which the subject breathes (Creton et al, 2010). In nose-only exposure systems, it will be the small volume in front of the nostrils. Furthermore, the aerosol composition in this zone should be uniform. If it is not, then measures must be taken to rectify the situation, such as better mixing or sampling at sufficient sites so that an average composition can be adequately described (Pauluhn, 2005).

With regards to the exposure, the study material concentration at the breathing zone and air-flow rate should be known throughout the exposure. If aerosol particles are being studied, the size distribution, typically the mass median aerodynamic diameter (MMAD) and geometric standard deviation (GSD), should be measured at least twice during each exposure in line with draft guidelines (see Table 2) set by the Organisation for European Cooperation and Development (OECD, 2004) for acute inhalation toxicity testing. In addition, the environmental conditions such as temperature, humidity, both inside and surrounding the inhalation exposure system, will need to be monitored and corrected if necessary (OECD, 2004).

Table 2: OECD Draft Guidelines for acute inhalation toxicity testing

Exposure conditions	**Levels**
Air flow nose-only (L/min/rat)	0.5
Whole body (air changes per hour)	12-15
Chamber temperature (°C)	22 ± 3
Relative humidity (%RH)	30-70
MMAD (µm) GSD	1-4.0 1.5-3.0
Exposure metric	**Frequency of sampling during exposure**
Airflow	Monitor at least 3 times
Temperature and Humidity	Monitor at least every 30 minutes
Particle size distribution	Monitor at least twice
Aerosol concentration	Monitor at least 5, on hourly basis in breathing zone

The mass concentration of an aerosol is the primary parameter for characterising a test atmosphere containing an aerosol. This measure may be specified in a mass per volume unit, such as micrograms per cubic meter ($\mu g/m^3$). Other measures of aerosol mass, such as the surface area, may provide a measure that better correlates with observed biological effects. Therefore, it is important to select the appropriate parameter that correlates with the biological response (Wong, 2007). Mass concentration is usually determined by pulling a sample of atmosphere through a filter located in the breathing zone at a known flow rate for a known period of time.

In addition, the particle size distribution of the study material must be characterised. This is typically done using a multistage cascade impaction instrument, such as the Marple Cascade Impactor (Tougas et al, 2009). The Multistage Impactor operates by separating the incoming sample into discrete fractions on the basis of particle inertia. Analysis of each fraction, typically by direct weighing or, more accurately, by high performance liquid chromatography, determines the amount of test material collected at each stage. Thereafter, metrics such as the MMAD and GSD are determined using a log-probit plot of the raw data. Together, the MMAD and GSD locate the central point of the particle size distribution and describe its spread (Tougas et al, 2009).

Furthermore, particle size distribution may be characterised using instruments based on the light-scattering principle, such as the aerodynamic particle size instrument (APS; TSI 3221). In this type of instrument, an optical sensor is placed in the flow field of the aerosol to be sampled. Consequently, different-sized particles will diffract the light at different angles. Thereafter, a computer algorithm is used to calculate the particle size. Limitations of the optical light-scattering methods include lack of standardisation amongst particle size instruments of this type as to the algorithm used to calculate the particle size, thus making comparison between different instruments very difficult (Mitchell et al, 2006).

2 Aim of the thesis

The objective of the thesis is to develop an *in vitro* model (IVR) of the rat respiratory tract. This model will attempt to account for the effect of drug product characteristics (aerodynamic particle size distribution, or APSD) and physiological parameters (breathing pattern and airway geometry) on total and regional deposition in the lungs. This investigation constitutes a critical step toward a better understanding of relationships among APSD, PK and local delivery for orally-inhaled drug products.

The primary endpoint of the project is the development of a quality-by-design tool that can be used to improve the performance of orally-inhaled drugs during the product development. Implementation of this method in drug development would enable the assessment of aerosol quality and regional dose distribution when animals are dosed during pre-candidate selection and during safety studies. In addition, use of the model may enable a better interpretation of data within and between species and for different powders; fewer dose variants will need to be developed, as the human dose can be predicted with more confidence from the animal data.

The following programme of work is proposed:

- Acquisition of Magnetic Resonance Imaging (MRI) scans of excised lungs from euthanased Sprague-Dawley rats and use of this data to reconstruct a physical hollow model of the rat lung by stereolithography. This will be carried out by a contract company.
- Develop and characterise an exposure system to assess deposition in the developed *in vitro* rat lung model.
- Assess the effect of ventilation parameters and particle characteristic on deposition in the *in vitro* model.
- For validation purposes, the *in vitro* results from the IVR model will be compared with corresponding outputs from published *in silico* methods and *in vivo* lung data.
- Subject to satisfactory results from the *in vitro* model validation work, the model will be used to investigate whether total or regional lung deposition are key drivers to pharmacokinetic and pharmacodynamic responses in rat animal models.

B. Results and Discussion

1 Development of aerosol delivery method

In order to study the effect of aerosol characteristics such as dose, particle size and duration exposure on both the *in vitro* rat lung model (IVR) and potentially live rats, an aerosol generation method was developed. However, the selection of a particular aerosol generation method requires careful consideration of the physical properties of both the bulk material and the aerosol. This, in turn, requires the relationship between the desired aerosol size and concentration and operating parameters to be established. In many cases, commercial aerosol generators may not be able to meet all the requirements and, therefore, need to be customised to fit the purpose they are intended for. Therefore, to address this issue, and prior to testing the IVR model, an aerosol generation was developed and characterised.

If particle dispersion and constant concentration are not required, then simple methods such as blowing a dust from a tube with a blast of air can be used. However, if it is required to obtain stable output, more sophisticated dust generators may be needed. Amongst these is the Jet-O-Mizer (Fluid Energy Corp, Plumsteadville, USA), which is useful for generating high concentrations (50-100 mg/m^3 at 200 L/min flow rate) and the Wright dust feeder, capable of generating 1-50 mg/m^3 at 20 L/min flow rate. However, a major drawback with using these generators is their inability to deagglomerate the aerosolised particles, particularly small-sized particles, which are difficult to aerosolise because of their cohesive nature (Y.S.Cheng and O.R.Moss, 1989).

One possible way of overcoming this agglomeration may be by the use of a fluidised bed, which should thoroughly deagglomerate the dust particles and, at the same time, act as a capacitor, thereby damping out unsteady dust injection into the bed. The TSI Model 3400A Fluidised Bed Aerosol Generator (FBAG) (St Paul, USA) operates by using this technique. It was chosen for this work as it is reported by the manufacturer to be able to thoroughly deagglomerate powders, have good feed rate control of the test powder and able to give a steady state concentration within a reasonable time frame (Marple et al, 1978).

The FBAG system has been previously used in a number of rodent inhalation studies, e.g. with nearly monodisperse polystyrene latex (PSL) microspheres (Yeh et al, 1987), talc powder (Pickrell et al, 1989) and a variety of bulk powders consisting of nanoparticles with a primary particle size < 25 nm (Schmoll et al, 2009).

The overall aim of the work was to develop and characterise an aerosol generation system that was capable dosing the IVR model and live rodents with airborne test material. Specifically, the following aims were to be investigated:

1. Assess the critical operating parameters of the generator and their relationship with measured outputs such as aerosol concentration, particle size and time required to achieve steady state concentration.

2. Assess the optimum delivery method for aerosolising test material. Two methods of delivery were to be investigated. The first was the chain-fed method, in which the test material is delivered to the fluidisation bed using a chain-operated variable controller. The second method of delivery was to pre-mix the test material with the bronze beads, and operate without adding any further powder during operation in order to reduce the time taken to achieve a steady state of aerosol concentration.

3. Assess the time required achieving a steady state of concentration of test material.

4. Determine the concentration range of test aerosol that can be achieved (mg/m^3).

5. Determine the duration of stable aerosol concentration required to deliver aerosol material to exposure ports.

6. Assess the suitability of using an on-line particle sizer instrument, the Aerodynamic Particle Sizer (APS), in measuring the aerosol concentration of exposure atmosphere compared to traditional method such as chemical and gravimetric analysis of filters.

7. Determine the particle size and distribution, average mass median aerodynamic particle size (MMAD, μm) and Geometric Standard Deviation (GSD, σg) of aerosol produced using this system.

1.1 Method used for generation of aerosol powder for inhalation

The fluidised bed aerosol generator (FBAG) was used to generate aerosol powder in the present study (see Figure 9). This is a relatively simple and commercially available apparatus that forms dry aerosol by the deagglormating bulk powder samples. It is reported by the manufacturer to be capable of generating aerosol particles in the size range of between 0.5 to 40 µm and thus should be suitable for the intended purposes in the planned studies.

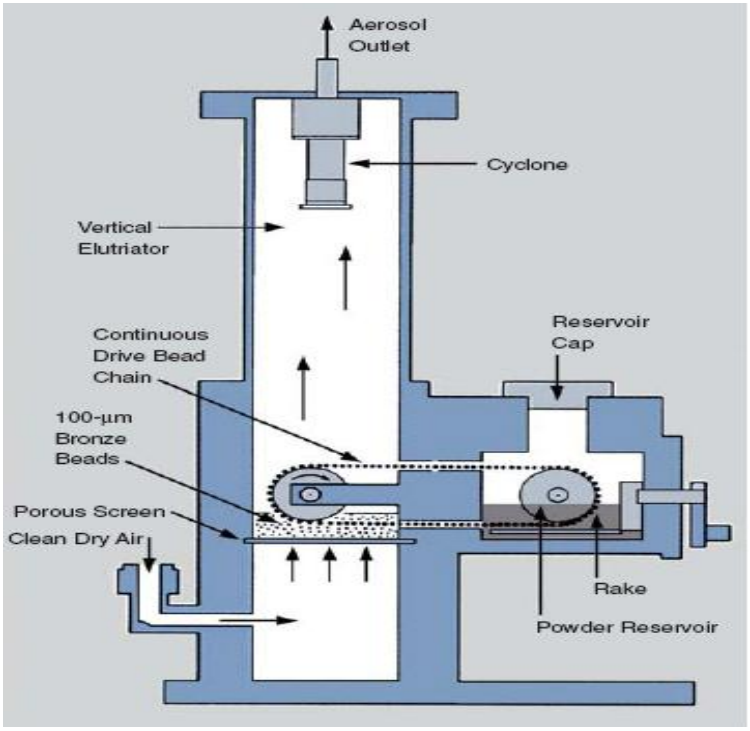

Figure 9: Schematic diagram of the FBAG 3400A. Reproduced with permission from TSI product literature.

The FBAG consists of a powder chamber into which the test material to be aerosolised is placed. From there, it is transported by a chain conveyor into the fluidised bed. The fluidised bed consists of a 1.5 cm thick layer of 100 µm bronze beads placed in a 5.1 cm diameter chamber. The beads are supported by a 250 mesh nylon screen placed above an air plenum (Marple et al, 1978).

The fluidising air flows from the plenum through the fluidised bed, in which the powder is dispersed and carried by the fluidising air through the elutriation chamber. This eluted aerosol is expected to be charged due to mechanical friction within the fluidised bed. Therefore, in order to overcome this charge, the aerosol is passed through a polonium charge neutraliser located in the elutriation chamber.

Aerosol neutralisation using a polonium source has been shown to impart a Boltzmann distribution of charge on low to moderately charged aerosols (Willeke et al, 1974). In this technique, the fluidised bed consists of two types of materials – a fluidising bed of spherical solids and the aerosol powder. The solids are larger than the aerosol particles, such that the upward airflow velocity of the fluidised bed is less than the gravitational settling velocity of the solids, but is greater than that of the aerosol particles.

These two components mix when exposed to an upward airflow velocity, which fluidises but does not entrain the larger bed solids. The fluidising action of these solids disperses the aerosol as individual particles by a combination of mechanical impact and micro scale turbulent shearing stresses. The particles are then elutriated from the fluidised bed, mainly by rising gas bubbles.

The bed solids used were bronze spheres, chosen because they possessed the following properties: smooth, spherical shape; hard material, low abrasion; inert at room temperature and pressure and low electrical charging effects (Willeke et al, 1974). A critical part of the dust generator is the chain conveyor system, which feeds the test powder material into the fluidised bed at a constant rate. The speed of the motor can be varied between 3% and 100% of the maximum speed by a variable speed controller.

The dust generated in this fashion is referred to as the “total” aerosol. It is also possible to use only a “respirable” portion of the aerosol by placing an optional 3 cm cyclone at the top of the elutriator tube and operating the fluidised bed at a flow rate of 9 L/min. As aerosol passes through this cyclone, the large agglomerate particles will be removed. Once the air velocity reaches a critical value, the bed becomes fluidised and produces aerosol. The flow rate flowing through the fluidised bed can be varied from 5 to 30 L/min and is supplied from compressed air source (Marple et al, 1978).

The FBAG may be operated in one of two modes: continuously-fed mode, using the chain system in the manner described earlier, and the “batch-fed” mode, in which test material is pre-mixed thoroughly with the bronze beads and introduced into the fluid bed chamber (Carpenter et al, 1980). Further technical details of this system are described in the Experimental Setup section (see Table 21, C. Experimental Setup).

1.2 Generator performance evaluation

The effect of varying the critical operating parameters of the FBAG and their relationship with measured outputs such as aerosol concentration, particle size and time required to achieve a steady state concentration were assessed. In addition, optimisation of the delivery method of the test material to the fluidisation chamber was investigated.

For this part of the investigation, two methods of delivery were evaluated: continuously-fed and batch-fed. This was done in order to assess which delivery method was most appropriate for the test materials under investigation. The experimental arrangements for evaluating the aerosol generator's performance are shown in Figure 10.

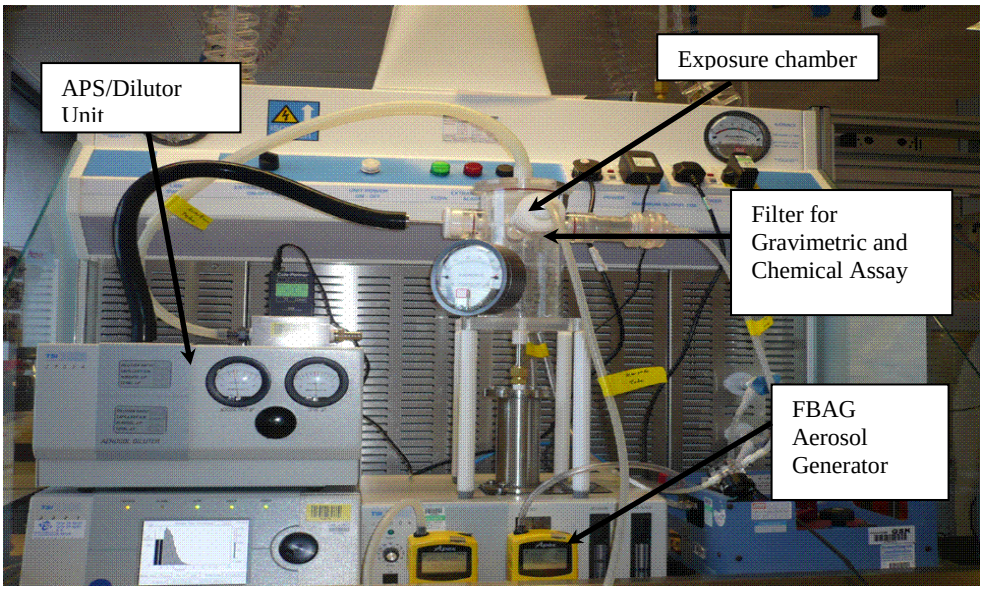

Figure 10: Test setup for evaluating dust generator

Several instruments were used to evaluate the aerosol generator. The mass concentration was measured by collecting particles on a filter and measuring the increase in filter weight. The aerosol concentration was then calculated knowing the mass of sample collected in the filter, the sampling rate and sampling time. In addition, a chemical analysis of some of the samples was also undertaken to determine aerosol concentration and chemical composition. Further details on the equipment used in the aerosol generator evaluation work are included in the Experimental Setup section (see Table 20, C. Experimental Setup).

1.3 Screening Study details

In order to investigate the significance of the critical method factors on the performance of the FBAG, an investigation utilising the statistical tool design of experiment (DOE) was used (Design Expert, DX7, USA).

The DOE statistical approach to process development offers several key advantages over the traditional one-variable-at-a-time approach. DOE studies allow for the evaluation of the statistical significance of individual process parameters, as well as the interaction between factors. Another advantage of the DOE approach is that the statistical significance of various mathematical models can be tested using the appropriate model-fitting functions provided in the DOE software package. The mathematical models can then be utilised to find the predicted optimum system response. Thereafter, the optimised set of conditions can then be verified experimentally to validate the model prediction.

In the current study, the factors chosen for evaluation were as follows: air flow rate into the fluidised bed, and chain speed. These parameters were selected as initial experimental investigations indicated that these factors are likely to affect the amount of aerosol concentration and particle size distribution produced to the greatest extent. The aerosol concentration and particle size distribution were determined by the use of an aerodynamic particle size instrument (APS; TSI 3221). For every factor, a high and low level were selected (see Table 3). Details of the test material and aerosol generation method are described in the Experimental Setup section (see Table 19 and 1.2.1, C – Experimental Setup).

Table 3: Summary of experimental details for the screening study

Factors		**Experimental Range**	
Test Material		Blend of Fluorescent Microspheres (2 µm sized) mixed with lactose (0.8% w/w)	
Powder Feed Rate		2 levels – 30 and 100% of the maximum speed by a variable speed controller	
FBAG Flow Rate		2 levels – 10.0 and 20.0 L/min(centre point 15 L/min)	
Dosing duration		1 level – 60 minutes	
Study Type: Factorial	Experiments: 11	Initial Design: 2-Level factorial	Centre points: 3

The combination of factors and levels for the experiment is shown in Table 4. These combinations were executed in a randomised order and repeated twice for the experiment. In addition, three replicates for the centre point were included to provide a measure of experimental variation (see Figure 11).

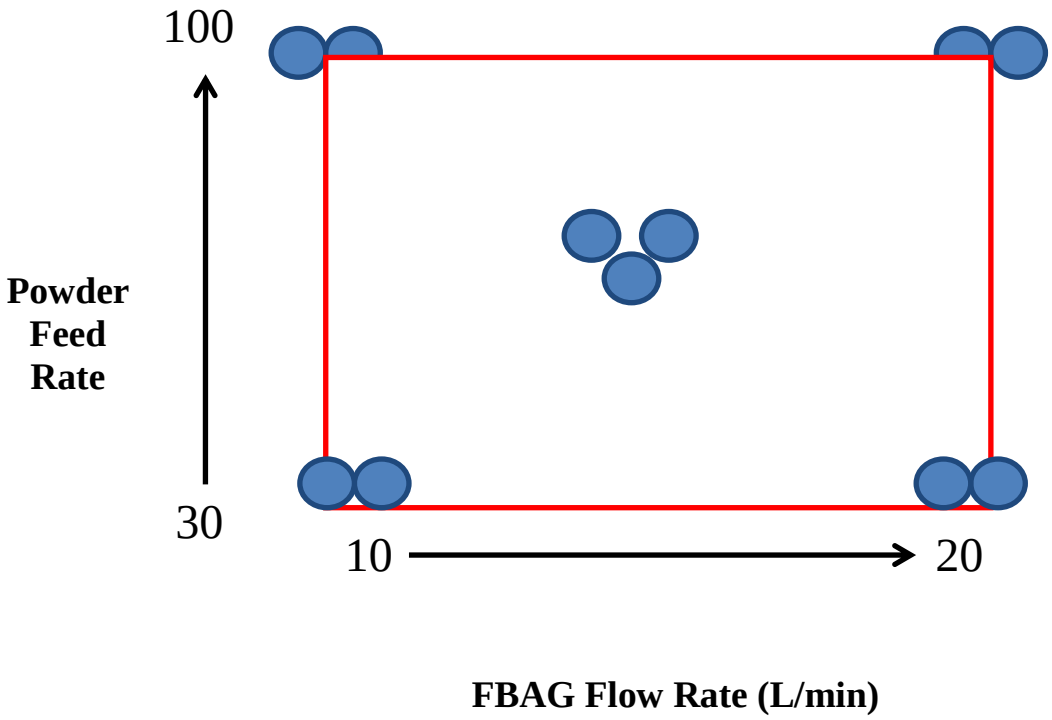

Figure 11: Schematic plot of the experimental design implemented for this investigation

Table 4: Experimental design model details for the screening study

Run number	Point Type	Nominal FBAG Flow rate (L/min)	Nominal powder feed rate	Dosing duration (min)
1	Corner	10	30	60.00
2	Corner	10	30	60.00
3	Corner	20	30	60.00
4	Corner	20	30	60.00
5	Corner	10	100	60.00
6	Corner	10	100	60.00
7	Corner	20	100	60.00
8	Corner	20	100	60.00
9	Centre	15	70	60.00
10	Centre	15	70	60.00
11	Centre	15	70	60.00

1.3.1 Screening study results

The effect of the parameter levels on the generator output in terms of producing an aerosol powder of consistent concentration and particle size distribution was measured using the APS instrument. Further technical details of this system are described in the Experimental Setup section (see 1.1.2.2, C – Experimental Setup). The results generated are listed in Table 5.

Table 5: Experimental results for screening study

Run number	Number particle concentration (n/cm^3)	Mass concentration (mg/m^3)	MMAD (µm)	Geo. Std Dev (σg)
1	7136.24	4.88	2.26	2.14
2	6651.22	4.42	2.29	2.17
3	17244.71	9.88	1.78	2.03
4	13357.32	7.53	1.70	2.10
5	6442.57	5.80	2.80	2.65
6	7643.81	8.93	3.27	2.14
7	20285.42	16.26	2.20	2.02
8	19187.35	13.70	2.14	2.07
9	20854.73	12.49	1.87	2.05
10	20389.96	14.25	2.29	2.20
11	21263.74	13.61	2.27	2.12

1.3.2 Mass particle size concentration (mg/m^3)

A statistically significant model accounting for 62.98% of the variance was fitted to the data describing the relationship between operation parameters and aerosol concentration ($p < 0.05$). The model identified both airflow and powder feed rate as a significant factor affecting aerosol concentration ($p < 0.05$) (see 1.3.1, D-Appendix, for a summary of the statistical analysis).

Figure 12 shows the aerosol concentration versus airflow into the fluidised bed. The plot clearly demonstrates the effect of airflow into the fluidised bed on aerosol concentration; as the air flow rate is increased over the experimental range, there is a corresponding increase in the output concentration. In addition, a similar trend with regards to the relationship between powder feed rate and aerosol concentration was demonstrated.

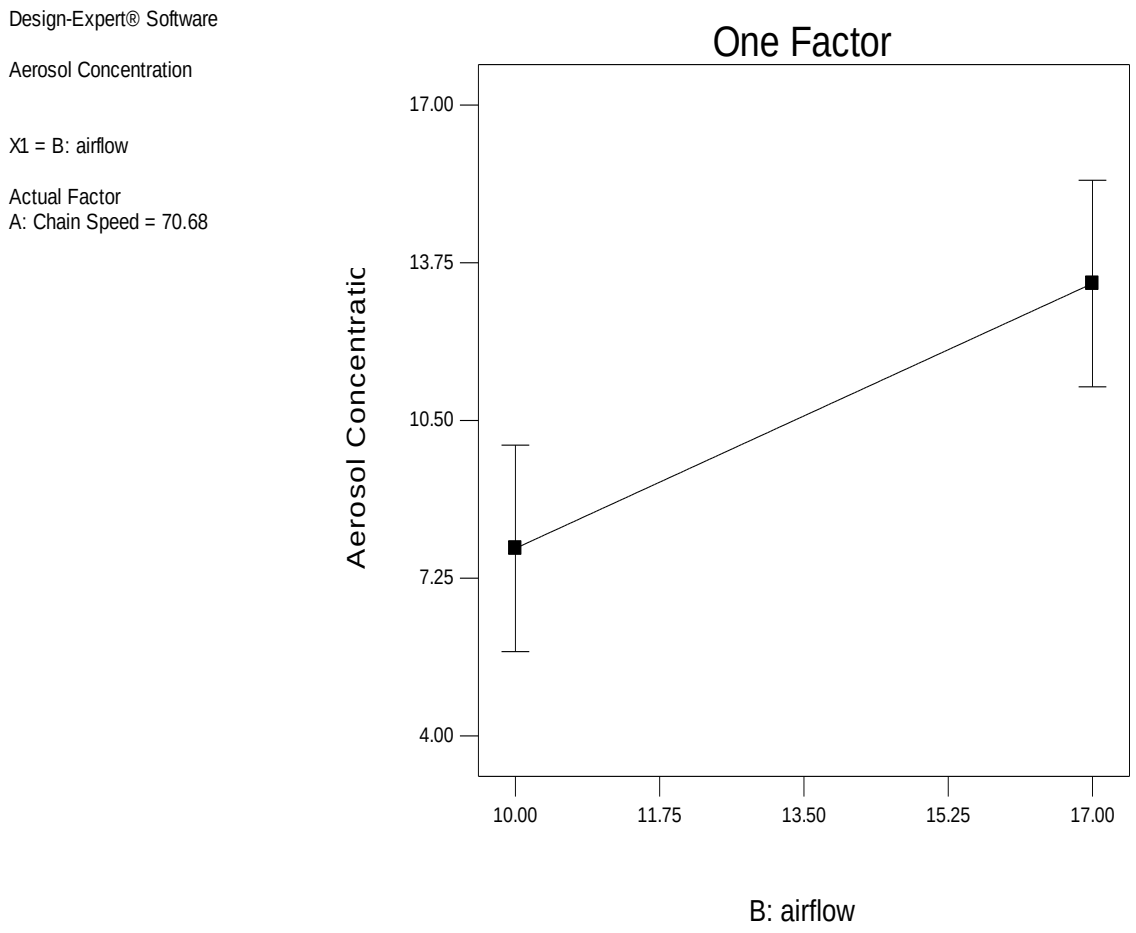

Figure 12: Statistical plot showing the effect of airflow into the fluidised bed on aerosol concentration produced.

1.3.3 Mass Median Aerodynamic Diameter (µM)

A statistically significant model accounting for 84.16% of the variance was fitted to the data describing the relationship between operation parameters and aerosol concentration ($p < 0.05$). The model identified airflow ($p = 0.003$) and powder feed rate ($p = 0.02$) as significant factors affecting particle size generation in the exposure chamber (see 1.3.2, D-Appendix for summary of statistical analysis).

Figure 13 shows the variation in MMAD as a function of powder feed rate and airflow into the fluidised bed. Increasing powder feed rate from 30.0 to 100% of maximum chain speed resulted in a corresponding increase in the size of aerosol particles generated. In addition, particle size decreased as a function of increasing airflow into the fluidisation chamber.

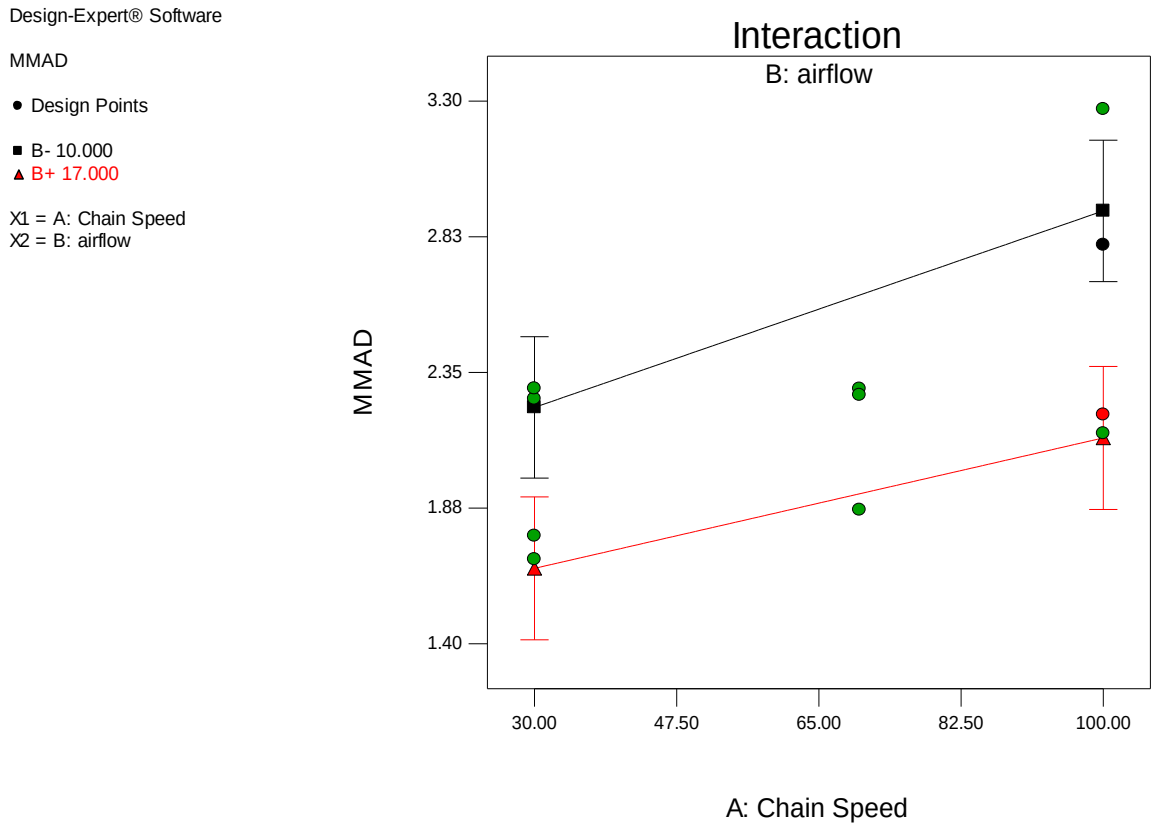

Figure 13: Statistical plot showing the effect of chain speed at two airflow settings on aerosol concentration produced. The red lines indicate airflow at 17.0 L/min, black lines indicate airflow at 10.0 L/min. Green dots indicate actual experimental values for MMAD for the different experimental conditions.

This trend would be scientifically expected, as increasing the airflow into the fluidised bed results in more particle deagglormation and, therefore, a greater number of smaller particles is detected in the aerosol chamber. This data indicated that the highest aerosol concentration was produced by operating the FBAG at high airflow. Conversely, increasing the airflow resulted in a reduction in aerosol size. Therefore, a balance between the desired aerosol size and aerosol concentration generated must be reached when selecting the generator operating conditions.

The results generated from this screening study were broadly in agreement with the published study by (Marple et al, 1978) assessing the performance of this generator. In that study, conducted on a range of materials such as coal, silica, rock and road dust, the authors concluded that the mass concentration is primarily controlled by the speed of the conveyor chain, i.e. powder feed rate. However, it was noted that output mass concentration is nearly the same for 9 and 25 L/min of flow in the fluidised bed, indicating that the same amount of particles were aerosolised in both cases. This is not in agreement with the findings from this study (see Figure 12), which showed a positive effect of varying the flow rate from 5 to 15 L/min on the mass concentration of aerosol generated.

However, it must be noted that the materials tested in the study by Marple *et al.* can be classified according to Geldart's classification of particles as belonging to group B (Geldart, 1973). Geldart divided particles into four groups according to their fluidisation characteristics. Type A particles are typically 50-100 µm in size, and are easily fluidised. Type B particles are sand-like, with most particles being 40 µm ≤ diameter< 500 µm, but are still fluidised relatively well. Type C particles are typically smaller than 10µm and are considered cohesive and extremely hard to fluidise. Type D particles are coarse, typically larger than 1 mm in diameter and tend to produce jets through the powder rather than being fluidised (Lind et al, 2010).

Therefore, the inherent characteristic of the test material used in the Marple study may explain the observed difference between the two studies with respect to the effect of airflow on aerosol concentration. In the Marple study, the solids tested tend to fluidise easily, hence the conclusion of the authors that the dust particles were found to be thoroughly deagglomerated and that particle size distribution of the generated aerosol is constant with respect to airflow.

In contrast, the fluorescent microspheres-lactose blend material used in the present investigation can be classified as belonging to Geldart group C, namely cohesive or very fine powders. Thus, normal fluidisation of particles is very difficult for these solids because inter-particle forces are greater than those resulting from the action of the fluidising gas. Consequently, the higher the airflow, the more deagglomeration of particles will result. Plus, the higher the aerosol concentration in the exposure chamber, the lower the resultant particle size.

1.4 Delivery method evaluation

The aerosol produced by the FBAG was studied as the function of the operating method: chain-fed versus batch-fed method. This was to ascertain how these operating modes affected the mass, aerosol concentration and aerosol size produced (see 1.2.2, C – Experimental Setup).

In the chain-fed mode, the powder feed rate was set at 70% of the maximum speed, as measured using the variable speed controller. This value was selected as the screening study (see Figure 13) showed the aerosol particle size generated began to reach a constant level once 50% of the maximum speed was exceeded. In the batch-fed method, the FMS-Lactose blend was thoroughly mixed with bronze beads and introduced into the fluidised bed chamber. Furthermore, the ratio of FMS blend to bed material required to produce the stable aerosol concentration was evaluated. Further details relating to the operating conditions for this experiment are detailed in Table 6.

Table 6: Experimental details for investigation to assess delivery method for FBAG

Conditions	**Levels**
Air flow into fluidised bed (L/min)	10 L/min
Operation modes	Batch-fed: Test material mixed with bronze beads in varying levels; 2.5 to 10% w/w prior to aerosolisation. Continuous-fed: 70% of the maximum speed using the variable speed controller.
Test material	Blend of Fluorescent Microspheres (2 and 4 µm sized) mixed with lactose (0.8% w/w)
Dosing duration (min)	45 minutes for Batch-fed 90 minutes for continues-fed
Filter type	Respigard 303A filter; Vital Signs, Ohio, USA
Air flow in to APS 3321/dilutor	5 L/min
Performances	**Comments**
Mass concentration of generator (mg/m^3)	Determined gravimetrically, using APS and chemical assay of filters.
MMAD (µm)	Determined using APS
S. Deviation of MMAD (σg)	Determined using APS

Figure 14 shows the aerosol concentration in the exposure chamber operating in the chain-fed mode. For experimental runs (two replicates per condition) employing clean bronze beads, the mass concentration was measured to be 8.89 ± 3.41 mg/m^3. However, the time taken for the aerosol concentration to stabilise was approximately 60 minutes.

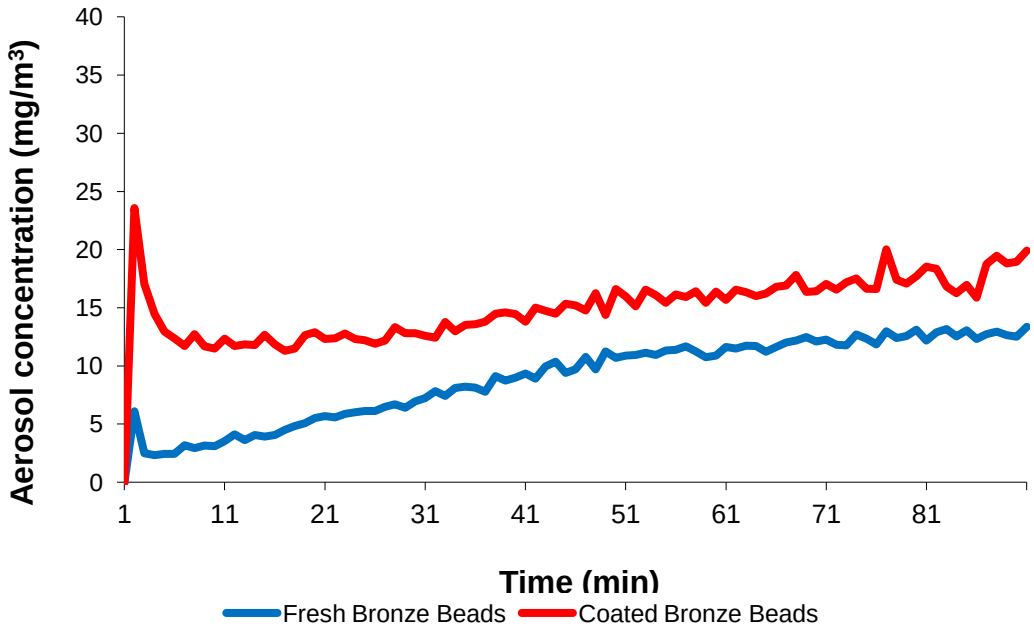

Figure 14: Aerosol concentration profiles versus time for 2 µm containing FMS-Lactose blends.

Thereafter, the two experimental runs were conducted using the same operating conditions as employed in the initial experiment, with the exception of the re-use of the same bronze beads as previously used in this investigation. The data showed that, in general, the aerosol concentration required much less time to reach stable concentration levels, being approximately 10 minutes. In addition, the average aerosol concentration was much higher than using clean beads at around 15.08 ± 2.44 mg/m^3.

For the coated bronze beads blends of FMS, the aerosol concentration (N/cm^3) as function of time was monitored for a representative two micron containing FMS-Lactose blend (see Figure 15). After an initial rise, the chamber aerosol concentration approached and maintained a stable equilibrium as the extraction and generation air flow rates were constant. On the termination of the airflow, the concentration shows a steep decline within a very short time period (< 1 minute).

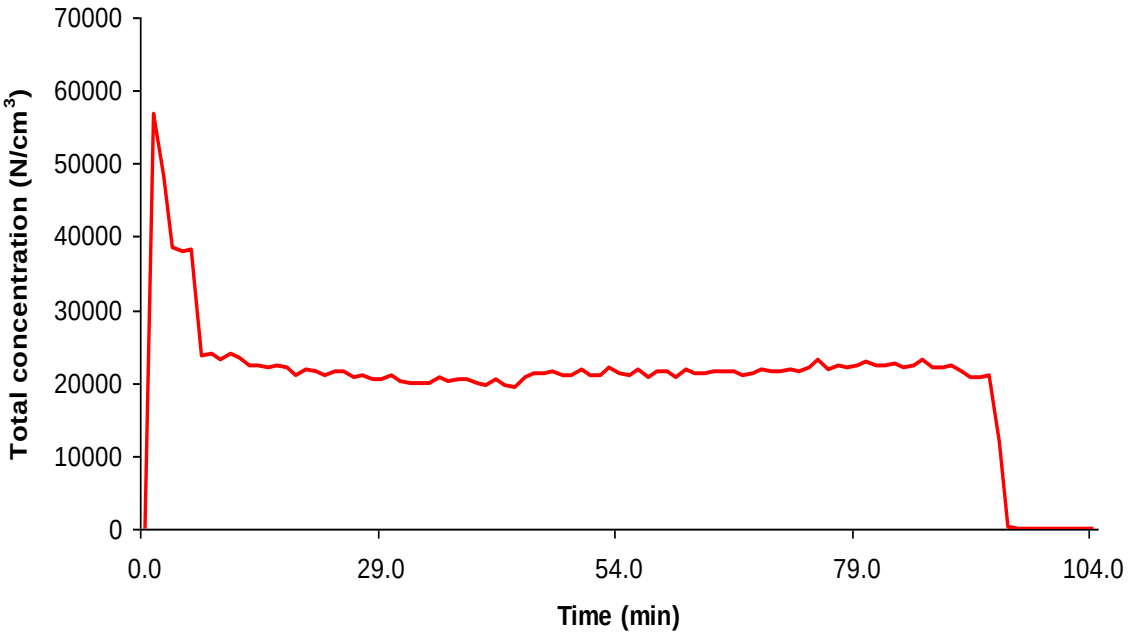

Figure 15: Real-time aerosol exposure monitoring during the entire exposure period using the APS monitoring system.

Therefore, this investigation showed that the aerosol concentration produced was dependent upon the previous history of the bed material. The aerosol concentration produced using fresh and previously unused bronze beads was much lower than using previously used bronze beads. Other researchers in this field have noted a similar trend using used bed material (Carpenter et al, 1980;Marple et al, 1978;O'Shaughnessy et al, 2003).

This behaviour may be attributed to the adhesion of fine particles to the larger fluidising beads used as bed particles, where the adhesion of fine particles on the surface of the fluidising beads frees the larger-sized aerosol particles to be generated into the exposure chamber (Carpenter et al, 1980). Thus, it can be concluded that a dynamic airflow system was attained using this exposure setup. Homogenous mixing of all airflows took place with the exposure chamber and the test atmosphere was continuously delivered to and exhausted from the exposure chamber.

For the batch-fed mode of delivery, different amounts of the FMS powder blends were mixed with a fixed mass of fresh bronze beads. The two powders were mixed thoroughly using a Turbula mixer and allowed to rest for a minimum of 24 hours in order to allow any electrostatic charges built up during the blending process to dissipate. Thereafter, the resultant powder mix was introduced into the fluid powder chamber.

Operating the FBAG in the batch-fed mode was used in a number of studies in the literature (Carpenter et al, 1980;Lind et al, 2010). This was to reduce the time taken to achieve a stable aerosol concentration, in comparison with the continuously-fed fluid bed aerosol generators. Figure 16 shows the observed relationship between the aerosol concentration and bed loading concentration over an exposure period of 45 minutes. The data shows a significant and sustained increase in aerosol concentration for the 5.0% w/w bed loading runs in comparison with the 2.5% w/w bed loading runs over the entire exposure period.

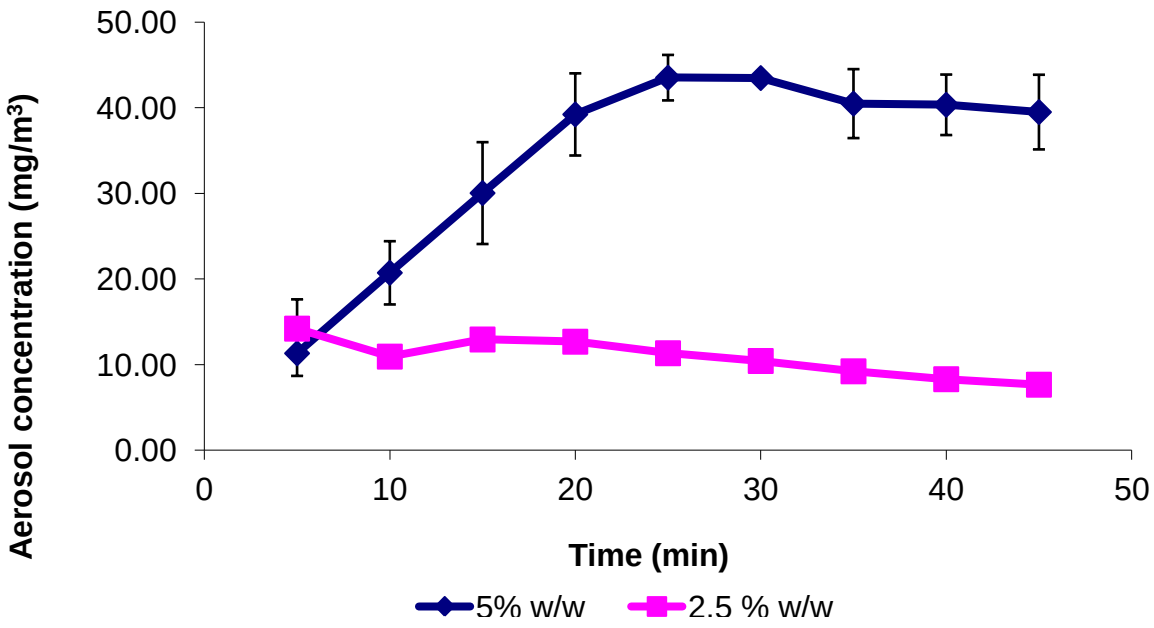

Figure 16: Aerosol concentrations profiles versus time for 2 µm containing FMS-Lactose blends directly mixed with bronze beads prior to aerosolisation. The number of replicates is two and three for the 2.5 and 5.0% bed loading runs respectively. Error bars are Mean ± SD from independent experiments.

However, whilst it is important to produce a high aerosol concentration in the exposure chamber, care must be taken to ensure that no excessive agglomeration of the test material arises. Therefore, the stability of aerosol generated in terms of particle size distribution was examined for the various bed loading levels and fresh and coated bronze bead material. This parameter was evaluated using the APS particle sizer to monitor the generated aerosol. In Figure 17, the size distributions for both delivery methods are shown.

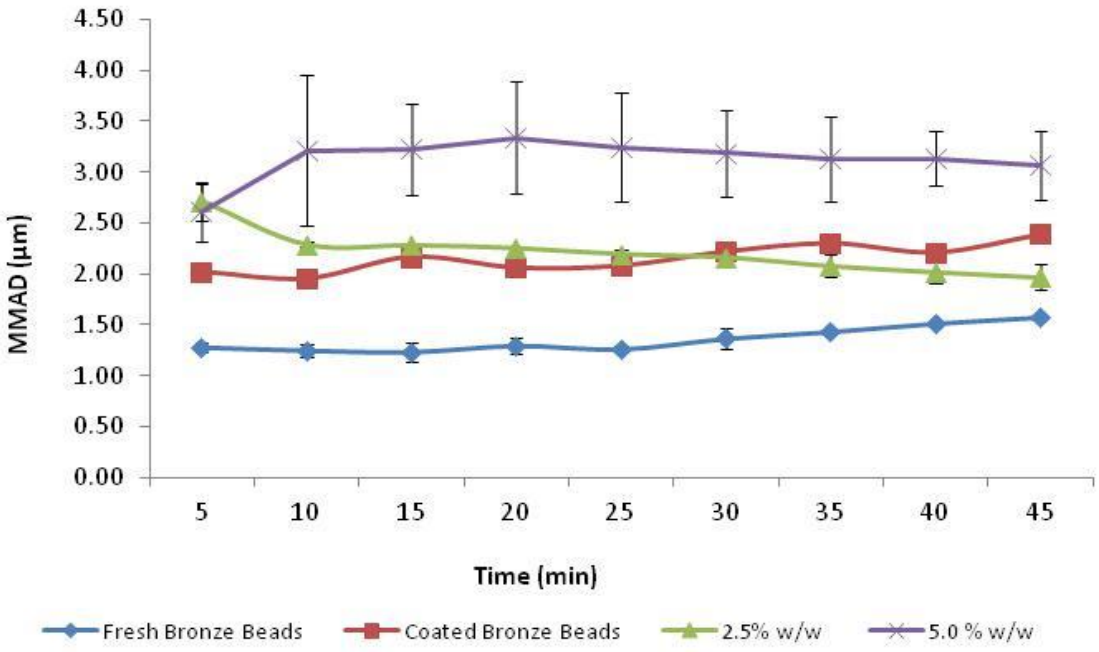

Figure 17: Aerosol mass median aerodynamic diameter vs. time for 2 µm containing FMS-Lactose blends delivered prepared using different methods: batch and continuous-fed methods. Error bars are Mean ± SD. The numbers of replicates were two for the fresh bronze beads, three for 2.5% bed loading and two for the 5.0% bed loading.

The data shows that the highest aerosol particle size of nominal 2 µm was recorded for the 5.0% w/w bed loading mix, followed by the chain-fed method in which coated bronze beads were used, followed by the 2.5% w/w bed loading mix. In addition, the lowest particle size was noted for the run in which the continuous chain feed system was operated using fresh bronze beads. However, the particle size produced using the 5.0% bed loading was around 3 µm, indicating agglomeration of particles was produced.

1.4.1 Experiment using 4 micron containing FMS blends

An important feature of any aerosol generator should be the ability to generate aerosol particles of different sizes, as the effect of this parameter on regional deposition in the IVR model will be investigated. For this reason, a number of experiments using 4 µm containing FMS blend were conducted.

Initial investigations evaluated the impact of increasing bed loading on aerosol concentration in the exposure chamber. The results of this experiment showed increasing the bed loading from 2.5 to 10% w/w resulted in a comparative increase in aerosol concentration in the exposure chamber.

As demonstrated with the 2 µm containing blend, operating the FBAG using the chain-fed mode showed essentially two types of curves (see Figure 18). One curve represents a start-up case, where the fluidised bed initially contains only clean brass beads. For this case, it takes on the order of two hours for the fluidised bed to reach stable operation. In the other case, the same coated brass beads were used and this time the time taken to reach stable aerosol concentration was about one hour.

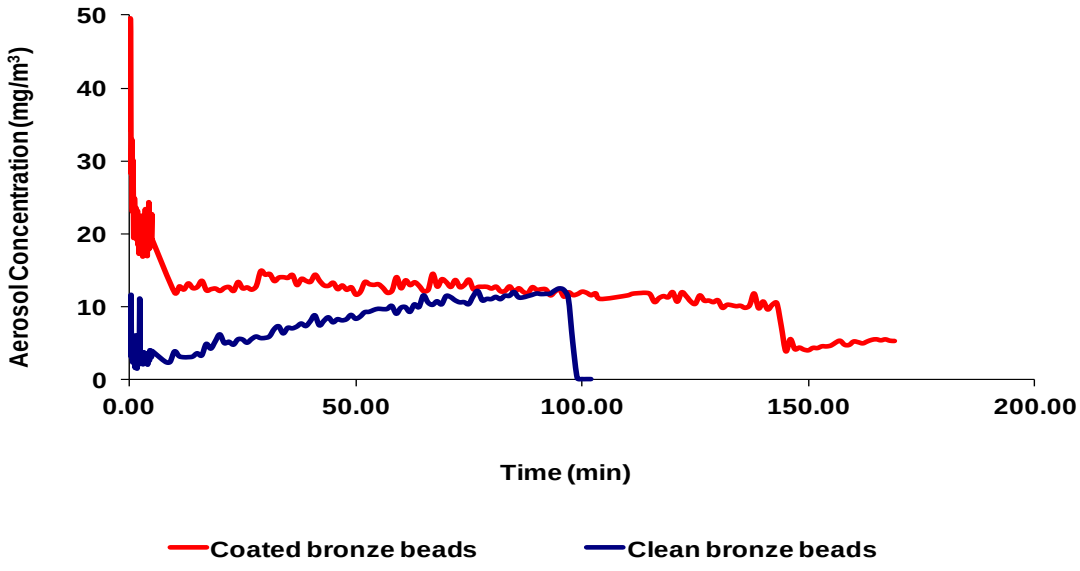

Figure 18: Aerosol concentration profiles versus time for 4.0 µm containing FMS-Lactose blends directly mixed with bronze beads prior to aerosolisation. The number of replicates per blends is two.

In Figure 19, the size distribution of the 4 µm containing FMS blend is shown for different levels of bed loading. The results shows that increasing the percentage bed loading levels resulted in increased particle size, which may be due to the agglomeration of particles which could not be deagglomerated by the aerosol generator.

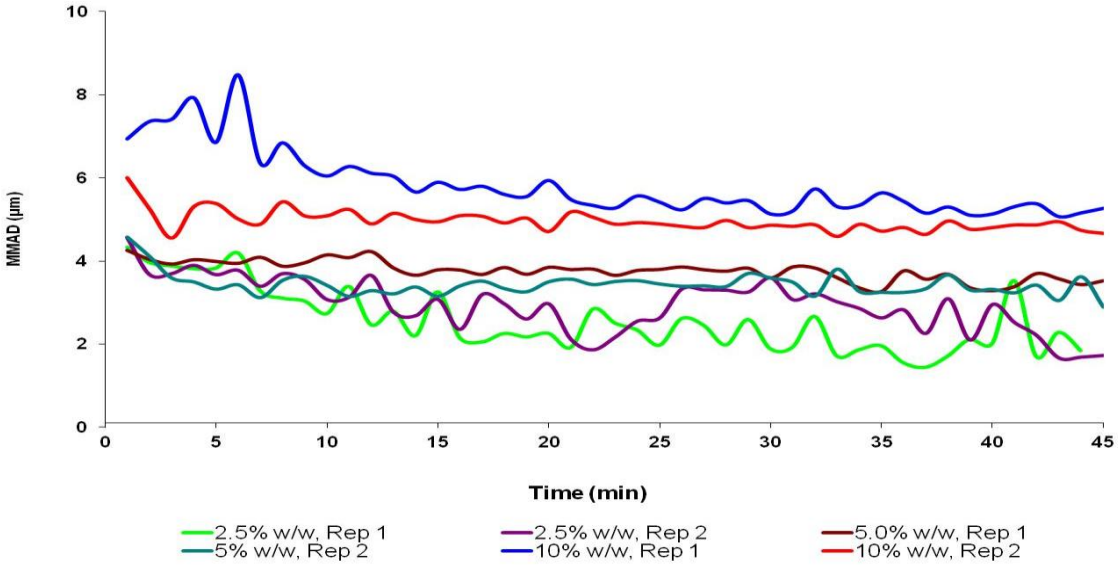

Figure 19: Aerosol mass median aerodynamic diameter (MMAD) as a function of bed loading for 4um containing FMS-Lactose blend. The number of replicates per blends is two, as indicated by Rep 1 and 2 for different bed loading levels.

Overall, the results of this study demonstrated the FBAG can be operated satisfactorily using both delivery methods. Similar aerosol concentrations and particle size were produced for the chain-fed delivery method using the coated bronze beads in comparison with the batch-fed method to fluidising material. However, the time taken to reach a steady aerosol concentration was much reduced using the continuous-fed method; more than 60 minutes on average was required to achieve a stable concentration. This compares with the almost immediate stabilisation of the aerosol concentration using batch-fed method.

Furthermore, the particle size data for both 2 and 4 µm containing blends demonstrate that, whilst using the FBAG in the batch-fed mode may offer an advantage in terms of reduced time to achieve steady aerosol concentration and produce particle of a small enough size (< 3.0 µm) to be inhaled into the rodent respiratory system, care must be taken to ensure that the bed loading level selected does not result in agglomerated particles. Whilst given adequate aerosol concentration, this method may produce particles that are too large to be inhaled in the rodent respiratory system (> 3.0 µm).

1.5 Validation of the use of the APS 3321 for use in rodent inhalation studies

Determination of the total aerosol concentrations in inhalation exposure studies that expose laboratory animals to dusts and particles is most often done by taking time-integrated filter samples (Wong, 2007). The aerosol concentration can then be calculated from the knowledge of the mass collected on the filter and sampling time, referred to as Total Particulate Matter (TPM) concentration. In addition, chemical analysis may also be used to determine the aerosol concentration for the active compound. However, one major drawback of the filter sample analysis is the time taken to collect enough material on the filter to accurately weigh. Furthermore, the data generated using this technique is time-delayed and reflective of past aerosol concentration history during the exposure period.

Thus, it is beneficial to use a real-time aerosol mass monitor in addition to filters for determining aerosol concentration throughout the exposure period. The use of a real-time monitor should enable the operator to monitor the stability of aerosol concentration and detect problems related to aerosol generation and delivery as they occur. In addition, the unit should be capable of characterising the size distribution of the aerosol produced. Commonly, this is described by two parameters: mass median aerodynamic diameter (MMAD), which is a measure of the particle diameter, and the spread of the distribution as described by the geometric standard deviation (GSD).

In addition, the validity of the APS to accurately measure a given dose of an active ingredient (FMS) was investigated. In this investigation, a number of timed samples over a set exposure period were collected by drawing air through filters (Respigard II) using a pump at 2L/min. The amounts of FMS trapped in the filters were determined by removing the filter material and washing with a dissolving solvent.

Furthermore, the utility of the APS to measure the particle size distribution of a given aerosol was evaluated. For this work, investigations involved comparing the results generated for MMAD and GSD versus a Marple Cascade Impactor sampling concurrently the same atmosphere and evaluating reproducibility of the APS response and changes in particle size distribution over the exposure period. The methodology used for conducting this work is described fully in the Experimental Setup section (see 1.2.3, C– Experimental Setup).

1.5.1 APS versus Gravimetric correlation

The aerosol concentration in the exposure chamber for lactose test material was measured using the APS and compared with time-integrated filter samples to determine the TPM. The APS was set up with a dilutor (model 3320A, St Paul, USA) at different ratios of 20:1 and 100:1, as well as the standard 1:1 ratio operated without the use of dilutor. This diluter is an accessory of the APS and is designed to reduce the concentration of high-concentration aerosol. Details of the method are described in the Experimental Setup section (see 1.2.3 , C–Experimental Setup)

Results showed the APS to significantly under-predict the aerosol concentration of lactose when compared to the measurement provided by the gravimetric filter sampling method. Almost two orders of magnitudes difference were recorded for the aerosol concentration recorded using both methods (see Figure 20).

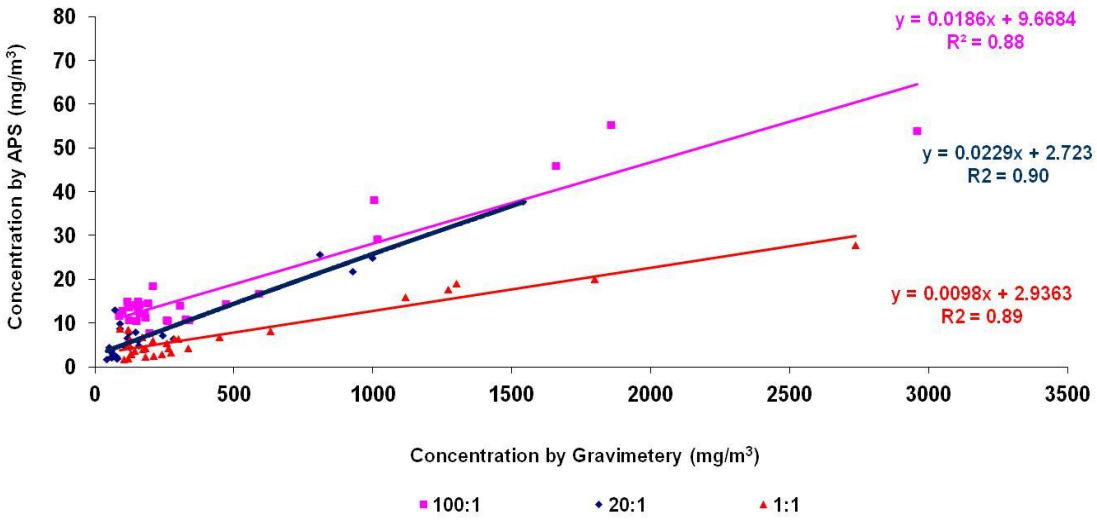

Figure 20: Correlation between APS reading and mass concentration reading by filter samples for lactose test material. Total airflow 20L/min split 15L/min to filter sample and 5L/min to APS.

This underestimation of aerosol concentration by the APS is assumed to be caused by a combination of impaction losses in the inner acceleration nozzle of the APS and transport lines for larger particles (> 5µm) prior to entry into the measurement zone of the instrument (Pagels et al, 2005). Whilst the expected larger aerosol particles may not have been a considerable fraction of the aerosol number, they clearly made up the bulk of the mass collected on the filter and, therefore, may have accounted for the difference in measured concentration recorded by these two methods.

Furthermore, the APS was calibrated to size particles in the range of 0.5-20 µm only, whereas the lactose material under investigation had MPPS of 60-80 µm, and fine content (< 8 µm) of 6 to 8%. Therefore, only the finest portion of the lactose would reasonably be expected to be collected and measured for mass by the APS instrument, which may explain to a large extent the difference observed between the two methods.

Other investigators have noted similar issues with under-measurement of aerosol concentration by the APS instrument in comparison with other instruments (Peters and Leith, 2003). This has been attributed to a number of reasons, including a lack of knowledge of particle characteristics of the material to be sampled. This factor is important, as the APS-estimated mass is strongly affected by shape factor (to the power 3/2) and particle density (to the power of ½) (Peters, 2006). However, in this case the particle density and shape factor (ρ = 1.5 g/cm-3, χ = 1) were known and input into the instrument set-up prior to start of the measurement.

Furthermore, work undertaken by Pagels *et al.* demonstrated that this instrument consistently underestimated the aerosol concentration of test particles greater than 5 µm. However, the authors noted that this instrument can, under many circumstances, give accurate time-resolved mass size distributions for particles less than 5 µm (Pagels et al, 2005). Nonetheless, the APS unit was shown to be capable of tracking changes in aerosol concentration, as evidenced by the reasonably good correlation coefficients (R^2 of 0.88 to 0.90) for comparison with the mass weighed sampling method.

In addition, the data showed the use of a dilutor in line with the APS instrument to improve the estimation of aerosol concentration. The agreement between both methods increases significantly from around 100 times underestimation of aerosol concentration when no dilutor is used (1:1), to 50 times underestimation when dilution of 20:1 and 1:100 are used in line with APS.

Figure 21 shows a percentage classification of events data as function of dilution ratios. Each detected particle was classified into one of four events depending on the structure of the continuous intensity signal recorded by the photo-detector. Event 1 consisted of either particle with time-of-flight shorter than for the lowest size channel (0.523 µm). Event 2 particles were correctly classified particles with two peaks above the detection threshold. Event 3 particles had three particles above the detection threshold. Events of this type were logged but not processed for concentration and particle size determination. Particles falling in this category were classified as coincidence particles. Event 4 particles resulted when signal was above the detection threshold and was recorded for particles above 20 µm.

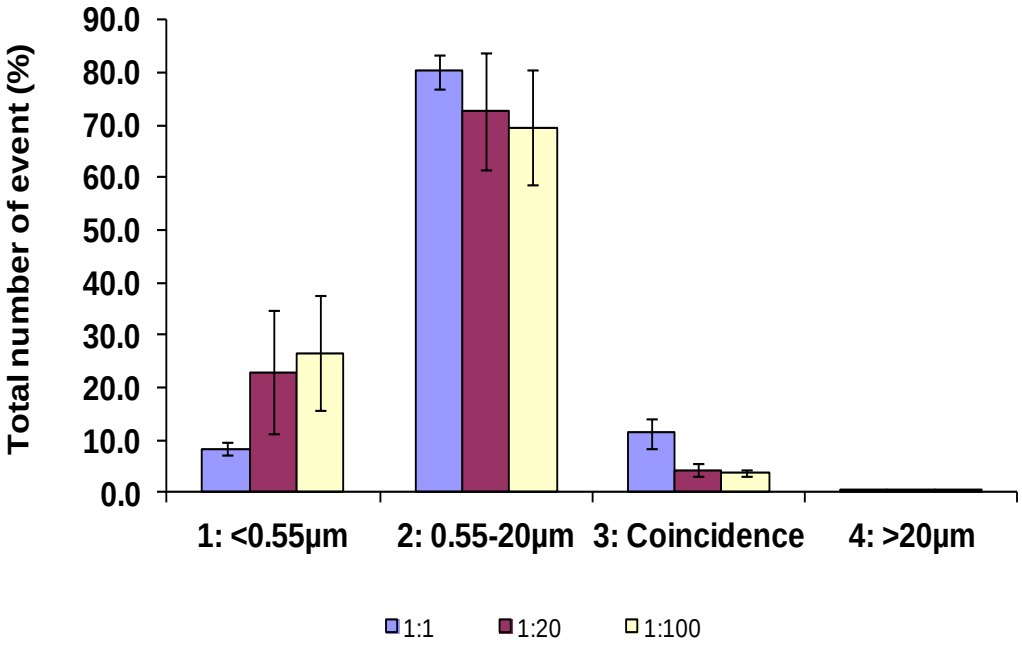

Figure 21: Event data as a function of dilution ratio used to dilute the aerosol prior to analysis by the APS particle-sizer. Error bars are Mean ± SD from five independent experiments.

The results clearly show a reduction in the detection of coincidence particles (event 3) with increased dilution ratios. In addition, operating at this dilution ratio resulted in an increased detection of particles of less than 0.523 µm and, as a consequence, resulted in improved correlation between APS and gravimetric determination of aerosol concentrations, as shown in Figure 20.

1.5.2 APS versus HPLC correlation

Having established that a reasonable correlation existed between gravimetric sampling and APS aerosol concentration measurements, the next stage of the work was to investigate whether the APS was capable of accurately measuring the same aerosol concentrations as collected on the filters for the active component of the aerosol exposure atmosphere.

For this comparison, data from a number of experiments, in which APS and filter samples for active determination using HPLC were taken concurrently, was compared. For these experiments, a blend of monosised fluorescent microspheres (2 µm sized) mixed with inhalation grade lactose was used. Details of the chromatography method used to assay for FMS content are listed in the Experimental Setup section (see 1.1.3, C – Experimental Setup).

Comparison of the aerosol concentration obtained by APS with those based on chromatographically determined airborne FMS concentration is shown in Figure 22. A measure of the accuracy of this relationship is shown by a linear regression analysis, and the trend line and associated equation is given.

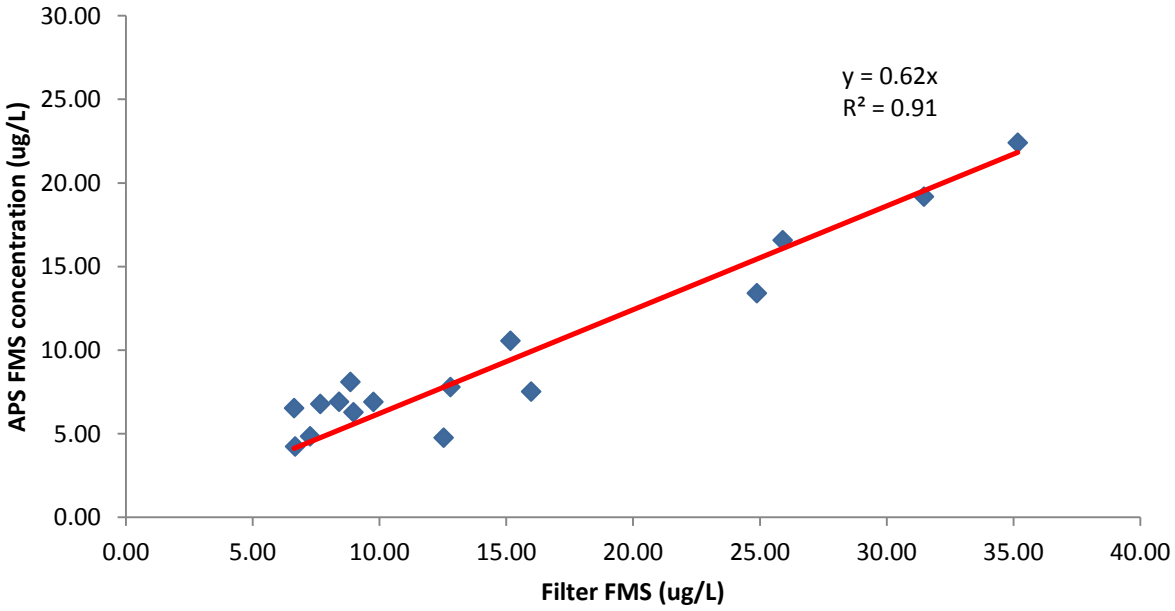

Figure 22: Comparison of drug concentrations collected in filters to those determined by the APS. Linear regression lines and their equations and R^2 values are shown.

Interestingly, the agreement between the APS and chromatographically determined aerosol concentrations is reasonably close, as indicated by gradient of the line of 0.62 (see Figure 22). This compares with the two orders of magnitude difference recorded for APS versus gravimetric aerosol concentration comparison. This may indicate the APS is much more capable of capturing the aerosol concentration for the primary active particles (< 2 µm) rather than TPM aerosol concentration.

Moreover, the results of regression analysis revealed good agreement between the two methods, with an R^2 of 0.92 for correlation coefficient between the two methods. This would indicate that APS may be used to track changes in the respirable mass of drug substances aerosolised in the exposure chamber during experimental runs.

1.5.3 APS versus Marple Cascade Impactor correlation

An important characteristic of the aerosol atmosphere generated for animal exposure studies, and which must be measured, is the particle size distribution of the test article. Traditionally, inertial cascade impactor instruments, such as the Marple Cascade Impactor (MCI), have been employed for this purpose.

However, the major drawbacks of this method are its complexity and time consumption. As a result, the data generated using this method is always post exposure period and does not offer the operator any information on the particle size distribution throughout the exposure period, or enable the operator to detect problems related to the aerosol generation and delivery as they occur. Alternative methods of testing aerosol particle size distribution, which are gaining increased usage, include techniques based on laser diffraction time of flight (TOF) methodology, such as the APS. The main benefits of this technique are ease of use and the ability to offer real-time information relating to the aerosol exposure concentration and size distribution throughout the exposure period.

For the assessment of the particle size distribution using the MCI, five replicate blends of fluorescent microspheres (FMS) mixed with lactose in proportions of 0.8% w/w were used as the test material. The mass fractional distribution was unimodal and hetrodisperse (see Figure 23). The particle size distribution was determined to have an MMAD of 2.64 µm and GSD of 2.19.

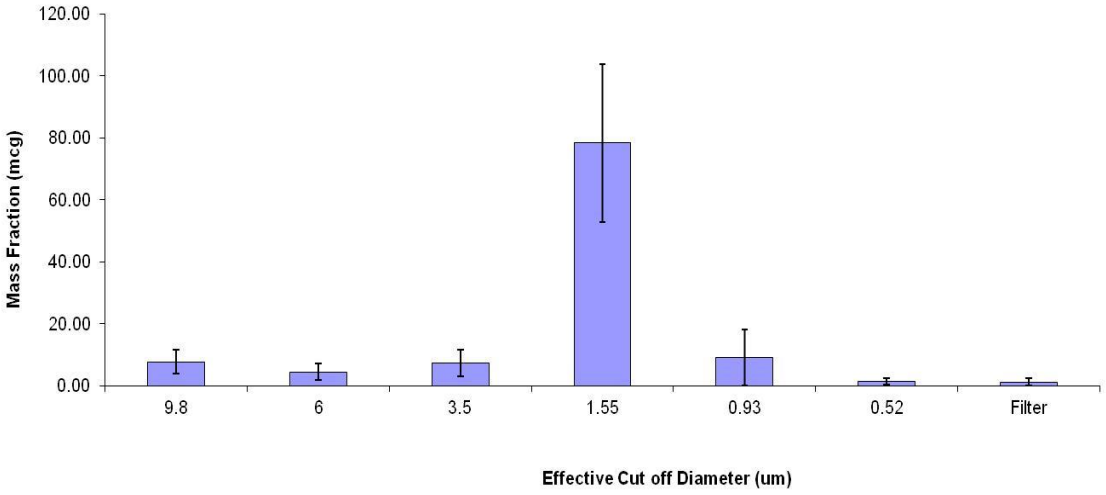

Figure 23: Particle size distribution for five replicate blends of 0.8% w/w FMS-Lactose inhalation blends. Data is presented as the mass of powder (in mcg) collected in each collection stage of the MCI, versus the median diameter (in µm) of particle sizes, which impacted on each stage of the cascade impactor, described as the Effective Cut-off Diameter (OECD, 2004).

In terms of comparison with the APS, content uniformity analysis of this blend material showed it to be homogenous; thus, the size distribution attributable to the FMS components will be the same as that attributable to the complete particles mix (Stein et al, 2003). Therefore, despite the fact that the APS measures the whole size distribution of the powder mix, including the lactose and FMS particles, the comparison with the MCI data, which will be FMS-specific, will still be valid.

Compared to the MCI, analysis of the particle size demonstrated a profile that was broadly similar, particularly at the larger end of the distribution > 5.0 µm. For the central and lower end of the size spectrum, the APS consistently produced smaller size measurements in comparison with the MCI method, with the average MMAD of 2.20 µm and GSD (2.00) for the APS method compared with an average MMAD of 2.64 µm and GSD (2.19) for the MCI method. Therefore, this data indicates that, for FMS containing blends, the APS is in broad agreement with the MCI method and shows it may be used for MMAD and GSD characterisation during aerosol exposure experiments (see Figure 24).

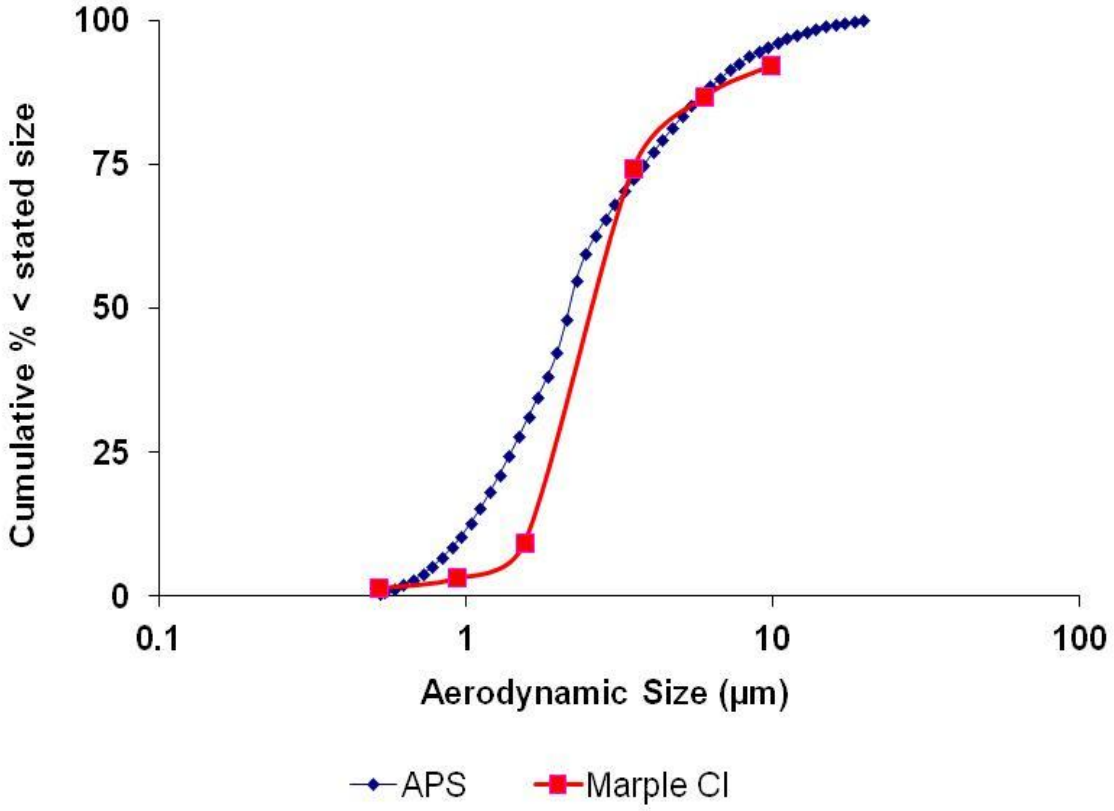

Figure 24: Particle size distributions of FMS inhalation blend (0.8% w/w) determined with MCI and APS. Each data point represents the average value of five determinations.

1.6 Conclusion

The present research evaluated the ability of the FBAG to produce an acceptable aerosol powder for use during an IVR model and rodent *in vivo* inhalation exposure studies. The results showed that the FBAG could efficiently produce an aerosol containing well-dispersed particles of test material.

The highest aerosol concentration was generated by operating the FBAG at high bed loadings, high airflow and high powder feed rate. These findings are in agreement with findings by Carpenter *et al.* (Carpenter et al, 1980), who showed similar trends with respect to the relationship between total aerosol concentration and variation of these operating parameters.

The total aerosol concentration output and particle size distribution was evaluated for two modes of operation, namely batch-fed and continuous-fed operated via a chain conveyor system, and was found to remain constant for the duration of the operation. However, the time taken to achieve a steady state concentration was considerably reduced when operating in the batch-fed mode, with only ten minutes required to attain a steady concentration level, as opposed to approximately one hour when operated in the continuous-fed mode.

Furthermore, much higher concentration levels were recorded when the FBAG was operated in the batch-fed mode. Thus, the batch-feed method presented in this study was a convenient technique for obtaining a constant and high aerosol concentration and particle size, without the need for a complicated feed device to deliver the test material to the fluidisation chamber. Therefore, the powder delivery method described here was an improvement over previous aerosol generation methods for dry aerosol generation.

The on-line particle spectrometer provided useful information for maintaining constant aerosol concentration. A reasonably good correlation, with mass concentration recorded for the active compound using the integrated filter method, was established as evidenced by R^2 of 0.91. The agreement with filter samples for determination of TPM was less good, showing the APS to underestimate the aerosol concentration by a factor of two orders of magnitude as compared to Gravimetric sampling. Thus, a sample specific calibration was needed to reconcile on-line light scattering instrument data with actual mass concentration.

In addition, the use of the APS to assess the particle size distribution was compared versus MCI. The data generated using the APS was found to be in broad agreement with that generated using the MCI method, therefore indicating it may be used for MMAD and GSD characterisation during aerosol exposure experiments.

2 Validation of Nose-only Exposure System for Rodents

One important feature of any exposure chamber should be the ability to achieve uniform distribution of the exposure test material aerosol. Variability in the resulting lung burden would then be solely as a result of biological factors and not the location within the chamber (Griffis et al, 1981). In addition, day-to-day experiments should produce similar exposures and, thus, all test animals would be exposed to approximately the same concentration of test aerosol.

However, this requirement does not often prevail. Therefore, it is important to characterise the distribution of test material within the exposure chamber to determine the impact of the non-uniformity of exposure, if any, on animal responses to the test material. Most importantly, knowledge of the chamber distribution characteristics is necessary in order to evaluate how representative selected sampling points are for routine measurements of the entire exposure chamber.

In this study, a directed-flow, nose-only exposure chamber was used. This system was a custom-made unit, consisting of a number of components. Principally, the exposure chamber was capable of exposing test subjects (maximum of 12 rodents) to the test material aerosol whilst minimising the amount of compound used. In addition, the system contained a fluidised bed aerosol generator (FBAG) to generate the aerosol powder and an on-line particle sizing instrument (APS) to monitor the exposure atmosphere. This inhalation chamber may be employed for acute inhalation studies with aerosols, dusts and vapours involving mice, rats or guinea pigs (see Figure 25).

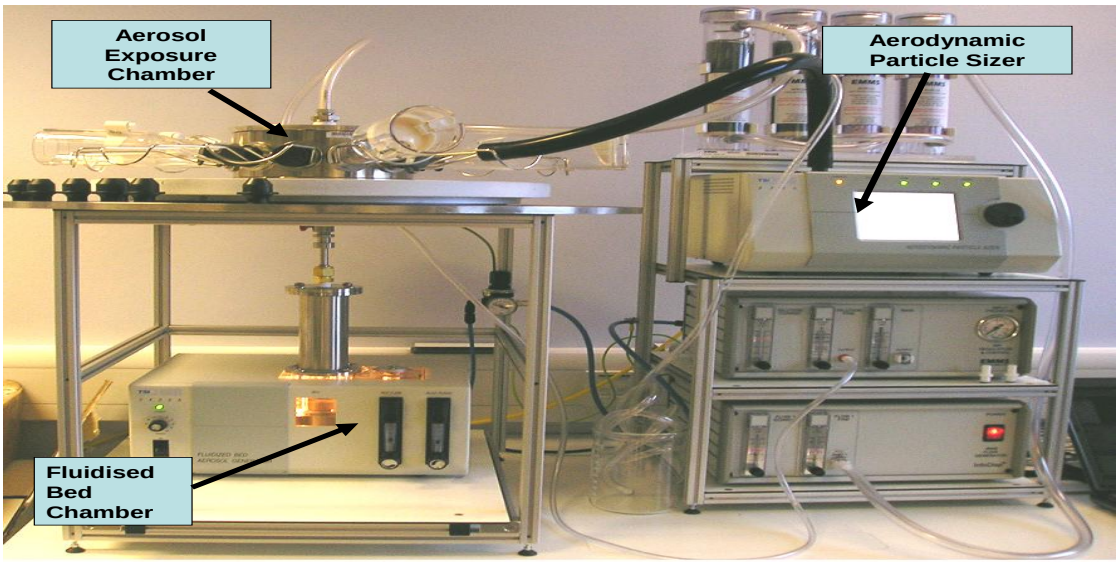

Figure 25: Photograph of the exposure system during operation

The purpose of this study was to evaluate performance of the exposure system prior to its use to assess the *in vitro* rat model (IVR). The performance in terms of uniform distribution of test material, fluorescent microspheres (FMS) throughout the exposure chamber, stability of concentration and size distribution of the aerosol generated was assessed.

2.1 Method used for characterisation of chamber atmosphere and its particle size distribution

The temporal variability, spatial distribution and particle size distribution of the aerosol generated within the exposure chamber were evaluated. Several instruments and/or methods were used for this purpose (see 2.2.1, C - Experimental Setup).

The sampling port manifold consisted of a spacer chamber (white colour) to which the tubes from the inhalation ports were attached. Airflow in the region of 10 L/min was pulled from an auxiliary pump attached at the exit of this attachment. This equated to airflow of ca. 1.0 L/min per sampling port and thus ensured equal division of airflow from each of the sampling port locations (see Figure 26).

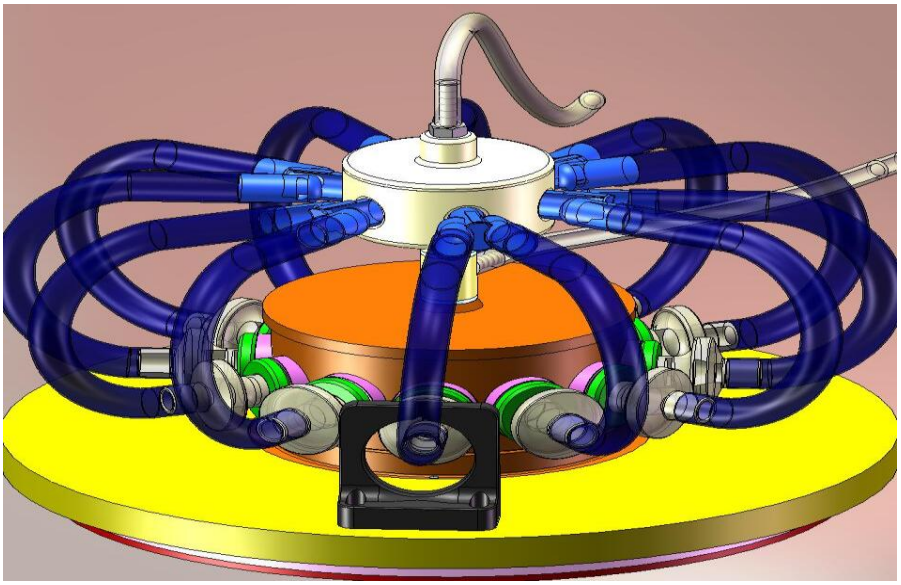

Figure 26: Exposure chamber and sampling port manifold. Reproduced with permission Aztec Precision Engineering, Letchworth, UK

Figure 27 depicts a schematic presentation of the experimental procedures undertaken as part of this study. Firstly, the study evaluated the homogeneity of exposure concentration at different chamber locations by determining the aerosol concentrations at different port locations. It used a variety of methods, such as a gravimetry, HPLC and real-time aerosol monitoring using the aerodynamic particle spectrometer (APS).

Secondly, the concentration-time relationship was evaluated in order to define the optimum exposure period for dosing animals. This was to be achieved by taking time-dependent samples at 5, 15, 30 and 45 minutes post exposure and determining the quantity of FMS collected on each filter, using the same techniques used to assess the homogeneity in the exposure

chamber. In addition, particle size distribution during the exposure period was investigated. Further technical details relating to the methodology used in this investigation have been described elsewhere (see 2.2.2, C - Experimental Setup).

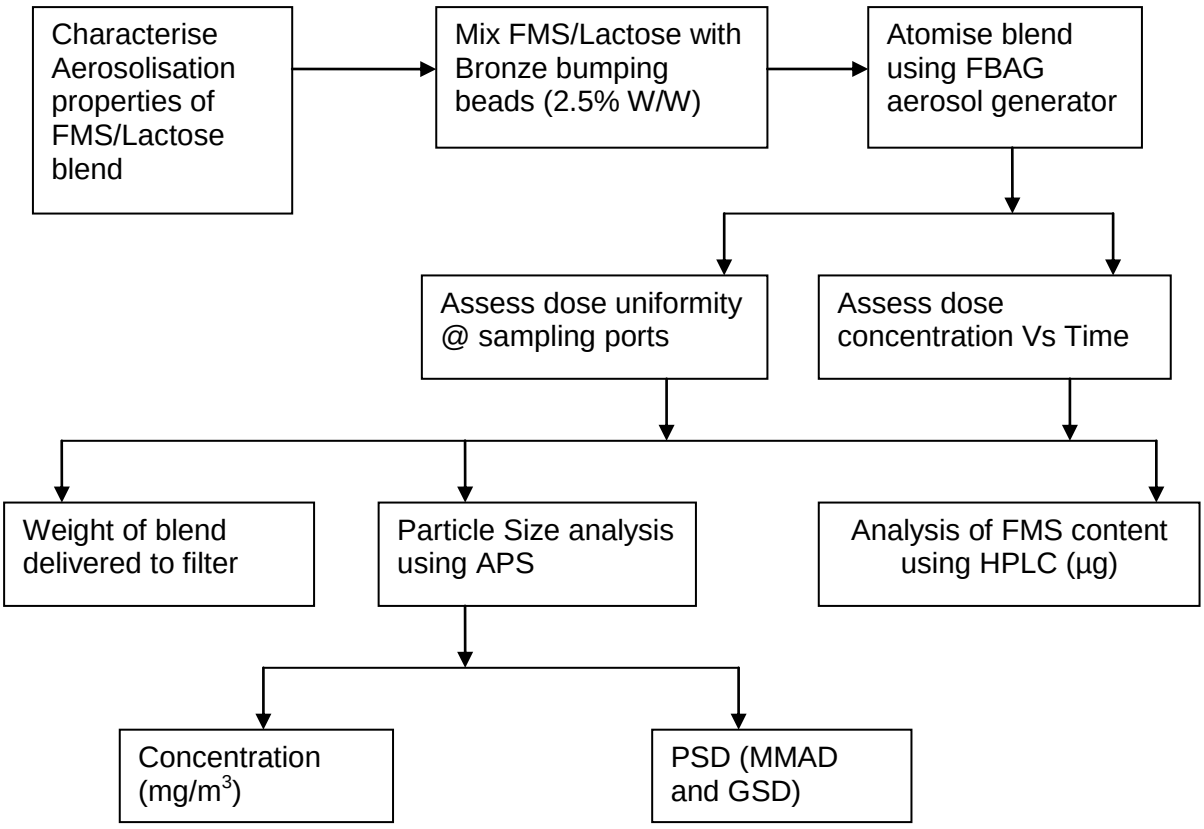

Figure 27: Schematic presentations of the experimental procedures to generate and characterise aerosol exposure atmospheres.

2.2 Modification of exposure chamber

The initial test showed that a significant amount of powder accumulated on the inner surface of the Elutriator during normal operation of the fluidised bed aerosol generator. This was attributed to the high level of electrostatic charges, which may have accumulated in the blend after mixing the FMS-Lactose blend with the fluidising beads.

This problem was partly overcome by leaving the blends to stand overnight under ambient storage conditions, in order to allow for static charges built up during the blending process to dissipate. Furthermore, charge neutralisation via the use of the Meech static eliminator (Meech Static Eliminators Ltd, Oxford, UK) was applied during aerosol generation to further reduce the electrostatic effect. After these modifications, it was noted that much higher levels of aerosol concentration (> 5.0 mg/m^3) were recorded by the on-line particle sizer than was the case without these modifications, as shown in Figure 28.

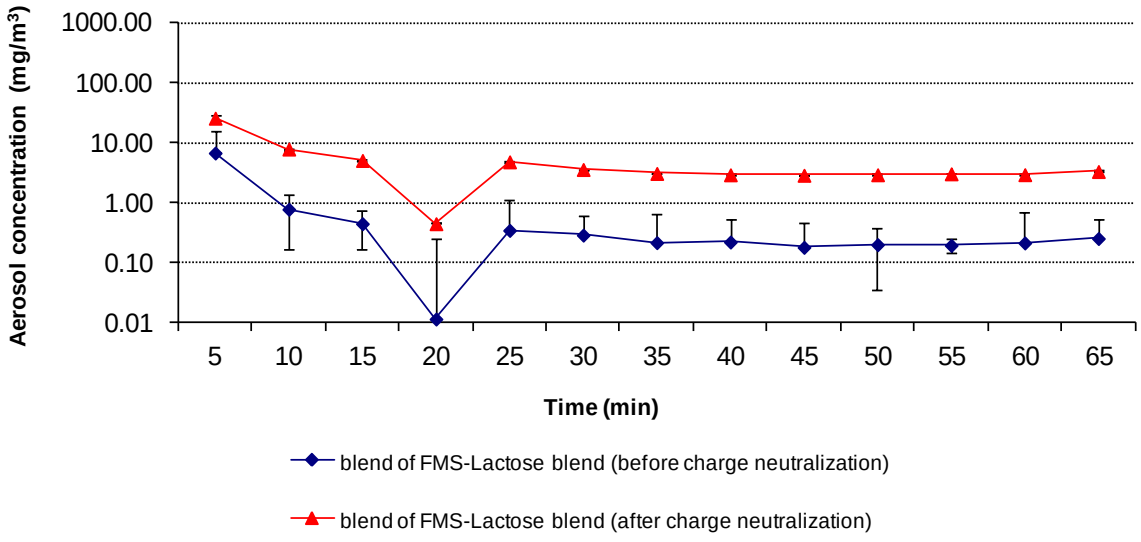

Figure 28: Comparison of the aerosol concentration of the FMS-Lactose blends before application of charge neutralisation (blue diamond) and after application of charge neutralisation (red triangle). Error bars are Mean ± SD from two independent experiments.

2.3 Assessing the variability of total particulate matter (TPM) in the exposure chamber

Total particulate matter (TPM) is a measure of the total mass of particles collected on the filters, including the active and carrier materials. This method is widely used in rodent aerosol exposure investigations to check whether the target aerosol concentration has been achieved (OECD, 2004;Wong, 2007). In addition, assuming the blend is well mixed, the variability in aerosol concentration for the TPM samples should be reflective of the variability in the concentration of active materials (Stein et al, 2003). However, the main drawback to this method is that the results generated are time-dependent and represent the aerosol concentration for a given period of time, rather than the actual aerosol concentrations at the time of measurement (Cheng et al, 1988).

The TPM concentrations in the exposure chamber were determined by measuring the increase in filter weight at five sampling port locations in the exposure chamber. The sampling ports used were located in diametrically opposite locations of the exposure chamber. The results of the determinations of TPM at different locations and sampling periods are shown in Figure 29. The overall Coefficient of Variation (CV) obtained by 60 measurements at five different inhalation chamber locations and over a duration of three consecutive days was 16.04%. This variability of aerosol generated is within the ±25% of the concentration limit for test materials, as recommended by OECD Guidelines for acute inhalation toxicity testing (OECD, 2004).

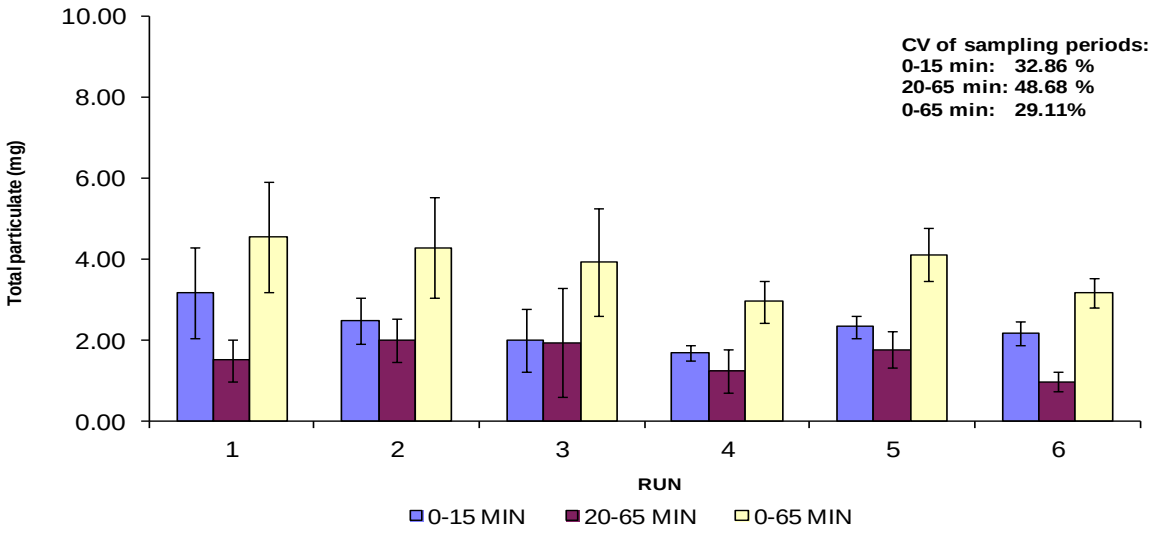

Figure 29: Comparison of the average aerosol concentrations of TPM and corresponding standard deviation. Data presented is grouped by time-intervals and run order.

2.4 Assessing the variability of active test material in the exposure chamber

The overall variability for active FMS aerosol concentration (obtained by 60 measurements at five different inhalation chamber locations over a period of three days) was 12.32% and hence demonstrates a high degree of spatial and temporal uniformity. The results for the determinations of FMS aerosol concentrations at different port locations of the exposure chamber over different sampling periods are summarised in Table 7.

Table 7: Comparison of the average aerosol concentrations of active and corresponding standard deviation. Data presented is grouped by time intervals and port location.

Time Interval (min)	FMS concentration (mg/m^3) at different Port Location [1]					Mean (1-11)	CV[2]
	1	3	5	8	11		
0-15	6.21±0.55	5.87±0.87	5.49±0.95	6.22±0.96	5.83±0.87	6.01±0.81	13.47
20-65	2.04±0.32	2.01±0.33	1.96±0.30	2.07±0.36	1.80±0.26	1.98±0.31	15.58
0-65	3.03±0.33	2.98±0.40	3.03±0.33	3.11±0.43	2.81±0.35	3.00±0.37	12.32

1. Six Gravimetric samples per port location and sampling period.
2. Coefficient of Variation.

These results are in keeping with temporal variability values of 5-19% as reported in other studies of animal exposure chambers (Liden et al, 1998;Lundgren et al, 2006;Yeh et al, 1986). They therefore indicate the achievement of adequate aerosol mixing in the exposure chamber.

In order to determine the degree of day-to-variability in aerosol concentrations, a comparison of the average aerosol concentrations for the various sampling period over a duration of three days was performed (see Figure 30).

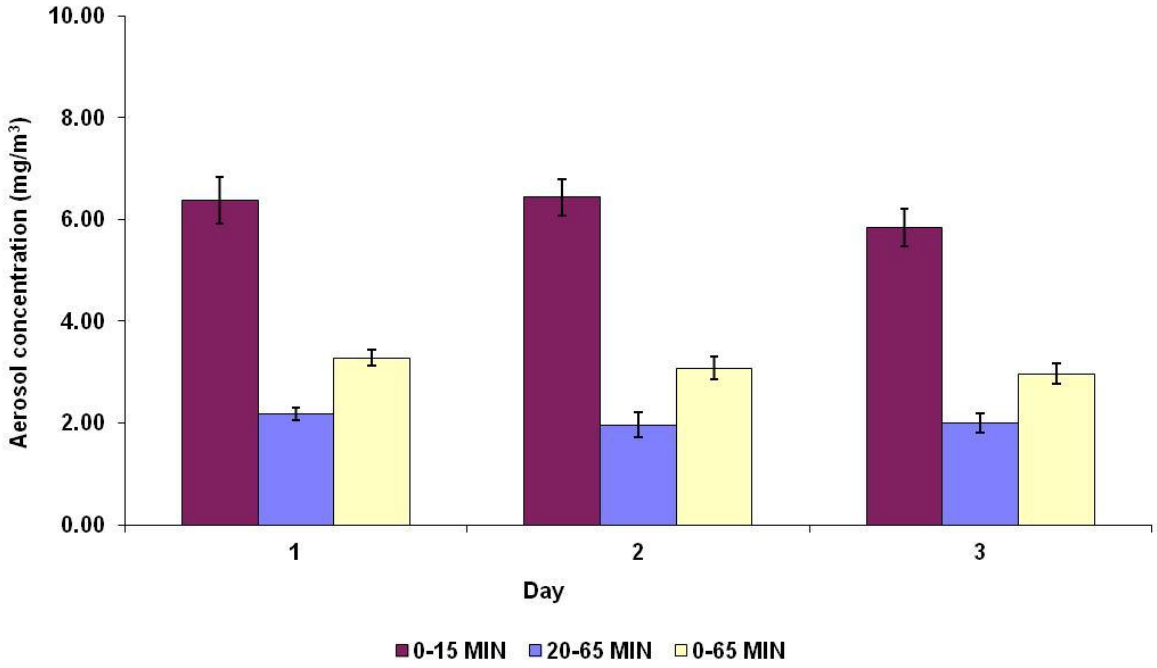

Figure 30: Comparison of the average aerosol concentrations of FMS and corresponding standard deviation for the various sampling period over a duration of three days. Error bars are Mean ± SD from six independent experiments.

A one-way analysis of variance (ANOVA) was used for statistical evaluation. A probability of $P < 0.05$ was chosen as the significance level. The results revealed no significant difference between the aerosol concentration of fluorescent microspheres (FMS) collected from sampling filters for the two exposure periods under evaluation: P= 0.87 and 0.61 for 0-15 and 20-65 minute exposure periods respectively over the three sampling days.

With respect to the degree of variability from port-to-port, ANOVA analysis was used for statistical evaluation. A probability of $P< 0.05$ was chosen as the significance level. Results revealed no significant difference between mass and aerosol concentration of fluorescent microspheres (FMS) collected on sampling port 1-11 during the two exposure periods under evaluation: P= 0.87 and 0.61 for 0-15 and 20-65 minute exposure periods respectively (see Figure 31). Therefore, any variation observed may be attributed to day-to-day variability of FMS in the exposure chamber, rather than an inhomogeneity of exposure concentrations at different inhalation chamber locations.

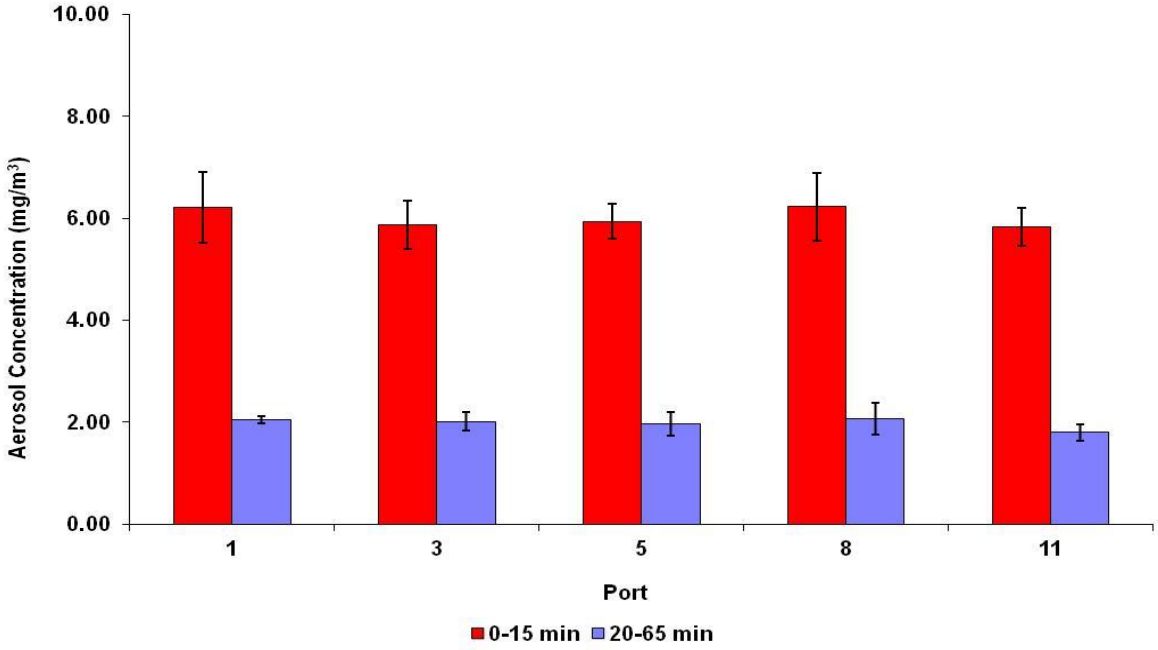

Figure 31: Comparison of the average aerosol concentrations of FMS and corresponding standard deviation at various locations of the exposure chamber. Error bars are Mean ± SD from six independent experiments.

The good temporal stability of the aerosol concentration found in the present study is probably due to several factors. Firstly, the mixing of the test material with bronze beads using low-shear Turbula mixer (Willy A. Bachofen, Mutternz, Switzerland) prior to fluidisation may have resulted in a more even distribution of the test material. Secondly, the charge neutralisation of the test powder was found to be critical for ensuring good mixing of the aerosol in the air supply chamber. Without this treatment, a significant amount of dust material would have accumulated on the inner surface of the elutriator and transport lines (see Figure 28).

2.5 Environmental conditions within exposure chamber

In order to assess the variability of environmental conditions and their impact on aerosol concentration, regular readings of the temperature and relative humidity readings were taken over the entire exposure period (65 minutes). Figure 32 shows the average measured relative humidity (% RH) and temperature (°C) within the exposure chamber to be in the region of 14% RH and 25°C during the operation of the exposure chamber.

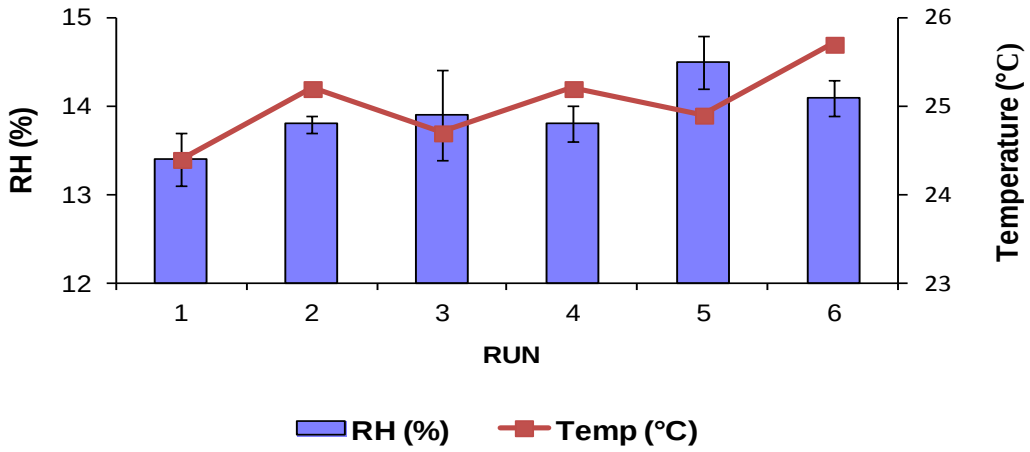

Figure 32: Recorded environmental (Temperature and Relative Humidity) conditions within the exposure chamber. Error bars are Mean ± SD from six independent experiments.

The relative humidity (RH) of approx 15% recorded in the exposure chamber is on the low side for animal studies. According to OECD draft guidelines 436, the relative humidity inside the exposure chamber should be in the range of between 30-70% RH. The temperature fluctuations within the exposure chamber were found to be mainly in the range of 25°C, well within the typical range of temperature variation noted in other rodent studies (OECD, 2004).

The relatively low RH levels recorded within the exposure chamber may explain some of the variability seen in the aerosol concentration, particularly the TPM concentration. Figure 33 shows the relationship between the level of variability for TPM content and RH within the exposure chamber. In general, the higher the RH levels within the chamber, the lower the degree of variation recorded for TPM aerosol concentrations. This trend may be explained with reference to electrostatic effects, where the low RH levels may have resulted in increased levels of electrostatic within the exposure chamber and thus contributed to the increased level of variability in the distribution of particles within the chamber (O'Shaughnessy et al, 2003).

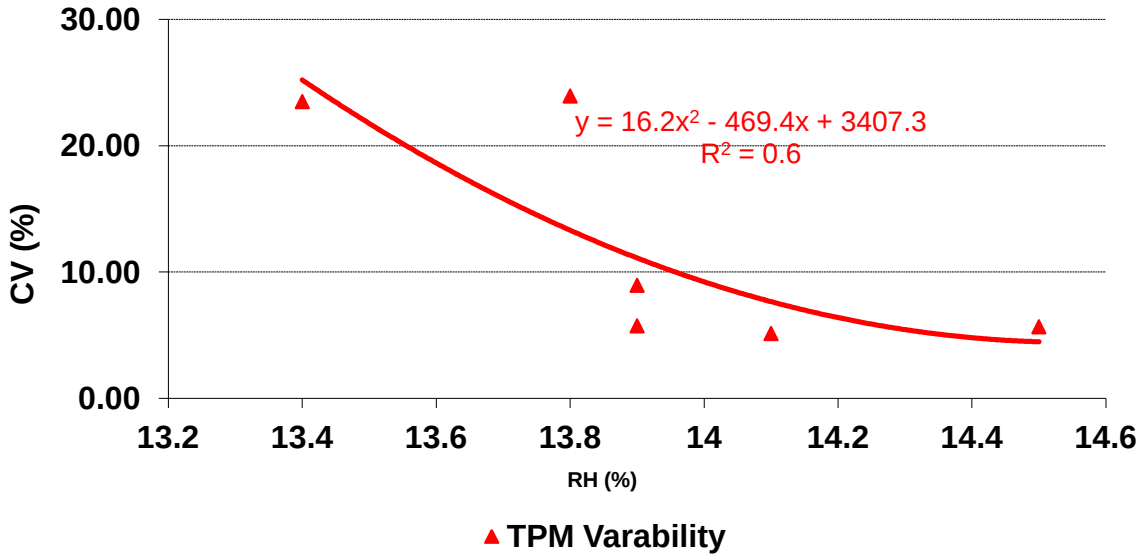

Figure 33: The relationship between the coefficients of variation of TPM (%CV) and corresponding measured RH within exposure chamber.

The influence of electrostatics on temporal variability has been stressed by Hinds (Hinds, 1999) and Liu *et al.* (Liu et al, 1986). Both have recommended the use of charge-neutralisation devices in the generation set-up as a means of overcoming, or at least reducing, the effect of this occurrence on the stability of chamber aerosol concentration. Furthermore, the highest CV values were found in studies that did not apply charge neutralisation (O'Shaughnessy et al, 2003;Taylor et al, 2000). Thus, this further supports the argument that some of the variability observed in this study may have been caused by electrostatic build-up in the exposure chamber.

As stated previously, the levels of variability recorded in this study for both TPM and active components of the formulation are within acceptable levels according to OCED draft guidelines. However, the trends seen in this experiment, coupled with the low relative humidity within the exposure chamber (<15% RH), clearly demonstrate the need for refinements of the re-humidification system. This, in turn, may result in obtaining even more stable and reproducible aerosol concentrations within the exposure chamber.

2.6 Characterisation of exposure atmosphere

The aerosol atmosphere was characterised using an Aerodynamic Particle Sizer (APS). The mean aerosol concentration for initial sampling period (0-15 min) was calculated to be 20.2 ± 9.7 mg/m^3. Thereafter, the generator was stopped for a period of five minutes in order to allow the filters to give an evaluation of the second dosing period (20-65 min). Data showed the aerosol concentration to recover rapidly to approximately the same levels before switch-off of the aerosol generator. However, the aerosol concentration continued to fall with increased operating time with mean aerosol concentrations of 6.1 ± 3.1 mg/m^3 for the remaining sample period of 20-65 minutes.

Figure 34 shows the aerosol concentration produced by the aerosol generator as a function of time for the six replicate runs. In all cases, the aerosol concentration started at a high level and fell rapidly thereafter.

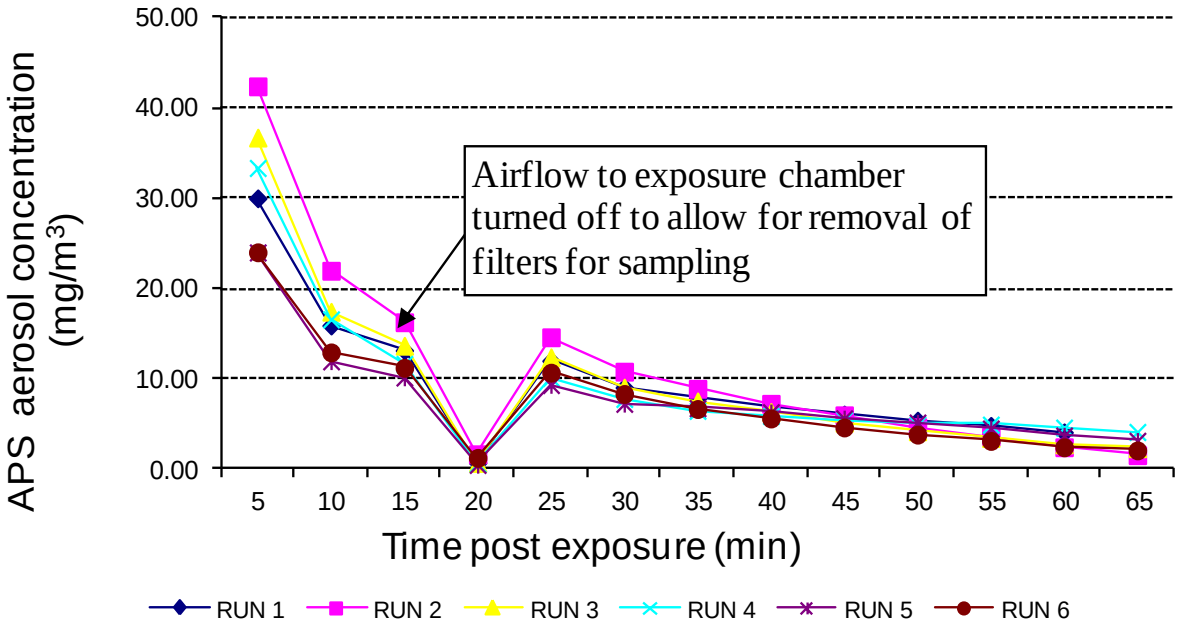

Figure 34: Aerosol concentration (mg/m^3) as a function of time

The mean mass median aerodynamic diameter (MMAD) was recorded as 2.41 µm, while the geometric standard deviation (GSD) was recorded as 1.80. Therefore, the particle size distribution generated was well suited for rodent inhalation studies and particles were in the size range that deposit throughout the entire rodent respiratory tract (see Figure 35).

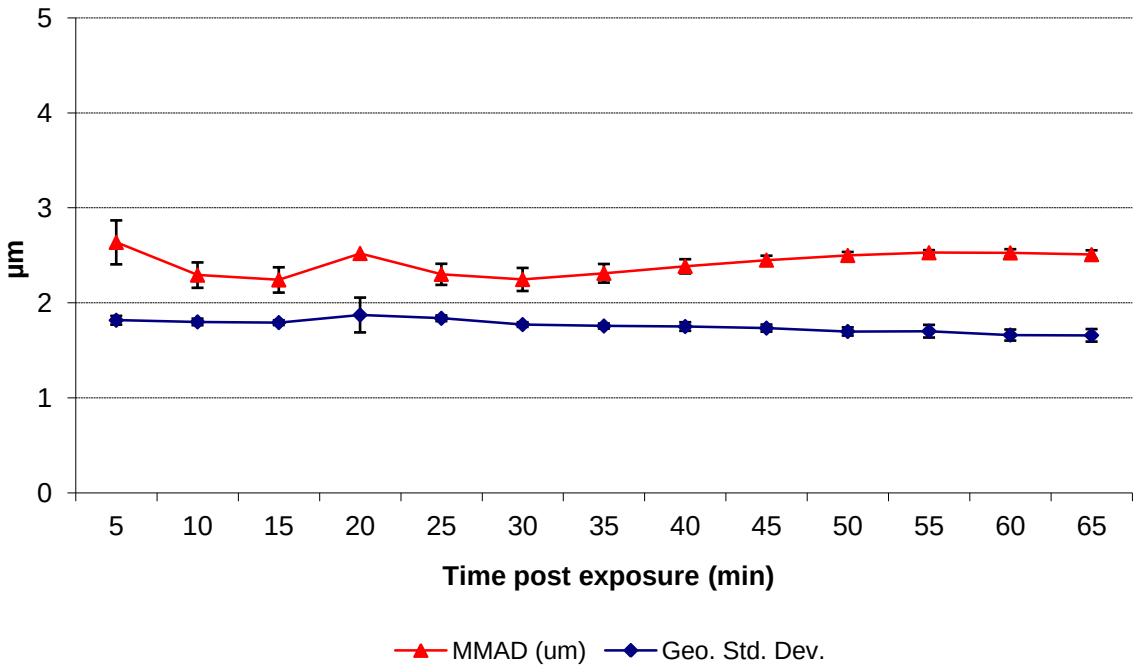

Figure 35: MMAD and GSD variation as function of time. Error bars are Mean ± SD from six independent experiments.

Furthermore, these results were in line with the requirement and recommendations of the current testing guidelines applied to inhalation studies such as the OECD draft guidelines, which state that an aerosol with a MMAD between 1.0 to 4.0 µm and GSD in the range 1.5 to 3.0 is recommended to ensure comprehensive respiratory tract exposure occurs (OECD, 2004;Wong, 2007).

2.7 Conclusion

Experimental evidence demonstrated that the aerosol generation and the exposure system developed provides uniform spatial exposure conditions. During the course of exposure, the temporal fluctuations in aerosol concentration as measured by CV were shown to be 12.4%. This finding is in keeping with temporal variability values of 5-19% reported in other studies of animal exposure chambers (Liden et al, 1998;Lundgren et al, 2006;Yeh et al, 1986).

In addition, the particle size distribution data generated, being MMAD of 2.41 µm and GSD of less than 2.00, indicates that the exposure atmosphere generated using this system is well suited for rodent inhalation studies and particles were in the size range that are likely to deposit throughout the entire rodent respiratory tract (Owen, 2013;Yeh et al, 1986). Furthermore, these results were in line with the requirement and recommendations of the current testing guidelines applied to inhalation studies such as the OECD draft guidelines, which state that an aerosol with a MMAD between 1.0 to 4.0 µm and GSD in the range 1.5 to 3.0 is recommended to ensure comprehensive respiratory tract exposure occurs (OECD, 2004).

This developed inhalation chamber system may be employed for acute inhalation studies with aerosols involving the IVR model and live rats. However, for experimental work assessing the effect of ventilation and formulation parameters on deposition in the IVR model, a simplified design version of the same type of exposure chamber detailed in this investigation was employed (see section 4, 5, B - Results and Discussion). The main difference was a reduction in the number of sampling ports, with 4 ports used as opposed to the 12 ports. Therefore, the results generated in this study are equally applicable to the simplified chamber design.

3 Development of the *In Vitro* Rat lung model

Small animals are widely used for the assessment of the efficacy and safety of inhaled medicines (Owen, 2013;Sakagami, 2006). As in the case of humans, there is a growing trend toward the use of computational models and *in vitro* models to simulate an animal lung, in order to better understand the impact of airway physiology and physical characteristics of inhaled particles on deposition in the lungs (Schroeter et al, 2012).

In addition, the development of such models could lead to a reduction in the amount of animals sacrificed for research purposes. Furthermore, such models can assist in the development of inhalation therapies and optimisation of inhaler devices (Coates et al, 2007;Kleinstreuer et al, 2007).

Whilst detailed *in silico* and *in vitro* models of the human lung have been developed and characterised, few investigators by comparison have developed similar models to study the deposition of drugs in the lungs of animals. However, advances in small animal imaging using micro-CT or MRI have made it possible to study the airway structure in greater detail (Minard et al, 2006).

As a result of this advance, a realistic computational model of the respiratory tract of Sprague-Dawley rats was developed using micro-CT scanning technology (De Backer et al, 2009). This model can subsequently be used to assess particle deposition behaviour.

This section summarises the work undertaken to generate the average model of the rat respiratory tract based on the CFD images produced from a study by De Backer *et al.* (De Backer et al, 2009). In addition, it details the subsequent manufacture of the physical model referred to as the *in vitro* rat lung model (IVR), as well as the general experimental setup used to validate the newly developed model.

3.1 Conduct of work

The micro-CT scanning process and generation of the CFD model, upon which the physical model of the rat lung was constructed, was conducted by a specialist contract research company (FluidDA, Antwerp, Belgium), which specialises in the acquisition and analysis of imaging data from a variety of preclinical species. In addition, the process of converting the CFD files into a physical model of the rat lung was undertaken by a specialist engineering Research Company (Aztec Precision Engineering, Letchworth, UK).

3.2 Micro-CT scanning of the rat respiratory system

A total of seven Sprague Dawley rats (weight: 372 ± 56 g) were used to develop a representative, realistic model of a rat's respiratory system. A combination of static and dynamic high micro-CT scans made it possible to reconstruct both the upper and lower airway region. The scanning process started from the nares and extended down to the central airways, up to the point where no distinction could be made between intraluminal air and air in the alveolar region. Full details of the scanning method used are described in the study by De Backer *et al.* (De Backer et al, 2009). Figure 36 illustrates the resultant model of the airways. As an additional reference in this figure, the skeletal structure and the skin were segmented and reconstructed.

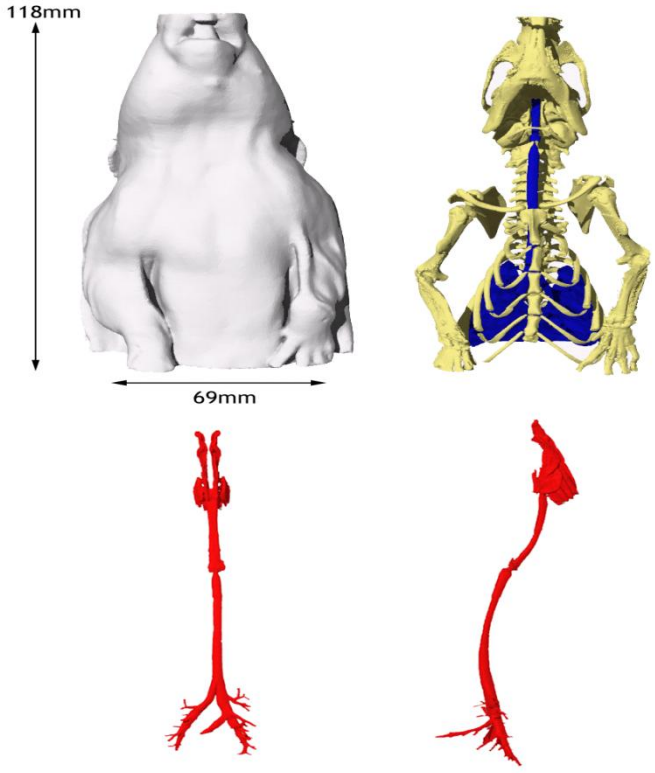

Figure 36: Model of Sprague Dawley rat derived from micro-CT scans. Taken from De Backer *et al.* (De Backer et al, 2009). Reproduced by permission of John Wiley and Sons

For the selection of the representative model, variables such as upper airway movement, segmentation length, airway volume and size are taken into account. The nasopharyngeal volume of the representative model was 373 mm^3, the tracheal volume was 173 mm^3 and the volume of the central airways amounted to 233 mm^3.

3.3 Physical model details

A number of identical physical models were constructed in Solidworks computer-assisted design (CAD) software (Solidworks, Concord, MA). These models were converted into Stereo Lithography file format (STL) for further processing, prior to transfer to a rapid prototyping (RP) machine for manufacture. This manufacturing process was carried out by Aztec Precision Engineering company (Letchworth, UK).

The designs were constructed as hollow plastic models using polycarbonate-based material, namely Accura 60 resin (3D System, Valencia, USA). In addition, the inner surface of the model cast was coated with Parylene N (Speciality Coating Systems, Woking, UK) material; this was to ensure the Accura resin did not come into contact with the organic solvents routinely used to extract drug material deposited on the model inner surface.

The resultant average model of a rat's airways (see Figure 37) consisted of the following sections: Extra-Thoracic region containing the Snout and Nasophyarynx (ET: sections 1and 2), Trachea-Bronchial region containing the Trachea, Bronchi and Bronchioles (TB: Sections 3, 4 and 5). All sections of the model were made to snap fit and were attached to one another in numerical order.

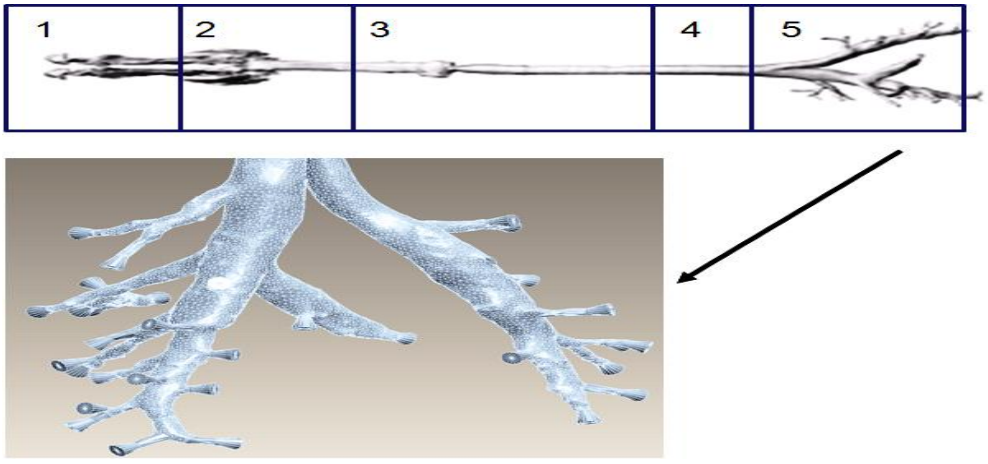

Figure 37: Average rat model derived from micro-CT scans (top). The model consisted of the following sections: 1 and 2 covered the Extrathoracic (ET) region; 3, 4, and 5 covered the Tracheobronchial (TB) region. The TB region was in more detail, showing the presence of some respiratory bronchioles (bottom)

Each airway model was installed in an identical custom-built cylindrical housing with an internal diameter and height of 3.4 and 16.0 cm respectively (see Figure 38). The volume of the containment section enclosing this diaphragm was approximately 7000 mm^3.

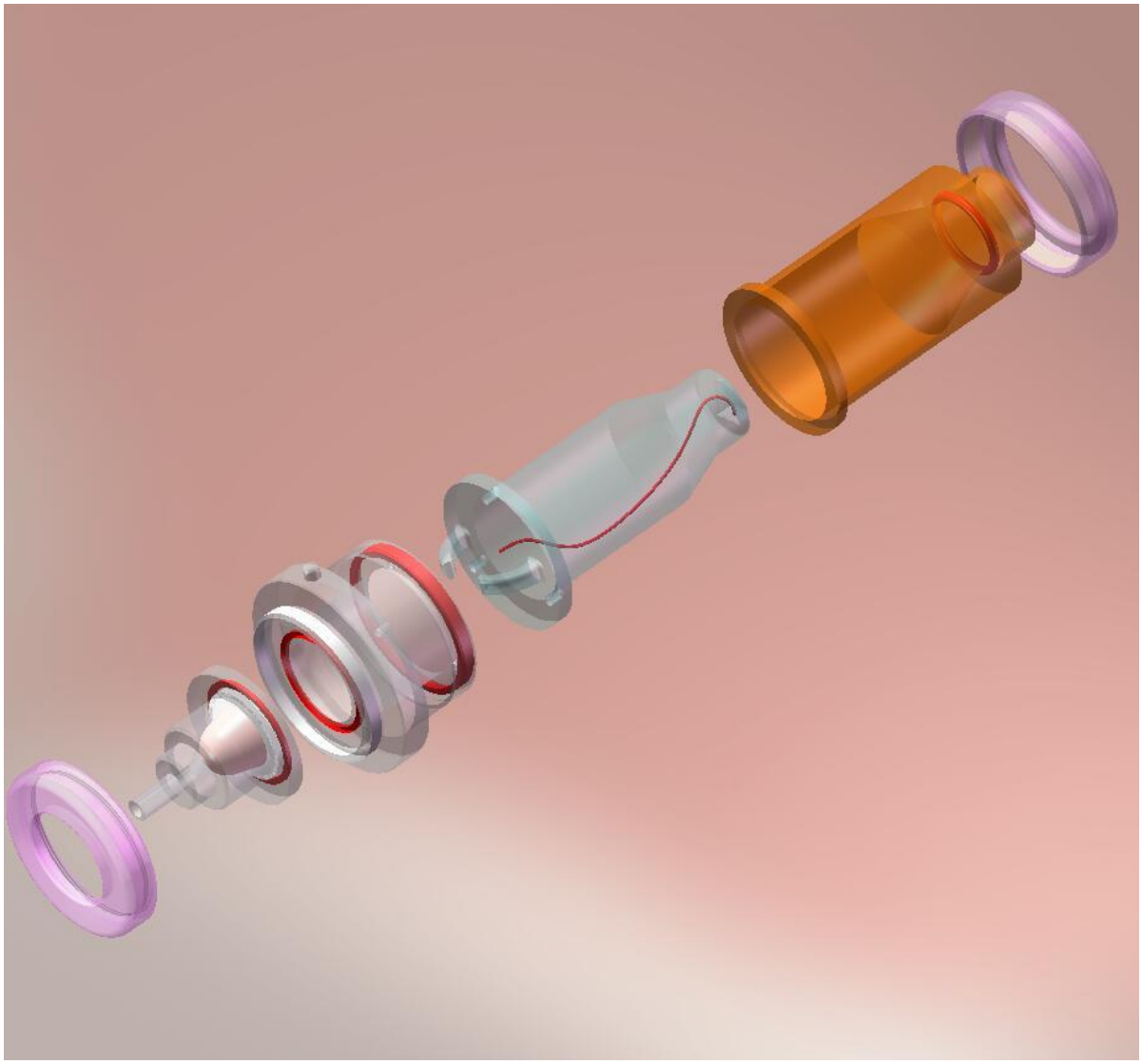

Figure 38: Three-dimensional image of the IVR model sections, encased in a custom-built cylindrical housing unit. Reproduced with permission from Aztec Precision Engineering, Letchworth, UK

3.4 Assessing the number of airways per generation for the IVR model

The numbers of airways in the IVR model were visually counted from three-dimensional CAD images of the rat model (see Figure 39).

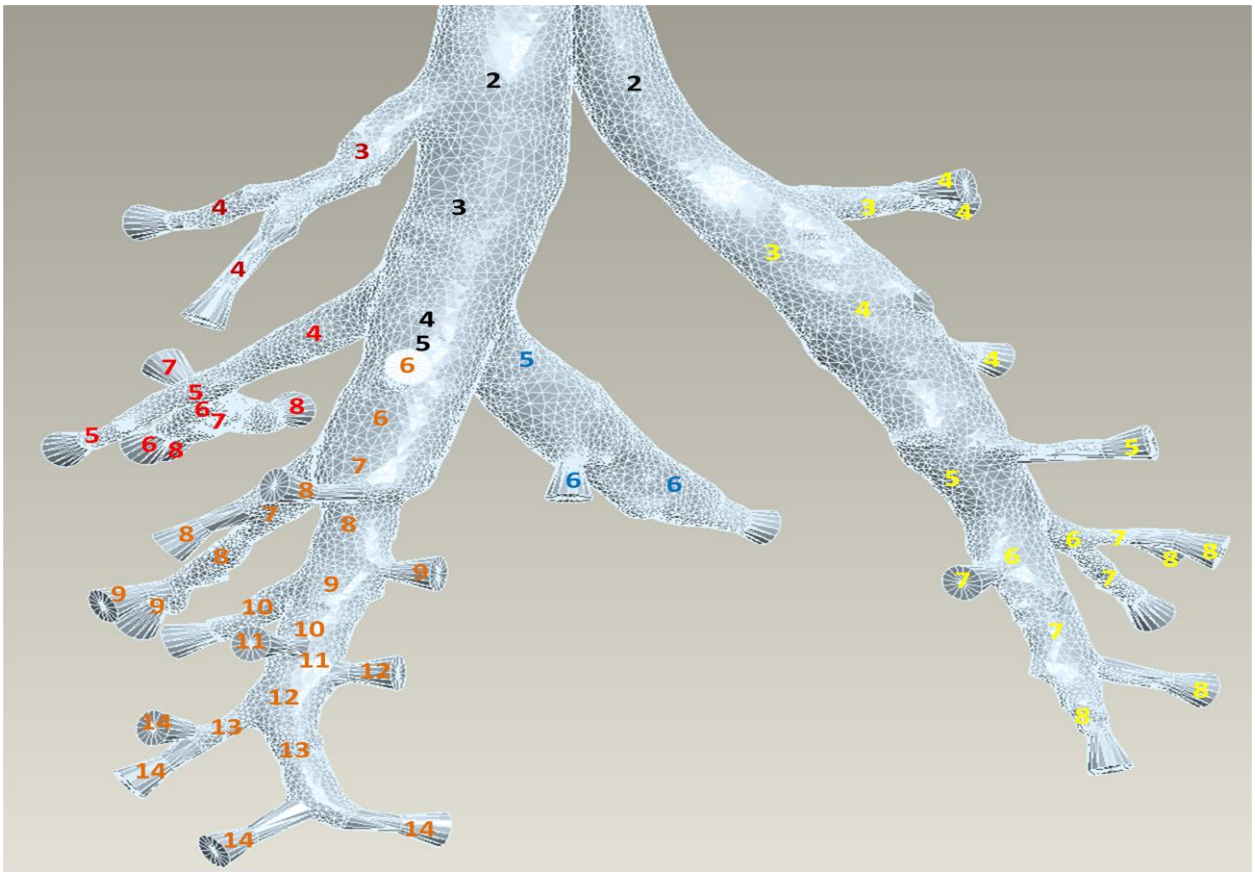

Figure 39: Three-dimensional model representation of the lower airway section of the IVR model. Reproduced with permission from GSK R&D Ware, UK

The results of this analysis showed that, in terms of airway morphology obtained from the scanning process, 100% coverage of the airways in generation 4 (Bronchiole) was achieved. However, the level of coverage thereafter decreased steadily and, by generation 15 (corresponding to the Alveolar region), less than 1% of total airways expected in this generation were covered (see Figure 40).

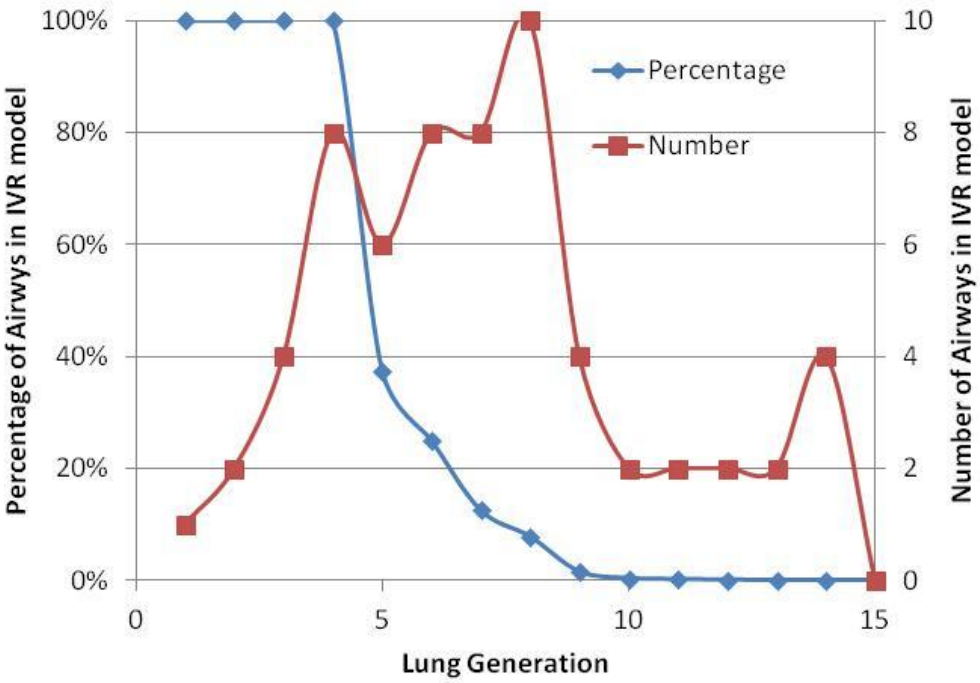

Figure 40: Number and percentage coverage of airways in the IVR model

Therefore, it could be concluded that this analysis provides confirmation that the developed lung model is a true representation of the lung structure for Sprague-Dawley rats, particularly for the head and tracheobronchial regions.

However, the lack of airways from the Alveolar region means deposition in the lower airway regions cannot be accurately determined in the present model. Nonetheless, a flexible diaphragm was attached at the rear of the model, after section 5, in order to collect the fraction of inhaled particles exiting the TB section and possibly reaching the lung. This section is referred to as the Post-TB region.

Therefore, the amount of particles collected in this section may be regarded as containing a combination of particles collected in the TB and pulmonary fractions. Thus, the results generated for this region should be treated with some caution and not interpreted as being reflective of actual deposition in the pulmonary region.

3.5 IVR model testing setup

To evaluate drug deposition during experimental procedures, the IVR model components were installed in a custom-built cylindrical housing unit. The rear end of this unit (at the far side of the diaphragm) was connected to the Ugo Basile Rodent ventilator (Model 6025; Comoro, Italy) in order to simulate breathing conditions, considered to be representative of various activity levels of a Sprague-Dawley rat. These conditions were simulated by varying the tidal volume and breathing frequency supplied to the model from the ventilator. A diagram of the general experimental set-up is shown in Figure 41. This set-up included, in addition to the IVR model, an aerosol generator, exposure tower and air filtration system.

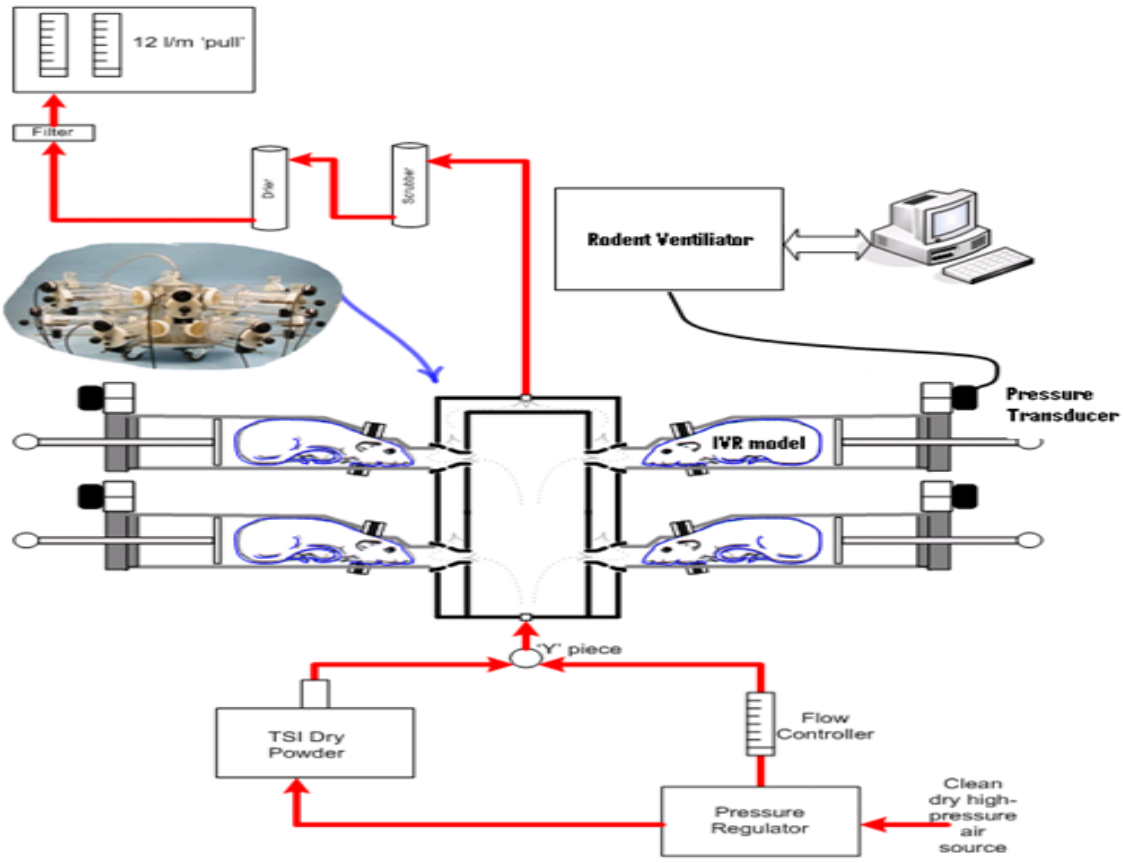

Figure 41: Diagram of the test set-up used to assess deposition of inhaled test material in the IVR model. Reproduced with permission from EMMS, Bordon, UK

During operation, the airflow conditions were continuously monitored via an airflow sensor (TPF 100 Pressure Transducer; EMMS, Bordon, UK) placed in the airflow path between the ventilator and rat model. This sensor was connected to a flow transducer (Adaptive Amplifier; AMP 110; EMMS, Bordon, UK), which transformed the electrical signals to flow traces of the inhalation manoeuvres and displayed on to a personal computer using a data acquisition program (eDacq software; EMMS, Bordon, UK).

3.6 Development of coating solution for the IVR model

It is widely recognised that the application of a coating material on the collection surfaces for the Cascade impactor stages is desired in order to avoid bias caused by particle bounce (Miller et al, 1998). In addition, a similar approach has been adopted for human throat and lung models (Delvadia et al, 2012). Furthermore, there is no standard approach in industry in terms of either materials used or method of applying the coating. Therefore, for the IVR model, a coating solution was developed and tested using fluorescent microsphere (FMS) as the test material.

Initial tests with standard coating material previously used in human throat cast models, such as a glycerol-methanol mixture or silicone fluid as described in Delvadia *et al.* (Delvadia et al, 2012), showed it to be too viscous for the rat model and led to blockage of the internal model tubes on drying. Therefore, a less viscous solution that is compatible with the plastic polymer (SLA resin) composition of the IVR model was required. Other requirements of the solution were that it should be adhesive enough to capture all the test material particles and be easily removable between preparations. In addition, the solution should not produce any interfering peaks in the HPLC system with the test material.

An iterative process was used in the development of the coating solution. A number of tests were applied, such as visual assessment of powder trapping properties on SLA resin blocks, flow using capillary tubes, as well as an investigation into the ability to recover the test material FMS from the coating solution. The final coating solution that developed, which satisfied all these criteria, consisted of a mixture of Brij: PEG 200 in Acetonitrile.

The application process consisted of dripping the coating solution into the model's individual sections and rolling the model to allow the coating of all surfaces. The model was then allowed to dry for approximately one hour post application. Thereafter, the model components were assembled together, ready for use in aerosol exposure experiments.

4 Assessing the effect of aerosol characteristics on deposition in the rat model

The understanding of the process and factors influencing particle deposition in specific regions of the respiratory tract has implications on the development of pharmaceutical inhalation products for aerosol therapy and to the risk assessment of air pollutants that concern toxicology.

The aerodynamic particle size distribution (APSD) of a pharmaceutical aerosol is known to influence its deposition in the respiratory tract, and must therefore influence both the efficacy and safety of inhaled drugs. In addition, there is sufficient evidence reported in the literature to show that the site of deposition in the respiratory tract for both human and preclinical species, such as rodents, is related to the APSD, with smaller particles in particular depositing in the lower portion of the respiratory tract (Kuehl et al, 2012;Raabe et al, 1988).

Besides pulmonary physiology, e.g. breathing pattern and lung geometry, particle deposition is known to be influenced by aerosol characteristics (Larhrib et al, 2003). The physicochemical properties of inhaled aerosols that can determine deposition are: particle size distribution, dose, shape, charge, density and hygroscopicity. An investigation into how these aerosol characteristics affect deposition and movement through the airway is required in order to optimise drug delivery through the inhaled route.

Inhaled formulations commonly consist of a carrier material (e.g. alpha-lactose monohydrate) included to ensure flowability, reducing agglomeration and providing bulk to make handling and dosing possible. In addition, a relative low amount (0.05–10.0% w/w) of active pharmaceutical ingredient (API), with particle size typically below 5.0 µm, is included. Furthermore, some recent inhaled products have been formulated using a ternary agent, such as magnesium stearate (MgSt), included as a chemical and fine particle stabiliser in powder formulations (Guchardi et al, 2008;Tuli et al, 2012).

The inclusion of MgSt in the inhaled formulation has been shown to increase the fine particle dose in *in vitro* assessment using the Anderson cascade Impactor. Peart and co-workers (Peart, 1997) reported blending magnesium stearate or L-leucine with 1.5 Salbutamol sulphate and coarse lactose (90-125 µm). The emitted fine particle fraction increased for both formulations, although the increase was more pronounced in the magnesium stearate formulation. It was suggested by the authors that the effect of a ternary agent on the fine particle dose depends on the quantity and also on the inter-particulate forces between the components.

For this work, the impact of particle size of API, dose of API and formulation changes by inclusion of MgSt in the final blend on deposition of particles in the *in vitro* rat (IVR) model were investigated. In addition, the experimental data generated using the IVR was compared with *in silico* model predictions and *in vivo* literature data. The overall aim of this work was to validate and assess the sensitivity of the IVR model with respect to changes in aerosol characteristics.

4.1 Assessing the influence of inhaled particle size on regional lung deposition in the *in vitro* rat model

In this study, the influence of aerosol particle size on the deposition pattern in the *in vitro* model of a rat lung was investigated. Triplicate blends containing FMS particles of 2.0 µm and 4.0 µm size and lactose were prepared. Full details are listed in section 4, C - Experimental Setup.

The aerosol generation of 2 and 4 µm FMS particles in the exposure chamber was successfully achieved. For the two micron-sized powder mixes, the average MMAD was 2.2 µm as measured using the APS. For the four micron-sized powder mixes, the average MMAD was 4.9 µm. Constant ventilation conditions of tidal volume (2.1 mL) and breathing frequency (102 min^{-1}) were supplied to the *in vitro* model throughout the duration of all experimental runs, which were conducted for a 45-minute period. The results are summarised in Table 8.

Table 8: Experimental results obtained with the *in vitro* rat model (IVR) using 2 and 4 µm FMS-Lactose inhalation blends.

Experimental Run Ref	Size of input FMS particle (µm)	Minute Volume ($L.min^{-1}$)	Aerosol concentration (mg/m^3)	MMAD (µm)	% Deposition in IVR model sections		
					Head	Tracheo-Bronchial	Post-TB
4µm blend Replicate 1	4	0.21	2.1	4.78	89.0	8.0	3.0
4µm blend Replicate 2	4	0.21	6.0	5.45	95.0	3.7	1.3
4µm blend Replicate 3	4	0.21	2.4	4.34	88.5	6.0	5.5
2µm blend Replicate 1	2	0.22	1.7	2.05	86.4	10.8	2.8
2µm blend Replicate 2	2	0.21	2.1	2.27	77.4	16.4	6.3
2µm blend Replicate 3	2	0.21	1.3	2.17	93.0	5.8	1.2

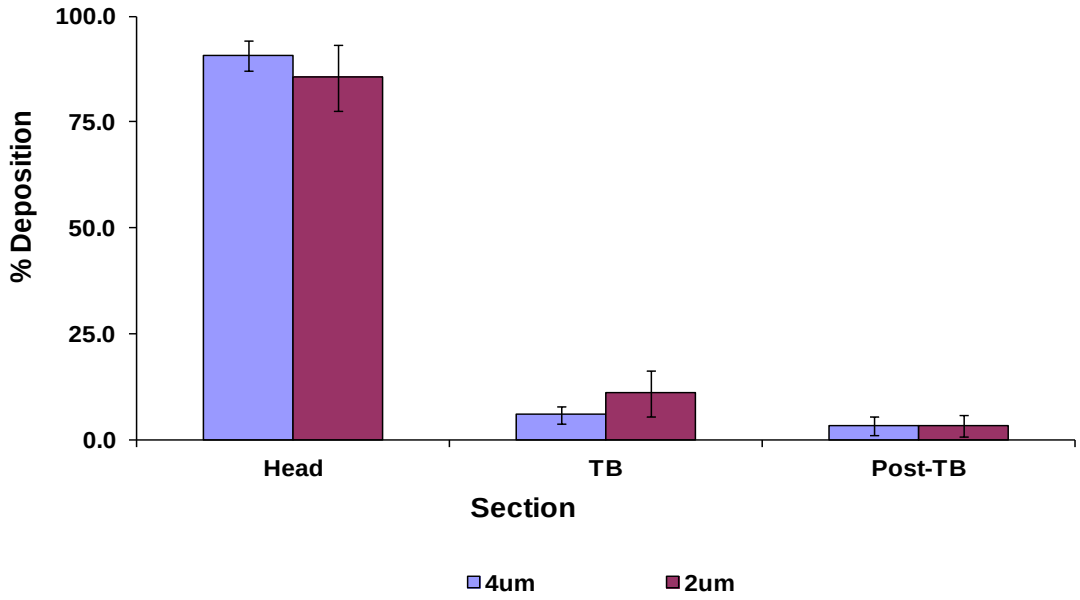

Figure 42: Comparison of particle deposition of FMS particles in the *in vitro* rat model (IVR) for 2.0 and 4.0 µm containing inhalation blends. Error bars are Mean ± SD from three independent experiments.

The results for regional distribution of FMS particles showed the majority of particles were deposited in the head region of the IVR (see Figure 42). In addition, slightly higher deposition levels were noted for the 4.0 µm sized particles versus 2.0 µm sized particles in this region, being 90.8 ± 3.6% and 85.6 ± 7.8% for 4 and 2 µm sized particles respectively. However, this difference did not reach statistical significance ($P > 0.05$), probably due to the relatively large variability in experimental data caused by the polydispersity of aerosolised FMS particles.

The high level of particle deposition in the head region can be attributed to an inertial impaction mechanism, as flow velocities in this area are relatively high and the residence time of the particle is short (Schulz, 1998). Consequently, a higher fraction of particle is expected to deposit in the upper regions of the IVR model. This observation is in general agreement with experimental and *in silico* models, assessing regional particle deposition in the respiratory tract for particles between 0.001 and 10 µm. In the model proposed by Schmid *et al.* for particles between 3.0 µm and 10.0 µm, most particles deposit by impaction in the extrathoracic region (Schmid et al, 2008).

For the tracheobronchial region, much higher deposition levels were noted for the 2 µm sized particles (11.0 ± 5.3%) in comparison with the 4 µm sized particles (5.9 ± 2.1%). This difference may be attributed to the higher deposition levels in the head region for the 4.0 µm sized particles in comparison with the 2.0 µm sized particles, as the head region acts as a highly efficient filter in removing the majority of inhaled FMS particles. Consequently, the fraction of particles reaching the TB region will be relatively reduced for the 4 µm sized particles in comparison with the 2 µm sized particles.

In the case of the pulmonary region (Post-TB), similar deposition levels were noted: 3.4 ± 2.6% and 3.3 ± 2.6% for 2.0 and 4.0 µm sized particles respectively. In both regions, the difference noted in deposition levels did not reach a significance level ($P > 0.05$), probably due to the relatively large variability in experimental data caused by the polydispersity of aerosolised FMS particles. In addition, the data generated from the IVR model were compared against historical *in vivo* data on deposition patterns in rats.

Table 9 shows a comparison to Otto Raabe's 1988 study undertaken using mono-sized ^{198}Y radiolabelled particles (Raabe et al, 1988). The IVR data showed lower pulmonary deposition fractions at the 2.0-3.0 µm particle size, and similar deposition levels at the 4.0 µm particle size. For the TB region, the IVR data showed a higher deposition fraction at the 2.0-3.0 µm particle size, and much lower deposition levels at the 4.0 µm particle size. In the case of the head region, similar deposition was shown at the 2.0-3.0 µm particle size, but significantly higher deposition was noted at the 4.0 µm particle size. Overall, the IVR data is broadly in agreement with the historical data, particularly at the 2.0-3.0 µm particle size range.

Table 9: Comparison of the regional lung deposition data for IVR model versus corresponding *in vivo* data from Raabe's 1988 study (Raabe et al, 1988).

Particle Size (µm)	Head deposition (% of Total)		TB deposition (% of Total)		Pulmonary deposition (% of Total)	
	Raabe	IVR	Raabe	IVR	Raabe	IVR
2.0	NA	85.6	NA	11.0	NA	3.4
3.0	86.5	N/A	5.7	NA	6.6	NA
4.0	71.4	90.6	23.9	5.9	4.8	3.0

A number of possible causes may explain the differences between the experimental and Raabe's data. Most importantly, the data generated in the present study was done using polydisperse particles, whereas the data reported in Raabe's study was generated using monodisperse particles, which may in turn account for the differences in deposition fractions between the studies. In addition, for the IVR, the breathing conditions were fixed at a respiratory minute volume of around 0.20 mL/min during the exposure period. However, for the Raabe rats, the breathing conditions were not monitored during the exposure period, and may have been different. As it is known that changes in ventilation conditions have a marked effect on deposition levels, it may be that differences in this factor could account for some of the apparent differences in lung deposition levels observed between the two data sets (Kuehl et al, 2012;Schulz, 1998).

Figure 43 shows a comparison of the regional distribution of FMS particles in the respiratory tract of rats, between the IVR and the *in silico* MPPD model predictions for 4µm sized FMS particles. Similar trends with respect to total and regional distribution were noted for the 4 µm FMS containing inhalation blends. Full details of the MPPD method are listed in section 3.4, C - Experimental Setup.

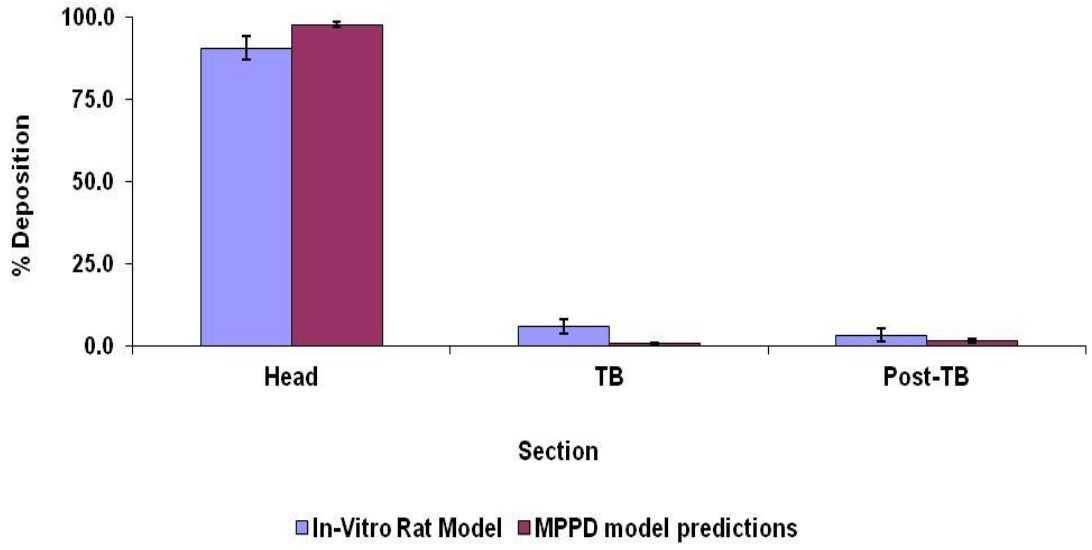

Figure 43: Comparison of particle deposition of FMS particles in the *in vitro* rat (IVR) and MPPD model for 4 µm containing inhalation blends. Error bars are Mean ± SD from three independent experiments.

For the MPPD estimated values, the amount of particles deposited in each region was normalised to the total dose of FMS particle deposited in rats. With this correction, the deposition fraction for the aerosols is only calculated for the aerosols that are assumed to be inhaled into the respiratory tract. This approach has been used by other investigators such as Menache *et al.*, who take into account the inhalability of the material to be deposited in the rats' respiratory tract, and is regarded as it allows for an improved understanding of the fate of aerosols after inhalation (Menache et al, 1996).

The results showed broad agreement between the two models with regards to the regional distribution of these particles, especially for the head region. In both cases, the highest deposition levels were seen in the head region, with 90.8 ± 3.6% and 97.90 ± 0.70% deposition recorded for the IVR and MPPD model respectively ($P < 0.05$).

In addition, higher levels of particle depositions were noted in the TB region for the IVR model in comparison with MPPD predictions for the 4µm sized FMS particles: 5.9 ± 2.1% versus 0.7 ± 0.3% ($P < 0.05$). For the pulmonary region, similar deposition fractions were observed for both models with 3.3 ± 2.2% and 1.3 ± 0.6% deposition recorded for the IVR and MPPD model predictions respectively ($P > 0.05$).

Also, the TB region of the MPPD model covers anatomical structures from the Trachea (generation 1) to the terminal Bronchioles (generation 22). Whereas, for the IVR model, the anatomical structures covered in this section are up to the level of respiratory Bronchiole (generation 4). Therefore, it would be expected that higher deposition levels are observed for the MPPD model in comparison with the IVR model owing to the higher surface area available for depositing particles of the former. Thus, this data indicate that the MPPD model may be significantly underestimating the level of deposition in the TB region of the rat respiratory tract.

4.2 Assessing the influence of dose increase and formulation changes on the total and regional deposition of FMS particles on the IVR model

In this study, the influence of increasing the dose of FMS on the total deposition of the test material in the IVR model was investigated. In addition, the effect of including the flowing agent, Magnesium Stearate (ternary blends) on regional deposition within the IVR model was assessed by comparison with the regional deposition results generated using blends containing FMS and lactose only (binary blends).

Four replicate blends containing 0.8% w/w FMS nominal content, with and without MgSt, were prepared. To assess the effect of dose increase on deposition, triplicate blends containing 3.0% w/w FMS nominal content were prepared. Full method details are listed in section 3, C - Experimental Setup. Constant ventilation conditions of tidal volume (2.1 mL) and breathing frequency (102 min^{-1}) were supplied to the *in vitro* model throughout the duration of all experimental runs, which were conducted for a 45-minute period. The results are summarised in Table 10.

Table 10: Experimental results obtained with the *in vitro* rat model (IVR) using 2 and 4 µm FMS-Lactose inhalation blends.

Experimental Run Description	Aerosol concentration (mg/m^3)	Marple MMAD (um)	Marple GSD (um)	Total mass deposited in IVR (µg)	% Deposition in IVR model sections		
					Head	TB	Post-TB
0.8% FMS-MgSt Rep 1	4.7	2.40	2.57	62.0	83.6	14.8	1.6
0.8% FMS-MgSt Rep 2	4.7	2.48	2.20	75.4	85.5	13.3	1.2
0.8% FMS-MgSt Rep 3	5.3	3..06	3.60	69.2	76.5	22.2	1.3
0.8% FMS-MgSt Rep 4	3.4	3.81	2.31	39.4	80.4	18.4	1.2
0.8% FMS-Lactose Rep 1	1.7	2.58	1.83	10.2	86.3	10.8	2.8
0.8% FMS-Lactose Rep 2	2.1	2.63	1.81	12.8	77.3	16.4	6.3
0.8% FMS-Lactose Rep 3	1.3	3.09	2.18	8.6	93	5.8	1.2
0.8% FMS-Lactose Rep 4	2.0	3.44	2.26	18.3	93.1	5.6	1.3
3.0% FMS-MgSt Rep 1	20.2	2.69	2.58	91.0	84.9	13.4	1.6
3.0% FMS-MgSt Rep 2	15.7	2.34	2.44	68.5	83.5	14.9	1.6
3.0% FMS-MgSt Rep 3	18.6	2.59	2.55	77.1	85.9	11.5	2.6

The results for the total mass of FMS particles deposited in the IVR model showed the expected trend with increased deposition in the model with increasing aerosol concentration. Furthermore, significantly higher aerosol concentrations were generated for the magnesium stearate containing blends of FMS in comparison with binary blends of the same formulation (0.8% FMS): 4.5 ± 0.8 mg/m^3 for ternary versus 1.8 ± 0.4 mg/m^3 for binary blends. This may indicate that magnesium stearate as a flowability agent has a beneficial effect on the flow of the FMS particles and their subsequent release from the formulation during aerosolisation.

The exact mechanism of how this may happen is unknown, but it may be that magnesium stearate reduces the electrostatic charge attraction between the bronze beads and FMS and lactose particles. Therefore, this frees more of the FMS particles into the atmosphere in comparison with binary formulation.

With regards to the effect of Magnesium Stearate (MgSt) inclusion in the formulation, the aerodynamic particle size data generated using the Marple cascade impactor (see Figure 44) showed differences in the distribution of FMS particles, depending on the addition of MgSt. Blends containing MgSt showed relatively higher levels of particle of FMS in the coarse fraction (diameter > 9.8 µm) versus blends without MgSt. However, blends containing MgSt showed a relatively higher percentage level of FMS particles in the fine fractions (diameter > 0.93 µm) in comparison with the blends without MgSt. Overall, the average MMAD was 2.89 µm for the MgSt containing blends, compared with the slightly higher MMAD of 2.95 µm for the blends without MgSt.

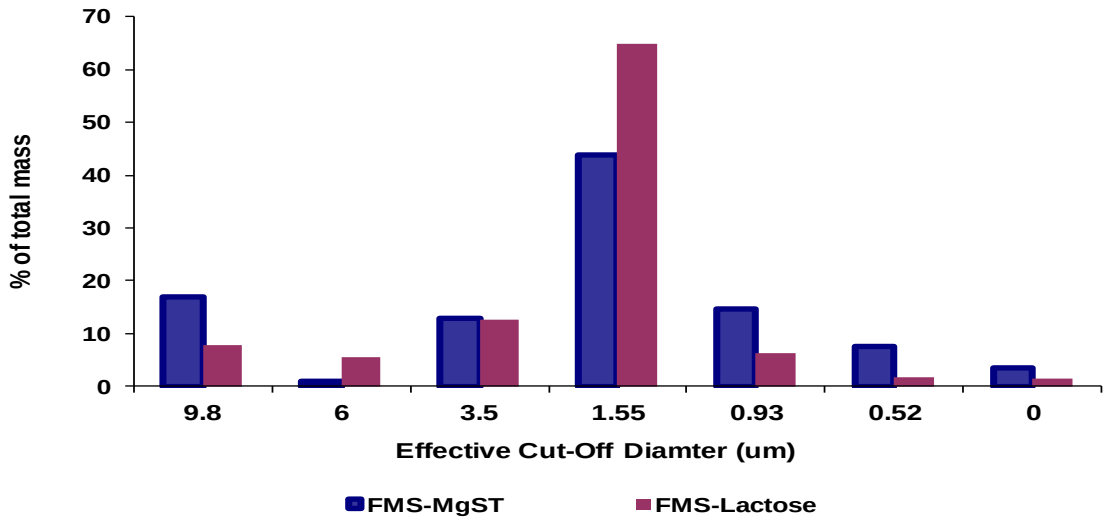

Figure 44: Aerodynamic particle size distribution of FMS formulations (0.8% FMS w/w), with and without Magnesium stearate.

This observation of increased fine particle dose using MgSt in inhaled formulations has been attributed to the influence of MgSt on the inter-particulate forces between the components of inhaled formulations. Young *et al.* (Young et al, 2002) investigated the interaction of beclomethasone dipropionate (BDP) and lactose surface modified with magnesium stearate using Atomic Force Microscopy. It was found that the separation energy of BP and MgSt modified lactose surface is significantly lower than that of BP and lactose surface without MgSt. Consequently, the *in vitro* performance of the formulations showed those formulations with magnesium stearate had a significantly higher fine particle dose.

In the present study, the *in vitro* performance of the formulations showed those formulations with magnesium stearate had a significantly higher fine particle dose. In terms of regional distribution in the IVR model, results for percentage deposition levels in the head region showed higher levels (87.5 ± 7.4%) for binary versus MgSt containing formulations (81.5 ± 3.9%). However, the difference between the two formulation types did not show a statistically significant difference (P > 0.05) (see Figure 45).

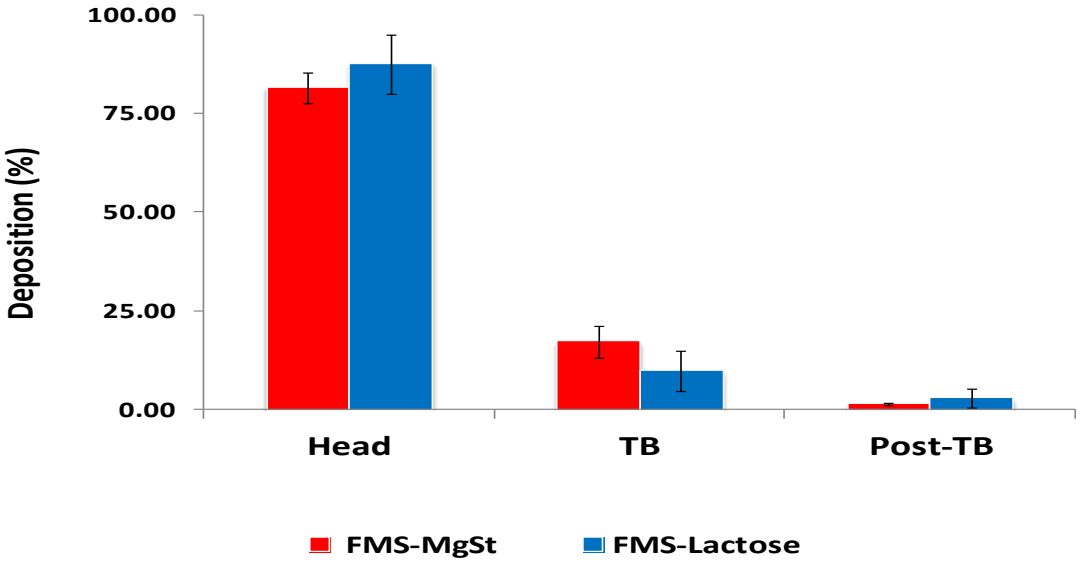

Figure 45: Comparison of particle deposition of FMS particles in the *in vitro* rat model (IVR) for FMS formulation, with (0.8% w/w FMS-MgSt) and without Magnesium Stearate (0.8% w/w FMS-Lactose). Error bars are Mean ± SD from four independent experiments.

For the Trachea-Bronchial (TB) region, higher deposition levels were shown for the MgSt containing formulation versus binary formulation: 17.2 ± 4.0 versus 9.7 ± 5.1% respectively. Although statistical significance was not achieved (p=0.06), results point to increased peripheral deposition for MgSt containing blends. Similar deposition levels were shown for the post-TB region, 2.9 ± 2.4% and 1.3 ± 0.20% for the binary and MgSt containing formulation respectively.

This observation may be explained with reference to the particle size distribution data (see Figure 44), which showed MgSt containing formulations to contain higher levels of fine particles than binary formulations. Consequently, a greater percentage level of FMS particles would be able to pass the head region and deposit deeper down the rat model in the TB region. Therefore, this data demonstrated the sensitivity of the IVR model to show the expected changes in particle deposition profiles, achieved by changes in formulation composition.

4.3 Conclusion

In this study, the influence of aerosol characteristics on deposition patterns in the *in vitro* model of a rat lung was investigated. Blends containing FMS particles of 2 µm and 4 µm size were generated in the nose-only exposure chamber. The results showed slightly higher deposition levels for the 4µm sized particles versus 2 µm sized particles in the head region: 90.8 ± 3.6% and 88.2 ± 6.6%. However, this difference did not reach statistical significance ($P > 0.05$), probably due to the polydispersity of aerosolised FMS particles. In addition, the regional deposition analysis showed an increased lung peripheral deposition with the smaller particles.

Furthermore, the effect of increasing the aerosol concentration on total deposition in the *in vitro* model of a rat lung was investigated. Results showed the expected trend of increased deposition in the model with increasing aerosol concentration.

The model was shown to be sensitive to changes in formulation composition. Binary blends containing FMS and lactose, and ternary blends containing FMS, lactose and MgSt were tested using *in vitro* model. Ternary blends produced smaller-sized FMS particles and this resulted in increased lung peripheral deposition in the *in vitro* model.

Thus, the developed *in vitro* model has been demonstrated to be sensitive to parameters known to effect the regional deposition of material in the rat respiratory tract such as size, size distribution mediated by formulation changes and aerosol concentration changes. Therefore, this model should facilitate a more complex regional deposition analysis that will benefit regional drug targeting in preclinical setting.

5 Assessing the effect of ventilation parameters on deposition in the rat model

As discussed previously (see section 1.1.2, Introduction), physiological parameters such as airflow conditions are known to strongly influence the site of aerosol deposition within the respiratory tract in both human and non-clinical species. Therefore, in order to assess the sensitivity of the IVR model with respect to changes to airflow conditions, the influence of inhalation parameters such as the breathing frequency and tidal volume on total and regional dose distribution was evaluated.

In addition, the experimental data generated using the IVR model was compared with *in silico* MPPD model predictions and *in vivo* literature data from a number of published rodent inhalation studies using particles of approximately the same size as generated in this investigation.

5.1 Study Design

A multi-factorial statistical design was implemented for this study. The parameters selected were Tidal Volume (VT, mL) and Breathing Frequency (f, min^{-1}). Typically, f ranged from 40 to 200 breaths/min, and VT between 1.4 to 4.0 mL.

Within the limits of the model selected, combinations of f and VT were evaluated (see Figure 46). These combinations are considered to be representative of the different breathing patterns which have been reported in rats (Schmid et al, 2008). For example, breathing with high VT (2.5-4 mL) and lower f (40-80 breaths/min) corresponds to deep anaesthesia, while breathing with lower VT (1.5-2.5 mL) and higher f (80-160 breaths/min) is considered to be representative of the breathing pattern of conscious animals. Conversely, breathing with large VT (4.0 mL) and low f (40-80 breaths/min) is considered to be representative of a sigh breath (Karrasch et al, 2009). Finally, a number of experimental runs (five runs) were operated under a normal rat's breathing conditions of VT of 2.1 mL and respiration frequency of 102 min^{-1} (Asgharian and Anjilvel, 1998).

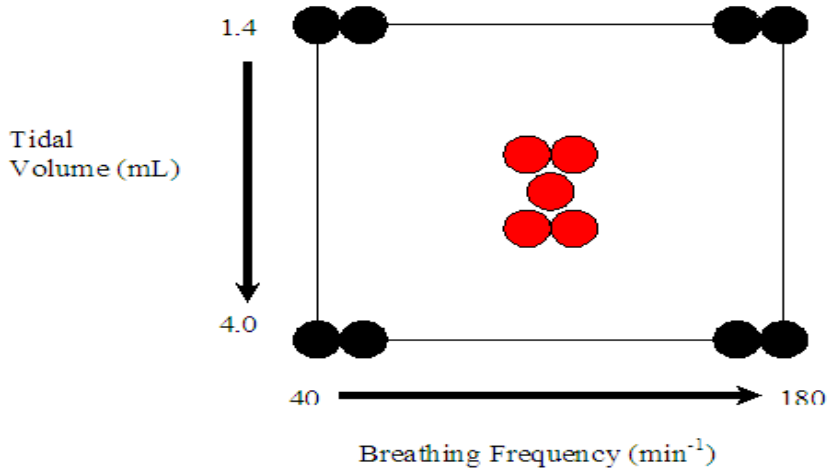

Figure 46: Schematic plot of the experimental design implemented for this investigation

The statistical design consisted of 13 experimental runs, 8 of which are for the corners of the design (2 replicates of each corner) and representative of intermediate conditions between high and low extremes, and 5 replicates for the centre point, which provide a measure of experimental variation. The resulting experimental matrix, exposure conditions and associated regional deposition levels in the IVR model for each experimental run are shown in Table 11. All experiments were carried out in randomised run order to mitigate the effect of environmental variance. The software Design Expert DX7 (Stat-Estate Corporation, USA) was employed for this work.

5.2 Aerosol generation and particle size analysis

The fluidised bed aerosol generator (FBAG) produced an average aerosol concentration of 2.2 ± 0.4 mg/m^3 for the 13 experimental runs of this study (see Table 11). This equates with an overall variability of 20.1% and is in keeping with temporal variability values of 5-19% reported in other studies of animal exposure chambers (Liden et al, 1998;Lundgren et al, 2006;Yeh et al, 1987).

In addition, particle size analysis using the Marple cascade impactor showed the average mass median aerodynamic diameter (MMAD) to be 3.1 µm and the geometric standard deviation (GSD) to be 2.10 (see Table 11). Thus, the particle size distribution generated is typical of rodent inhalation studies. This demonstrates the suitability of the experimental set-up for evaluating the deposition behaviour of test material in the *in vitro* respiratory rodent model (IVR).

This set-up also enabled the determination of the impact of breathing patterns on total and regional deposition of the IVR model to be assessed and compared against existing literature data and *in silico* predictions using the MPPD model. Full method details are listed in section 4, C - Experimental Setup.

Table 11: Table detailing the experimental conditions for each run of the IVR experiment: aerosol concentration, particle size and ventilation condition. In addition, the regional deposition levels per run are listed.

Run	Tidal Volume (V_T, *ml*)	Breathing Frequency (*f*, min^{-1})	Aerosol concentration (mg/m^3)	MMAD (µm)	GSD (µm)	% Deposition in IVR model sections		
						Head	TB	Post-TB fraction
1	2.12	103.3	1.7	2.58	1.83	86.4	10.8	2.8
2	1.91	109.0	2.1	2.63	1.81	77.3	16.4	6.3
3	2.02	106.0	1.3	3.09	2.18	93.0	5.8	1.2
4	1.40	180.0	3.0	2.80	2.12	88.0	8.3	3.8
5	4.00	40.0	2.3	3.21	2.34	70.2	20.2	9.7
6	4.00	182.4	2.7	2.88	2.08	97.7	2.0	0.3
7	1.40	40.0	2.4	2.28	1.97	80.4	10.7	8.9
8	1.21	181.6	2.1	2.93	2.08	91.8	6.5	1.7
9	4.18	43.3	2.1	4.22	2.49	75.1	13.3	11.6
10	1.50	45.2	2.7	3.97	2.30	76.8	19.2	4.0
11	3.78	177.0	2.1	3.51	2.29	98.0	1.6	0.4
12	2.38	104.0	2.0	3.44	2.26	93.1	5.6	1.3
13	2.10	103.4	2.1	3.44	2.26	90.9	6.1	3.0

5.3 Influence of ventilation parameters on lung deposition in the IVR model

The impact of the tidal volume and breathing frequency variation on the deposition levels (in µg) in the head region of the IVR model is shown in Figure 47. In general, the data reveals an increase in particle deposition levels with an increase in breathing frequency; variation in the tidal volume at low breathing frequency (40 min^{-1}) had almost no impact on the fraction of particle deposited in the head region. However, variation in the tidal volume at higher breathing frequency (180 min^{-1}) resulted in an increased fraction of particles in the head region.

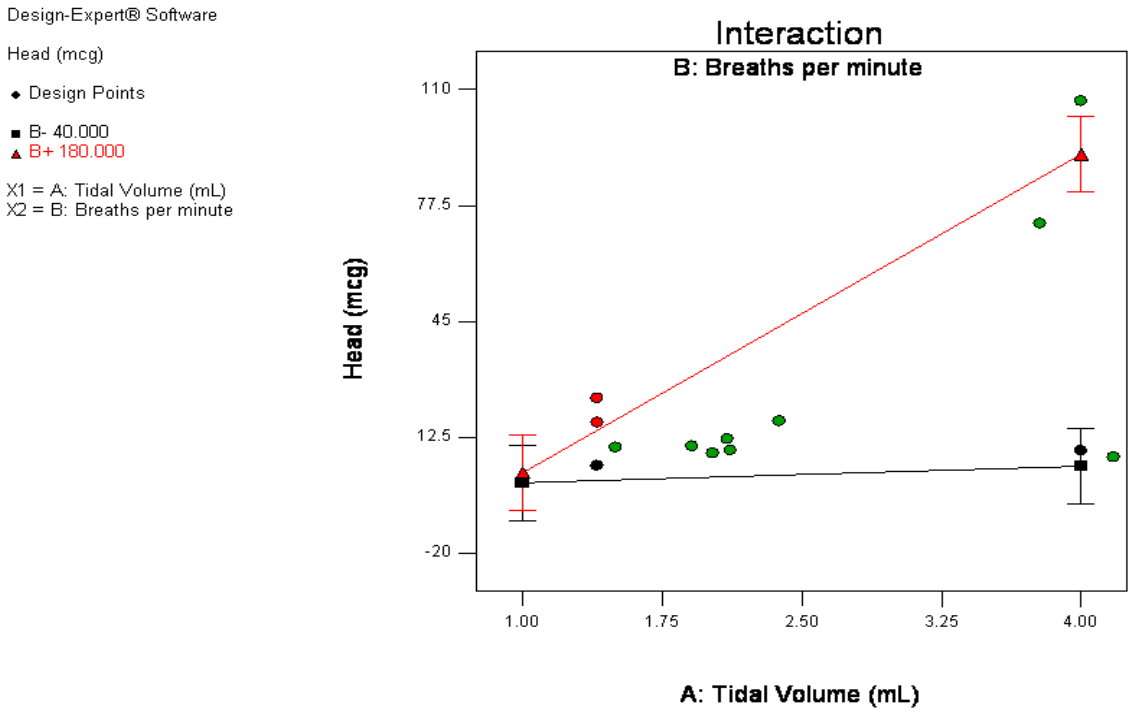

Figure 47: Interaction plot showing the effect of tidal volume and breathing frequency on absolute deposition levels (mcg) in the head region. Black line shows Head deposition levels (mcg) at 40 breaths per minute. Red line shows Head deposition levels (mcg) at 180 breaths per minute. Coloured circles represent experimentally derived data points.

The high level of deposition seen in this region may be explained if we consider that the particle deposition in the head region is governed by inertial impaction, as flow velocities in this area are relatively high and the residence time of the particle is short. Consequently, a higher particle fraction is expected to deposit in the upper regions of the model (Schulz, 1998). Other investigators have demonstrated similar trends, with higher particle deposition noted in the nasal regions in comparison with the tracheobronchial and pulmonary regions of the rat respiratory tract (Wichers et al, 2006).

The experimental data (in µg) for deposition in the head region was fitted to a statistically significant quadratic model accounting for 93.8% of the variance. The final equation to describe the deposition in the head region (*D*) as function of tidal volume (α) and breathing frequency (ß) was as follows (Equation 7):

$$D = 5.4 - 6.5\alpha - 0.2\beta + 0.2\alpha.\beta \qquad \textbf{Equation 7}$$

The effects of ventilation parameters variation on TB deposition are shown in Figure 48. The data showed that changes in tidal volume did not have a significant impact on deposition levels, whereas a reduction in breathing frequency for different tidal volumes resulted in significantly higher deposition levels. As the predominant deposition mechanisms acting in this region are inertial impaction and gravitational sedimentation, lowering the breathing frequency leads to a substantial increase in the residence time of particles in the conducting airways and greater deposition levels due to sedimentation (Schulz, 1998).

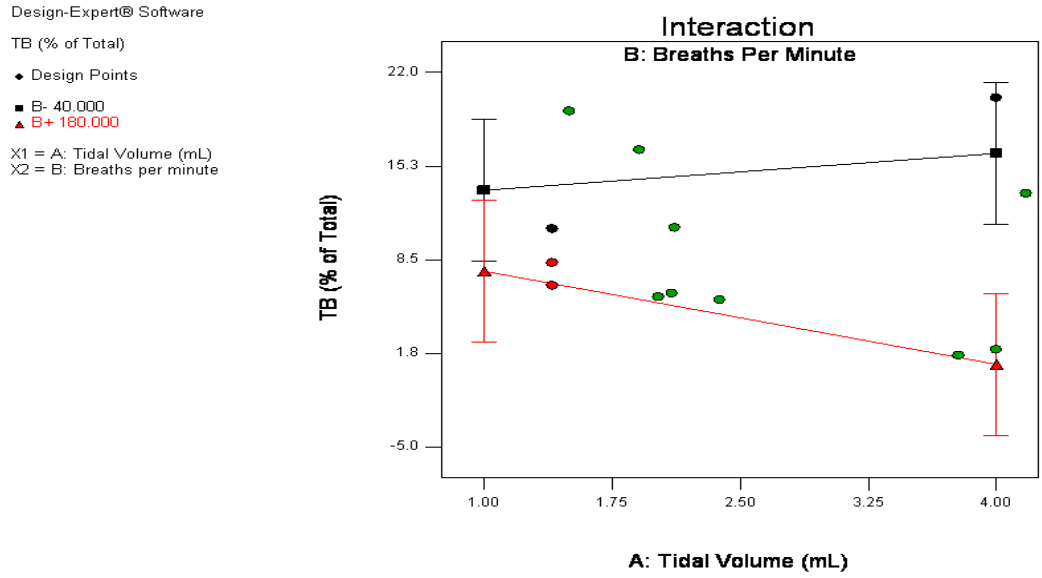

Figure 48: The simultaneous effects of two parameters, namely tidal volume and breathing frequency, on the percentage deposition in the TB region are shown in this interaction plot. Black line shows Head deposition levels (mcg) at 40 breaths per minute. Red line shows Head deposition levels (mcg) at 180 breaths per minute. Coloured circles represent experimentally derived data points.

A 3-dimensional plot visualised the relation of breathing frequency and tidal volume with deposition in the post-TB region (see Figure 49). The model identified breathing frequency as a statistically significant factor affecting deposition (P< 0.05), with the lower the breathing

frequency the higher the deposition in the pulmonary region. Whereas, variation in tidal volume in the range explored (1.4-4.0 mL) did not affect deposition in the pulmonary region.

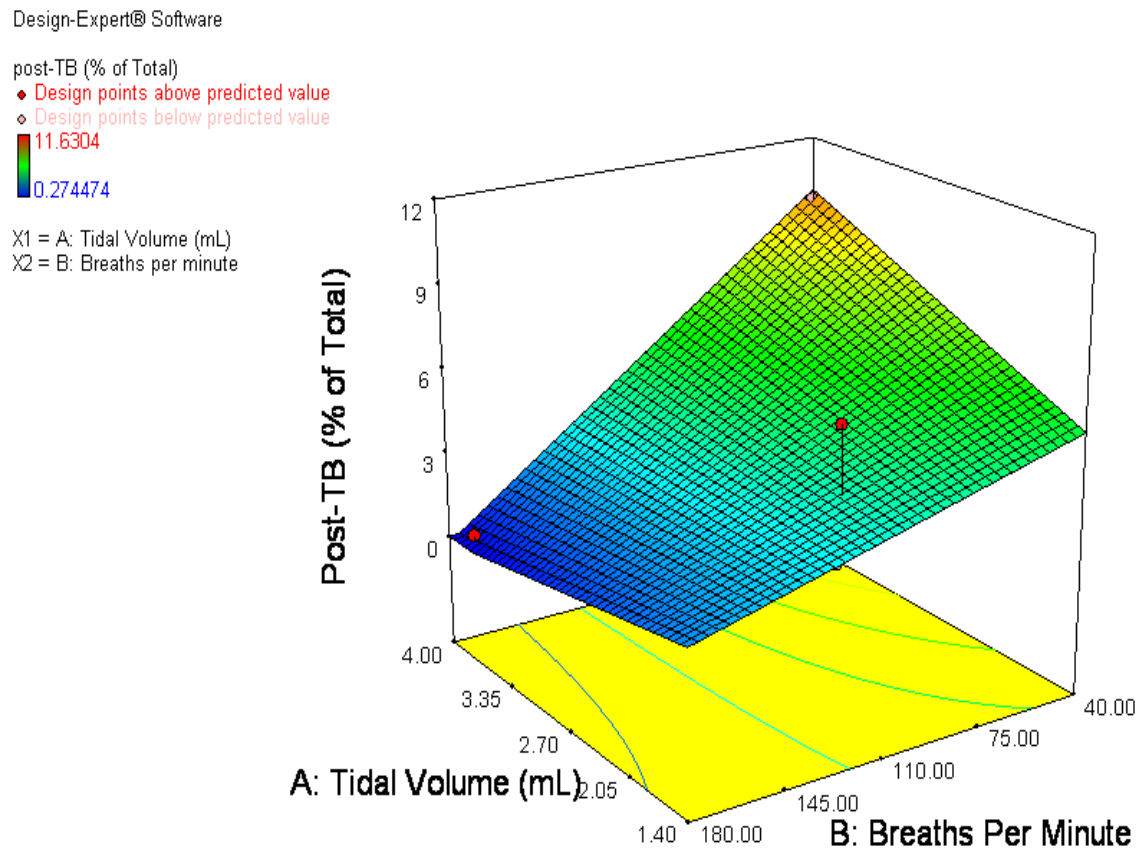

Figure 49: The simultaneous effect of two parameters, namely tidal volume and breathing frequency, on the percentage depositions in the post-TB region are shown in the 3D surface response plot. The changes in response surface colour from blue to red correspond with an increase in deposition levels. Red pins represent experimentally derived data points.

This trend is consistent with the hypothesis that, for a given particle size, the residence time in the pulmonary region is the main factor affecting deposition. Particle deposition by sedimentation and Brownian diffusion are the main deposition mechanisms in this region and both are dependent on residence time; thus, any factor which increases this time, such as reduction in breathing frequency, will result in higher deposition levels (Schulz, 1998).

5.4 Total deposition in the IVR model compared to the MPPD model predictions

After calculating the theoretical total dose of inhaled fluorescent microspheres deposited (M_{inh}) for each IVR model experimental condition, it was possible to compare this calculated dose with the measured deposition in the IVR model. In addition, comparison was made between the measured deposition to that predicted by the MPPD model using the run-specific conditions and default inputs (see Table 12).

The data showed that the experimentally determined total deposition in the IVR model underestimated the theoretical total dose prediction by an average factor of 0.86 ± 0.29 (CV= 33.2%). These findings are in line with expectations, as the theoretical model assumes 100% deposition of inhaled particles in the rat; the IVR model, on the other hand, is operated under tidal volume conditions and only a fraction of the total dose is inhaled and the remainder is exhaled. Therefore, the IVR model should underestimate the total dose deposited in comparison with the theoretical calculations.

In terms of comparison between the IVR and MPPD model predictions, the IVR model exceeded the MPPD model predictions by an average factor of 1.51 ± 0.70 (CV= 46.5%). However, the agreement between the two models is much closer when the MPPD default breathing conditions were used: 102 breaths/min for *f,* 2.1 ml for V_T. In this case, the agreement between the two models is much closer and agree with a factor of 1.08 ± 0.15 (CV= 13.6%).

Interestingly, in a study conducted by Casse *et al.* comparing the MPPD model prediction with measured pulmonary deposition levels for cadmium chloride aerosol, the MPPD model overestimated the measured pulmonary deposition when *f* and V_T were entered as experimentally determined rather than default-breathing parameters (Cassee et al, 2002).

Another study by Wichers *et al.* involving rats exposed to oil combustion-derived particulate matter showed the MPPD model to underestimate the measured pulmonary fraction by more than 60% of the measured dose. As in the study by Casse *et al.*, experimentally determined rather than default-breathing parameters were entered into the MMPD model (Wichers et al, 2006). Therefore, these findings in addition to our study, albeit for total deposition levels, may highlight the limitation of the MPPD model for estimation of the total and pulmonary inhaled dose for breathing conditions other than those under normal levels.

Table 12: Comparison between the total deposition levels for the in-vitro rat model (IVR) versus MPPD versus theoretical models estimate

Run	Aerosol Concentration (mg/m^3)	RMV[1] (L/min)	Total mass deposited in IVR (µg)[2, 3]	M_{inh}[4] (µg)	Inhaled Fraction[5]	Total mass deposited (MPPD adjusted; µg)[6]	MPPD inhaled Fraction	IVR: M_{inh} ratio	IVR: MPPD ratio
1	1.7	0.22	10.2	16.73	1	11.21	0.67	0.61	0.91
2	2.1	0.21	12.8	19.67	1	12.59	0.64	0.65	1.02
3	1.3	0.21	8.6	12.54	1	7.52	0.60	0.69	1.14
4	3.0	0.25	26.6	34.02	1	21.09	0.62	0.78	1.26
5	2.3	0.16	12.4	16.56	1	9.27	0.56	0.75	1.34
6	2.7	0.73	109.3	88.65	1	63.83	0.72	1.23	1.71
7	2.4	0.06	5.6	6.05	1	2.43	0.40	0.93	2.30
8	2.1	0.22	18.2	20.76	1	12.46	0.60	0.88	1.46
9	2.1	0.18	9.2	17.09	1	9.91	0.58	0.54	0.93
10	2.7	0.07	12.5	8.24	1	3.62	0.44	1.52	3.45
11	2.1	0.67	73.8	63.23	1	42.36	0.67	1.17	1.74
12	2.0	0.25	18.3	22.28	1	14.03	0.63	0.82	1.30
13	2.1	0.22	13.2	20.52	1	12.52	0.61	0.64	1.05

1. RMV: Respiratory Minute Volume
2. Duration of exposure: 45 minutes.
3. Average body weight of rats: 0.37 kg
4. M_{inh}: calculated theoretical total dose of inhaled fluorescent microspheres deposited for each IVR model experimental condition
5. This is assumed to be 100% for particles < 7 µm.
6. Predicted using both rat-specific and default inputs.

5.5 Regional deposition in the IVR model compared to the MPPD model predictions

The percentage deposition level of FMS particles in the IVR and MPPD model for the five replicate centre point experimental runs were compared (see Figure 50). These runs used a tidal volume of 2.1 mL and breathing frequency of 102 min^{-1} to mechanically ventilate the IVR model. These ventilation settings are the default settings for the MPPD model (Asgharian and Anjilvel, 1998). The aerosol concentrations levels (mg/m^3) and particle size distribution (µm) for all the replicate runs were input into the MPPD model in order to generate regional distribution predictions for the inhaled dose of FMS particles.

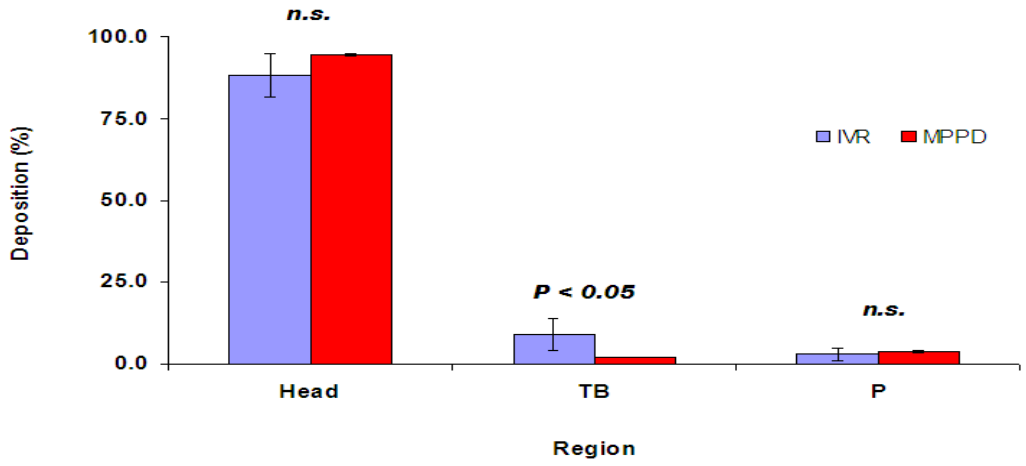

3

Figure 50: Plot showing regional deposition of FMS particle deposition in the different regions of the rat's respiratory tract: Head, Tracheobronchial (TB) and Pulmonary (P) regions in the IVR and MPPD models. For the IVR model, the pulmonary fraction refers to the percentage of particles in the diaphragm placed at the rear of the TB section of the model. Error bars are Mean ± SD from five independent experiments.

The results showed good agreement between the IVR and MPPD model with regards to the regional distribution of the FMS particles, especially for the head region. In both cases, the highest deposition levels were seen in the head region, with 88.14 ± 6.63% and 94.50 ± 0.34% deposition recorded for the IVR and MPPD model respectively (P = 0.065).

For the tracheobronchial region, much higher deposition levels were noted for the IVR (8.93 ± 4.7%) in comparison with the MPPD model (1.85 ± 0.16%), ($P<0.05$). This difference may be attributed to the higher deposition levels in the head region for the MPPD in comparison with the IVR model, as the head region acts as a highly efficient filter in removing the majority of the inhaled FMS particles. Consequently, the fraction of particles reaching the TB region will be relatively reduced for the MPPD in comparison with the IVR model owing to the higher head filtration efficiency of the former.

For the pulmonary region, comparisons between the fraction of FMS particles collected in the diaphragm section post the tracheobronchial region of the IVR model and the pulmonary region of the MPPD model were made. In the case of the IVR model, the current limitations of the µ-CT scanning technology did not enable scanning much beyond generation 4 of the model to be made. Hence, the amount of particles collected in this section may be regarded as containing a combination of particles collected in the TB and pulmonary fractions. Therefore, the results generated for this region should be treated with some caution and not interpreted as being absolutely reflective of actual deposition in the pulmonary region.

Nonetheless, despite these limitations for a direct comparison between the two models, similar deposition fractions were observed for both with 2.92 ± 2.05% and 3.69 ± 0.23% deposition recorded for the IVR and MPPD model predictions respectively ($P > 0.05$). Overall, there is reasonable general agreement for regional deposition in the rat respiratory tract for the inhaled FMS particles between the two models.

5.6 Deposition in the IVR model compared to *in vivo* data from literature

The measured deposition levels in the Lung region of the IVR model versus changes in the breathing frequency were compared with data from a number of published rodent inhalation studies, which used particles of approximately the same size as generated in this investigation (MMAD: 2-4 µm) (Asgharain et al, 2003;Benson et al, 1994;Karrasch et al, 2009).

For the purpose of this comparison, the Lung region is regarded as consisting of the sections in TB and post-TB regions of the IVR model. This definition is required, as the *in vivo* data for pulmonary deposition of particles is generally stated in the literature as lung fraction and contains particles deposited in both the tracheobronchial and pulmonary region. Therefore, in order to generate a valid comparison, the fraction of particles deposited in the TB and post-TB region of the IVR model were summed and compared with the corresponding literature data. Additionally, the corresponding MPPD predicted levels (TB and Pulmonary fractions) for the IVR settings were included for comparison (see Figure 51).

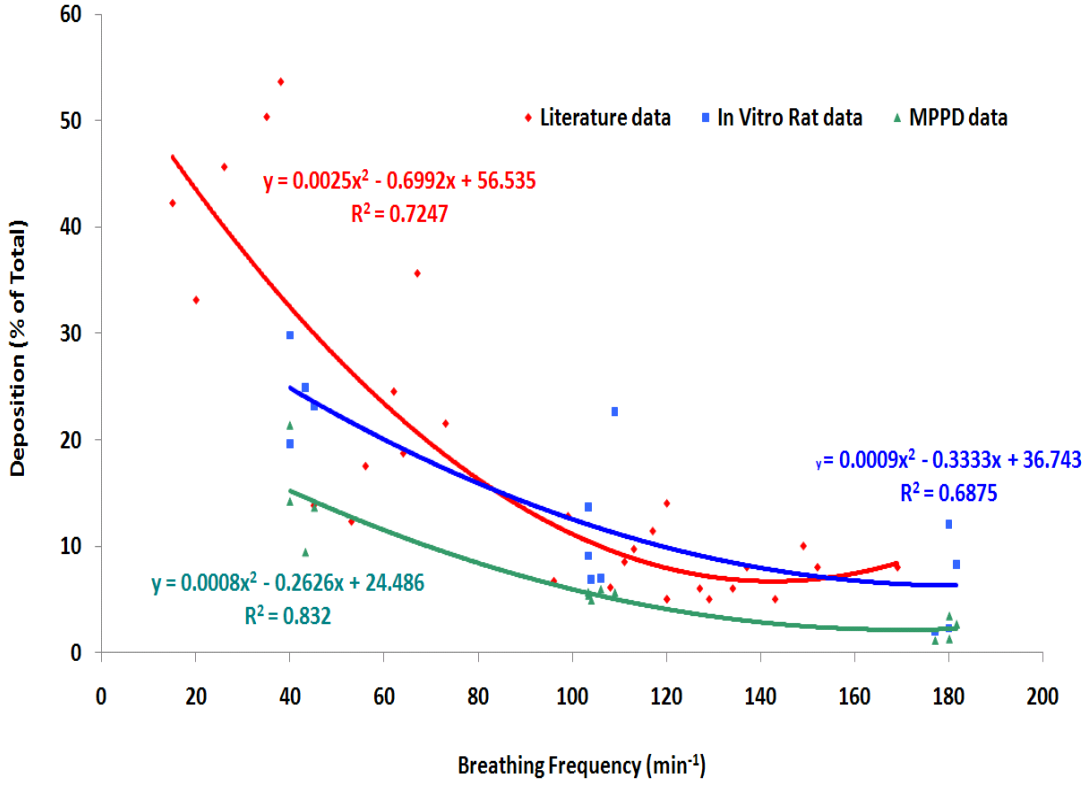

Figure 51: Comparison of Lung deposition in the in *vitro* rat model Vs literature Vs MPPD data. Literature data sources (Asgharain et al, 2003;Benson et al, 1994;Karrasch et al, 2009).

In general, the data shows an inverse relationship between the measured breathing frequency of the rats and deposition in the pulmonary region, a trend which is consistent for all three data sets. The MPPD predicted levels are consistently the lowest of the three sets and across the entire range of breathing frequencies under evaluation. This observation is in general agreement with a number of published studies, which showed the MPPD model to consistently underestimate deposition in the lung region (Cassee et al, 2002;Wichers et al, 2006).

Notably, the data for the IVR model is in good agreement with data published in *in vivo* rodent studies. This is despite the fact that the data pool from rodent studies assessing the deposition in the pulmonary region are relatively scarce and show greater levels of variability in comparison with the extrathoracic and tracheobronchial regions.

5.7 Impact of polydispersity of aerosolised FMS particle on the variability in experimental data

Some of the variability exhibited in the IVR model, especially for the post-TB region, can be attributed to variations in the particle size characteristics of the FMS particles aerosolised in the exposure chamber. Despite using monosised FMS particles as input material with a Geometric diameter of 2 um and GSD of 1.2, the resultant particle size distribution of FMS particles in the exposure chamber varied from 2.28 to 4 microns for MMAD and 1.81 to 2.49 microns for GSD, indicating that polydisperse aerosols of FMS particles were produced. This can be attributed in part to the inefficiency of the FBAG aerosol generator system used in our experimental setup to adequately de-agglomerate the FMS particles.

However, it is expected in principle that the regional distribution of polydisperse aerosol should exhibit the same trend as the corresponding distribution levels for monodisperse MMAD-aerosol, with the fraction of particles deposited in the head and pulmonary region flattened out to some extent (Rudolf, 1988).

In addition, various models of particle deposition in the respiratory tract of rats show that, for particles in the range of 3 to 10 micron, most particles will deposit in the extrathoracic region. This trend has been demonstrated in the experimental data for this study (see Figure 50) (Schmid et al, 2008).

5.8 Limitation of the IVR model

The present IVR approach also has some limitations. Firstly, the model is based on scans up to generation four of the rat respiratory tract as this represents the current limits of the micro-CT scanning technology. Thus, particle deposition in deeper lung regions might not be reflected precisely in the IVR model.

Secondly, the current model does not take into account lung clearance. However, data on mucociliary clearance is sparse and is generally not reflected accurately in silico models. Consequently, the results generated using this IVR model for drug molecules with high mucociliary clearance rate should be treated with some caution.

A further limitation of the IVR model is that it does not account for hygroscopic growth of particles in the rat's respiratory tract. It is known from studies in human airways that drug particles can change in size during respiration due to the high relative humidity and this, in turn, can lead to a change in the total and lung deposition profile (Londahl et al, 2007).

This is a common limitation of most deposition models with the exception of the recently proposed model by Ferron *et al.* (Ferron et al, 2013). In this model, the effect of hygroscopicity on lung deposition in rat and human airways was demonstrated for inorganic salts and three drugs, representing large, medium and small particle growth in humid air.

5.9 Conclusions

An *in vitro* deposition (IVR) model for the respiratory tract of rats has been developed. Studies using this model with polydisperse fluorescent microsphere particles (MMAD; 3.1 µm, GSD: 2.1) showed it to be sensitive to changes in breathing parameters, especially respiratory frequency (f), where the data showed an increased pulmonary deposition with decreased respiratory frequency. This observation is in good agreement with previously published *in vivo* rodent studies for particles of the same size.

Comparison of the experimental data for total and regional deposition levels with predicted outputs using the *in silico* MPPD model showed reasonably good relative agreement between the two models. The predictions were closest to the experimental values, when default respiratory conditions of 102 breaths/min and tidal volume 2.0 mL were used. To summarise, the reasonably good agreement of the data generated with our IVR model and the MPPD model, together with the high correlation with *in vivo* data of the rat, support the validity of our rat respiratory tract model. Using the IVR model allows an easy, fast and reasonably precise estimation of the inhaled dose in rodent inhalation studies.

The IVR has the potential to be used along with live rats in an inhalation rig in pulmonary pharmaceutics research. Thus, it provides the unique possibility to run an internal standard for dose deposition in the respiratory tract in each inhalation experiment. This should contribute to a greater understanding of drug pharmacokinetics and dynamics in rats; it may also improve dose extrapolation from animal to man and interpretation of data from rodent inhalation studies.

6 Comparative deposition of inhaled aerosols in experimental rats and *In Vitro* rat lung model

Previous studies have shown the IVR model to exhibit the expected regional distribution of particles mediated via alteration of particle properties, such as changes in particle size, dose and formulation composition (see section 4, B-Results and Discussion). In addition, the model was shown to be sensitive to changes in breathing parameters such as breathing frequency and tidal volume changes (Ahmed et al, 2012). However, for the model to be used routinely in drug development, extensive validation in terms of the comparison of deposition levels with *in vivo* rats needs to be demonstrated. Thus, the work outlined in this section aims to address this issue.

The most complete data set to date on total and regional particle deposition in the rat lung is that published by Raabe *et al.* (Raabe et al, 1988). This study was conducted with monodispersed radio-labelled aerosol particles in the range of between 0.5 and 5.0 µm MMAD, and results showed the majority of particles to be deposited in the head and stomach of the rodents. For peripheral deposition, an inverse relationship with particle size was demonstrated, with the highest deposition level (8.75%) recorded for 1.0 µm sized particles and lowest deposition levels (4.60%) recorded for 5.0 µm sized particles. Other investigators have noted similar deposition levels; for instance, in a study by Dahlback *et al.* (1998), rats were exposed to a polydisperse Evans blue aerosol generated from an air jet nebuliser and the estimated total deposition, lung burden and the site of deposition within the lung were determined. Twenty per cent of the total deposition of Evans blue droplets was found in the lung and 80.0% in the extrathoracic region (Dahlback et al, 1989).

Furthermore, the majority of the published deposition studies in preclinical species have been conducted with monodispersed aerosols (Asgharian and Anjilvel, 1998;Raabe et al, 1988). This is in contrast to the majority of current inhaled pharmaceutical aerosols, which are primarily polydisperse. Therefore, there is a potential that existing models based on this data, such as the *in silico* MPPD model, may not accurately predict the deposition of today's polydisperse aerosol.

For this work, the IVR model was placed onto the exposure chamber concurrently with live rodents exposed to a range of test materials. The intended inhaled dose delivered to the rodents' lungs ranged from 100 to 1000 µg/kg/day. In addition, ranges of particle size were delivered to the rodents and *in vitro* rat, from approximately 1.77 to 5.21 µm MMAD (GSD> 1.2). Thus, this wide range of MMAD should cover the particle size distribution of the majority of today's pharmaceutical aerosols.

Specifically, the following aims were investigated:

1. Compare the lung deposition in the IVR model versus the standard tissue analysis method of measuring the drug concentration in lung homogenate samples.

2. Compare the regional deposition profile generated using the IVR model with the MPPD model estimates for the same test material and exposure conditions.

3. Assess the effect of formulation characteristic on deposition levels in the IVR, *in vivo* and *in silico* models. For this investigation, compound X formulated with either a micronised or spray-dried form of the drug substance served as the test material.

4. Combine the deposition data from all studies conducted using the IVR model to assess the effect of the particle size on lung deposition. In addition, where available, the corresponding data from lung homogenate samples and MPPD estimates will be included in order to provide a comparison for all three models.

6.1 Study design

Rats were exposed to aerosol drug materials as part of routine preclinical studies undertaken to assess the safety and efficacy of inhaled compounds. As part of these studies, the IVR lung model was placed onto the exposure chamber in order to evaluate the ability of this model in estimating the total lung dose as well as its distribution in the lung. Both the IVR model and live rats were exposed to the same test compound and for the same duration of exposure (see Figure 52). After exposure, the IVR model was removed from the rig, disassembled and its sections washed down with appropriate solvents and assayed for drug content.

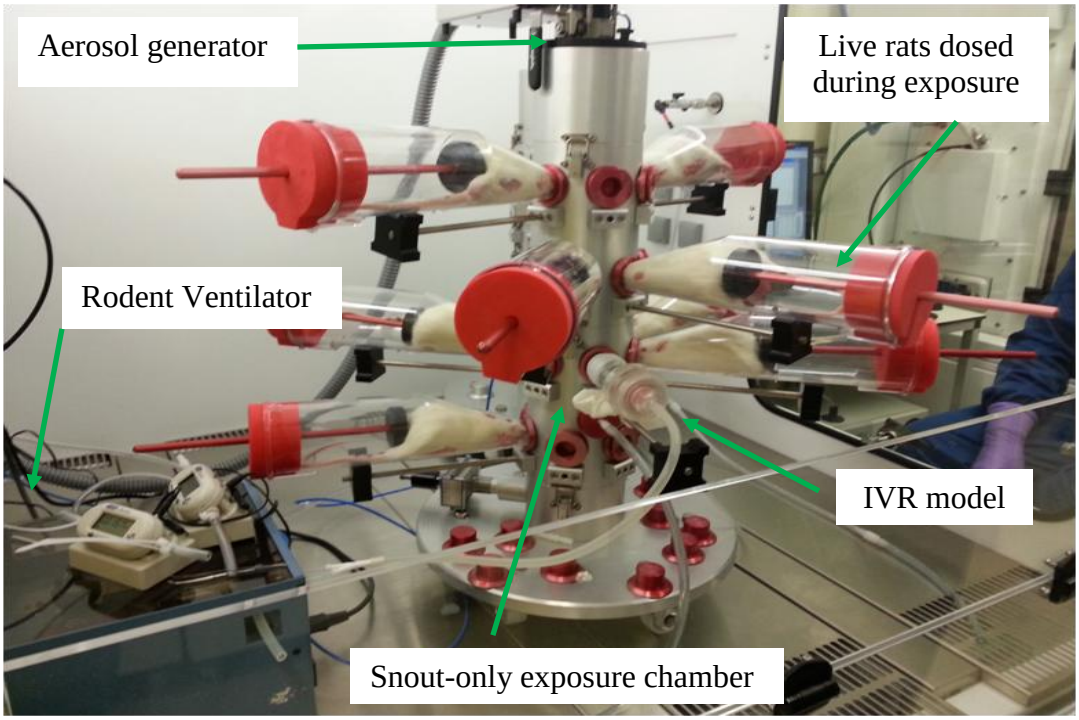

Figure 52: Photograph of the exposure setup used to evaluate the performance of the IVR model as part of live dosing studies exposing rats to various inhaled compounds.

For comparison with the lung concentration data, deposition from rats sacrificed immediately after exposure (IAD) was assessed in order to minimise the impact of mucociliary clearance on the results. In addition, it should be noted that, in order to generate additional replicate data points for the IVR model for each exposure scenario tested, the IVR was placed onto the exposure chamber on occasions other than when the live rat IAD samples were taken. However, on such occasions, the exposure atmosphere in terms of target dose, aerosol concentration and particle size distribution was the same as in the IAD exposure occasions. Full details of the method are described in section 5, C-Experimental Setup.

6.2 Total deposition in the IVR model compared to estimates of total deposition based on filter samples

The total masses of aerosol particles deposited in the IVR model for the three drug compounds tested were compared with the theoretical estimates of the total inhaled dose (see Table 13). In the absence of a direct measure of total drug burden in the body, a theoretical calculation based on the aerosol filter concentration readings, breathing conditions and duration of exposure was used to estimate the total inhaled dose (see Equation 8). The data showed that the experimentally determined total deposition in the IVR model underestimated the theoretical total dose prediction by an average factor of 0.70 ± 0.35.

This estimate of total deposition (70.1 ± 34.6%) provided by the IVR model was compared with theoretical predictions provided by two studies assessing particle deposition in the respiratory tract of rats (Koblinger and Hofmann, 1995;Schmid et al, 2008). Both of these *in silico* models showed total deposition profiles fitting the well-known, bell-shaped filter efficiency curve, with approximately 100% deposition for particles smaller than 0.01 µm and larger than 10.0 µm. However, in the range of particle size between 3 and 10 µm, which is the closest to the particles tested in the IVR studies, deposition levels of 70.0% and greater of total inhaled particles were predicted. Therefore, the data provided by the IVR for total deposition is in good agreement with the range of theoretical predictions provided by these *in silico* models.

The variability shown in the *in vitro* rat model data may be attributed to a number of factors. Firstly, a major source of variability is driven by changes in the aerosol concentration readings taken from the filter samples from compound-to-compound; these are estimated to be 12.4 and 21.1% CV for the filter and IVR samples respectively. Second, differences in the sampling flow rates between the two methods may have contributed to the variability (see section 5.5, C-Experimental Setup). For filter samples, the flow rate was set at 2.0 L/min for the majority of experiments with the exception of the fluticasone propionate (MMAD < 2 µm) experiments, where a flow rate of 0.20 L/min was employed. For the IVR experiments, however, the sampling flow was set at 0.214 L/min in order to simulate typical ventilation conditions for the rat. In addition, differences in duration of exposure between the two methods may have played a role; for example, a duration of two minutes was used for filter samples and for the entire duration of exposure in the case of the IVR models.

Table 13: Comparison between the total deposition levels for the *in vitro* rat model (IVR) versus theoretical models estimate

Test compound	Target Dose (µg/kg/Day)	Aerosol Concentration (mg/m^3)	Duration of exposure (min)	Size distribution (MMAD + GSD)[1]	Estimated Delivered Dose(µg)[2,3,4]	Total mass deposited in IVR (µg)	IVR: Estimated Delivered Dose ratio	Number of IVR Samples Tested
Compound Y, Micronised	1000	28.0 ± 9.1 (CV: 32.6%)	60	2.22 ± 2.39	439.3 ± 160.1	177.7 ± 68.0 (CV: 38.3%)	0.42	6(3 x 2)[5]
Fluticasone propionate (MMAD > 4um)	100	5.0	18	4.9 ± 2.65	23.6	23.6	0.90	1
Fluticasone propionate (MMAD > 4um)	1000	78.8 ± 14.5 (CV: 18.4%)	18	3.90 ± 3.99	371.1 ± 68.3	214.3 ± 0.90 (CV: 0.4%)	0.59	2
Fluticasone propionate (MMAD < 2um)	100	5.1 ± 0.2 (CV: 3.9%)	18	1.80 ± 1.60	23.9 ± 1.0	31.1 ± 7.4 (CV: 23.8%)	1.33	3
Fluticasone propionate (MMAD < 2um)	1000	34.7 ± 7.3 (CV: 21.0%)	18	1.90 ± 1.50	163.7 ± 34.4	88.4 ± 30.5 (CV: 34.5%)	0.57	2
Compound X, Micronised	600	14.3 ± 0.3 (CV: 2.0%)	30	5.28 ± 2.55	224.6 ± 4.4	194.4 ± 49.3 (CV: 25.4%)	0.87	2
Compound X, Spray-Dried Form 1	600	14.9 ± 1.1 (CV: 7.1%)	30	2.46 ± 2.96	219.1 ± 16.7	218.8 ± 45.3 (CV: 20.7%)	0.95	2
Compound X, Spray-Dried Form 2	600	13.7 ± 0.2 (CV: 1.6%)	30	1.77 ± 3.22	214.4 ± 3.4	136.5 ± 6.4 (CV: 4.8%)	0.64	2

1. Average particle size distribution determined for dosing group.
2. Calculated theoretical total dose of inhaled test compound deposited in rat lung.
3. Respired minute volume (L/min) = 0.608 x $BW^{0.852}$ (Alexander et al, 2008).
4. Based on average body weight of 372 g of IVR model.
5. Two IVR samples were taken per exposure period; one sample covered an exposure period of 0-30 minutes, the second sample covered an exposure period of 30-60 minutes.

6.3 Lung region comparison between IVR model, live animals and *in silico* MPPD model

Differences in how the various anatomical structures of the rat respiratory tract are grouped to represent the main regions of the rat airways, namely the Head, Trachea-Bronchial (TB) and Pulmonary (P) regions for the three models under investigation, mean direct comparison between them is very difficult. This is especially the case for the pulmonary region comparison between the *in vivo* and *in vitro* data (see Table 14).

Table 14: Comparison between IVR, *in silico* MPPD and *in vivo* models in terms of anatomical structures covered.

Region	**Rat respiratory system models**		
	***In vitro* (IVR)**	***In silico* (MPPD)**	***In vivo***
Head	Nose, Nasophyarynx	Nose, Nasophyarynx	Not determined
TB	Trachea, Bronchi and Bronchioles	Trachea, Bronchi, bronchioles , terminal bronchioles	Trachea, First few Bronchi
P	Collection diaphragm to capture particles deposited past TB section of the rat model	Alveolar duct, Alveolar sac, Alveoli	Remaining Bronchi, terminal bronchioles Alveolar duct, Alveolar sac, Alveoli

For the *in vivo* data, the lungs are dissected into the trachea and bronchia and the left and right lungs. As the lung fraction contains some anatomical features of the TB region, such as the remaining portion of bronchus which could not be dissected, the lung region will contain some drug particles deposited in the TB region.

For the IVR model, the TB portion is made up of sections 3, 4 and 5 (see Figure 37). In addition, some of the anatomical features considered to be representative of the pulmonary region, such as terminal bronchioles, are also present in section 5 of the model. Therefore, it is not possible to have an accurate head-to-head comparison between the pulmonary fractions for both models due to the overlap of these anatomical features.

Thus, in order to overcome these differences between the two models, drug depositions in the TB (S3, S4 and S5) and diaphragm sections of the IVR model were combined. This combination provides a general estimate of drug deposition in the *in vitro* rat lung as opposed to deposition

in the Head region (S1 and S2). However, although combining the deposition data in this manner does not allow for a distinction between deposition in the TB and peripheral lung regions, it does permit for a direct and valid comparison between the *in vitro* and *in vivo* lung deposition data.

In terms of comparison with the MPPD model, a head-to-head comparison for the Head region of the IVR model (sections 1 and 2) with the MPPD model outputs for the same region was possible. For the *in vivo* data, the amount of particles deposited in the Head region was not determined, so a comparison between the IVR and *in vivo* and MPPD was not possible.

For the TB region comparison, the MPPD model covers anatomical structures from the Trachea (generation 1) to the terminal Bronchioles (generation 22). For the IVR model, however, the anatomical structures covered in this section are up to the level of the respiratory Bronchiole (generation 4).

For the pulmonary region, the MPPD model covers anatomical structures of the Alveolar duct, Alveolar sac and Alveoli. Whereas, for the IVR model, a collection diaphragm is placed to capture particles deposited past the TB section of the rat model, which may be regarded as representing the particles collected in the peripheral region of rat airways (referred to as the Post-TB region).

6.3.1 Comparative lung deposition

This section compares the lung deposition levels (absolute and percentage) in the IVR model versus corresponding levels in the lung tissue, as well as estimates using the *in silico* model: MPPD. Full details of the methods used to measure the deposition in the *in vivo* lung tissue, IVR and MPPD models are described in sections 5.7, 5.9 and 3.4, C-Experimental Setup respectively.

6.3.1.1 **Lung deposition in the IVR model versus *in vivo* lung homogenate data**

The mass of aerosol particles deposited in the lung portion of the IVR model (TB and Post TB sections) was compared with the corresponding mass of particles deposited in the lung and tracheal portions of the rat lungs, sacrificed immediately after exposure in order to minimise the impact of mucociliary clearance on the results (see Figure 53).

The data for both methods was normalised to the weight of rats in order to remove the body weight of rats as a possible factor in confounding the results. For the live rats, the average weight was recorded to be 376.7 ± 82.64 g, whereas for the IVR model the average weight of the rats, upon which the model was constructed, was 372 ± 56 g (see section 5.1, E-Appendix).

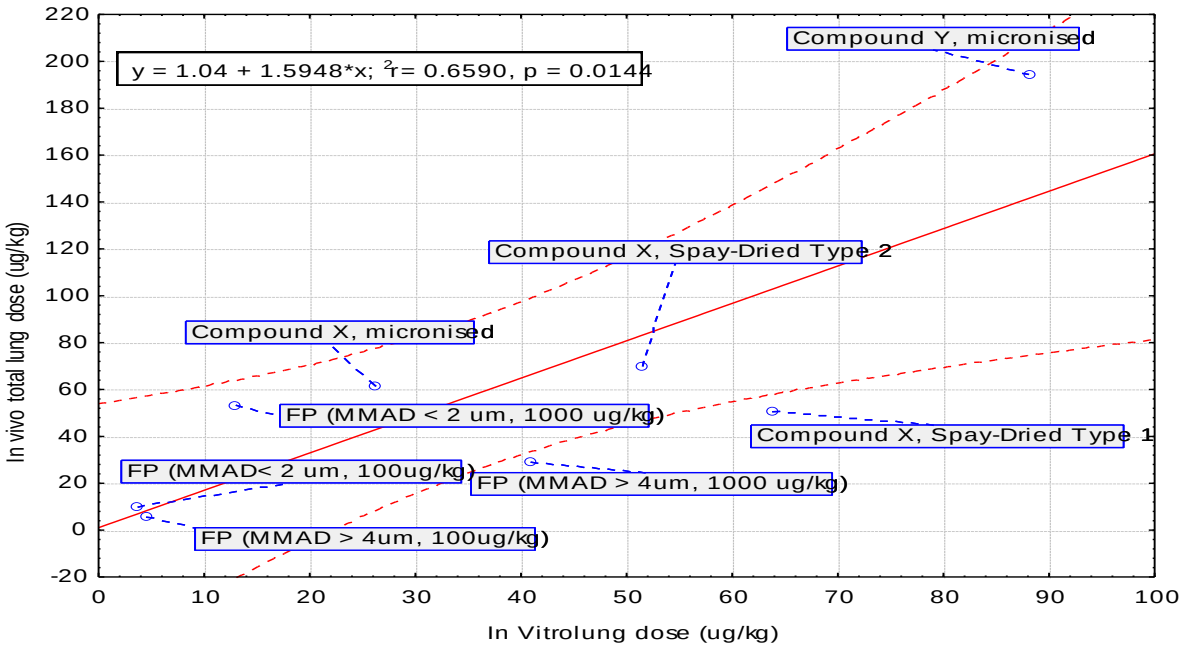

Figure 53: Plot of linear regression with 95% confidence intervals (dashed lines) for the relationship between drug dose deposited in the *in vitro* rat lung (IVR), and the corresponding measured drug dose in the lung tissue of a rat exposed to the same test materials during exposure period. Values for *in vivo and in vitro* data points are presented as average absolute figures (µg) relative to body weight (kg). Number of replicates: Compound Y, *in vivo* = 3, *in vitro*= 3. Compound X (all forms), *in vivo* = 3, *in vitro* = 2. FP (MMAD > 4 um) 100 and 1000 µg/kg, *in vivo* = 2, *in vitro* = 2. FP (MMAD < 2 um) 100 and 1000 µg/kg, *in vivo* = 3, *in vitro* = 2.

The data indicates a reasonably strong and significant correlation existed between the measured lung dose in the IVR model and the actual lung dose for all compounds tested (R^2 = 0.66, $P < 0.05$). In addition, predicted lung doses were within 2-folds of the measured lung deposition values. With respect to the comparison between the two methods, there are a number of potential causes for the differences and general underestimation of the lung dose in the IVR in contrast with the *in vivo* lung data.

Firstly, the regional deposition data generated using the IVR model tended to show high deposition levels in the head region (> 85.0% of total inhaled; see Figure 55). This may be due to the highly convoluted nature of the airway passages in the nasophyarynx region of the model, which may lead to a high relative deposition of particles in this region due to impaction and agglomeration mechanisms. Consequently, the relative deposition of particles in the regions downstream of the head section is reduced. This may account for the general trend of underestimation of deposition in the peripheral regions of the lung, in comparison with *in vivo* lung deposition data.

Secondly, differences in the segmentation of the lung fraction between the two methods may be account for some of the divergence in the data. The IVR model was based on micro-CT scans up to generation four of the rat respiratory tract; here, the lung fraction is composed of particles collected in the TB, as well as particles exiting the TB section and possibly reaching the lung (referred to as the Post-TB section). This is in contrast to the *in vivo* lung tissue analysis methodology, where the whole lungs, including some sections of the bronchial tree as well as the main lung lobes, are dissected, homogenised and the drug content determined. Thus, it is reasonable to expect the total surface area available for the collection of particles in the IVR model to be significantly less than that of the *in vivo* situation; consequently, the total amount of drug likely to deposit in the IVR is much less than that in the *in vivo* situation.

Thirdly, some of the differences in results may be explained due to differences in the ventilation parameters between the two methods. For the IVR, the breathing conditions were fixed at a respiratory minute volume of around 0.20 mL/min during the exposure period. However, for the live rat, the breathing conditions were not monitored during the same exposure period, and may have been different. As it is known that changes in ventilation conditions have a marked effect on deposition level, it may be that differences in this factor could account for some of the apparent differences in lung deposition levels observed (Kuehl et al, 2012;Schulz, 1998).

Other possible causes include the effect of mechanical clearance mechanism and particle dissolution on the *in vivo* lung deposition data. Studies assessing the rate of clearance in rat lungs have shown retention half-times in the TB region to vary from one to two hours (Hofmann and Asgharian, 2003). However, clearance from the alveolar region is much slower with retention half-times of 60 to 80 days (Brown et al, 2005). Thus, the extent to which the drugs are retained in the *in vivo* lungs is likely to vary to some degree, particularly for the TB region, as the duration of exposure for the drugs tested in this investigation varied from 18 to 60 minutes (see Table 13). This is in contrast with the IVR model, which does not account for clearance; thus, the amount deposited in the lung is likely to provide an overestimate in comparison with the *in vivo* situation.

Furthermore, differences in the strains of rats used in both methods, namely Sprague-Dawley for the IVR model and a combination of Sprague-Dawley and Wistar Han for *in vivo* rats, may have contributed to some of the differences in lung deposition levels observed for the two methods.

However, studies assessing the effect of strain differences of rat lung morphology on lung deposition are scarce. Nonetheless, a study by Hoffman *et al.* comparing the TB geometry of Long Evans and Sprague-Dawley rats revealed some differences, as well as similarities, between the two strains. Excellent agreement was found for branching angles and airway lengths, whereas the diameters were somewhat smaller for Sprague-Dawley rats (Hofmann et al, 1999). Therefore, it would be logical to assume that these differences in lung morphology may affect lung deposition and hence contribute to some of the variability seen in the data, both between *in vivo* rats and between IVR and *in vivo* rats.

Nonetheless, knowing the already discussed variability in biological systems and the multiple components required to estimate lung doses, it seems that the IVR predictions within 2-fold of the measured *in vivo* lung values, and $R^2 = 0.66$, would seem very reasonable.

6.3.1.2 Fractional lung deposition comparison in the IVR model versus *in vivo* lung homogenate data versus *in silico* MPPD estimates

For fractional deposition comparison, the amount of drug deposited in the lung sections of the IVR model (TB + post-TB) was expressed as a percentage of the total inhaled dose. This was then compared against the corresponding *in vivo* lung data, as well as estimates using the MPPD model (see Figure 54). Further details of the individual data determinations for the *in vivo* and IVR methods are listed in Section 5, E-Appendix. For details of the determinations of the MPPD data, see Table 15. The data revealed a number of interesting trends.

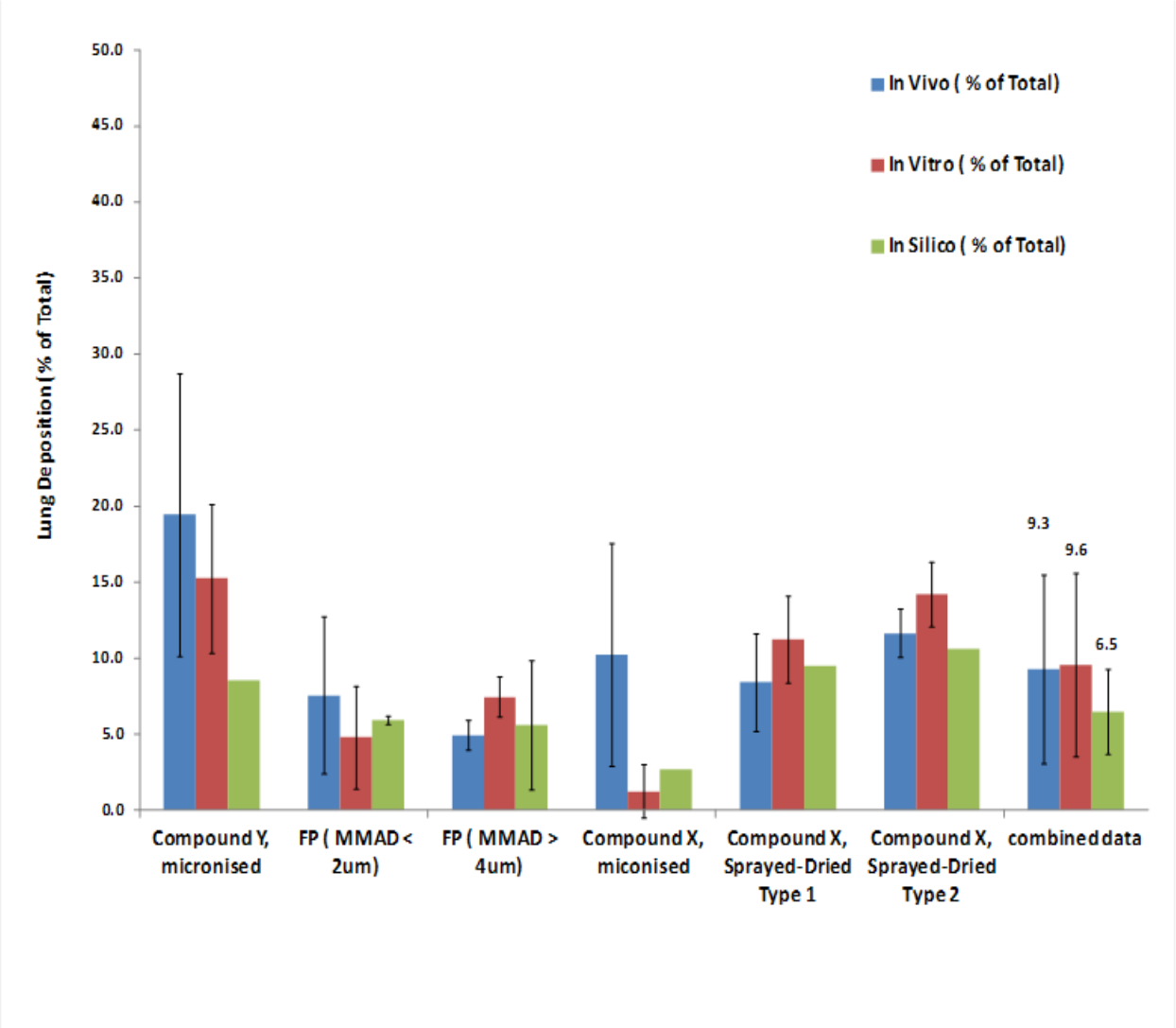

Figure 54: Comparison of the relative deposition levels assayed in rat tissue lung samples (blue=*in vivo),* collected in IVR model *(red=in vitro),* and estimated using MPPD model (green=*in silico*) for three test compounds exposed to a rat with various inhaled doses and particle diameters. Error bars are means ± SD. Total number of experimental replicates for the *in vivo,* IVR and MPPD models was 28, 35 and 26 respectively. The numbers above the combined data columns indicate the mean lung deposition levels in percentage terms for the three models.

First, the overall lung deposition levels for all compounds under investigation were very similar; 9.3 ± 6.2% and 9.6 ± 6.0% for *in vivo* and *in vitro* data respectively. Second, the MPPD model estimates were consistently lower than the corresponding *in vivo* data for all compounds. Overall, the combined MMPD lung deposition level was estimated to be 6.5 ± 2.9%. Third, the ranking order of lung deposition in percentage terms was as follows: *in vitro* > *in vivo* > *in silico*.

In terms of statistical analysis, ANOVA comparison between the three data sets revealed no statistically significant differences between the IVR and *in vivo* data ($P < 0.05$). However, a statistical difference was demonstrated between the MPPD model estimates and *in vivo* and IVR data ($P < 0.05$).

With respect to the deposition comparison between the three models for each test compound, in general the data followed the trend exhibited for the combined data set. However, for compound Y (micronised form), higher percentage deposition levels were noted for the *in vivo* data (19.4 ± 9.3%) in comparison with the *in vitro* data (15.2 ± 4.9%). In addition, similar relative deposition trends were demonstrated for FP (MMAD < 2 µm) and compound X (micronised form).

As already discussed (see section 6.3.1.1, B-Results and Discussion), multiple factors such as variability in biological systems and differences in segmentation of the lung fraction between the IVR model and *in vivo* lung dose determination method may account for differences between them. In addition, the effect of particle size and formulation characteristics may be responsible for some of the differences between the two models (see section 6.5, B-Results and Discussion).

The reasons for the general underestimation of the lung dose for the *in silico* MPPD model in comparison with the IVR and *in vivo* data are discussed in greater detail in the following section (6.4, B-Results and Discussion).

6.4 Deposition measurements in the IVR model versus *in silico* MPPD modelling estimates

The average percentage deposition levels of aerosol particles in the IVR and MPPD model for all experimental runs conducted was compared (see Figure 55). In addition, the data for individual compounds are summarised in Table 15.

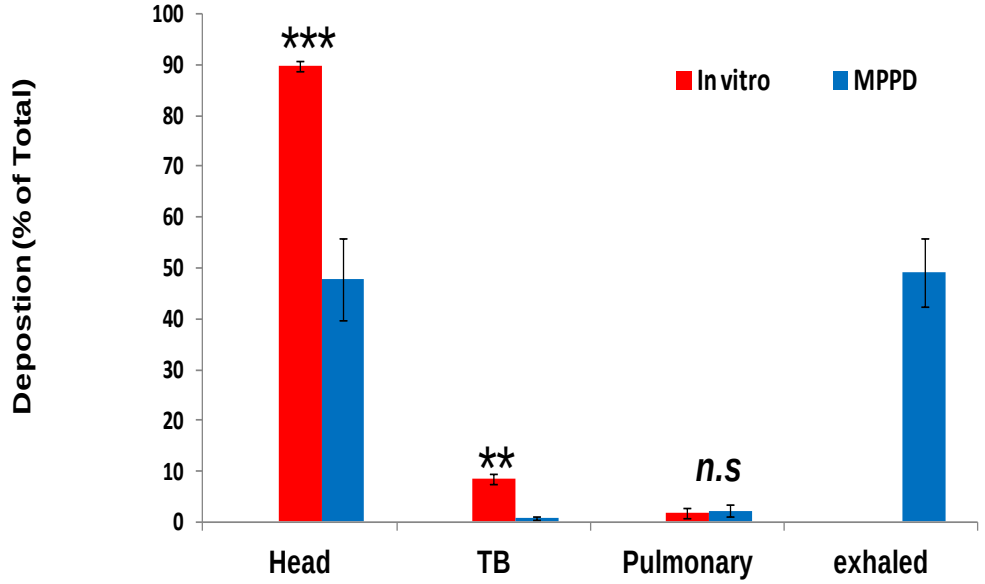

Figure 55: Comparison of the relative deposition of three different test drugs between measured doses in the *in vitro* rat model versus estimated doses using the MPPD model for deposition expressed as percentage of total dose. A statistically significant difference was found between the two models for Head (***P = 0.001) and TB (***P = 0.01) fractions of the rat lung. No significant difference was found between the two models for the pulmonary fraction. Error bars are Mean ± SD from six independent experiments.

The MPPD fractional deposition data is presented as percentage of the total dose, including the exhaled fraction. Whereas, for the IVR model, due to the practical difficulties in measuring the amount of aerosol particles that are exhaled, no attempt was made to quantify these losses or differentiate between inspiratory and expiratory deposition fractions.

The results showed poor agreement between the IVR and MPPD model with regard to the regional distribution of the aerosol particles. In both cases, the highest deposition levels were seen in the head region, with 90.4 ± 6.0% and 50.4 ± 7.4% deposition recorded for the IVR and MPPD model respectively ($p = 0.001$). For the Tracheo-Bronchial (TB) region, significantly higher deposition levels were noted in the *in vitro* rat model in comparison with MPPD model predictions: 8.1 ± 5.2% versus 1.2 ± 0.5% deposition for the IVR and MPPD model respectively ($p = 0.01$). For the peripheral lung structures, similar fractional deposition levels were noted between the two models: 1.5 ± 1.7% versus 2.8 ± 1.1% deposition for the IVR and MPPD model respectively ($p > 0.05$).

However, a significant proportion of the total dose is predicted by the MPPD model to be exhaled: 45.6 ± 7.5% of the total dose. This may be an overestimate, however, as numerous published *in silico* models of deposition in rat lungs, such as work by Menache *et al.* or the model by Schmid *et al.,* have shown that, for particles in the range of 3.0 to 10.0 µm, the inhaled portion was in excess of 70.0% of the total dose (Menache et al, 1996;Schmid et al, 2008).

Table 15: Comparison of the regional deposition levels for the *in vitro* rat model (IVR) versus MPPD estimates

Test compound	Size distribution (MMAD ± GSD)	IVR (% of Total)			MPPD (% of Total)[1,2]				MPPD (% of Inhaled)		
		Head	TB	Post- TB	Head	TB	Pulmonary	Exhaled	Head	TB	Post- TB
Compound Y, micronised	2.22 ± 2.39	84.8 ± 4.9	13.8 ± 4.0	1.4 ± 1.7	46.2	1.2	3.1	49.6	91.7	2.4	6.2
Compound X, micronised	5.28 ± 2.55	98.8 ± 1.8	0.8 ± 1.2	0.4 ± 0.6	54.2	0.5	1.0	44.3	97.3	0.9	1.7
Compound X, spray-dried Type 1	2.46 ± 2.96	88.8 ± 2.8	6.9 ± 1.5	4.4 ± 1.4	41.0	1.1	3.2	54.8	90.7	2.4	7.1
Compound X, spray-dried Type 2	1.77 ± 3.22	85.8 ± 2.1	10.6 ± 0.6	3.6 ± 1.5	37.6	1.0	3.5	57.9	89.3	2.3	8.3
Fluticasone propionate (MMAD > 4um)	4.63 ± 3.05	92.6 ± 1.3	7.4 ± 1.3	0.1 ± 0.1	49.2 ± 9.3	0.9 ± 0.4	1.8 ± 1.2	48.0 ± 7.8	94.3 ± 4.2	1.8 ± 1.1	3.8 ± 3.1
Fluticasone propionate (MMAD < 2um)[3]	1.86 ± 1.58	95.2 ± 3.4	3.9 ± 2.8	0.8 ± 0.7	55.5 ± 2.2	1.7 ± 0.1	3.6 ± 0.1	39.3 ± 2.2	91.4 ± 0.3	2.7 ± 0.1	5.9 ± 0.3

1. Input parameters for MPPD: Tidal volume: 2.1, Breaths per minute: 102.
2. Inhalability Adjustment is applied.
3. Particle size distribution was determined using APS instrument.

NR: Not Recorded

When the exhaled portion of the total dose was excluded from the MPPD outputs and the fractional deposition levels for the various regions of the rat respiratory tract were expressed as percentages of the inhaled fraction, similar deposition levels were observed in comparison with IVR model outputs (see Figure 56).

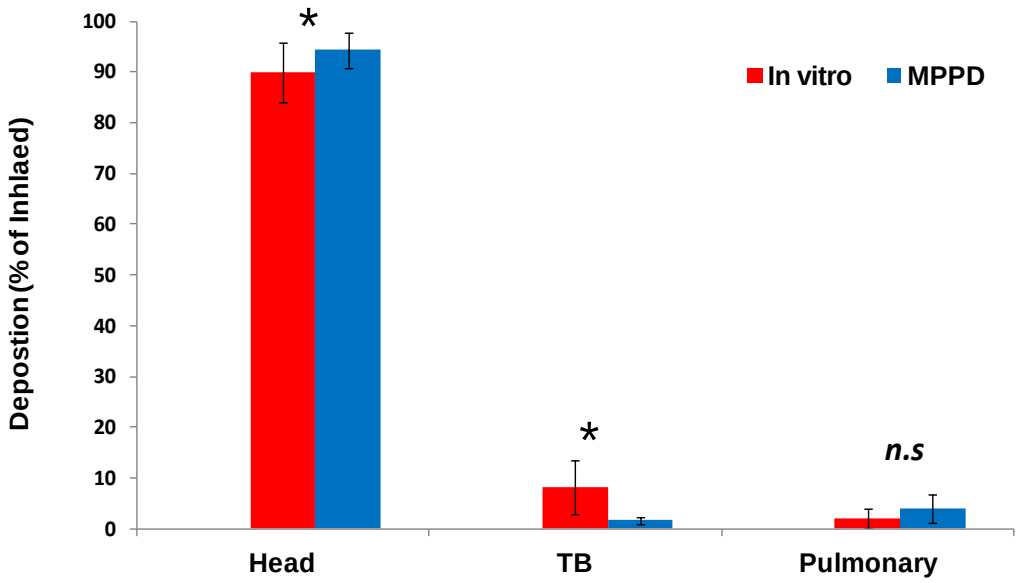

Figure 56: Comparison of the relative deposition of three different test drugs between measured doses in the *in vitro* rat model versus estimated doses using the MPPD model for deposition expressed as a percentage of inhaled dose. A statistically significant difference was found between the Head and TB (*P<0.05) regions of the rat respiratory tract. No significant difference was found between the two models for the pulmonary fraction. Error bars are Mean ± SD from six independent experiments.

Furthermore, normalising the fractional deposition data for inhalable fraction only, as shown in Figure 56, allows for direct comparison between the two models. It also allows for an improved understanding of the deposition of test materials after inhalation, as only the particles considered to be respirable are compared.

The results showed good agreement between the IVR and MPPD model with regard to the regional distribution of the aerosol particles. In both cases, the highest deposition levels were seen in the head region, with 90.4 ± 6.0% and 92.4 ± 2.8% deposition recorded for the IVR and MPPD model respectively ($p = 0.01$). For the Tracheobronchial (TB) region, significantly higher deposition levels were noted in the *in vitro* rat model in comparison with MPPD model predictions: 8.1 ± 5.2% versus 2.3 ± 0.7% deposition for the IVR and MPPD model respectively

($p = 0.01$). Furthermore, a similarly good agreement between the IVR and MPPD models for the deposition of Fluorescent Microsphere Particles (FMS) was demonstrated (see Figure 50).

In addition, as discussed previously (see section 4.1, B-Results and Discussion), the TB region of the MPPD model covers anatomical structures from the Trachea (generation 1) to the terminal Bronchioles (generation 22). Whereas for the IVR model, the anatomical structures covered in this section are up to the level of the respiratory Bronchiole (generation 4). Therefore, it would be expected that higher deposition levels are observed for the MPPD model in comparison with the IVR model owing to the higher surface area available for depositing particles of the former. Thus, the data indicate that the MPPD model may be significantly underestimating the level of deposition in the TB section.

However, caution must be exercised in using the airway generation number for the purposes of comparison between different methods, as recent works from Oakes *et al.* showed that the variability of measurements for each rat airway generation was high and often larger than intergeneration variability. This suggests that generation organisation may not be the most appropriate method to compare different rat airways or to describe the rat airways (Oakes et al, 2012). Nonetheless, the lower deposition in the TB region of the MPPD model in comparison with the IVR model does highlight an important limitation of MPPD for estimating the TB dose and fraction in the rat lung.

For the peripheral lung structures, similar fractional deposition levels were noted between the two models, being 1.5 ± 1.7% versus 5.4 ± 2.2% deposition for the IVR and MPPD model respectively ($p > 0.05$). The corresponding level of lung deposition in the *in vivo* rats was 10.1 ± 7.8% of total deposition.

Therefore, both the MPPD and IVR model underestimated lung deposition in comparison with the *in vivo* situation. However, the high variability (SD of 7.8%) recorded for the *in vivo* results clearly demonstrate the inherent variability in the *in vivo* rats due to differences in multiple factors; for example, strain, weight, particle characteristics and physiological factors are known to affect deposition in the rat lungs (Schmid et al, 2008). With regards to comparison of the MPPD results with *in vivo* data in the literature, most studies have reported an underestimation of lung dose using MPPD in comparison with *in vivo* lung dose (Cassee et al, 2002;Wichers et al, 2006).

6.5 Assessing the effect of formulation characteristics on regional deposition of inhaled particles in the IVR model versus *in vivo* lung homogenate data

In order to assess the effect of formulation changes on lung deposition, different physical forms of the test material compound X were prepared. A micronised and spray-dried form of the active drug was mixed with lactose to make an inhalation blend. This compound was selected as it has been shown previously to be very difficult to achieve a reduction in particle size of its primary particles using conventional particle reduction techniques such as micronisation (MMAD < 5µm), due to the inherent property of its particles to agglomerate post micronisation (internal GSK data). Therefore, a combination of wet-bead milling and a spray-drying technique was used in order to effect a reduction in particle size, as this method has been demonstrated in the literature to produce the desired reduction in particle size (Sheth et al, 2012;Yang et al, 2008).

These test materials were exposed to the test animals for the same duration and chamber aerosol concentration. As expected, the different forms of compound X gave rise to quite distinct particle sizes of the active drug in the exposure atmosphere: MMAD of 5.28 µm for the micronised form of the drug, 2.46 and 1.77 µm for the sprayed-dried forms 1 and 2 respectively. In addition, the IVR model was exposed to the same exposure atmosphere for each of the particle size groups investigated.

Thus, this investigation allowed for the effect of particle size on deposition in the lung to be elucidated, as all other variables such as dose and duration of exposure remained constant.

The data (see Figure 57) for the *in vivo* rats showed the expected trend of increased lung deposition fraction for the spray-dried compounds with decreased particle size. A similar comparative increase in lung deposition with decreasing particle size was demonstrated in the IVR model exposed to the same forms of the compound.

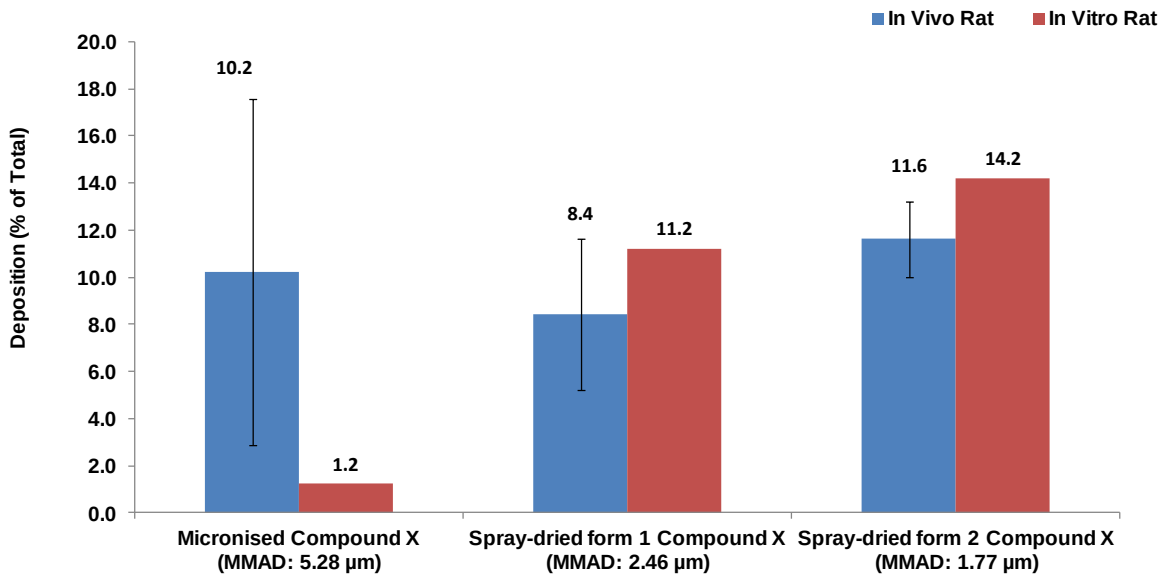

Figure 57: Deposition fraction for the lung portion of the *in vivo* rats and corresponding fraction in the IVR model for each particle size. Error bars are Mean ± SD from three rats sacrificed for each particle size dosing group. Numbers above the columns indicate the mean lung deposition levels in percentage terms using the IVR model (red columns) and in the *in vivo* rat lungs (blue columns).

However, for the group of live rats exposed to the micronised form of the same drug, which produced an MMAD of 5.28 µm, the average lung deposition was 10.2 ± 7.3% of total lung dose. The equivalent lung deposition fraction for the IVR models was 1.2% of total lung dose. Further evaluation of the *in vivo* lung data showed one rat to have deposited a significantly high level of the drug in comparison with the two remaining rats in the same groups; rat one received 18.7% versus 6.5 and 5.5% lung dose for rats two and three respectively. The reason for the relatively high lung dose received by rat one is not known.

A possible cause of this high deposition fraction includes a much reduced breathing rate in comparison with the two other rats in the same group. A reduction in the breathing rate has been shown to result in increased peripheral deposition in the lung in both *in vivo* and *in vitro* situations (see section 5). However, the absence of ventilation monitoring data for the *in vivo* rats means this hypothesis cannot be confirmed.

Nonetheless, and despite the high variability observed in the lung data for the rat group dosed with the micronised form of drug, in general the data showed the expected trend of increased lung deposition with decreased particle size. The trend for the IVR model was much stronger and demonstrated a clear step-wise increase in lung deposition with decreased particle size.

In addition, the fractional deposition data for the IVR model were compared against historical data on deposition patterns in rats provided in Otto Raabe's 1988 study using monodispersed, insoluble aluminosilicate particles and labelled with radioactive ^{169}Yb (Raabe et al, 1988) (see Table 16).

Table 16: Comparison of Raabe's 1988 pulmonary deposition data for rats with experimental data (IVR and *in vivo*) from present study using compound X

Particle Size (µm)	Pulmonary deposition (% of Total)		
	Raabe	IVR	In vivo
1.0	8.75*	NA	NA
1.8	NA	14.2 ± 2.1	11.6 ± 1.6
2.5	6.6 ± 0.5	11.2 ± 2.8	8.4 ± 3.2
5.0	4.8 ± 0.9	NA	N/A
5.2	NA	1.2#	10.2 ± 7.3

* Two data points of 6.5 and 11.0% averaged.
# Two data points of 0.0 and 2.5% averaged.

For the largest-sized particle generated in this study, compound X had an MMAD of 5.2 µm, while the lung deposition fraction was 1.2%. This compared with a deposition level 4.8 ± 0.9% for 5.0 µm reported in Raabe's study. For particles in the range of 3.0 µm, lung deposition was 11.2 ± 2.8% and 6.6 ± 0.5% for the *in vitro* (MMAD: 2.46 µm) and Raabe study respectively.

For the smallest-sized particles generated in the study, at particle size of 1.77 µm MMAD compound X (Spray-dried form 2) deposition levels of 14.2 ± 2.1% were noted. For Raabe's studies, no particles were generated at the 2.0 µm size, although lung deposition levels of around 8.75% were noted for 1.0 µm sized particles.

A number of possible causes may explain the differences between the results generated in this study and published data. Most importantly, the data generated in the present study was done using polydisperse particles, whereas the data reported in the Raabe study was generated using monodisperse particles. This may, in turn, account for the differences in deposition fractions between the studies.

Other potential causes of differences between the experimental data and the published data may have been differences in exposure duration. It is possible that the Raabe lung data may underestimate the lung deposition, as mucociliary clearance of particles was occurring throughout the 45-minute exposure duration that was used (Hofmann and Asgharian, 2003). This is in contrast to the present study, where the duration of exposure was shorter at 30 minutes (see Table 13). Therefore, the impact of clearance on deposition is reduced and may explain why the *in vivo* results from the present are generally higher than reported in Raabe's study.

6.5.1 Combining deposition data from all studies to assess the effect of MMAD on lung deposition

Pooling the deposition data for all the test materials evaluated as part of this thesis, including FMS, fluticasone propionate, compound X, and compound Y, allowed the effect of particle size in the range of 2.0-6.0 µm MMAD on deposition in the rat lungs to be assessed. For all IVR data points selected, the same ventilation parameters of respiratory minute volume (0.204 L/min) were used to ventilate the *in vitro* model, therefore removing the ventilation effect as a possible factor confounding the results. In addition, where available, the corresponding data from lung homogenate samples and MPPD estimates were included in order to provide a comparison for all three models (see Figure 58).

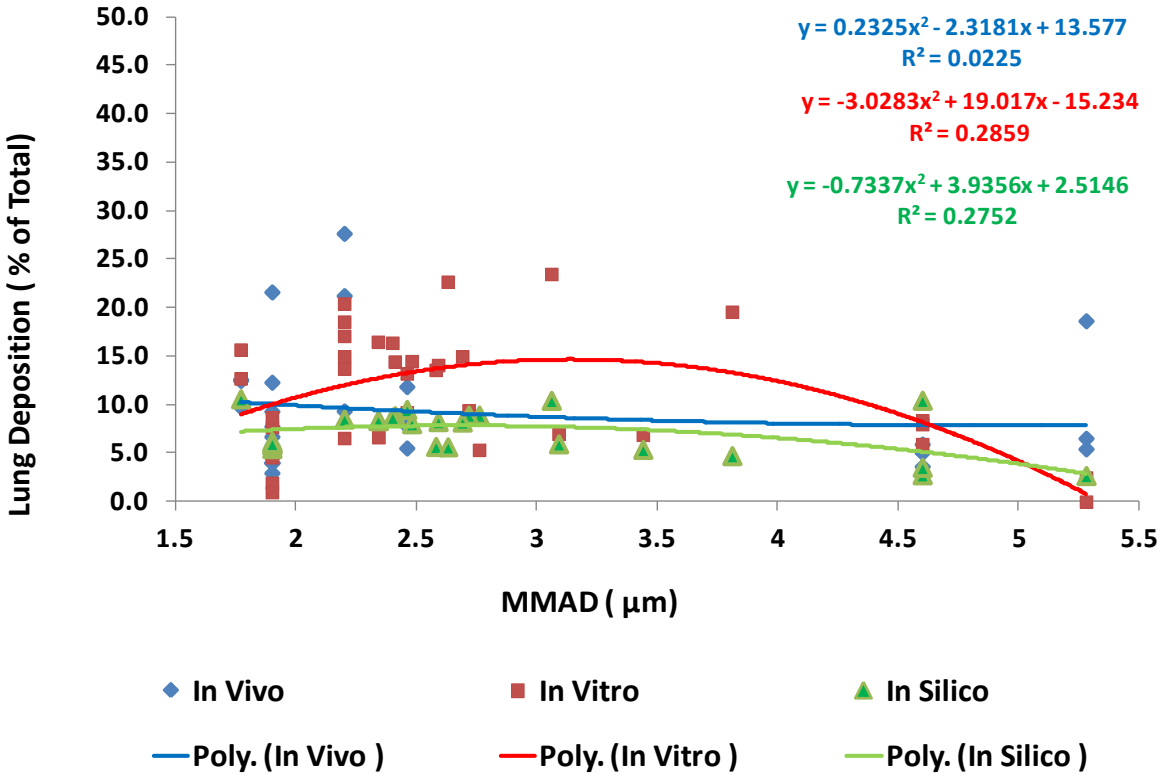

Figure 58: The relationship between percentage deposition in the *in vitro, in vivo* lungs and *in silico* estimates (MPPD) and the aerodynamic particle size of test material during exposure period. The numbers of data points are 35, 28 and 26 for *in vitro, in vivo* lungs and *in silico* estimates respectively.

For the IVR model, the lung deposition data showed a great deal of variability, with deposition in the range of 1.77-3.0 µm showing no consistent trend in terms of the effect of particle size on the lung deposition (R^2 = 0.29). This lack of trend in this size range can be attributed primarily to the polydispersity of the test particle, resulting in significant overlap in the size distribution between particles in this size. Consequently, all particles in this size range can be regarded as having an equal opportunity of depositing in the peripheral regions of the lung. Overall, for a mean particle size of 2.2 ± 0.4 µm MMAD, the corresponding deposition levels recorded were 12.3 ± 5.9% of total inhaled.

However, in the range of 3.0-6.0 µm, an inverse relationship between increased particle size and deposition in the lung region was demonstrated (see Figure 58). In this size range, the overall particle size was 4.9 ± 0.3 µm MMAD, and the corresponding average deposition lung deposition levels recorded were 5.0 ± 3.6%. Thus, in general terms, the IVR model demonstrated the scientifically expected trend of decreased deposition with increased particle size. This observation is consistent with a number of published studies, which showed a similar trend with respect to these two factors, namely the imaging model developed by Kuehl *et al.* and the live rat study by Raabe (Kuehl et al, 2012;Raabe et al, 1988).

For the corresponding *in vivo* data, a similarly poor correlation was demonstrated for the relationship between particle size and lung deposition (R^2 = 0.02). This finding is consistent with data reported in the literature, where there is no well-defined relationship between deposition in the TB region and particle size (Schlesinger, 1985). This relative insensitivity of the size has been attributed to the monopodial branching pattern in rat airways, where airways of considerable diameter differences may be found in the same branching level. Thus, a monopodial system results in a constant deposition level over a wide particle size range. For the pulmonary region, in general, deposition increases as particle size decreases, after a minimum deposition is reached. However, the efficient removal of large particles in regions upstream of the pulmonary airways may result in less pulmonary deposition than would be expected for a given particle size (Schlesinger, 1985).

Theoretical models of deposition in the rat lung have demonstrated that, between 3.0 and 10 µm, most particles deposit by impaction in the extrathoracic region (Schmid et al, 2008). Consequently, this efficient removal of particles in the extrathoracic region results in a reduced fraction of particles reaching the TB and alveolar region. However, between 1 and 3 µm, particle deposition can occur to approximately the same level in this region due to the polydispersity of particles in this size range (Schmid et al, 2008).

Furthermore, the large variability in the experimental *in vivo* data can be attributed to variations in aerosol characteristics, namely the density and polydisperse nature of the test compounds. In addition, there is variability in physiological parameters such as strain, body size and activity levels. This is in contrast with the IVR model, where the physiological parameters are fixed for the duration of the exposure and thus may explain the stronger correlation shown for the relationship between particle size and deposition in the peripheral regions of the lung.

In addition, comparison of the *in vivo* and IVR model data was made with the MPPD model predictions of the equivalent lung deposition fraction. This analysis showed the estimated lung deposition fraction to have an average value of 7.1 ± 2.3%, which is significantly lower than the equivalent lung deposition faction from lung homogeniate analysis (9.3 ± 6.2%) and the IVR model (11.3 ± 6.2%). However, the degree of variability in the MPPD model estimates was much less, being 31.9% CV in comparison with CV values of 67.1% and 54.6% for the *in vivo* and IVR model data respectively.

In terms of trends, the MPPD data did not show a strong trend with respect to the effect of particle size on lung deposition fraction (R^2 = 0.28). However, at the extremes of the data distribution, higher deposition levels were observed at low MMAD: 10.7% at 1.77 µm versus 2.7% at 5.28 µm. As in the case of the *in vivo* and *in vitro* data, the relatively high degree variability and lack of clear trend between particle size and lung deposition fractions may be attributed to the polydispersity of the test materials, resulting in a significant overlap between the different particle sizes in terms of where they are likely to be deposited in the airways. This is in contrast to studies using monodisperse 198Y radiolabelled particles over a wide size range, such as the 1988 Raabe's study using mono-sized 198Y radiolabelled particles (MMAD range: 0.29 to 10.16 µm), which demonstrated a clear inverse relationship between increased lung deposition and decreased particle size.

Overall, the lung deposition fractions generated using the IVR model and compared with the equivalent *in vivo* and *in silico* estimates showed comparable levels. Furthermore, the results from this investigation showed that, for the range of particle size studied (1.8-5.3 µm), the actual deposition fraction varied from 0.0 to 20.5%, in contrast to the deposition fraction often used for preclinical toxicological studies, where it is assumed that the deposition fraction for particles between 1.0 and 5.0 µm MMAD is 10.0% regardless of particle size (Forbes et al, 2011). Therefore, this comparison provides further support for the validity of using the IVR rat lung model for assessing the deposition of inhaled material in the lungs of the live rats during exposure.

6.6 Conclusions

The lung deposition data from exposure studies with three different drugs were compared with the lung deposition fraction in the newly developed IVR model, which was exposed to the same exposure atmosphere.

For total deposition, the amount deposited in the IVR model was compared with estimates of the total lung dose. The data showed the IVR model underestimated the theoretical total dose prediction by an average factor of 0.78 ± 0.29. The variability in the data was attributed to a number of factors, primarily changes in aerosol exposure concentrations, which in turn affected the variability seen in the IVR data. Furthermore, differences in the sampling flow rate and duration of exposure between the filter methods, upon which the theoretical estimates of total lung dose are based, and IVR method may have contributed to the variability observed.

The lung deposition amount in the IVR lung model showed reasonably strong significant correlation with the *in vivo* lung concentration data, particularly when the data is expressed in absolute terms (R^2= 0.66, $P < 0.05$). Compounds were predicted well and within 2-fold of the measured lung deposition values. This estimate would seem reasonable considering the variability in biological systems and the multiple components required to estimate lung doses. However, further work would be required to determine the true confidence intervals around these predictions.

Analysis of the lung deposition data in both *in vivo* rat lungs and the IVR model showed an increase in the lung deposition fraction as the particle size of the test materials decreased. In addition, it was demonstrated that, for the range of particle size studied (1.8-5.3 µm), the actual deposition fraction varied from 0.0 to 20.5%, in contrast to the commonly used 10% deposition fraction, based on the work of Snipes *et al*. (Snipes et al, 1989) and accepted widely in the pharmaceutical industry for estimating the deposited dose (Forbes et al, 2011).

However, there is a growing consensus amongst researchers in this field that this 10.0% default value is not particularly accurate and tends to underestimate the deposition in non-clinical species. Therefore, the use of the IVR model may enable a more accurate measurement of drug deposition and would improve the analysis of non-clinical safety data. Thus, it would make it easier to define realistic clinical dose ranges.

In terms of comparison with the IVR model deposition with *in silico* estimates, the MPPD model estimates were consistently lower than the corresponding *in vitro* as well as *in vivo* data for all compounds under investigation. Furthermore, this underestimation of deposited lung fraction, as predicted using MPPD, is consistent with findings reported in the literature for a number of studies (Cassee et al, 2002;Wichers et al, 2006).

In addition, a major advantage of using the IVR in preference to the MPPD model is the ability of the former to assess the effect of formulation characteristics on deposition, as demonstrated in the differing deposition profiles shown for micronised and spray-dried forms of compound X. Whereas, in the case of the MPPD model, particle size and geometric standard deviation are the only particle characteristics that can be factored into the model estimates for lung deposition.

Therefore, the developed IVR model has been demonstrated to allow a more accurate and detailed regional deposition analysis than existing techniques, such as the *in silico* MPPD model, and may benefit optimisation development studies aimed at regional drug targeting.

7 Assessing the relationship between efficacy of inhaled fluticasone propionate in an allergen-induced rodent model with regional lung deposition

One of the biggest concerns of using inhaled corticosteroid therapy in humans is the level of systemic side effects at high doses. To reduce the level of these side effects, research in this field has focused efforts on developing new drugs which maximise topical efficacy and minimise side effects (Chiang et al, 2009). Moreover, Pharmacokinetic/Pharmacodynamic (PK/PD) modeling suggests that enhanced pulmonary targeting may be achieved via modification of pharmacokinetic profiles. Pharmacokinetic parameters such as high lung deposition, high receptor binding, long lung retention and high lipid conjugation have been sought to improve the efficacy of such drugs (Rohatagi et al, 2004).

In addition, drugs with appropriate physiochemical properties, primarily particle size, could further optimise the PK profile (Tayab and Hochhaus, 2005). However, despite this understanding of what is required, the major hurdle for pulmonary drug discovery is to develop animal models of sufficient sensitivity to assess efficacy of inhaled corticosteroids prior to clinical testing. In addition, a greater understanding of the relationship between physiochemical, PK and PD characteristics is needed in order to achieve these goals.

Animal models such as the acute primary allergen model are widely used in the evaluation and development of topical anti-inflammatory medicines such as inhaled corticosteroids (Shin et al, 2009). As rats do not develop airway hyperresponsiveness (Adams et al, 2010) or allergic airway inflammation, an artificial asthma-like reaction has to be induced in the airways of the animals. Single or multiple systemic injections of an allergen, such as lipopolysaccharides (LPS), can be used to induce sensitisation. Two to four weeks following sensitisation, the challenge phase follows, during which allergens are administered in a nebulised form or administered by deposition through the intranasal route.

The response elicited is primarily lung inflammation, characterised by infiltration of large numbers of neutrophils, eosinophils, macrophages and lymphocytes into the lung (Chiang et al, 2010). These factors can be monitored by examination of inflammatory cells in bronchoalveolar lavage fluid (BAL) fluid (Natiello et al, 2009). In humans, measurement of these cell infiltrates has been shown to correlate with disease severity. For example, an increased number of eosinophils in BAL fluid are seen in patients with asthma.

However, an increased level of neutrophils coupled with low eosinophils is typically seen in patients with chronic obstructive pulmonary disease (Fabbri et al, 2003). Limitations of the primary allergen challenge model include minimal airway remodeling, transient airway inflammation and AHR due to the short-term nature of the model. Therefore, as this model is most often used in pre-clinical studies, the results are often over-interpreted to represent asthma. As a result, it is not surprising that most extensions to asthma have failed in the clinic (Blyth et al, 1996).

Possible reasons for this lack of translation from animal models to the clinical settings include a poor understanding of the impact of particle size on regional deposition in the rat lungs. For instance, in a study by Sorkness *et al.,* there was no distinct anti-inflammatory effect of fluticasone propionate (FP), despite an increase in the dose administered. The authors speculated that the lack of distinct dose response for anti-inflammatory effect suggests that the distribution of an aerosolised drug within the airways might be an important determinant of efficacy (Sorkness et al, 2004).

In addition, this observation is consistent with the growing recognition of distal airway involvement in human asthma and the concern that inhaled steroid therapies do not reach these areas effectively. Studies in human subjects with radiotracer techniques have identified aerosol particle size and inhalation techniques as important variables affecting total pulmonary and regional deposition of inhaled drugs (Martin, 2002). Furthermore, Leach *et al.* have compared two formulations of beclomethasone dipropionate MDIs; they revealed that the one, having a median particle diameter of 1.1 µm, deposited a larger total amount of drug in the human lungs, as well as a larger proportion in the peripheral regions of the lungs, compared with the MDI that generated particles with a median diameter of 3.5µm (Leach et al, 1998).

Therefore, in order to better understand the relationship between particle size, dose and PD effects, a study using FP was conducted. FP was selected as the test compound as it is a highly lipophilic corticosteroid and is commonly used in the treatment of bronchial asthma (Mollmann et al, 1998). In addition, as FP is characterised by having an oral bioavailability of less than 1.0%, prolonged residence and slow absorption from the lungs makes it an excellent comparator compound for a comparison of deposition in the IVR model, which does not account for clearance mechanisms in determining the lung dose.

The primary aim of the present study was to test the hypothesis that pharmacodynamic responses of inhaled corticosteroids are more strongly correlated with the regional lung deposition mediated using FP with small particle size (MMAD < 2 µm) rather than total deposition in the body. The study compared the efficacy of FP administered at different doses with particle sizes on the suppression of the acute anti-inflammatory response using the LPS-challenge model. Furthermore, the lung deposition in the IVR model and MPPD estimates were used to provide supporting evidence to test this hypothesis.

The study was conducted as two separate investigations. In the initial investigation, particle size in the range of MMAD > 4 µm was generated and an estimated inhaled dose in the range of between 10 to 1000 µg/kg of body weight was achieved. The follow-up investigation (study 2) produced FP powder with a particle size of less than 2.0 µm and an estimated inhaled dose in the range of between 10 to 1000 µg/kg of body weight was achieved. Thus, because of the differences in particle size and doses, the effect of these parameters on the anti-inflammatory response can be assessed.

7.1 Study Design

The rats were assessed for suppression of the pulmonary allergic inflammatory response in order to evaluate the efficacy of the drug delivery through the pulmonary route. There were five treatment groups per study, each with six rats, except for the control group which had three rats only (see Table 17). Full details of the methods used in this study are described in section 6, C-Experimental Setup.

Table 17: Treatment groups for assessing the effect of FP on inflammatory response in rat lungs

Group	Treatment	Challenge	Number of Animals
Control	**Lactose + Saline**	**Saline**	**3**
Placebo	**Lactose + LPS**	**LPS**	**6**
FP 0.01 mg/kg	**FP 0.01 mg/kg +LPS**	**LPS**	**6**
FP 0.1 mg/kg	**FP 0.1 mg/kg +LPS**	**LPS**	**6**
FP 1.0 mg/kg	**FP 1.0 mg/kg +LPS**	**LPS**	**6**

For study 1, FP with an MMAD greater than 4.0 µm was generated. All animals were dosed with either vehicle (lactose) or FP (nominal dose 0.01, 0.1 and 1.0 mg/kg) by inhalation for approximately 18 minutes in a nose-only exposure chamber (see section 6.1.2, C-Experimental Setup). Thereafter, the animals were administered LPS (0.15 mg/ml) by inhalation in a cloud chamber for 15 minutes. Following this, the animals were returned to their cages and placed in the holding rooms.

However, for study 1 the Placebo group and FP (0.01 mg/kg) groups were administered FP in error at a dose of 0.1 mg/kg. This error in administration was confirmed by filter analysis, which showed aerosol concentration readings of similar levels at 9.5 and 5.9 µg/L for the placebo and 0.01 mg/kg dose group respectively. This was compared with a target aerosol concentration reading of 5.0 µg/L for the 0.1 mg/kg FP dose group, thus confirming the error in administration. Therefore, the rat data from these groups (placebo and 0.1 mg/kg) were excluded from the data analysis.

For study 2, which generated an MMAD for FP of less than 2.0 µm, all animals were dosed with the same treatment groups as detailed in study 1. However, approximately 30 minutes post exposure, the rats were anaesthetised with 5.0% isoflurane in 2l/min oxygen and intratracheally administered saline or LPS (2ug/kg in 200ul saline).

In both studies, at four hours post LPS exposure, the rats were euthanased with 2.5 ml of 200 mg/ml sodium pentobarbitone administered intraperitoneally. After confirmation of death (cervical dislocation at the end of all procedures), the trachea was exposed and cannulated, and the lungs lavaged with 3x 5 ml of BAL fluid. Differential cell count was performed on the pooled BAL fluid using a Sysmex XT2000i vet cell analyser (Sysmex Corporation, Kobe, Japan) to determine the level of inflammatory infiltrates in the lung tissue.

7.2 Results and Discussion

In Figure 59, the effects of different doses of FP and particle sizes from both studies on neutrophil numbers released in the BAL fluid are shown. The results demonstrated that exposure to FP resulted in a dose-dependent inhibition of BAL neutrophils, particularly for the rats dosed with an MMAD of less than 2.0 µm. However, for the 4.0 µm dosed rats, a flat response for the relationship between neutrophil numbers and dose was demonstrated, with relatively similar neutrophil suppression levels noted for the 0.1 and 1.0 mcg/kg dose groups. This lack of dose response for the anti-inflammatory effect suggests that a regional distribution of drug in the rat lung, rather than dose administered, may be an important parameter affecting efficacy.

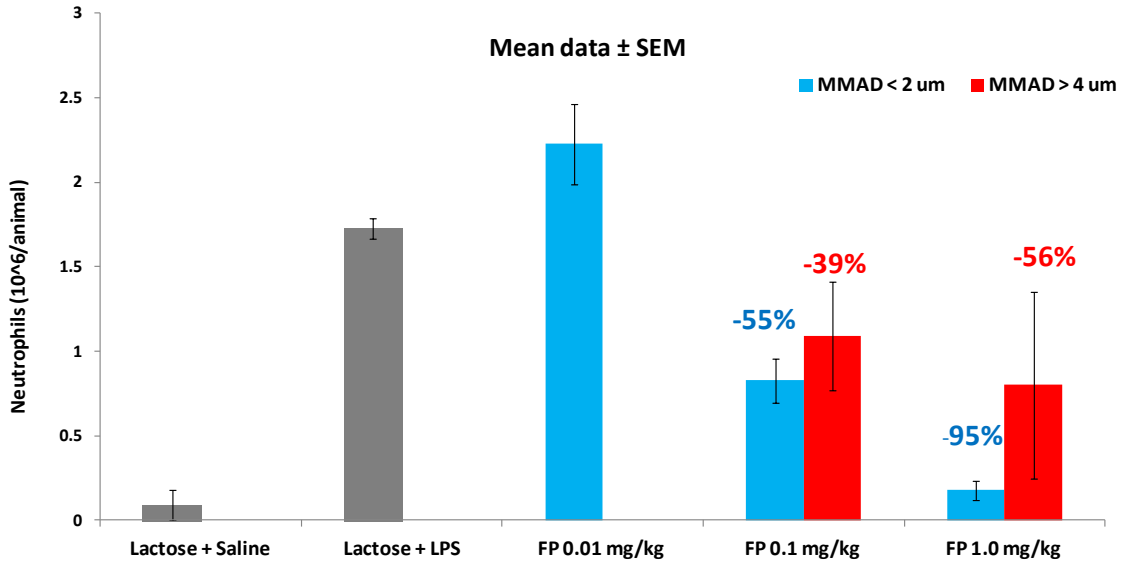

Figure 59: Effects of inhaled FP on LPS-induced BAL neutrophil infiltration. Data is presented as mean ± SEM (n= 3-6 per group). Percentage values in the above bar chart represent the level of neutrophil suppression relative to the placebo and control groups.

As previously stated, the work by Sorkness *et al.* (Sorkness et al, 2004) provides further support to the argument that regional lung dose distribution, rather than total inhaled dose, may be an important determinant of efficacy. In the study carried out by Sorkness *et al.*, inhaled FP was delivered through a metered-dose inhaler to rats and compared with systemic dexamethasone for acute pulmonary allergic inflammatory response. The results showed a lack of dose-related response for the anti-inflammatory effect of the inhaled therapies. This lack of response was attributed to the inability of the FP at higher doses to reach the most distal airways and induce an anti-inflammatory response, therefore demonstrating the importance of peripheral deposition of inhaled drug on efficacy.

In the present study, a similar lack of dose response is demonstrated for the 4 µm FP doses. Increasing the dose by ten-fold from 100 to 1000 µg/kg did not result in a corresponding increase in the level of inhibition of the pro-inflammatory neutrophil numbers. This may indicate that, in order to achieve higher neutrophil suppression, a greater level of peripheral deposition in the rat lung is required, which is clearly demonstrated for the 2 µm FP doses.

In terms of the relationship between particle size and the lung deposition fraction, the data showed the reduction in the particle size of FP resulted in the scientifically expected trend of increased deposition in the periphery of the lung for all three lung deposition models, namely IVR, *in vivo* and MPPD. However, this trend was not as strong as expected (see Table 18). For instance, in the case of the *in vivo* rat data, the trend between particle size and lung deposition fraction was largely flat, with similar deposition levels demonstrated for rats dosed with FP particles with an MMAD of 1.8 µm (7.6 ± 5.2%) and an MMAD of 4.9 µm (4.9 ± 1.0 %).

Table 18: Comparison of the percent deposited fractions at each particle size and dose between IVR, *in vivo* and MPPD models

Target dose (µg/kg)	**100**	**1000**	**100**	**1000**
size (MMAD: µm)[1]	**4.9**	**4.5**	**1.8**	**1.9**
% of targeted dose in lung (in vivo)[2]	**5.5 ± 0.6**	**4.4 ± 1.0**	**10.7 ± 9.5**	**5.4 ± 3.4**
IVR lung dose (% of total)[3]	**8**	**7.2 ± 1.7**	**4.8 ± 3.9**	**4.8 ± 4.1**
IVR post-TB dose (% of total)	**NR**	**0.1 ± .03**	**0.8 ± 0.7**	**0.9 ± 0.9**
MPPD Pulmonary fraction (% of total)	**2.3**	**4.6 ± 4.0**	**6.0 ± 0.2**	**5.7 ± 0.4**

1. Based on particle size determination from one study per group.
2. Estimated from dividing the lung dose (µg/g of lung) by the total inhaled dose.
3. Based on number of samples per group: 1.

NR: No Results recorded

Whilst it is expected that a reduction in particle size will lead to increased deposition in the periphery of the lung (Raabe et al, 1988), the monopodial nature of the rat airways and the efficient filtering in the nasal and TB region mean this relationship is not always clear-cut. Also, deposition levels may be similar in the range of between 2.0 and 5.0 µm (Schlesinger, 1985).

In addition, the data generated in the present study was done using polydisperse particles, whereas the data reported in the literature (Raabe et al, 1988) showing a clear trend of increased lung deposition with decreased particle size was generated using monodisperse particles, which tend to better demonstrate the effect of particle size on regional lung deposition.

Furthermore, some of the *in vivo* data showed a high degree of variability, i.e. for a target dose of 100 µg/kg (MMAD: 1.8 µm) the lung deposition fraction ranged from 5.8 to 21.6% of the total inhaled dose. This is likely to have contributed to the lack of clear trend between decreased particle size and increased lung deposition. In addition, previous works have shown the *in vivo* lung data to exhibit a high degree of variability (see Figure 54). This was attributed to a combination of factors such as difference in breathing conditions, body size and activity levels.

For the IVR model, the lung fraction data showed an increased deposition for a change between 2.0 and 5.0 µm. As in the case of the *in vivo* data, this trend is not in line with scientific expectations, in which the fractional lung deposition is expected to show an increase with decreased particle size (Kuehl et al, 2012;Raabe et al, 1988). However, if the data for the IVR model is expressed as post-TB fractions versus particle size, the trend is consistent with scientific expectations, albeit with a high degree of variability. This suggests this fraction of the IVR model may be a more accurate representation of the peripheral lung deposition than the total lung fraction, which encompasses both the TB and post-TB regions of the IVR model.

Moreover, this decrease in particle size was associated with enhanced efficacy as measured by the associated reduction in neutrophil number (see Figure 60). However, it must be stated that this trend did not reach statistical significance (P= 0.3319), probably due to the clear differentiation in response between the 100 and 1000 µg/kg doses at the 2 µm particle size.

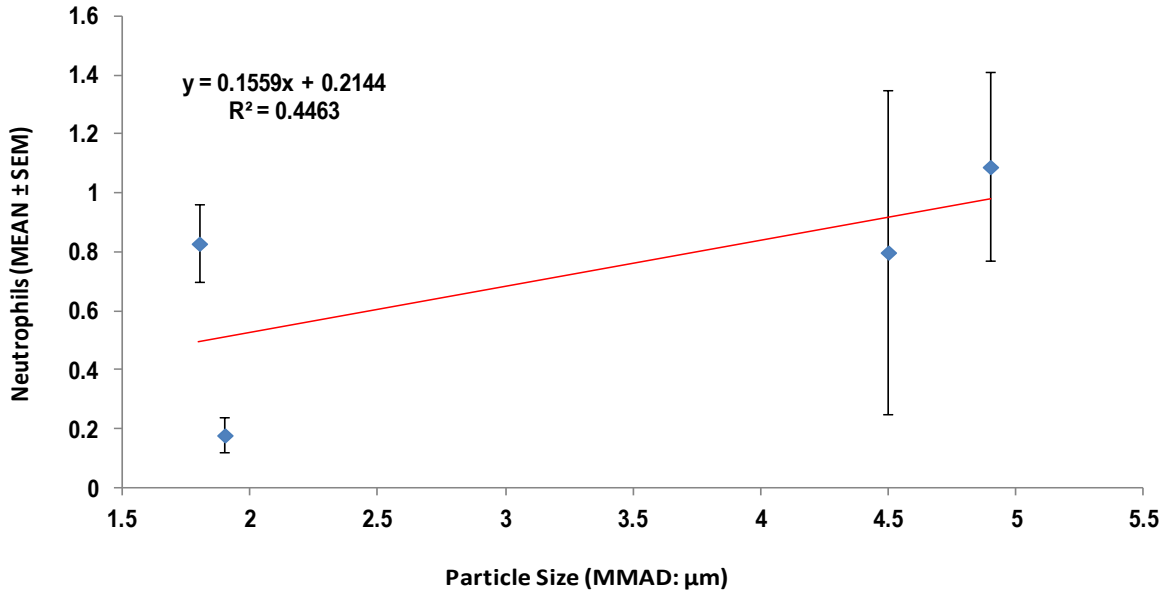

Figure 60: Effects of inhaled FP particle size (MMAD) on LPS-induced BAL neutrophil infiltration in the rat lung.

Consequently, when the data is plotted as neutrophil numbers versus percentage lung dose for the *in vivo* rats, a flat relationship between the two variables results (see Figure 61).

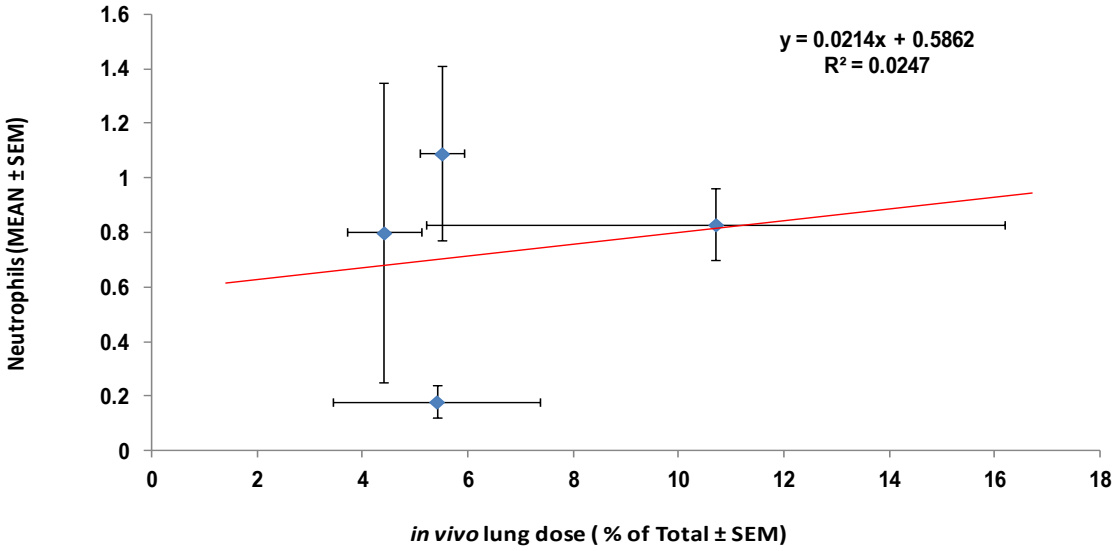

Figure 61: Neutrophil numbers versus percentage of targeted dose in lung for *in vivo* rats

However, when the neutrophil numbers versus the MPPD pulmonary fraction and IVR post-TB fraction (see Figure 62) are plotted, an inverse trend is demonstrated. This suggests a lack of agreement between the *in vivo* lung deposition and the IVR and MPPD model data with respect to the effect of particle size on the fractional deposition in the lung.

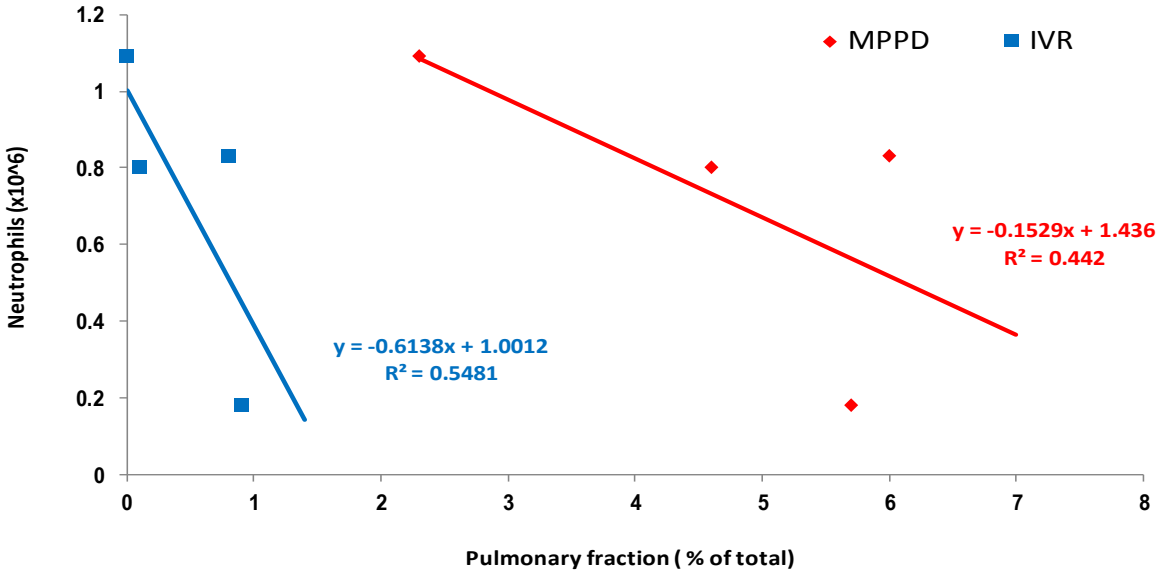

Figure 62: Neutrophil numbers versus MPPD pulmonary fraction estimates (red diamonds) and IVR post-TB deposition (blue squares)

There are several possible reasons why the *in vivo* lung homogenate data (% of deposited dose) failed to show a differentiation at different deposition fractions of FP in contrast with MPPD and the IVR model. Firstly, as previously stated, the *in vivo* lung dose data have tended to show a high degree of inherent variability due to differences in animal breathing conditions during exposure (see section 6.3.1.2, B-Results and Discussion). This is in contrast with the MPPD model estimate which uses default breathing parameters and the IVR model, which used a ventilator set at a set value of 0.214 L/min to ventilate the model during exposure.

Secondly, the LPS challenge method may not be sensitive enough to show differences in efficacy over the range of doses explored. Therefore, additional higher doses may be required in order to demonstrate the relationship between dose and efficacy (Chiang et al, 2010).

Nonetheless, these observations for the relationship between increased peripheral deposition in the IVR model and MPPD model estimates and increased efficacy are consistent with studies in human subjects. They suggest an increasing airway deposition of inhaled corticosteroids through formulation changes, enhanced anti-inflammatory effects and clinical efficacy with increased deposition in the small airways (Cohen et al, 2008;Gentile and Skoner, 2010;Menzies et al, 2007).

7.3 Conclusion

This study demonstrated that exposure of rats to FP powder resulted in a dose-dependent inhibition of neutrophils in BAL fluids. However, a clear difference in neutrophil suppression was demonstrated for equivalent doses but different particle sizes of FP, where the smaller FP particles (2.0 µm) induced a greater level of neutrophil suppression in comparison with larger FP particles (4.0 µm). This difference in efficacy response was attributed to greater peripheral deposition for smaller-sized FP particles and the induction of a greater efficacy response.

However, the *in vivo* fractional deposition data (% deposited of target dose) did not support this hypothesis, where a flat response between fractional deposition level and neutrophil numbers was demonstrated. This is in contrast to the IVR model and MPPD estimates, which showed an inverse correlation between increased peripheral deposition and greater efficacy, as measured by suppression of neutrophil numbers in the BAL fluids. This lack of agreement between the *in vivo* fractional deposition data and IVR and MPPD model estimates was attributed to a number of factors. Principally, the *in vivo* lung dose data is known to exhibit a high degree of inherent variability (Schlesinger, 1985), probably due to the difference in animal breathing conditions during exposure. For instance, for the target dose of 100µg/kg, the lung dose ranged from 4.6 to 21.6%.

This is in contrast with the MPPD model estimates, which use default breathing parameters and an IVR model using a ventilator set at a constant value of 0.214 L/min to ventilate the model during exposure. In addition, the LPS challenge method may not be sensitive enough to show differences in efficacy over the range of doses explored; thus, additional higher doses may be required to demonstrate the relationship between dose and efficacy.

In summary, a reasonably clear correlation for the relationship between lung deposition in the IVR model and neutrophil suppression levels was demonstrated. Furthermore, this data support the hypothesis that regional deposition is an important determinant in efficacy. Therefore, this suggests that the IVR model may be useful as a tool to describe *in vivo* efficacy with *in vitro* data. To my knowledge, this is the first time an *in vitro* model of the rat lung has been used as part of the assessment of efficacy of inhaled drugs in preclinical animal models. Further work would be required to evaluate the validity of this model and relationship with efficacy for a range of inhaled drug classes.

C. Experimental Setup

1 Development of aerosol delivery method

1.1 Materials and Equipment

1.1.1 Materials

1. Blends of monodispersed fluorescent microsphere (FMS), particle size 2 and 4 µm and GSD 0.095 and 0.094 respectively mixed with inhalation grade lactose in proportion of 0.8% w/w were used as the test materials to evaluate aerosol generation performance and assess the impact of particle size of the active ingredient (FMS) on aerosilisation properties in the exposure chamber. FMS is proprietary product of Polysciences Inc, Warrington, USA. Inhalation grade lactose (Grade A) was obtained from Friesland Food Domo, Zwolle, Netherlands. The percent level of fines is stated as 4.4% for % < 4.5um on the certificate of analysis. Blends were prepared using Turbula mixer, operated for 60 min at 42 rpm.

2. Inhalation grade A lactose; FFD lactose, manufacture Batch No: 15284. This material was obtained from Friesland Food Domo, Zwolle, Netherlands. Particle size analysis using Symapetc showed this material to have the following distribution: Mass Median Particle Size (MMPS) of 60-80 µm and % fines level (< 8 µm); 6-8% w/w.

Table 19 contains information on which investigations the test materials were used and justification for their use.

Table 19: Details of where the test materials were used and justification for their use

Material	Uses	Justification
FMS (2µm) mixed with inhalation grade Lactose (0.8% w/w)	Screening study (see 1.3, B–Results and Discussion) APS Vs HPLC filter correlation (see 1.5.2, B–Results and Discussion) APS Vs Marple Cascade Impactor evaluation(see 1.5.3, B–Results and Discussion)	FMS was chosen at the test material as it is widely used in rodent inhalation studies to investigate particle deposition in site-specific regions of the lung (Pinkerton et al, 1993). In addition, FMS due to its monodisperse particle size act as "surrogate" marker of drug substance and enable generalised understanding of particle deposition in specific regions of the lung and the subsequent action of these particles, such as translocation and clearance from distinct sites within the lung
FMS (4µm) mixed with inhalation grade Lactose (0.8% w/w)	Delivery method evaluation (see 1.4, B–Results and Discussion)	
Inhalation grade A Lactose	APS dilution ratio study (see 1.5.1, B– Results and Discussion)	This material was selected as it is likely to be mixed with micronised drug substance of much smaller particle size distribution (X50: 2-5 µm) in future animal dosing studies. Therefore, understanding the behaviour of this carrier is important in the overall evaluation of the performance of exposure chamber and the carrier physical properties are likely to dominate.

1.1.2 Equipment

Table 20 details the equipment used in the development of aerosol delivery method investigations.

Table 20: Equipment

Equipment	Manufacturer/Supplier
Aerosol generator	Model 3400A Fluidised Bed Aerosol Generator TSI Incorporated, Shoreview, U.S.A
Aerosol Diluter	Model 3302A (TSI Incorporated, Shoreview, U.S.A)
Animal exposure chamber	12-port animal exposure system (CH Technologies, USA) 4-port animal exposure system (EMMS, Bordon UK)
Balance, analytical	Mettler Toledo XP204 (Mettler Toledo, Columbus, USA) Readability 0.1 mg Repeatability 0.05 - 0.07 mg Linearity 0.2 mg
Balance, precision	Mettler MT5 (Mettler Toledo, Columbus, USA) Readability- 0.001mg Reapeatability-0.0008mg Linearity-0.004mg
Blender	Turbula Shaker-Mixer (Willy A. Bachofen, Mutternz, Switzerland)
Filters	Respigard II™ Filters, Vital Signs Ltd (Littlehampton, U.K)
Cascade Impactor	Marple Personal Cascade Impactors, model 298. Andersen Samplers Incorporated (Smyrna, USA)
Mass Flow meters	Cole-Parmer Instrument Co. Ltd (Hanwell, U.K)
Particle size spectrometer	Model 3321 Aerodynamic Particle Sizer (APS) spectrometer (TSI Incorporated, Shoreview, U.S.A)
Static eliminator	Meech Static Eliminators Ltd (Oxford, UK)

1.1.2.1 Operation of Fluidised Bed Aerosol Generator (FBAG)

The following table describes the operating limits of most important parameters of the fluidised bed Aerosol generator.

Table 21: Specification of the model 3400A Fluidised Bed Aerosol Generator

Aerosol flow rate	5 to 15 L/min
Particle size distribution	Similar to powder to be dispersed; maximum size is about 40 µm aerodynamic diameter; particles smaller than 0.5 µm do not deagglomerate efficiently.
Output concentration (adjustable)	10 to 100 mg/m^3
Powder feed rate (adjustable)	3 to 30 mm^3/min
Flow meter	Two, rotameter type: bed flow and bead-purge flow
Cyclone (½-inch stainless-steel)	classified respirable dust at 9 L/min
Environmental Conditions	Indoor use Altitude up to 2000 m (6500 ft) Ambient Temperature 10 to 50°C Ambient humidity 0-90% RH non-condensing
Power Requirements	85 to 260 VAC, 50/60 Hz, 25 W maximum

1.1.2.2 Operation of the real-time Aerodynamic Particle Sizer

When size and number concentration analysis was required, the aerosol sample was drawn through the aerodynamic particle spectrometer (APS 3321; TSI Inc, Shoreview, MN). The APS 3321 uses time-of-flight technique to calculate number-weighted aerodynamic size distributions that are transformed to a mass-weighted basis using software provided with the instrument (Aerosol Instrument Manager Program 5.2.1, TSI Inc., St. Paul, MN).

The APS sizes particles by accelerating the aerosol sample flow through an accelerating orifice (see Figure 63).The aerodynamic size of a particle determines its rate of acceleration, with larger particles accelerating more slowly due to increased inertia. As particle exit the nozzle, they cross through two partially overlapping laser beams in the detection area. Light is then scattered as particles crosses through the overlapping beams. The emergent light is then focussed onto an avalanche photo-detector (APD). The APD then converts the light pulses into electrical signal for further processing using instrument software.

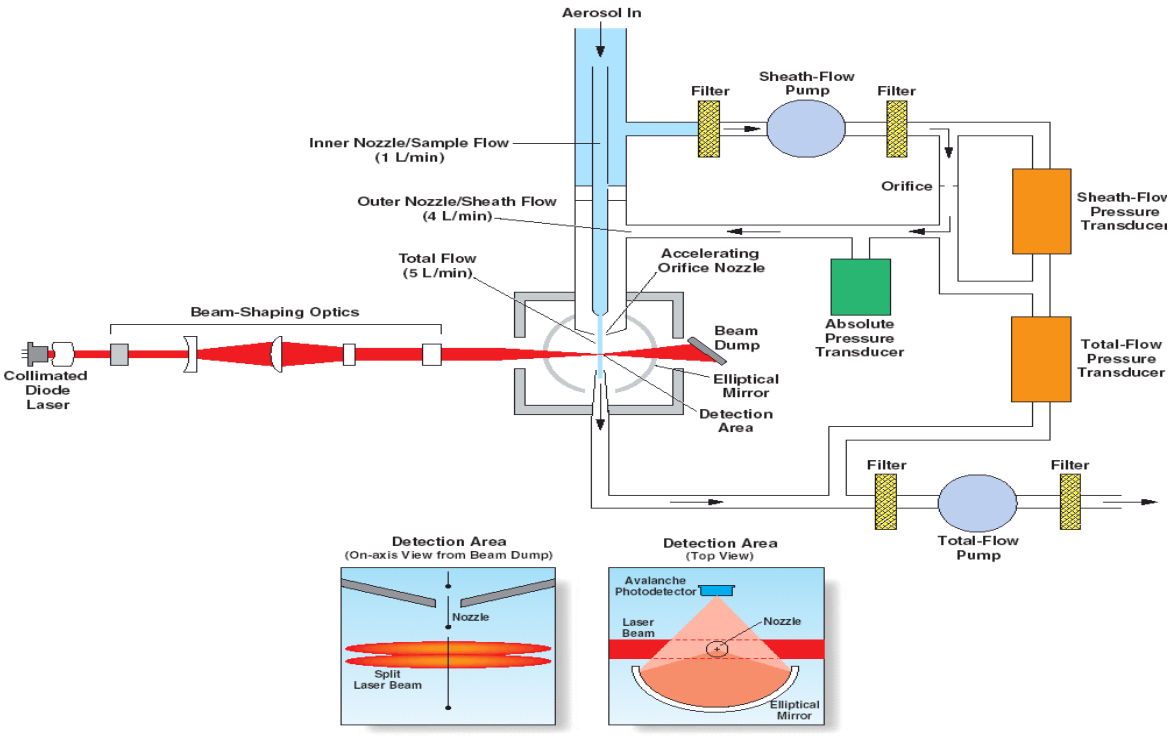

Figure 63: Aerosol flow through the APS 3321.Reproduced with permission from TSI product literature.

Prior to the start of the investigation the instrument was calibrated using polystyrene latex beads particles of size distribution between 0.5 to 20µm. The peak in signal for these particles fell in the appropriate size bin to their size thus confirming the accuracy and precision of the instrument. In addition, in cases where highly concentration aerosols are under evaluation, the APS may be configured with an optional dilutor (Model 3302A) designed to specifically reduce the particle concentration, reduce the frequency of coincidence events and improve the accuracy of particle size and total concentration determinations. The dilutor is calibrated for dilution ratios of 100:1 and 20:1 at a total flow rate of 5 litres per minute.

Furthermore, the APS has the capability to processes and logs every particle single into four distinct events dependent on its aerodynamic properties. This is a useful diagnostic feature which allows the operator to diagnose any problems which may arise during data collection and thus enable corrective actions to be employed to resolve these issues. Figure 64 summarises these events data and their impact on the particle size measurements produced.

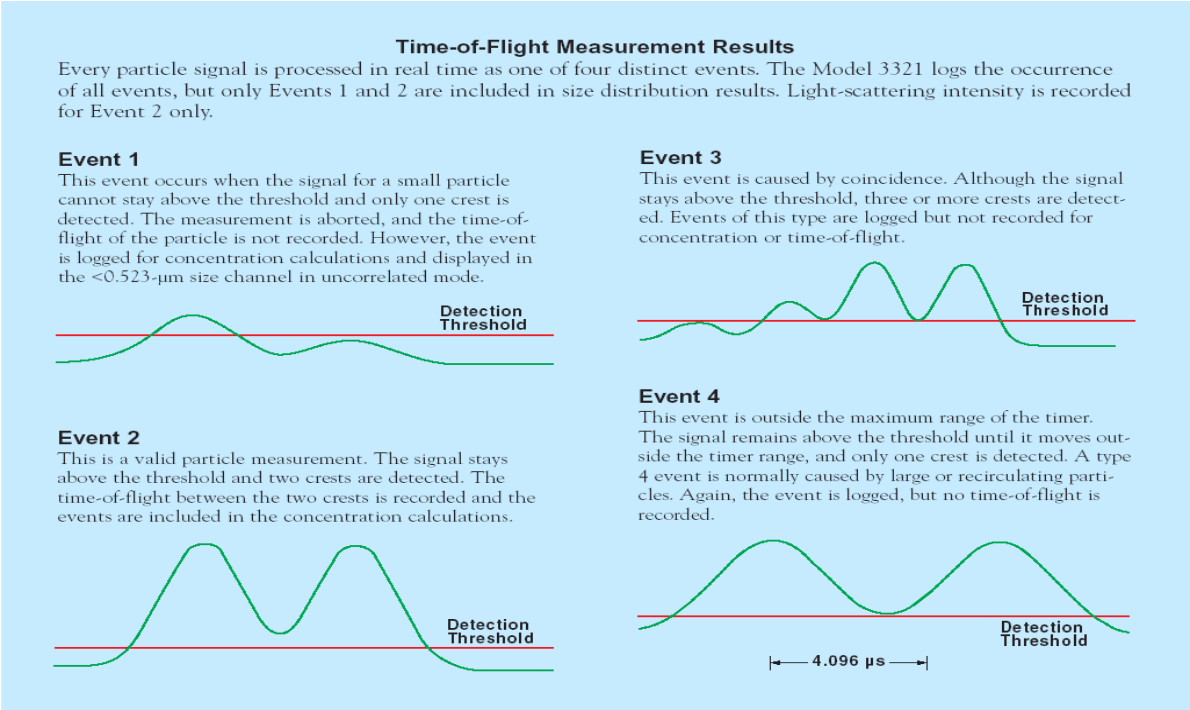

Figure 64: Classification of particle size data by Event number, dependent on its aerodynamic properties. Reproduced with permission from TSI product literature

The following Table describes the most important data of the major components of APS particle sizer.

Table 22: Specification of the Model 3321 Aerodynamic Particle Sizer

Measurement technique	The time-of-flight of individual particles is measured in an accelerating flow field. Processing electronics measure the time-of-flight of the particle using a single high-speed timing processor. Phantom particle rejection is achieved through the use of a patent pending double crested optical system. The particle size binning is based on an internally stored calibration curve.
Particle Type	Airborne solids and non-volatile liquids
Particle Size Range	0.5 to 20 µm aerodynamic size, 0.3 to 20µm optical size (PSL equivalent)
Maximum Particle Concentration	1000 pt/cm^3 at 0.5 µm with less than 2% coincidence. 1,000 pt/cm^3 at 10.0 µm with less than 6% coincidence.
Display	32 channels per decade of particle size (logarithmic). This results in 52channels total. 1,024 bins of raw time-of-flight data (4 ns per bin)
Resolution	0.02 µm at 1.0 µm diameter. 0.03 m µ at 10 m µ diameter.
Sampling Time	Programmable from 1 second to 18 hours
Flow Rates	Total flow: 5.0 L/min ± 1%, Sheath flow 4.0 L/min ±1%, Aerosol Sample 1.0 L/min ± 10% (feedback controlled).
Atmospheric Pressure Correction	Automatic correction between 400 and 1,030 mbar (full correction between 700 and 1,030 mbar)
Concentration Accuracy	±10% of reading plus variation from counting statistics.
Operating Temperature **Operating Humidity**	10 to 40°C (50 to 104°F). 10 to 90% RH non-condensing.
Laser Source	30 mW, 655 nm laser diode.

1.1.3 HPLC quantification of Fluorescent Microspheres

1.1.3.1 Reagents

Acetonitrile (MeCN, HPLC – gradient – grade) was purchased from Sigma-Aldrich (St. Louis, US). The mobile phase was Acetonitrile: Water at a ratio of 80:20 (v/v). Fluorescent Microspheres (FMS) was purchased from Polysciences Inc, Warrington, USA and was used to prepare the working standard solutions. FMS was extracted using 2-Ethoxyethyl acetate (Cellosolve, 98% purity grade) purchased from Sigma-Aldrich (St. Louis, US). Water was obtained by an in-house filter system (Milli – Q; reagent grade water system) from Millipore (Schwalbach, Germany).

1.1.3.2 Sample preparation

The fluorescent microspheres were extracted from the Respirgard filters using 2-Ethoxyethyl acetate (Cellosolve, 98% purity grade) purchased from Sigma-Aldrich (St. Louis, US). The filter was initially rinsed with cellosolve and extracted from the housing using tweezers. The casing, filter and tweezers were rinsed down into an emitted dose pot (plastic container with screw top lid) using 25ml of cellosolve and sonicated for 5 minutes. The filter and emitted dose pot were washed down into a 50ml volumetric flask using cellosolve. A secondary dilution was performed, taking 10ml into 100ml (or an equivalent dilution ratio) and diluting with 70:30 Acetonitrile: Water. Acetonitrile (MeCN, HPLC – gradient – grade) was purchased from Sigma-Aldrich (St. Louis, US). Water was obtained by an in-house filter system (Milli - Q® - reagent grade water system) from Millipore (Schwalbach, Germany).

1.1.3.3 Analytical equipment

The HPLC system (Agilent Technologies, Placerville, CA, USA) consisted of a quaternary pump, a degasser, a fluorescent detector, a column oven, and an auto sampler. The column used was Zorbax SB-C18 3.5µm, 4.6 x 50mm. The column was maintained at 30°C. The flow rate was set at 1.0 mL/min. The injection volume was 50 µL. Detection was by fluorescence (Excitation at 441 nm; Emission at 486 nm).The fluorescence excitation and emission of each sample was measured to be 441 and 486 nm respectively. The method was developed and validated at GSK.

1.1.3.4 **Analytical method validation details**

The HPLC method was developed and validated at GSK Ware. Details of the method are described in Table 23.

Table 23: Validation details for determination of the Fluorescent Microsphere content in filter samples

Parameter	Result
Specificity of the Chromatographic System	Resolution demonstrated for FMS when using FLD at 441nm exc, 486nm emis
Linearity of Detector Response for FMS (Range 0.15 - 1540ng on column)	Linearity demonstrated for the response due to FMS Correlation coefficient R^2 > 0.9999. Intercept = 0.57% of nominal
Accuracy of FMS from solution containing Lactose	FMS recovery in the presence of Lactose in solution has been demonstrated.
Standard Solution Stability	The dilute standard solutions have been demonstrated to be stable for 10 days (including the day of preparation) when stored at ambient temperature on the bench top in a sealed container.
Limit of Quantification (LOQ)	0.003 µg/mL
Range	0.003-30.8 µg/mL

The chromatograms obtained were comparable to the example chromatograms shown in Figure 65.

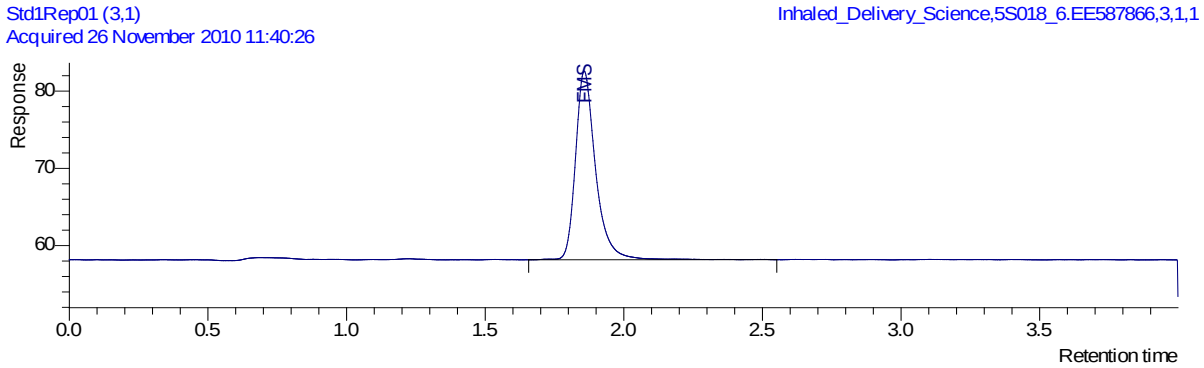

Figure 65: Example chromatogram for FMS test material. Retention time for of the FMS peak should be in the range of 1-3 minutes.

1.1.4 Determination of particle size distribution using Marple Cascade Impactor (MCI)

Particle size distribution was determined using the MCI (see 1.5.3, B- Results and Discussion). A measured volume of air was drawn from the exposure chamber at a flow rate of 2.0 L/min through the impactor (model 269), attached to one of the sampling port. Aerosol was collected on stainless steel substrates and a final glass fibre filter. After the sampling period was completed, each substrate is wash down with a known volume of solvent (50 mL of Methanol: Water, 70:30 v/v). Concentration of actives (Fluorescent Microspheres; FMS) was determined using the HPLC method described in section 1.1.3, C- Experimental Setup.

The data from the cascade impactor was used to estimate the median diameter and GSD of an aerosol if the aerosol has a log-normal size distribution. The cumulative fraction of particle number or mass below each stage was converted to a z-score (number of standard deviations away from the mean, based on a normal cumulative distribution) for each stage. The log of the particle size cut-off for each stage is then plotted as a function of those z-scores.

The resulting graph will be linear if the distribution is log-normal and all of the particles deposited in the impactor. The y-intercept of the fitted line corresponds to peak of the distribution and the median diameter found by finding the inverse log of that intercept. Because the particle diameter relevant to inertial impaction is the aerodynamic diameter, the median diameter is referred to as the mass median aerodynamic diameter (MMAD). The GSD is found by dividing the particle size associated with the 16th or 84th percentile (z-score = 1) with the median particle size (Christopher et al, 2010).

1.1.5 Statistical data analysis

The statistical analyses for the screening study (see 1.3, B- Results and Discussion) were performed using Design Expert 7 (Stat-Ease, Inc.2021 East Hennepin Ave., Suite 480 Minneapolis, MN55413 (Version 7.1.1). For each response the final ANOVA model is shown. If a factor has a p-value of less than 0.05 then it is statistically significant at the 5% significance level. If a factor has a p-value between 0.05 and 0.1 then there is an indication of statistically significant effect (see 1.3, D-Appendix for summary of statistical analysis).

1.2 Aerosol generation methods

1.2.1 Screening study

For the screening study (see 1.3, B – Results and Discussion), the chain-feed operating mechanism was used to deliver the test material to the fluidised bed. Prior to the start of the experimental runs, the chamber was operated for 60 minutes using fresh bronze breads, in order to allow time for the aerosol exposure concentration and particle size output to stabilise. Thereafter, the chamber was operated for 60 minutes per experimental run, and the readings for the aerosol concentration and particle size distribution were captured using the APS instrument. Details of the operation steps followed in the conduct of this study are listed below.

Operating steps for the operation of the exposure equipment:

1. Connect the generator to the source of compressed air.
2. Remove plug from the bed chamber and fill the chamber with the bronze beads to the line inscribed on the inside of the chamber.
3. Remove the cover of the powder reservoir chamber and fill the powder reservoir with the selected powder using approximately 20 cm^3 and reinstall the powder reservoir cover.
4. Connect the dust outlet of the generator to the test chamber.
5. Switch on the AC POWER on the back panel of the generator.
6. Adjust the flow rate to the required level.
7. Switch on the motor switch and set the chain speed switch to the desired level.
8. Switch the APS instrument and ensure its connected to a personal computer to capture the exposure conditions.
9. Check the APS aerosol diluter settings are correct.
10. Operate the generator for 60 minutes.
11. On completion of experiment, switch off the APS and compressed air supply.

1.2.2 Delivery method evaluation

For the batch-fed delivery method evaluation study (see 1.4, B–Results and Discussion), the required amount of FMS-Lactose test materials (2 and 4µm) was mixed thoroughly with bronze beads before being transferred into the fluidisation chamber. The percentage level of FMS in the bronze bead material ranged from 2.5 to 10% w/w of total content. Thereafter, the generator was operated for a total of 45 minutes. The readings for the aerosol concentration and particle size distribution were captured using the APS instrument. Details of the operation steps followed in the conduct of this study are listed below.

Operating steps for the operation of the exposure equipment:

1. Weigh 3.8 and 7.8 grams of the test material into amber glass jar using analytical balance.
2. Weigh 150 grams of the fluidising bronze beads into a separate appropriately amber glass jar.
3. Sequentially transfer the bronze beads from its container to the jar containing the test material. Mix thoroughly and continue adding more material until all the brass beads have been transferred.
4. Shake the mixture thoroughly using a Turbula mixer for at least thirty minute in order to ensure even mixing of the test material within the fluidising beads.
5. Leave the mix to rest for a minimum of 24 hours in order to allow any electrostatic charges built up during the blending process to dissipate
6. Transfer the mixture into the fluidised chamber.
7. Fill the chamber with mixture to the line inscribed on the inside of the chamber. The beads must cover the lower part of the chain when the bed is inactive.
8. Connect the dust outlet of the generator to the test chamber
9. Switch the APS instrument and ensure its connected to a personal computer to capture the exposure conditions.
10. Seal all remaining port with the exception of APS and sampling port
11. Turn on the compressed air supply.
12. Adjust the aerosol flow rate in the FBAG to 10 L/min.
13. Operate the generator for 45min.

1.2.3 Validation the APS 3321 for use in rodent inhalation studies

For all studies conducted, the batch-fed delivery method as described in section 1.2.2, C – Experimental Setup, was used to generate the aerosol powder for evaluation. For studies comparing the aerosol concentrations generated using gravimetric versus APS and assessing the effect of using dilutors on measured aerosol concentrations (see 1.5.1, B-Result and Discussions) inhalation grade lactose (6-8% W/W <15 micron, MMPS= 60-80 micron) was used as the test material. The two powders were thoroughly mixed and introduced into the fluid bed chamber. The ratio of lactose to bed material was reported as volume percent (nominal; 2.5% w/w). The fluidised bed was operated at a flow rate of 20 litres/minutes for duration of 45 minutes per run. A total of 5 runs per dilution ratio were conducted.

In addition to the standard 1:1 sample dilution ratio, two dilution ratios were used: 20:1 and 100:1. The model 3320A diluter is an accessory of the APS and is designed to reduce the concentration of high-concentration aerosol. The diluter is calibrated for dilution ratios of 1:1, 20:1 and 100:1 at a standard flow rate of 5 litres per minute. The sample flow enters the diluter and separates into two paths. In the case of 100:1 dilution, 99% of the flow is removed for filtering (4.95 LPM) is removed and 1% (0.05 LPM) is drawn isokinetically through a capillary tube measuring 13.4 cm long and 0.09 cm in diameter.

The methodology used for correlating the APS readings with gravimetric readings involved weighing filters before and after each sampling period using an electrobalance (Mettler Toledo, Columbus, USA) and the aerosol masses was calculated. The corresponding readings from the APS were then used to establish correlation coefficient between the two methods for determining the mass concentration of aerosol in the exposure chamber.

For studies comparing aerosol concentration using HPLC versus APS, a blend of monosised fluorescent microspheres (2µm sized) mixed with inhalation grade lactose was used as used as the test material. The amount of FMS collected on filters after a given sampling period was extracted with acetonitrile solvent (Baker, HPLC gradient grade) and analysed by HPLC as detailed in section 1.1.3, C-Experimental Setup.Thereafter, the aerosol concentrations results for FMS generated were compared against the corresponding readings given by the APS.

For studies comparing particle size distribution using Marple Cascade Impactor (MCI) versus APS, a blend of monosised fluorescent microspheres (2µm sized) mixed with inhalation grade lactose was used as used as the test material. A total of five experimental runs were conducted. Details of the MCI and APS method are listed in section 1.1.4 and 1.1.2.2, C-Experimental Setup respectively. Thereafter, the particle size distribution in terms of MMAD, GSD and profile for both methods were compared.

2 Validation of Nose-Only Exposure System for Rodents

2.1 Materials and equipments

2.1.1 Materials

A blend of monodispersed fluorescent microsphere (FMS), particle size 2 µm and GSD 0.095 mixed with inhalation grade lactose in proportion of 0.8 w/w served as the test compounds. Section 1.1.1, C-Experimental Setup details the material and manufacturing method used to prepare this blend. Blend content uniformity analysis showed mean content of 98.8% of Label Claim and 2.7% CV

2.1.2 Equipments

Refer to Table 20 for details the equipments used in validation of nose-only exposure system for rodents investigation.

2.2 Methods

2.2.1 Exposure technique and generation of aerosol

The test material (FMS-Lactose) was mixed with fluidising beads before addition to the generator. The nominal blend concentration was 2.5% w/w. A Turbula mixer operated at speed of 49 revolutions per minutes and 30 minutes duration was used to ensure adequate coating of the bronze beads with the test material. The use of Turbula mixer ensured a standardised method was used for the preparation of all samples and removed this factor as a possible of source of variability in the aerosol concentrations in the various locations of the exposure chamber.

Following on from this, the mixture was then transferred to the fluidised bed chamber. The flow rate in the fluidised bed aerosol generator (FBAG) was set at 25 L/min; 5 L of which was required for operation of the aerodynamic particle sizer (APS 3200A). Technical details of the air flow rates of the inhalation chamber are given in Table 24. Experimental procedures of the operation of the exposure system are detailed in section 2.2.3, C-Experimental Setup.

Table 24: Inhalation chamber, airflows and generation of aerosol atmosphere details

Parameter	Values
Volume of inner cylinder	1250mL
Equilibrium concentration (t_{99})	13.82 sec
Airflow into fluidised bed	25 L/min
Dilution Air	0 L/min
Total air flow fed into chamber	25 L/min
Airflow rate/exposure port	0.89 L/min
Exhaust air	8.0 L/min
Auxiliary pump	9.0 L/min
APS	5 L/min
APS Dilution Ratio	1:100
Total air flow extracted from chamber	22 L/min
Per cent extracted from the chamber	88% of total airflow fed into chamber
Aerosol Generation Delivery Method	Batch-Fed

Under the assumption that the internal the internal cylinder of the inhalation chamber behaves as a completely mixed chamber, the time required to reach 99% of its equilibrium concentration (t_{99}) is given by the term 4.605 (V/F), where V is the internal volume of inner cylinder of the inhalation chamber and F is the total air flow rate through the chamber (Silver, 1949). Under these conditions, a steady state should be attained in the chamber within 20 seconds.

2.2.2 Aerosol monitoring and evaluation

The inhalation chamber consisted of one segment accommodating a maximum of 12 animals. Of the 12 exposure ports, one was used for sampling the exposure atmosphere for concentration and particle size using the APS. Another port was fitted with a Relative Humidity/Temperature probe in order to allow for evaluation of environmental conditions within the exposure chamber during operation. In addition, 10 of the remaining ports were fitted with high efficiency collection filters (Respigard 303A). These filters allowed for evaluation of the aerosol concentration and size distribution with respect to time using gravimetric and chemical assay techniques.

Chemical assay of the filters samples at different time periods and locations was used to estimate temporal variability within exposure chamber. This was performed using the Respigard filters placed in various port locations of the exposure system and analysing the quantity of fluorescent microspheres collected on each filter. To determine the uniformity of the exposure to all ports multiple runs were performed with the filters located in different ports. The exposure system was run for 65 minutes to minimise any fluctuations over the duration of dosing.

For the time dependant dosing experiments samples were collected continuously, beginning immediately after aerosol generation (0-15 minutes) and from 20-65 minutes time interval in order to allow 5 minutes for replacement of filters. Each filter was attached to identical tubing and attached to a Copley pump to give a flow of approximately 1.0 L/min through each filter. The fluorescent microspheres were extracted and analysed using HPLC using the method detailed in section 1.1.3, C-Experimental Setup.

In gravimetric analysis the mass concentration was measured by collecting particles on a filter and measuring the increase in filter weight using an electronic balance (Mettler Toledo, Columbus, USA). The weight difference before and after exposure was then noted and represented the Total Particulate Matter (TPM) per exposure period. Filter samples for gravimetric determinations were taken from sampling ports located in diametrically opposite locations of the exposure chamber.

Samples for the analysis of particle size distribution and aerosol concentration using the aerodynamic particle spectrometer (APS TSI 3321) were obtained exclusively from a fixed sampling location in the exposure chamber to enable comparison with the gravimetric and HPLC samples.

2.2.3 Experimental procedure for operating the exposure system

2.2.3.1 Experimental checks prior to start of exposure period

1. Check air flow from FBAG is set at 25L/min
2. Check the airflow from auxiliary pump is set at 9 L/min
3. Check the airflow after APS is turned on and airflow is set at 5 L/min
4. Turn on the vacuum source and set airflow to 8L/min
5. Check the aerosol diluter settings are correct.
6. Record the Temperature and Relative humidity (RH) in exposure chamber.

2.2.3.2 Experimental procedure for Start-Up and Operation

1. Drain compressor of any remaining water before start of experiment
2. Instil lid on top of exposure chamber and grease joints.
3. Install the elutriator with four ¾- inch Phillips pan-head screws. Grease Joints
4. Connect the Elutriator tube of the generator to the Central Dosing Chamber.
5. Install the APS probe into port numbered 6.
6. Install the RH probe into port numbered 12.
7. Number, weigh and place the 10 Respigard filters into the inhalation ports of the exposure chamber (ports 1-5, 7-11)
8. Switch on the APS.
9. Turn on the compressed air supply for the main extraction pump and set at 8 L/min
10. Switch on the air supply to auxiliary pump and set to 9 L/min
11. Adjust the aerosol flow rate in the FBAG to 25 L/min.
12. Check the airflow is balanced and record values in experimental log book.
13. Transfer the FMS-Lactose-Bronze beads mixture into the fluidised chamber.
14. Fill the chamber with mixture to the line inscribed on the inside of the chamber. The beads must cover the lower part of the chain when the bed is inactive.

15. Install the elutriator with four ¾- inch Phillips pan-head screws.
16. Connect the Elutriator tube of the generator to the Central Dosing Chamber.
17. Operate the generator for 15 min.
18. Stop the FBAG operation by turning off the airflow to the compressor
19. Remove filter 1-11 sequentially and replace with new filters.
20. Reweigh and record filter weights of removed filters
21. At 20 min post exposure exactly, restart operation of FBAG by turning the airflow to previous settings.
22. Operate Exposure Chamber for a further 45 minutes (total sampling time including 5 min stop for removal of filter: 65 minutes).
23. Remove filter samples and reweigh.
24. Power down the aerosol generator, FBAG.
25. Check the airflow settings and record values in experimental log book
26. Perform dry clean on all components of the exposure chamber.

3 Assessing the effect of aerosol characteristics on deposition in the rat model

3.1 Materials and equipments

3.1.1 Materials

A blend of monodispersed fluorescent microsphere (FMS), particle size 2 µm and GSD 0.095 mixed with inhalation grade lactose in proportion of 0.8 w/w served as the test compounds. Section 1.1.1, C-Experimental Setup provides more details on this test material.

The 2.0 µm and 4.0 µm FMS-Lactose blends were prepared using a high shear M-Pro mixer (ProCepT nv, Zelzate, Belgium), operated for a total of 30 min at 900 rpm. Blend content uniformity analysis using high performance liquid chromatography showed a mean content of 0.70% w/w and CV of 3.0% for the 2.0 µm blend. For the 4.0µm FMS-Lactose blend, content uniformity analysis using high performance liquid chromatography showed a mean content of 0.84% w/w and CV of 1.8%.

For the MgSt containing inhalation blends, FMS was initially mixed with a mixture containing MgSt and lactose (1.0% w/w) using a pestle and mortar. Thereafter, the mixture was transferred to an amber glass jar and blended using Turbula mixer for 30 min at 42 rpm. Blend content uniformity analysis using high performance liquid chromatography showed an average content of 0.67% w/w and CV of 7.3% for the 0.8% FMS containing blends. For the 3.0% FMS blend, blend content uniformity results showed an average content of 2.7% w/w and CV of 3.8%.

3.1.2 Equipment

Refer to Table 20 for details the equipments used in this investigation. Furthermore, Table 25 details additional equipments used.

Table 25: Details of equipment used in assessing the effect of aerosol characteristics on deposition in the rat model experiment.

Equipment	Manufacturer/Supplier
Rodent Ventilator	Ugo Basile Rodent ventilator (Model 6025; Comoro, Italy)
TPF 100 Flow Transducer and Adaptive Amplifier	EMMS, Bordon, UK
Preamp module controller	EMMS, Bordon, UK
ventilation manoeuvres monitoring software (eDacq)	EMMS, Bordon, UK

3.2 Aerosol Generation and characterisation of chamber atmospheres

For experimental work assessing the effect of ventilation and aerosol characteristics on deposition in the IVR model (see section 4, 5, B- Results and Discussion) a simplified design version of the 12-port exposure chamber was employed. The main difference was a reduction in the number of sampling ports, with 4 ports used as opposed to the 12 ports. The test aerosol material was generated using a fluidised bed aerosol generator (FBAG) and connection of the generator output to the exposure chamber (see Figure 66).

Figure 66: Schematic of the four-port exposure chamber, used for evaluation of the *in vitro* rat model. Reproduced with permission from Aztec Precision Engineering, Letchworth, UK

Of the four exposure ports, one was used for sampling the test atmosphere for concentration and particle size in real-time using an aerodynamic particle spectrometer (APS 3321; TSI Inc, Shoreview, USA). Another port was fitted with a cascade impactor (Marple Personal 298, Smyrna, USA) in order to allow for simultaneous determination of particle size distribution using the cascade impaction method outlined in section 1.1.4, C- Experimental Setup.

A third port was fitted with the *in vitro* rat model (IVR) connected to an Ugo Basile ventilator (Model 6025, Comoro, Italy) in order to simulate physiologically realistic inspiratory and expiratory flow conditions. In addition, two of the remaining ports were fitted with high efficiency collection filters (Respigard 303A). These filters allowed for evaluation of the aerosol concentration and size distribution with respect to time using gravimetric and chemical assay techniques. The test material, fluorescent microspheres (FMS) were extracted and analysed using HPLC using the method detailed in section 1.1.3, C-Experimental Setup.

The test materials (FMS-Lactose blends) were thoroughly mixed with fluidising beads prior to introduction into the fluidising bed using the batch-delivery method outlined in section 1.2.2, C-Experimental Setup. The air flow rate into the FBAG was set at 12 L/min; 5 L of which was required for operation of the aerodynamic particle sizer (APS 3321). Further technical details of the air flow rates of the inhalation chamber components are given in Table 26.

Table 26: Inhalation chamber details, airflows and generation of aerosol atmosphere

Parameter	**Values**
Volume of inner cylinder	1500 mL
Equilibrium concentration (t_{99})	34.5 sec
Airflow into fluidised bed	12 L/min
Dilution Air	0 L/min
Total air flow fed into chamber	12 L/min
Auxiliary pump	2 L/min
Marple Cascade Impactor (MCI)	2 L/min
Filter Air flow conditions	3 L/min
APS	5 L/min
Total air flow extracted from chamber	12 L/min
Aerosol Generation Delivery Method	Batch-Fed

3.3 Ventilation parameters monitoring

During experimental procedure, the airflow conditions were continuously monitored via an airflow sensor (TPF 100 Flow Transducer; EMMS, Bordon, UK) placed in the airflow path between the ventilator and IVR model. This sensor was connected to a flow transducer (Adaptive Amplifier; AMP 110; EMMS, Bordon, UK) which transformed the electrical signals to flow traces of the inhalation manoeuvres was achieved by connecting a notepad (Dell, USA) directly to the COM – port of the ventilator using a USB adapter cable with serial 9 pin interface.

Online recording of ventilation parameters such as breathing frequency, tidal volume and respiratory minute volume (see Table 27) was displayed on personal computer using a data acquisition program (eDacq software; EMMS, Bordon, UK). In addition, there was the possibility to monitor all recorded data listed in an excel spreadsheet updated every ten seconds for trend data and all ventilation values were saved automatically.

Table 27: Selection of ventilation parameters reported and documented by eDacq software

Parameter	Abbreviation	Unit
Breathing rate	f	1/min
Expiratory Tidal Volume	V_{Te}	mL
Flow	-	L/min
Minute Volume	MV	L/min

Several displays of the eDacq software was displayed either trend data like V_{Te}, f, and MV. In addition, curve data for a maximum of three ventilation parameters like flow, mean airway pressure and respiratory volume can be displayed and recorded simultaneously throughout the running of the experiments (see Figure 67).

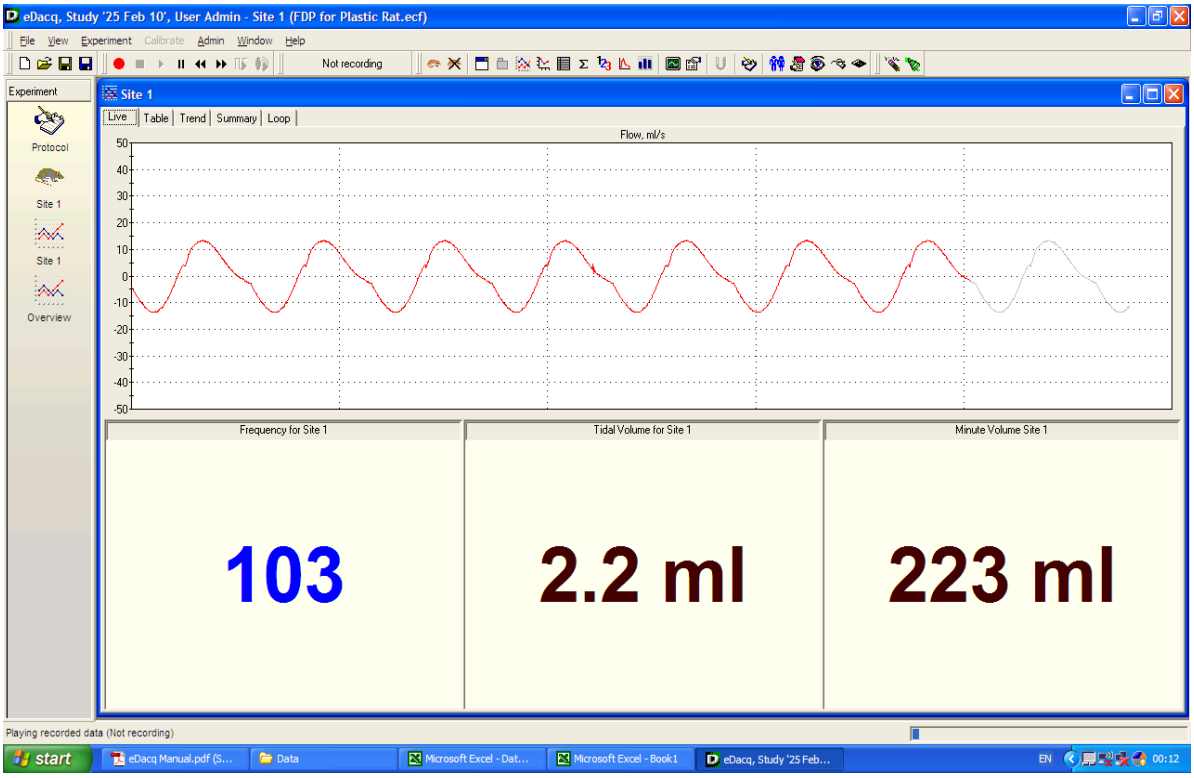

Figure 67: Display of ventilation parameters during experimental procedure, acquired using the data acquisition program (eDacq).

For all experimental procedures the breathing rate was kept constant at 102 breaths per minute throughout the experiments, whereas the tidal volume was set at 2.1 mL. These conditions are considered to be representative of day time activity levels of a Sprague-Dawley rat (Schmid *et al.*, 2008)

3.4 Dose estimation using Multiple-Path Particle Dosimetery Model (MPPD)

The MPPD modelling software (v1.1; National Institute for Public Health and the Environment; Bilthoven; The Netherlands) was used to predict deposition, of FMS particles for each IVR experimental run conditions.

The model takes into account a detailed description of the airway and lung geometry for Long Evans rats. The model consisted of detailed morphometric mapping of 2404 conducting airways collected by Raabe *et al.*, 1975 (Raab et al, 1975). A symmetric 9-generation model acinus was attached to the end of each terminal bronchiole in order to model the pulmonary region in the rat lung. Deposition within each region or airway is calculated using theoretically derived equations for deposition by diffusion, sedimentation and impaction within the airways. The model allows the assessor to test a variety of inputs, such as lung geometry, breathing conditions and particle characteristics such as size distribution and mass density (Asgharian and Anjilvel, 1998).

Model output included deposition for the following regions: (1) Nasopharyngeal; (2) Tracheobronchial; and (3) Pulmonary. IVR run-specific respiration data obtained using the eDacq data acquisition software were input into the model; these parameters included breathing frequency (f, min^{-1}) and tidal volume (V_T, mL). In addition, exposure aerosol conditions of aerosol concentration and particle size distribution (MMAD and GSD) were input into the model. Finally, for all model runs, the inhalability adjustment was selected, and the pause fraction was the default value (0.0).

4 Assessing the effect of ventilation parameters on deposition in the rat model

4.1 Materials and equipments

4.1.1 Blend Manufacture

A blend of monodispersed fluorescent microsphere (FMS), particle size 2 µm and GSD 0.095 mixed with inhalation grade lactose in proportion of 0.8 w/w served as the test compounds. Section 1.1.1, C-Experimental Setup details the material and manufacturing method used to prepare this blend. Blend content uniformity analysis using high performance liquid chromatography showed a mean content of 0.704% w/w and 3.01% CV.

4.1.2 Equipment

Details of equipments used are described in Table 20 and Table 25, C-Experimental Setup.

4.2 Aerosol Generation and characterisation of chamber atmospheres

Details of aerosol generation method used are described in section 3.2, C-Experimental Setup.

4.3 In Vitro Rat (IVR) model details

Details of IVR model used are described in section 3, B- Results and Discussion.

4.4 Ventilation parameters monitoring

Details of ventilation parameter monitoring procedure used are described in section 3.3, C-Experimental Setup.

4.5 Sample preparation and HPLC method details

The FMS deposited in the various sections of the IVR model and filters were recovered using appropriate volumes of 2-Ethoxyethyl acetate solvent (98% purity; Sigma-Aldrich) and analysed using an isocratic validated HPLC assay method as described in section 1.1.3, C-Experimental Setup.

Total drug recovery was calculated by adding the drug deposited in all sections of the model. Regional deposition results were expressed as the percentage of the total drug delivery.

4.6 Dose estimation using Multiple-Path Particle Dosimetery Model (MPPD)

IVR run-specific respiration data obtained using the eDacq data acquisition software were input into the model; these parameters included breathing frequency (f, min^{-1}) and tidal volume (VT, mL). In addition, exposure aerosol conditions of aerosol concentration and particle size distribution (MMAD and GSD) were input into the model. For all model runs, the inhalability adjustment was selected, and the pause fraction was the default value (0.0). Details of the *in silico* MPPD model are described in section 3.4, C-Experimental Setup.

4.7 Dose estimation based on filter samples

The theoretical total dose of inhaled fluorescent microspheres deposited (M_{inh}) for each IVR model experimental conditions were calculated using the equation as described in Equation 8:

$$M_{inh} = [\text{Aerosol concentration}] \times RMV \times t \times IF \qquad \textbf{Equation 8}$$

Where [Aerosol concentration] is the aerosol concentration of FMS, expressed in µg/L. This value is derived from knowledge of the mass of FMS collected on filter samples and assayed using HPLC, duration of exposure period and sampling flow rate. RMV is the respiratory minute volume, *t* is the time of aerosol exposure (usually 45 minutes), and IF is the inhaled fraction which is assumed to be 100% for particles < 7 µm (Bide et al, 2000).

4.7.1 Statistical data analysis

The statistical analyses for the screening study (see 5.3, B- Results and Discussion) were performed using Design Expert 7 (Stat-Ease, Inc.2021 East Hennepin Ave., Suite 480 Minneapolis, MN55413 (Version 7.1.1). For each response the final ANOVA model is shown. If a factor has a p-value of less than 0.05 then it is statistically significant at the 5% significance level. If a factor has a p-value between 0.05 and 0.1 then there is an indication of statistically significant effect (see 4.3, D-Appendix for summary of statistical analysis).

5 Comparative deposition of inhaled aerosols in experimental rats and *In Vitro* rat lung model

5.1 Materials

The test materials included the following classes of inhaled therapeutic drugs; corticosteroid, (Fluticasone propionate) p38 Kinase inhibitor (compound Y) and novel corticosteroid (compound X). All drug compounds tested were prepared as blends composed of lactose with either micronised form of the active drug substance or spray-dried version of the same. All inhalation material tested here are proprietary products of GlaxoSmithKline (Uxbridge, UK). Table 28 summarises the details of the drug materials, target aerosol dose and exposure conditions used in these studies. In addition, the strain of rat used in each study in this work is listed.

5.2 Animal Care and Ethical Approval

All animal studies were ethically reviewed and carried out in accordance with Animals (Scientific Procedures) Act 1986 and the GSK Policy on the Care, Welfare and Treatment of Animals.

5.3 Conduct of experimental procedure

The experimental procedure (section 5.4, C- Experimental Setup) involved in the generation of the aerosol and characterisation of the exposure atmosphere as well as the handling of the live rats and subsequent preparation of lungs samples for analysis and determination of the drug content was done by the staff of the GSK Safety Assessment department (Ware, UK). The analysis of the drug content in the biological matrices (section 5.7, C- Experimental Setup) was undertaken by staff of the Drug Metabolism and Pharmacokinetic department (Ware, UK).

5.4 Method of aerosol Generation and exposure setup

5.4.1 Compound X and Y

Aerosols were generated from compound Y and compound X-lactose dry powder blends using Mark II Wright Dust Feed (WDF) system. The system is the most widely used aerosol generator in inhalation toxicology studies due to its reliability and ease of use (Wong, 2007). Further details describing its mechanism of action, uses and limitation are detailed in section 1.7.2.3, A-Introduction.

A regulated flow of compressed air (10 L/min) transported the aerosol from the dust feed into an inhalation chamber. Generation of aerosol from the WDF generator was checked for all groups at approximately 15 minute intervals during exposure. Preliminary work was conducted prior to Day 1 (the first day of dosing) to establish the operating conditions required to generate the target aerosol concentrations. The operating conditions were adjusted during the course of the study to maintain the desired aerosol concentration.

Standard (top section, 3 animal exposure rings, base section) snout only exposure chambers operating under conditions of dynamic airflow were employed. Extract rate was set at 16 L/minute for all exposure chambers. The extract from the chamber was slightly greater than the total volume of air input into the chamber ensuring a flow of aerosol throughout the chamber.

A temperature and relative humidity probe was placed below the animals being exposed, using a dedicated sampling port on the lowest animal exposure ring, in order to monitor chamber environmental conditions during exposure.

5.4.2 Fluticasone propionate (FP)

For FP powder, aerosol was generated from a novel dry powder using a prototype capsule based aerosol generator (CBAG).The CBAG is designed to produce and maintain atmospheres containing dust, by dispersing material from pierced capsules using a pulse of dried air (Paul, 2012). The main advantages of using the CBAG in comparison with conventional aerosol generation systems such as the Wright–Dust feeder included utilisation of powder without compression and elimination of dead spaces (see Figure 68).

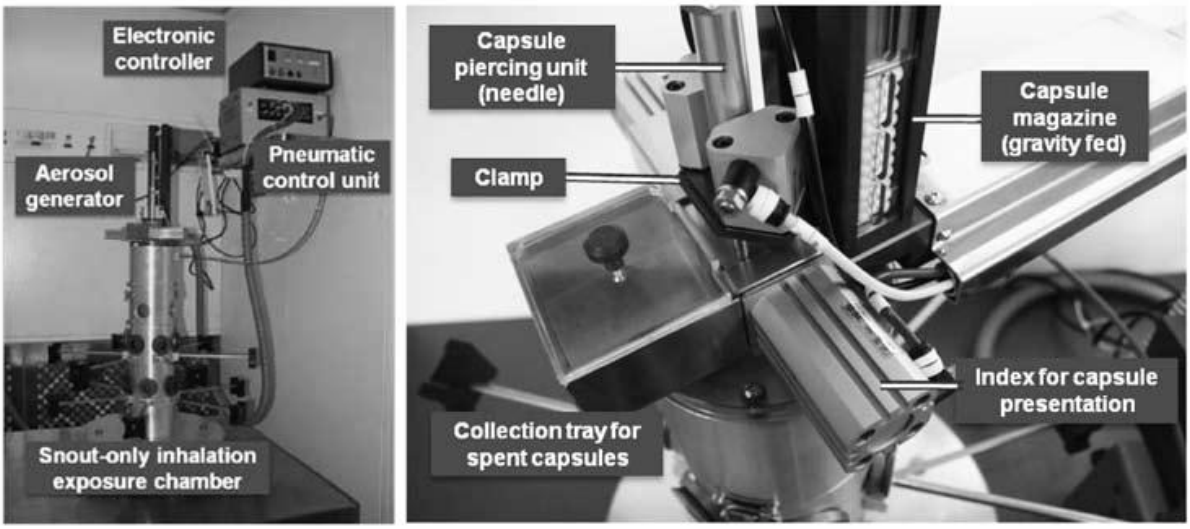

Figure 68: The Capsule Based Aerosol Generator (CBAG) mounted on top of a flow through chamber for snout-only inhalation exposure of rodents. Reproduced with permission from GSK R&D Ware, UK

A regulated flow of compressed air (5 L/min) conducted the aerosol from the dust feed into an inhalation chamber and entered the exposure chamber whilst the pneumatically controlled capsule preparation cycle is in operation (i.e. between airbursts).

Table 28: Details of drug material tested, exposure conditions and strains of rats from the various studies used to compare the lung concentration data with the IVR lung model.

Test compound	Therapeutic class	Target aerosol concentration (µg/L)[1]	Target dose (µg/kg/day)[2]	Size distribution (MMAD + GSD)[3]	Rat strain	Exposure Condition
Compound Y	P38 Kinase inhibitor	24.0	1000	2.22 ± 2.39	Sprague Dawley	Exposure 60 minutes. Mark II Wright dust feeder and snout only exposure chamber
Fluticasone propionate	Corticosteroid	5.00 68.5 4.92 29.58	100 1000 100 1000	4.9 ± 2.65 3.9 ± 3.99 1.78 ± 1.67 1.92 ± 1.49	Wistar Han	Exposure 20 minutes. Capsule based aerosol generator and snout only exposure chamber
Compound X: Micronised Spray-Dried Form 1 Spray-Dried Form 2	Novel Corticosteroid	14.1	600	5.28 ± 2.55 2.46 ± 2.96 1.77 ± 3.22	Wistar Han	Exposure 30 minutes. Mark II Wright dust feeder and snout only exposure chamber

1) Chamber concentrations and doses are expressed in terms of test compound.
2) Target dose (µg/kg/day) is based on a body weight of 300g. Respiratory Minute Volume determined using equation: $RMV = 0.608 \times BW\ (kg)^{0.852}$ (Alexander et al, 2008).
3) MMAD: Mass Median Aerodynamic Diameter, GSD; Geometric Standard Deviation

5.5 Chamber Aerosol Characterisation

Aerosol concentrations of the test drugs were determined in the test atmosphere by taking filter samples at regular intervals throughout the duration of the studies. Determinations were made by drawing a measured volume of air at a rate of 2.0 L/min through a glass fibre filter, fitted to an open face sampler attached to the sampling port of the chamber. In addition, samples were taken from the same port location on the top animal dosing ring.

Determination of particle size distribution was made during the preliminary trials as well as other selected times as specified in the study protocols. A measured volume of air was drawn from each exposure chamber containing the test material, at a rate of 2.0 L/min through a Marple Personal Cascade Impactor (model 296) attached to a sampling port located on the top layer of the dosing rig. Aerosol was collected on stainless steel substrates and a final glass fibre filter. Following sampling, a visual assessment of the substrates and glass fibre filter was performed and each foil substrate was washed in a solution of solvent appropriate for the test material under investigation.

Following sample collection for both aerosol concentration and particle size determination, the filters were analysed for active drug concentration using high performance liquid chromatography. Details of the columns used, mobile phases, detection wavelength and linearity per test drug under investigation are shown in Table 29.

Table 29: Details of HPLC methods used for drug assay of test materials

Drug	Mobile Phase	Drug solvent used for recovery	Analytical Column	Detection Wavelength (mm)	Linear Calibration range (µg/mL)
Compound Y	Phase A: 0.1% Formic Acid Phase B: Methanol A:B (59:41 v/v)	Methanol: Water in the ratio of 50:50 by volume + 0.1% Formic acid	50 x 2.1 mm i.d. Waters BEH C18 1.7 µm	342 nm	0.2 to 20 µg/ML
Fluticasone propionate	Mobile phase A: 0.010M Sodium Dodecyl Sulphate containing 0.10% glacial acetic acid: Methanol in the ratio of 80:20 by volume Mobile Phase B: Acetonitrile. A:B(50:50 v/v)	Methanol: Water in the ratio 70:30 by volume	5 cm x 4.6 mm i.d. 3.5 µm Zorbax Stable Bond SB C-18	239 nm	0.1 to 20 µg/ML
Compound X	Phase A: 10mM Ammonia Phase B: Acetonitrile A:B (42:58 v/v)	Methanol: Water in the ratio 80:20 by volume	50 x 2.1 mm i.d. Waters BEH C18 1.7 µm	254 nm	0.4 to 30 µg/ML

5.6 Dose Estimation

The target dose listed in Table 13, B-Results and Discussions for the live rats was determined using the equation described in Equation 4.

5.7 Lung concentration determination for compound X and Y

5.7.1 Sample preparation

For the immediately after dosing (IAD) samples, lung tissues were collected from a selected number of rats (n = 3) immediately after the end of the dosing period. Samples were then frozen prior to further processing. . It was sometimes necessary to stop the homogenisation process and remove any trapped material from the homogeniser blades before continuing homogenisation. Homogenates were stored frozen until analysed for drug.

Lung and trachea homogenate samples from rats were analysed for parent drug (and metabolite, if required and an authentic standard existed) using a validated analytical methods based upon protein precipitation followed by Liquid Chromatography-Mass Spectroscopy (LC/MS) analysis as detailed below.

5.7.2 Sample extraction for compound X

The extraction process for compound X consisted of the following steps:

1. Aliquot 25 µL of sample, standard or QC into tube
2. Add 100 µL Acetonitrile to double blank
3. Add 100 µL internal standard working solution (C1; 100 ng/mL) to all other tubes
4. Cap tubes and vortex mix thoroughly
5. Centrifuge the tubes for at least 10 minutes at approximately 3000 g
6. Transfer the supernatant to a clean tube
7. Inject onto HPLC-MS/MS system for analysis as detailed in Table 30 and Table 31

For compound X, the lower limit of quantification (LLQ) was 10ng/mL using 100uL sample of rat lung homogenate with a higher limit of quantification (HLQ) of 2500 ng/ML. The concentrations of the test article and metabolite in the lung homogenates of the rats (µg/g lung) were calculated by multiplying each measured lung homogenate concentration by the respective homogenate: lung weight ratio (see Table 67).

5.7.3 Sample extraction for compound Y

The extraction process for compound X consisted of the following steps:

1. Aliquot 100 µL of sample, standard or QC into tube
2. Add 300 µL Acetonitrile to double blank
3. Add 300 µL internal standard working solution (C1; 500 µg/mL) to all other tubes
4. Cap tubes and vortex mix thoroughly
5. Centrifuge the tubes for at least 5 minutes at approximately 3000 g
6. Transfer the supernatant to a fresh tube
7. Cap tubes and vortex mix briefly
8. Inject onto HPLC-MS/MS system for analysis as detailed in Table 30 and Table 31

For compound Y, the lower limit of quantification (LLQ) was 20 ng/mL using 100uL sample of rat lung homogenate with a higher limit of quantification (HLQ) of 2000 ng/mL. The concentrations of the test article and metabolite in the lung homogenates of the rats (µg/g lung) were calculated by multiplying each measured lung homogenate concentration by the respective homogenate: lung weight ratio (see Table 67).

5.8 Lung concentration determination for fluticasone propionate

Full details of the analytical method used to determine the lung concentration of fluticasone propionate in the lung homogenate samples are detailed in section 6.4, C- Experimental Setup.

Table 30: HPLC conditions for the determination of drug content of test material in Rat Lung Homogenate

Drug	**Compound Y**	**Compound X**	**Fluticasone propionate**
Auto sampler	Waters Acquity (Milford, USA)	Waters Acquity (Milford, USA)	Jasco X-LC (Tokyo, Japan)
Injector Wash Solvent 1	4:3:3 Acetonitrile: Water: IPA containing 0.1% Formic Acid	4:3:3 Acetonitrile: Water: IPA containing 0.1% Formic Acid	NR
Injector Wash Solvent 2	70/30 (v/v) Acetonitrile / UPW (0.1% formic acid)	Water containing 0.1% Formic Acid	NR
Typical Injection Volume	2 µL	3.5 µL (partial loop fill)	15.0 µL (5µL for ion suppression check samples)
Chromatography System	Waters Acquity UPLC	Agilent 1100 binary solvent delivery HPLC system	Jasco X-UPLC
Flow Rate	1.5 mL/min	0.8 mL/min	1.1 mL/min
Analytical Column	Spherisorb S5CN-100A, 100 x 4.6 mm i.d.	Acquity BEH phenyl 50 x 2.1 mm i.d.,1.7 µm	Ascentis Express C18
Column Temperature	40°C	50°C	
Run Time	3.2 minutes	2.0 minutes	4 minutes
Mobile Phase A	10mM Ammonium Acetate (pH 2.5 with formic acid)	Water containing 0.1% Formic Acid	0.1% Formic acid in HPLC grade water
Mobile Phase B	Acetonitrile	Acetonitrile containing 0.1% Formic Acid	0.1% Formic acid in Acetonitrile

* NR: Not Recorded
* Alternative, equivalent HPLC equipment may be used as appropriate.

Table 31: LC/MS conditions for the determination of drug content of test material in Rat Lung Homogenate

Drug	**Compound Y**	**Compound X**	**Fluticasone propionate**
Mass Spectrometer	API-4000 (MDS Sciex, Concord, Canada)	API-4000 (MDS Sciex, Concord, Canada)	API-4000 (MDS Sciex, Concord, Canada)
Ionisation Interface and Temperature	TurboIonSpray™ at 750°C	Heated Nebuliser at 400 °C	Heated Nebuliser at 650 °C
Pause Time	5 msec	5 msec	5 msec
Gas 1 Setting (nitrogen)	70 psi	40 psi	NR
Gas 2 Setting (nitrogen)	50 psi	50 Psi	NR
Curtain Gas Setting (nitrogen)	30	40	NR
Collision Gas (Nitrogen)	4	7	NR
DP Value	84	69	46
CE Value	71	25	19

* NR: Not Recorded
* Analytical method parameters are typical but may vary from instrument to instrument in order to achieve an equivalent response

5.9 Sample preparation for the In Vitro (IVR) Rat model details

Details of IVR model used are described in section 3, B- Results and Discussion.

The drugs deposited in the various sections of the IVR model during aerosol exposure were recovered by rinsing the model sections with appropriate solvent into volumetric cylinders as listed in Table 29. Thereafter, the samples were analysed using an isocratic validated HPLC assay method. Details of the columns used, mobile phases, detection wavelength and linearity per test drug under investigation are shown in Table 29. Total drug recovery was calculated by adding the drug deposited in all sections of the model. Regional deposition results were expressed as the percentage of the total drug delivery.

5.10 Dose estimation using Multiple-Path Particle Dosimetery Model (MPPD)

The MPPD modelling software was used to predict deposition of compound X, Y and FP particles for each experimental group conditions. The exposure aerosol conditions of concentration and particle size distribution (MMAD and GSD) were input into the model (see Table 13). In addition, the respiratory parameters in terms of breathing frequency (f, min^{-1}) and tidal volume (VT, mL) were input into the model. Model output included deposition for the following regions: Nasopharyngeal, Tracheobronchial and Pulmonary (% of total).

5.11 Statistics

Regional deposition comparison between the IVR model and MPPD model predictions were analysed using Student's t-test. All pair-wise comparisons were two-tailed. Group mean differences with an associated probability <0.05 were considered to be statistically significant.

6 Assessing the relationship between efficacy of inhaled fluticasone propionate in an allergen-induced rodent model with regional lung deposition

6.1 Conduct of experimental procedure

The experimental procedure involved in the generation of the aerosol and characterisation of the exposure atmosphere as well as the handling of the live rats and subsequent preparation of lungs samples for analysis and determination of the drug content was done by the staff of the GSK Safety Assessment department (Ware, UK).

The analysis of the drug content in the biological matrices was undertaken by staff of the Drug Metabolism and Pharmacokinetic department (Ware, UK).The determination of the level of inflammatory infiltrates in the lung tissue (section 7.2, B- Results and Discussion) was done by the staff of the GSK Respiratory department (Stevenage, UK). Section 6, D- Appendix provides comprehensive summary of all the experimental results generated for this study

6.2 Animals used in study

Male Wistar Han rats were used in both studies. The age of the rats was approximately 6 to 8 weeks of age at start of studies. Weight of rats ranged from 200 to 275 g at the start of studies. All animal studies were ethically reviewed and carried out in accordance with Animals (Scientific Procedures) Act 1986 and the GSK Policy on the Care, Welfare and Treatment of Animals.

6.3 Inhalation methodology

The capsule based aerosol generator was selected for aerosol generation due to its high generation efficiency (Paul, 2012). The instrument sequentially loads, pierces and then aerosolises the content and discharge individual capsules through a sequential mechanical cycle. Compressed air was used to aerosolise the content of individual capsules into the exposure chamber. The capsule fill weight employed was nominally 1 mg at the blend strengths of 1.0%, 10.0% and 100.0% for the low, intermediate and high dose group respectively. The capsules were filled using a semi-automated system. Further details describing this generation system are detailed in section 5.4.2, C- Experimental Setup.

Standard (top section, 3 animal exposure rings, base section) snout only exposure chamber operating under conditions of dynamic airflow was employed. Rats were placed in restraint cones and attached randomly to the 24 ports exposure tower. The tower was calibrated for an air input of 10 L/min and an air extract of 10.5 L/min.

Both aerosol concentration and particle size samples were removed directly from the animal exposure levels and analysed for FP content using a validated HPLC-UV method (see section 5.5, C- Experimental Setup). In addition, for the second study, the APS instrument was used in place of Marple cascade impactor to monitor the particle size generated during exposure. However, previous experimental work using FMS has shown broad agreement between particle size determination using the APS and Marple instruments, although the APS tended to slightly underestimate the particle size in comparison with the Marple instrument (see section 1.5.3, B- Result and Discussion).

6.4 In vivo Lung dose determination

6.4.1.1 Sample preparation

Study lungs were collected into Falcon tubes (Falcon Plastics, Los Angeles, USA) and stored frozen until analysis. On the day of analysis all lung samples and control lungs were removed from the freezer and thawed. In addition, the study lung weights were determined.

6.4.1.2 Preparation of compound standards in lung homogenate

A 1mg/mL stock solution of FP was prepared. This solution was then used to prepare 200µg/mL spiking solutions by diluting 20µL in 80µL acetonitrile: water (50:50). 40µL of the 200ug/mL spiking solution was pipetted directly on to either the right or left hand-side of a control rat lung in a Precellys 7ml homogenising tube with ceramic beads ceramic beads (Precellys, France). 4ml of water was then be added. A second tube with the corresponding side of the rat lung and 4mL of water was also homogenised. The resulting homogenate from the two tubes was then combined in a scintillation vial to produce an 8000ng/lung top standard that is used for generation of calibration line. The calibration line was prepared by serial dilution of 8000ng standard FP. Control lungs and all study samples were also be taken and homogenised as detailed above.

6.4.1.3 Sample extraction

100 µL of the resulting homogenate was transferred from all standards and samples into eppendorfs (Hamburg, Germany) and 300µL of 95:5 ACN: EtOH containing 10ng/ml of GR160288A as an internal standard was added and then vortex mixed before being centrifuged at 6,500rpm for 10 minutes. 200mL of the resulting supernatant was transferred in to a clean 96 well plate.

Samples were dried down under heated nitrogen and reconstituted in 200µl of 10:90 (v/v) Acetonitrile: water and shaken on the plate shaker for at least 5 min before analysis by UHPLC-MS/MS, as detailed in Table 30 and Table 31 respectively. The resulting sample lung homogenate levels in µg/ lung were then be adjusted for the individual lung weights to give the results in µg/g (see Table 67). For fluticasone propionate, the lower limit of quantification (LLQ) was 20 ng/mL using 100uL sample of rat lung homogenate with a higher limit of quantification (HLQ) of 4000 ng/mL.

6.5 IVR analysis

An IVR model was placed in the exposure chamber for each treatment group. The model sampled the inhalation atmosphere for the same duration as the live animal during the entire exposure period. Furthermore, when possible additional replicate samples for each exposure scenario were taken. However, in such occasions, the exposure atmosphere in terms of target dose, aerosol concentration and particle size distribution was the same as in the live exposure occasions. Table 32 provides details of the number of samples taken per treatment group.

Table 32: Number of IVR samples taken per FP treatment group

Study	Group	Target MMAD (µm)	Number of replicates
1	FP 0.1 mg/kg	≥ 4µm	1
1	FP 1.0 mg/kg	≥ 4µm	2
2	FP 0.1 mg/kg	≤ 2µm	3
2	FP 1.0 mg/kg	≤ 2µm	2

The IVR model was connected to a rodent ventilator with the breathing rate kept constant at 102 breaths per minute, and the tidal volume was set at 2.1 mL throughout the experiments. These conditions are considered to be representative of day time activity levels of a Sprague-Dawley rat (Schmid et al, 2008). After sampling is completed, the component of the model were dissembled and the drug deposited in the various sections of the IVR model during aerosol exposure were recovered by rinsing the model sections with appropriate solvent into volumetric cylinders. Thereafter, the samples were analysed using an isocratic validated HPLC assay method (see section 5.5, C-Experimental Setup).

6.6 MPPD analysis

The MPPD modeling software was used to predict deposition of FP particles for each experimental group conditions (Asgharian and Anjilvel, 1998). The exposure aerosol conditions of concentration and particle size distribution (MMAD and GSD) were input into the model. In addition, the respiratory parameters in terms of breathing frequency (f, min^{-1}) and tidal volume (VT, mL) were input into the model. Model output included deposition for the following regions: Nasopharyngeal, Tracheobronchial and Pulmonary (% of total).

D. Appendix

1 Development of aerosol delivery method

To analyse and quantify the effect of experimental parameters on aerosol exposure, values for aerosol concentration (µg/m^3) and particle size (MMAD) were recorded every sixty seconds. The consecutive values per experimental run were captured in real-time using the APS software. After completion of the experiment, the CSV data files were exported into Excel format for further analysis. Tables below summarises the data generated.

1.1 **Table 33:** Aerosol concentration (mg/m^3) input into DoE model (Table 5)

Experimental No	**735266**	**735266**	**735266**	**735266**	**735266**	**735266**	**735266**	**735266**	**735266**	**735266**	**735266**
Run No	**1**	**2**	**3**	**4**	**5**	**6**	**7**	**8**	**9**	**10**	**11**
Airflow (l/min)	**10**	**10**	**17**	**17**	**10**	**10**	**17**	**17**	**13**	**13**	**13**
Chain Speed	**30**	**30**	**30**	**30**	**100**	**100**	**100**	**100**	**70**	**70**	**70**
Actual time (min)	**Aerosol Concentrations (mg/m^3)**										
1.0	5.50	4.17	13.45	9.64	2.56	8.57	23.75	13.98	10.37	29.41	17.73
2.0	5.41	4.27	12.64	8.25	3.52	7.40	22.51	13.83	11.56	17.11	16.98
3.0	5.10	5.65	12.08	7.56	4.02	7.57	20.91	12.63	9.96	12.58	16.32
4.0	4.82	4.91	11.73	7.85	3.36	7.75	20.74	14.33	14.11	11.58	14.32
5.0	4.79	4.72	11.78	7.43	3.17	7.92	20.93	14.32	13.04	10.21	14.56
6.0	4.81	4.88	11.61	8.15	3.71	7.84	19.68	14.56	13.29	9.95	13.49
7.0	6.19	4.03	10.71	8.42	3.53	7.75	18.32	13.55	13.30	10.19	15.27
8.0	5.00	4.15	11.74	7.90	4.76	9.11	19.97	13.50	13.26	10.28	13.10
9.0	5.42	6.23	10.64	8.29	3.67	7.89	19.49	14.38	12.58	9.82	13.18
10.0	4.36	3.99	11.26	7.85	3.14	8.07	16.56	14.96	12.61	10.88	13.80
11.0	4.80	4.57	10.52	8.06	2.14	9.30	17.45	15.52	11.90	10.35	13.09
12.0	4.81	4.05	9.38	8.52	2.68	7.80	16.91	15.13	11.92	10.68	13.01
13.0	4.77	4.49	10.55	7.02	4.42	9.79	16.04	13.89	13.05	10.88	12.71
14.0	5.45	4.17	11.93	7.32	2.47	8.18	16.19	13.89	12.44	12.23	13.11
15.0	4.70	4.51	11.20	7.80	2.82	9.51	15.83	14.83	12.93	11.90	11.80

Table 33 Continued

Experimental No	735266	735266	735266	735266	735266	735266	735266	735266	735266	735266	735266
Run No	1	2	3	4	5	6	7	8	9	10	11
Airflow (l/min)	10	10	17	17	10	10	17	17	13	13	13
Chain Speed	30	30	30	30	100	100	100	100	70	70	70
Actual time (min)	Aerosol Concentrations (mg/m^3)										
16.0	4.63	4.60	12.37	7.77	2.67	8.82	16.85	13.54	12.69	10.24	12.34
17.0	4.95	4.36	10.91	7.87	3.06	9.79	16.31	14.05	12.68	11.18	11.79
18.0	4.76	4.44	10.86	7.43	3.15	10.85	15.30	15.86	13.19	12.51	12.80
19.0	5.08	4.53	10.60	8.12	3.72	8.95	16.71	14.28	11.71	12.87	12.90
20.0	4.87	5.26	10.66	7.51	3.92	8.82	15.37	13.80	12.39	11.92	12.71
21.0	4.66	4.24	11.82	7.26	3.66	8.83	17.34	13.24	13.40	11.74	12.99
22.0	5.37	4.57	10.34	8.10	5.48	8.07	15.26	14.57	13.41	12.66	12.89
23.0	4.96	4.01	11.06	7.71	7.85	8.67	13.71	13.78	12.45	13.14	11.49
24.0	4.68	4.34	9.72	7.82	5.40	10.87	17.06	13.59	13.62	12.71	11.69
25.0	5.91	4.62	10.52	7.90	5.59	8.01	11.80	14.50	14.08	12.20	11.62
26.0	4.65	4.58	10.81	7.50	5.16	8.75	17.23	12.63	12.29	12.43	11.93
27.0	4.96	4.14	10.48	7.49	5.49	7.54	16.53	14.66	13.51	14.41	12.27
28.0	5.05	4.41	9.65	7.73	6.63	8.74	17.21	13.20	12.63	12.84	12.79
29.0	4.59	3.90	9.03	7.07	6.53	9.39	17.30	13.21	11.91	13.96	11.63
30.0	4.69	4.06	9.77	7.41	6.36	8.36	16.68	14.37	11.76	13.68	11.49
31.0	4.39	4.49	9.94	8.02	6.14	8.66	16.30	15.80	12.45	13.37	11.50
32.0	5.10	4.90	10.18	7.82	5.92	10.28	17.04	13.79	12.57	14.57	13.00
33.0	4.75	4.12	10.00	7.38	6.63	8.81	16.29	12.75	13.00	14.42	11.53
34.0	4.63	4.78	9.78	7.74	6.99	8.36	14.70	12.61	13.85	15.17	11.91
35.0	5.01	4.41	9.09	6.96	7.04	7.56	15.60	13.14	13.02	14.79	12.36
36.0	6.01	4.14	9.46	8.31	6.23	12.17	14.53	13.63	14.77	13.94	13.68
37.0	5.66	4.15	8.89	7.15	7.15	8.59	15.07	14.29	12.33	15.30	13.70
38.0	4.43	4.37	9.36	8.73	7.24	8.67	15.12	13.40	12.38	15.52	13.66

Table 33 Continued

Experimental No	735266	735266	735266	735266	735266	735266	735266	735266	735266	735266	735266
Run No	**1**	**2**	**3**	**4**	**5**	**6**	**7**	**8**	**9**	**10**	**11**
Airflow (l/min)	**10**	**10**	**17**	**17**	**10**	**10**	**17**	**17**	**13**	**13**	**13**
Chain Speed	**30**	**30**	**30**	**30**	**100**	**100**	**100**	**100**	**70**	**70**	**70**
Actual time (min)	**Aerosol Concentrations (mg/m^3)**										
40.0	4.11	4.22	9.35	6.65	6.42	10.21	14.69	13.23	11.96	14.37	13.25
41.0	4.81	4.12	9.25	7.64	6.43	8.92	15.17	13.01	12.35	15.04	14.99
42.0	5.95	4.27	8.55	7.18	6.58	8.43	14.22	12.81	12.87	15.40	14.07
43.0	4.49	4.89	8.13	7.41	7.84	9.14	15.15	14.91	13.04	15.34	13.63
44.0	4.38	3.90	7.99	7.65	6.66	8.23	13.03	13.51	11.48	15.99	14.71
45.0	5.11	4.75	8.77	7.38	7.42	7.89	14.56	13.75	11.42	15.83	14.59
46.0	5.08	3.97	7.85	6.56	6.46	9.03	14.25	13.66	12.32	15.76	13.76
47.0	4.81	3.92	8.82	7.03	8.72	9.86	14.75	13.47	12.32	15.97	16.53
48.0	4.38	4.21	8.26	7.35	7.91	8.88	14.48	12.31	12.12	15.17	13.61
49.0	4.58	3.71	7.93	6.37	8.90	11.17	14.43	12.69	12.38	19.22	14.01
50.0	4.74	4.02	8.58	7.85	7.85	10.60	15.29	13.86	11.66	17.07	14.91
51.0	4.02	4.49	7.86	7.39	7.40	8.80	16.62	13.84	12.36	15.96	14.28
52.0	4.99	4.61	8.92	7.16	7.46	9.39	15.61	12.59	11.82	18.34	14.79
53.0	4.75	4.27	8.56	6.58	9.53	8.73	16.45	13.19	11.64	17.95	14.24
54.0	4.76	5.33	8.75	6.61	7.50	8.93	16.30	12.70	11.54	16.84	13.98
55.0	4.62	4.47	8.44	7.19	7.52	8.65	14.04	12.29	12.08	17.31	14.96
56.0	4.88	3.71	8.40	6.41	7.43	9.06	15.02	13.20	11.48	17.34	14.48
57.0	4.51	4.05	8.73	6.76	8.47	9.51	14.60	13.19	10.97	17.49	15.36
58.0	4.58	4.09	8.11	7.58	8.15	9.52	14.84	11.99	12.55	17.01	13.82
59.0	4.33	4.66	8.23	7.06	8.85	9.75	13.48	13.53	12.58	16.94	15.82
60.0	4.21	4.21	7.59	6.56	8.98	9.55	13.50	13.18	13.47	16.32	15.05
MEAN	**4.88**	**4.42**	**9.88**	**7.53**	**5.80**	**8.93**	**16.26**	**13.70**	**12.49**	**14.25**	**13.61**
STDEV	0.45	0.46	1.41	0.62	2.05	0.97	2.30	0.86	0.87	3.17	1.44

1.2 **Table 34:** Mass Median Aerodynamic Diameter (µM) input into DoE model (Table 5)

Experimental No	**735266**	**735266**	**735266**	**735266**	**735266**	**735266**	**735266**	**735266**	**735266**	**735266**	**735266**
Run No	**1**	**2**	**3**	**4**	**5**	**6**	**7**	**8**	**9**	**10**	**11**
Airflow (l/min)	**10**	**10**	**17**	**17**	**10**	**10**	**17**	**17**	**13**	**13**	**13**
Chain Speed	**30**	**30**	**30**	**30**	**100**	**100**	**100**	**100**	**70**	**70**	**70**
Actual time (min)	**MMAD (µm)**										
1.0	2.42	1.86	1.84	2.42	1.36	3.28	2.32	2.11	1.69	4.43	2.85
2.0	2.50	1.83	1.80	1.80	1.98	2.67	2.35	2.01	1.83	2.76	2.63
3.0	2.14	2.80	1.81	1.76	2.67	3.00	2.32	1.93	1.84	2.75	2.68
4.0	2.01	2.79	1.75	1.74	1.81	3.01	2.31	2.15	1.92	2.29	2.12
5.0	1.93	2.19	1.74	1.66	1.64	3.14	2.42	2.27	1.77	2.02	2.27
6.0	1.94	2.62	1.76	1.81	2.06	2.75	2.21	2.22	1.94	1.93	2.14
7.0	3.51	1.85	1.69	1.70	1.83	2.75	2.19	2.10	1.97	1.89	2.50
8.0	2.17	1.84	1.78	1.80	4.34	3.48	2.39	2.11	1.92	1.98	2.13
9.0	2.32	4.00	1.64	1.65	2.51	2.75	2.36	2.24	1.77	1.82	2.11
10.0	1.75	1.84	1.79	1.76	2.25	3.06	2.08	2.25	1.85	1.95	2.26
11.0	1.97	2.54	1.65	1.70	2.08	3.39	2.12	2.43	1.80	1.91	2.27
12.0	2.03	2.08	1.60	1.87	2.77	2.93	2.08	2.18	1.75	1.93	2.12
13.0	1.97	2.06	1.71	1.59	4.63	3.43	2.09	2.17	1.82	1.89	2.11
14.0	2.46	2.00	1.78	1.68	2.31	2.91	2.11	2.13	1.81	2.26	2.25
15.0	2.06	2.24	1.83	1.75	2.43	3.42	2.10	2.23	1.82	2.16	1.90
16.0	1.82	2.39	1.98	1.64	2.31	2.88	2.21	2.06	1.91	1.79	2.01
17.0	2.20	2.18	1.76	1.59	2.83	3.66	2.35	1.99	1.81	1.99	2.04
18.0	1.94	2.15	1.78	1.74	2.37	3.76	2.26	2.63	1.91	2.16	2.17
19.0	2.16	2.50	1.78	1.87	2.68	3.31	2.29	2.27	1.77	2.32	2.38
20.0	2.05	2.70	1.87	1.78	2.80	3.08	2.15	2.21	1.84	2.06	2.24
21.0	1.86	2.13	2.01	1.79	2.44	3.19	2.49	2.16	1.90	1.99	2.18

Table 34 Continued

Experimental No	735266	735266	735266	735266	735266	735266	735266	735266	735266	735266	735266
Run No	1	2	3	4	5	6	7	8	9	10	11
Airflow (l/min)	10	10	17	17	10	10	17	17	13	13	13
Chain Speed	30	30	30	30	100	100	100	100	70	70	70
Actual time (min)	MMAD (µm)										
23.0	2.29	1.85	1.91	1.78	3.71	2.90	2.24	2.16	1.83	2.24	2.01
24.0	2.01	2.39	1.75	1.71	2.59	3.97	2.45	2.15	2.01	2.10	2.06
25.0	3.22	2.25	1.78	1.84	2.67	2.85	2.22	2.24	2.03	2.08	2.05
26.0	1.98	2.44	2.06	1.66	2.47	3.16	2.16	2.07	1.82	2.02	2.09
27.0	2.36	2.10	1.81	1.78	2.65	2.77	2.14	2.21	1.98	2.33	2.21
28.0	2.33	2.28	1.72	1.68	3.06	3.21	2.27	1.99	1.87	2.16	2.32
29.0	2.00	1.87	1.67	1.71	2.95	3.22	2.21	2.08	1.78	2.25	2.01
30.0	2.11	1.86	1.67	1.64	2.97	3.15	2.22	2.12	1.74	2.22	2.04
31.0	1.85	2.23	1.87	1.79	2.73	3.19	2.20	2.50	1.81	2.15	2.07
32.0	2.45	2.53	1.99	1.75	2.73	3.75	2.23	2.12	1.83	2.32	2.28
33.0	2.11	1.92	1.91	1.73	2.93	3.10	2.34	1.96	1.87	2.27	2.09
34.0	1.93	2.77	1.84	1.65	3.08	3.02	2.04	2.10	2.10	2.42	2.17
35.0	2.37	2.17	1.73	1.56	3.11	3.09	2.21	2.10	1.91	2.30	2.10
36.0	3.23	2.13	1.81	1.83	2.57	4.87	2.03	2.04	2.17	2.26	2.29
37.0	3.19	2.03	1.67	1.68	3.10	3.05	2.13	2.30	1.85	2.47	2.29
38.0	2.06	2.27	1.79	1.85	3.15	3.11	2.13	2.11	1.85	2.33	2.16
39.0	2.23	2.81	1.89	1.51	2.97	3.29	2.13	2.11	1.94	2.22	2.40
40.0	1.80	2.13	1.87	1.55	2.78	3.72	2.05	2.07	1.78	2.21	2.19
41.0	2.24	2.09	1.91	1.61	2.67	3.36	2.28	2.04	1.85	2.23	2.42
42.0	3.52	2.05	1.78	1.63	2.90	3.14	2.10	2.03	2.02	2.30	2.37
43.0	2.01	2.42	1.72	1.74	2.99	3.32	2.16	2.21	1.91	2.32	2.26
44.0	1.99	1.97	1.69	1.71	2.75	3.17	2.12	2.07	1.76	2.35	2.33

Table 34 Continued

Experimental No	735266	735266	735266	735266	735266	735266	735266	735266	735266	735266	735266
Run No	**1**	**2**	**3**	**4**	**5**	**6**	**7**	**8**	**9**	**10**	**11**
Airflow (l/min)	**10**	**10**	**17**	**17**	**10**	**10**	**17**	**17**	**13**	**13**	**13**
Chain Speed	**30**	**30**	**30**	**30**	**100**	**100**	**100**	**100**	**70**	**70**	**70**
Actual time (min)	**MMAD (µm)**										
45.0	2.55	2.64	1.92	1.64	2.90	3.14	2.19	2.10	1.74	2.39	2.43
46.0	2.65	2.03	1.68	1.55	2.54	3.24	2.17	2.06	1.91	2.35	2.32
47.0	2.23	1.93	1.73	1.59	3.36	3.50	2.24	2.11	1.86	2.36	2.74
48.0	2.06	2.37	1.65	1.60	2.90	2.97	2.17	1.92	1.87	2.31	2.30
49.0	2.04	1.90	1.69	1.57	3.42	4.41	2.26	2.04	1.91	2.81	2.25
50.0	2.32	1.97	1.82	1.72	3.48	3.78	2.41	2.20	1.76	2.45	2.44
51.0	1.76	2.58	1.62	1.60	2.94	3.42	2.11	2.10	1.84	2.39	2.41
52.0	2.76	2.71	1.95	1.62	2.86	3.51	2.10	1.98	1.84	2.59	2.38
53.0	2.42	2.39	1.73	1.52	3.69	3.07	2.16	2.20	1.84	2.61	2.30
54.0	2.39	3.53	1.79	1.56	2.81	3.29	2.30	1.96	1.78	2.44	2.28
55.0	2.27	2.50	1.70	1.66	2.98	3.24	2.05	2.02	1.90	2.53	2.39
56.0	2.54	2.00	1.66	1.49	2.71	3.31	2.15	2.15	1.78	2.47	2.38
57.0	2.21	2.10	1.70	1.57	3.31	3.55	2.17	2.19	1.76	2.42	2.52
58.0	2.29	2.27	1.70	1.70	2.88	3.42	2.23	2.04	1.85	2.45	2.28
59.0	1.90	2.77	1.79	1.59	3.16	3.40	1.97	2.11	1.94	2.53	2.58
60.0	1.92	2.36	1.63	1.50	3.36	3.73	1.98	2.12	2.30	2.48	2.34
MEAN	**2.26**	**2.29**	**1.78**	**1.70**	**2.80**	**3.27**	**2.20**	**2.14**	**1.87**	**2.29**	**2.27**
STDEV	**0.40**	**0.40**	**0.10**	**0.14**	**0.56**	**0.39**	**0.11**	**0.13**	**0.11**	**0.36**	**0.19**

1.3 Statistical analysis for screening study

1.3.1 Aerosol concentration

Table 35: ANOVA Table assessing the effect of various FBAG operating factors on aerosol concentration

Response	Factor	Degree of Freedom (DF)	F Value	P-Value	Significant?
Aerosol Concentration (µg/m^3)	Model	2	6.80	0.0188	Yes
	A-Chain Speed	1	5.96	0.0404	Yes
	B-airflow	1	7.75	0.0238	Yes
	Lack of Fit	5	10.37	0.0413	Yes

From Table 35, the chain speed (Factor A) and airflow (Factor B) had a statistically significant effect on Aerosol Concentration. The Model F-value of 6.80 implies the model is significant. There is only a 1.88% chance that a "Model F-Value" this large could occur due to noise.

For the lack of Fit test, the results showed there was significant lack of fit (p=0.0413). This implies that the model can be used to predict Aerosol Concentration using the significant factors but that there may be other factors not included in the experimental design that are required to fully fit the model to the results.

1.3.2 Particle size

Table 36: ANOVA Table assessing the effect of various FBAG operating factors on particle size (MMAD)

Response	Factor	Degree of Freedom (DF)	F Value	P-Value	Significant?
MMAD (µm)	Model	3	12.39	0.0034	Yes
	A-Chain Speed	1	9.94	0.0161	Yes
	B-airflow	1	20.18	0.0028	Yes
	Lack of Fit	4	2.10	0.2846	No

From Table 36, the chain speed (Factor A) and airflow (Factor B) had a statistically significant effect on particle size. The Model F-value of 12.39 implies the model is significant. There is only a 0.34% chance that a "Model F-Value" this large could occur due to noise.

1.4 **Table 37:** Mass Median Aerodynamic Diameter (µM) data for Figure 14

Experimental No	**735268**	**735268**	**735268**	**735268**	**735268**	**735268**
Run No	**7a**	**7b**	**7c**	**7d**	**Average for Run 7a and 7c**	**Average for Run 7b and 7d**
Description	**Fresh Bronze Beads**	**Coated Bronze Beads**	**Fresh Bronze Beads**	**Coated Bronze Beads**		
Time (min)	**Total Conc (mg/m^3)**	**Total Conc (mg/m^3)**	**Total Conc (mg/m^3)**	**Total Conc (mg/m^3)**	**Total Conc (mg/m^3)**	**Total Conc (mg/m^3)**
0	0	0	0	0	0	0
1	0.32	29.41	6.09	17.73	6.09	23.57
2	0.30	17.11	2.50	16.98	2.50	17.05
3	0.32	12.58	2.33	16.32	2.33	14.45
4	0.40	11.58	2.43	14.32	2.43	12.95
5	0.60	10.21	2.42	14.56	2.42	12.38
6	0.67	9.95	3.19	13.49	3.19	11.72
7	0.56	10.19	2.93	15.27	2.93	12.73
8	0.69	10.28	3.15	13.10	3.15	11.69
9	0.73	9.82	3.09	13.18	3.09	11.50
10	1.45	10.88	3.54	13.80	3.54	12.34
11	1.35	10.35	4.12	13.09	4.12	11.72
12	1.30	10.68	3.61	13.01	3.61	11.84
13	1.39	10.88	4.05	12.71	4.05	11.79
14	1.49	12.23	3.92	13.11	3.92	12.67
15	2.02	11.90	4.07	11.80	4.07	11.85
16	2.02	10.24	4.51	12.34	4.51	11.29

Table 37 Continued

Experimental No	735268	735268	735268	735268	735268	735268
Run No	7a	7b	7c	7d	Average for Run 7a and 7c	Average for Run 7b and 7d
Description	Fresh Bronze Beads	Coated Bronze Beads	Fresh Bronze Beads	Coated Bronze Beads		
Time (min)	Total Conc (mg/m^3)	Total Conc (mg/m^3)	Total Conc (mg/m^3)	Total Conc (mg/m^3)	Total Conc (mg/m^3)	Total Conc (mg/m^3)
17	2.21	11.18	4.82	11.79	4.82	11.48
18	2.37	12.51	5.08	12.80	5.08	12.65
19	2.35	12.87	5.53	12.90	5.53	12.89
20	2.67	11.92	5.68	12.71	5.68	12.31
21	3.06	11.74	5.58	12.99	5.58	12.36
22	2.88	12.66	5.87	12.89	5.87	12.78
23	2.71	13.14	6.01	11.49	6.01	12.31
24	3.13	12.71	6.12	11.69	6.12	12.20
25	3.27	12.20	6.13	11.62	6.13	11.91
26	3.51	12.43	6.49	11.93	6.49	12.18
27	4.31	14.41	6.71	12.27	6.71	13.34
28	4.72	12.84	6.41	12.79	6.41	12.81
29	4.96	13.96	6.94	11.63	6.94	12.80
30	5.11	13.68	7.24	11.49	7.24	12.59
31	5.81	13.37	7.82	11.50	7.82	12.44
32	6.00	14.57	7.41	13.00	7.41	13.78
33	6.39	14.42	8.11	11.53	8.11	12.98
34	6.05	15.17	8.23	11.91	8.23	13.54
35	6.52	14.79	8.14	12.36	8.14	13.57
36	6.62	13.94	7.78	13.68	7.78	13.81

Table 37 Continued

Experimental No	735268	735268	735268	735268	735268	735268
Run No	7a	7b	7c	7d	Average for Run 7a and 7c	Average for Run 7b and 7d
Description	Fresh Bronze Beads	Coated Bronze Beads	Fresh Bronze Beads	Coated Bronze Beads		
Time (min)	Total Conc (mg/m^3)	Total Conc (mg/m^3)	Total Conc (mg/m^3)	Total Conc (mg/m^3)	Total Conc (mg/m^3)	Total Conc (mg/m^3)
37	6.83	15.30	9.12	13.70	9.12	14.50
38	7.71	15.52	8.73	13.66	8.73	14.59
39	7.26	14.55	8.99	14.37	8.99	14.46
40	7.42	14.37	9.34	13.25	9.34	13.81
41	8.42	15.04	8.91	14.99	8.91	15.01
42	7.93	15.40	9.94	14.07	9.94	14.73
43	8.34	15.34	10.36	13.63	10.36	14.49
44	9.18	15.99	9.41	14.71	9.41	15.35
45	9.08	15.83	9.71	14.59	9.71	15.21
46	9.60	15.76	10.77	13.76	10.77	14.76
47	9.72	15.97	9.71	16.53	9.71	16.25
48	9.80	15.17	11.24	13.61	11.24	14.39
49	9.81	19.22	10.68	14.01	10.68	16.62
50	10.19	17.07	10.87	14.91	10.87	15.99
51	9.81	15.96	10.94	14.28	10.94	15.12
52	11.94	18.34	11.14	14.79	11.14	16.56
53	11.34	17.95	10.94	14.24	10.94	16.10
54	11.59	16.84	11.32	13.98	11.32	15.41
55	12.55	17.31	11.37	14.96	11.37	16.14
56	12.36	17.34	11.68	14.48	11.68	15.91

Table 37 Continued

Experimental No	735268	735268	735268	735268	735268	735268
Run No	7a	7b	7c	7d	Average for Run 7a and 7c	Average for Run 7b and 7d
Description	Fresh Bronze Beads	Coated Bronze Beads	Fresh Bronze Beads	Coated Bronze Beads		
Time (min)	Total Conc (mg/m^3)	Total Conc (mg/m^3)	Total Conc (mg/m^3)	Total Conc (mg/m^3)	Total Conc (mg/m^3)	Total Conc (mg/m^3)
57	12.10	17.49	11.23	15.36	11.23	16.42
58	14.11	17.01	10.76	13.82	10.76	15.42
59	12.67	16.94	10.88	15.82	10.88	16.38
60	12.97	16.32	11.63	15.05	11.63	15.69
61	12.92	18.36	11.49	14.77	11.49	16.56
62	12.63	17.86	11.74	14.80	11.74	16.33
63	13.28	16.23	11.71	15.75	11.71	15.99
64	14.06	17.77	11.22	14.66	11.22	16.22
65	13.86	18.70	11.64	14.91	11.64	16.81
66	14.44	17.42	12.00	16.38	12.00	16.90
67	13.83	20.33	12.17	15.32	12.17	17.82
68	14.66	18.10	12.49	14.64	12.49	16.37
69	15.45	17.60	12.09	15.21	12.09	16.41
70	15.27	19.55	12.27	14.57	12.27	17.06
71	15.59	16.71	11.82	16.38	11.82	16.54
72	15.19	18.53	11.76	15.82	11.76	17.18
73	15.99	19.89	12.71	15.16	12.71	17.52
74	16.28	17.98	12.35	15.32	12.35	16.65
75	16.88	18.23	11.84	14.98	11.84	16.60
76	16.13	21.13	12.99	18.89	12.99	20.01

Table 37 Continued

Experimental No	735268	735268	735268	735268	735268	735268
Run No	7a	7b	7c	7d	Average for Run 7a and 7c	Average for Run 7b and 7d
Description	Fresh Bronze Beads	Coated Bronze Beads	Fresh Bronze Beads	Coated Bronze Beads		
Time (min)	Total Conc (mg/m^3)	Total Conc (mg/m^3)	Total Conc (mg/m^3)	Total Conc (mg/m^3)	Total Conc (mg/m^3)	Total Conc (mg/m^3)
77	16.21	17.24	12.41	17.57	12.41	17.40
78	17.03	18.44	12.56	15.73	12.56	17.08
79	16.47	19.99	13.10	15.45	13.10	17.72
80	16.62	20.68	12.19	16.37	12.19	18.53
81	16.06	20.71	12.89	15.99	12.89	18.35
82	15.99	19.55	13.17	14.10	13.17	16.83
83	17.52	18.34	12.52	14.16	12.52	16.25
84	18.29	19.41	13.07	14.51	13.07	16.96
85	16.80	19.68	12.31	12.05	12.31	15.86
86	16.64	18.76	12.73	-	12.73	18.76
87	17.25	19.46	12.94	-	12.94	19.46
88	17.54	18.80	12.64	-	12.64	18.80
89	16.49	18.95	12.51	-	12.51	18.95
90	17.59	19.92	13.37	-	13.37	19.92
MEAN	**9.07**	**15.77**	**8.98**	**14.12**	**8.98**	**15.08**
STDEV	**5.90**	**3.44**	**3.41**	**1.59**	**3.41**	**2.44**
%RSD	**65.12**	**21.81**	**38.01**	**11.26**	**38.01**	**16.18**

1.5 **Table 38:** Aerosol concentration (mg/m^3) data for **Figure** 15

Experimental No	**735268**		
Run No	**7d**		
Time (min)	**Total Conc.(N/cm^3)**	**Time (min)**	**Total Conc.(N/cm^3)**
0	0	56	21854
1	56690	57	20694
2	48081	58	21464
3	38557	59	21434
4	38020	60	20678
5	38229	61	21788
10	23726	62	21385
11	23867	63	21325
12	23243	64	21553
13	23830	65	21455
14	23317	66	21593
15	22235	67	21116
16	22464	68	21251
17	21980	69	21760
18	22217	70	21465
19	22115	71	21464
20	20929	72	21923
21	21781	73	21481
22	21498	74	22178
23	21104	75	23278
24	21598	76	21723
25	21557	77	22323
26	20820	78	21978
27	21083	79	22227
28	20350	80	22903
29	20489	81	22387
30	21077	82	22286
31	20072	83	22722
32	19911	84	22187
33	19796	85	22381
34	19957	86	23020
35	20732	87	22028
36	20279	88	22098
37	20367	89	22225
38	20475	90	21538
39	19997	91	20858
40	19655	92	20739
41	20404	93	21078

Table 38 Continued

Experimental No	735268		
Run No	7d		
Time (min)	Total Conc.(N/cm^3)	Time (min)	Total Conc.(N/cm^3)
42	19646	94	11948
43	19419	95	286
44	20617	96	14
45	21255	97	7
46	21282	98	5
47	21594	99	5
48	21078	100	4
49	21016	101	4
50	21750	102	4
51	20931	103	4
52	21020	104	5
53	21978	-	-
54	21368	-	-
55	20896	-	-
56	21854	-	-
57	20694	-	-
58	21464	-	-
59	21434	-	-
60	20678	-	-

1.6 **Table 39:** Aerosol concentration (mg/m^3) data for **Figure** 16

Experimental No	**735268**	**735268**
Run No	**5a, 5b, 5c**	**6a, 6b**
Blend	**5.00**	**2.50**
Time (min)	**Aerosol concentration (mg/m^3) ± SD**	
5	11.33 ± 2.63	14.21 ± 3.42
10	20.73 ± 3.69	10.94 ± 0.72
15	30.04 ± 5.95	12.95 ± 0.60
20	39.23 ± 4.80	12.68 ± 1.12
25	43.52 ± 2.66	11.34 ± 0.82
30	43.47 ± 0.15	10.43 ± 0.86
35	40.49 ± 4.03	9.23 ± 1.01
40	40.35 ± 3.53	8.31 ± 1.01
45	39.50 ± 4.36]	7.63 ± 1.10

1.7 **Table 40:** Mass Median Aerodynamic Diameter (µM) data for **Figure** 17

Experimental No	**735268**	**735268**	**735268**	**735268**
Run No	**7a, 7c**	**7b**	**5a, 5b and 5c**	**6a, 6b**
Description	**Fresh Bronze Beads**	**Coated Bronze Beads**	**2.5% w/w**	**5.0% w/w**
Time (min)	**MMAD (um) ± SD**	**MMAD (um) ± SD**	**MMAD (um) ± SD**	**MMAD (um) ± SD**
5	1.28 ± 0.05	2.02	2.71 ± 0.19	2.61 ± 0.28
10	1.25 ± 0.06	1.95	2.29 ± 0.02	3.21 ± 0.74
15	1.23 ± 0.10	2.16	2.28 ± 0.02	3.22 ± 0.45
20	1.29 ± 0.09	2.06	2.25 ± 0.02	3.34 ± 0.55
25	1.26 ± 0.03	2.08	2.2 ± 0.04	3.24 ± 0.53
30	1.36 ± 0.10	2.22	2.16 ± 0.06	3.18 ± 0.43
35	1.43 ± 0.03	2.30	2.08 ± 0.11	3.13 ± 0.42
40	1.51 ± 0.03	2.21	2.02 ± 0.10	3.13 ± 0.26
45	1.57 ± 0.02	2.39	1.97 ± 0.13	3.07 ± 0.34

1.8 **Table 41:** Aerosol concentration (mg/m^3) data for **Figure** 18

Experimental No	**735268**				
Run No	**4a, 4b**		**Run No**	**4c, 4d**	
Type	**Coated bronze beads**		**Type**	**Clean bronze beads**	
Start Time	**(min)**	**Total Conc.(mg/m^3)**	**Start Time**	**(min)**	**Total Conc.(mg/m^3)**
	0	0		0	0
11:17:50	0.08	34.30	09:18:38	0.08	3.28
11:18:40	1.00	20.55	09:19:28	1.00	2.91
11:22:45	5.00	19.21	09:23:33	5.00	3.85
11:26:52	10.00	11.88	09:26:30	7.95	2.37
11:31:52	15.00	12.70	09:31:30	12.95	3.01
11:36:52	20.00	12.14	09:36:30	17.95	4.19
11:41:52	25.00	12.49	09:41:30	22.95	4.72
11:46:52	30.00	14.38	09:46:30	27.95	5.84
11:51:52	35.00	13.94	09:51:30	32.95	7.26
11:56:52	40.00	13.40	09:56:30	37.95	7.63
12:01:52	45.00	13.27	10:01:30	42.95	8.00
12:06:52	50.00	11.64	10:06:30	47.95	8.22
12:11:52	55.00	13.06	10:11:30	52.95	9.24
12:16:52	60.00	12.50	10:16:30	57.95	10.05
12:21:52	65.00	12.10	10:21:30	62.95	10.25
12:26:52	70.00	13.34	10:26:30	67.95	10.68
12:31:52	75.00	13.70	10:31:30	72.95	10.54
12:36:52	80.00	12.47	10:36:30	77.95	10.81
12:41:52	85.00	11.97	10:41:30	82.95	11.45
12:46:52	90.00	12.28	10:46:30	87.95	11.38
12:51:52	95.00	12.38	10:51:30	92.95	11.73
12:56:52	100.00	12.05	10:56:30	97.95	5.07

1.9 **Table 42:** Aerosol concentration (mg/m^3) data for **Figure** 19

Experimental No	735268	735268	735268	735268	735268	735268
Run No	1a	2a	3a	1b	2b	3b
Blend	2.5% w/w	5.0% w/w	10% w/w	2.5% w/w	5% w/w	10% w/w
Time (min)	MMAD (um)					
1	4.33	4.26	6.93	4.56	4.58	6.00
2	3.96	4.04	7.35	3.68	4.11	5.26
3	3.87	3.93	7.40	3.70	3.59	4.56
4	3.81	4.03	7.92	3.90	3.50	5.31
5	3.83	3.99	6.85	3.67	3.32	5.38
6	4.19	3.95	8.47	3.78	3.43	5.01
7	3.27	4.09	6.34	3.39	3.11	4.89
8	3.10	3.88	6.84	3.70	3.53	5.42
9	3.03	3.96	6.28	3.56	3.63	5.09
10	2.73	4.15	6.04	3.07	3.41	5.09
11	3.38	4.08	6.27	3.13	3.15	5.24
12	2.46	4.23	6.11	3.66	3.29	4.90
13	2.79	3.83	6.03	2.77	3.21	5.15
14	2.20	3.66	5.65	2.69	3.37	5.00
15	3.25	3.79	5.89	3.08	3.15	4.95
16	2.14	3.78	5.71	2.36	3.40	5.09
17	2.05	3.68	5.79	3.19	3.52	5.08
18	2.25	3.85	5.59	2.97	3.33	4.92
19	2.17	3.68	5.54	2.61	3.26	5.04
20	2.25	3.85	5.93	2.97	3.50	4.72
21	1.92	3.80	5.47	2.11	3.56	5.18
22	2.84	3.81	5.33	1.86	3.43	5.05
23	2.50	3.66	5.27	2.17	3.51	4.89
24	2.33	3.78	5.56	2.56	3.53	4.93
25	1.97	3.80	5.41	2.63	3.44	4.90
26	2.61	3.86	5.23	3.33	3.39	4.84
27	2.45	3.79	5.50	3.31	3.40	4.81
28	1.97	3.76	5.39	3.30	3.39	4.98
29	2.59	3.83	5.45	3.26	3.70	4.81
30	1.89	3.59	5.12	3.60	3.59	4.87
31	1.92	3.86	5.20	3.07	3.49	4.84
32	2.66	3.83	5.73	3.21	3.15	4.88
33	1.71	3.60	5.30	3.02	3.81	4.60
34	1.86	3.36	5.33	2.86	3.26	4.89
35	1.96	3.27	5.63	2.63	3.24	4.72
36	1.55	3.77	5.43	2.83	3.24	4.81
37	1.44	3.56	5.14	2.26	3.33	4.65
38	1.71	3.68	5.29	3.10	3.66	4.97
39	2.11	3.36	5.09	2.10	3.30	4.77

Table 42 Continued

Experimental No	735268	735268	735268	735268	735268	735268
Run No	1a	2a	3a	1b	2b	3b
Blend	2.5% w/w	5.0% w/w	10% w/w	2.5% w/w	5% w/w	10% w/w
Time (min)	MMAD (um)					
40	2.00	3.29	5.12	2.95	3.32	4.81
41	3.52	3.39	5.30	2.52	3.23	4.87
42	1.70	3.70	5.37	2.21	3.42	4.87
43	2.28	3.57	5.06	1.67	3.05	4.95
44	1.84	3.44	5.15	1.69	3.62	4.74
45		3.53	5.26	1.73	2.89	4.67
MEAN	2.55	3.77	5.82	2.94	3.43	4.96
STDEV	0.76	0.23	0.78	0.64	0.27	0.25

1.10 **Table 43:** Gravimetric and APS aerosol concentration (mg/m^3) data for **Figure** 20

	Aerosol concentration (mg/m^3). Dilution ratio 1:1. Experimental Reference: 356680									
RUN	**1**		**2**		**3**		**4**		**5**	
Time (min)	**Gravimetric**	**APS**	**Gravimetric**	**APS**	**Gravimetric**	**APS**	**Gravimetric**	**APS**	**Gravimetric**	**APS**
5	1798.63	20.05	1272.37	17.67	2736.62	27.84	1300.00	19.13	1117.24	15.90
10	335.66	4.20	273.68	3.29	631.94	8.13	240.56	2.96	181.94	2.39
15	263.89	4.19	143.05	3.67	448.61	6.80	212.68	2.59	103.50	1.77
20	260.14	5.37	122.37	5.02	299.30	6.34	132.87	2.87	120.83	1.96
30	169.50	6.75	126.49	6.16	286.81	6.42	173.94	4.14	129.86	3.01
45	118.78	8.63	89.62	8.71	207.87	6.10	112.68	5.52	181.15	4.31
	Aerosol concentration (mg/m^3). Dilution ratio 1:20. Experimental Reference: 356680									
RUN	**1**		**2**		**3**		**4**		**5**	
Time (min)	**Gravimetric**	**APS**	**Gravimetric**	**APS**	**Gravimetric**	**APS**	**Gravimetric**	**APS**	**Gravimetric**	**APS**
5	809.46	25.62	1541.03	37.76			998.65	25.02	929.25	21.81
10	106.12	4.92	245.03	7.22	124.00	7.74	124.32	4.43	282.19	6.35
15	43.84	1.81	158.94	4.83	77.33	2.37	81.08	1.99	154.48	6.00
20	76.71	1.95	123.81	5.64	60.00	2.33	59.86	2.08	146.21	7.91
30	59.31	2.40	118.00	6.72	67.33	2.49	62.59	3.20	89.58	9.98
45	61.61	3.85	90.95	8.73	54.75	3.68	51.70	4.45	71.76	12.99
	Aerosol concentration (mg/m^3). Dilution ratio 1:100. Experimental Reference: 356680									
RUN	**6**		**7**		**8**		**9**		**10**	
Time (min)	**Gravimetric**	**APS**	**Gravimetric**	**APS**	**Gravimetric**	**APS**	**Gravimetric**	**APS**	**Gravimetric**	**APS**
5	1660.27	46.04	1016.11	29.17	1005.44	38.09	1856.55	55.21	2958.39	54.00
10	260.69	10.50	338.78	10.66	327.89	11.00	305.63	14.05	589.26	16.67
15	181.94	11.30	197.30	7.71	258.90	10.78	208.45	18.55	470.67	14.45
20	160.84	12.34	148.30	10.56	179.31	12.28	155.24	14.91	191.89	14.63
30	123.08	13.76	122.45	10.66	144.83	14.12	161.27	14.20	189.86	14.62
45	97.90	12.87	87.07	11.67	119.08	13.60	116.43	15.02	154.65	12.89

1.11 **Table 44:** APS event data for **Figure** 21

RUN / EVENT DATA	Dilution ratio 1:1. Experimental Reference: 356680						
	1	**2**	**3**	**4**	**5**	**MEAN**	**STDEV**
1: <0.55µm	8.03	7.77	7.32	10.41	8.83	8.47	1.21
2: 0.55-20µm	78.18	80.83	82.22	75.69	83.82	80.15	3.24
3: Coincidence	13.78	11.40	10.46	13.90	7.34	11.38	2.71
4: >20µm	0.00	0.00	0.00	0.00	0.01	0.00	0.00

RUN / EVENT DATA	Dilution ratio 1:20. Experimental Reference: 356680						
	1	**2**	**3**	**4**	**5**	**MEAN**	**STDEV**
1: <0.55µm	14.95	10.13	40.65	24.10	25.21	23.01	11.70
2: 0.55-20µm	80.57	85.76	57.02	70.63	69.53	72.70	11.10
3: Coincidence	4.48	4.11	2.33	5.26	5.26	4.29	1.21
4: >20µm	0.00	0.00	0.00	0.00	0.00	0.00	0.00

RUN / EVENT DATA	Dilution ratio 1:100. Experimental Reference: 356680						
	1	**2**	**3**	**4**	**5**	**MEAN**	**STDEV**
1: <0.55µm	16.50	38.14	35.20	13.62	29.89	26.67	11.05
2: 0.55-20µm	79.43	58.92	61.21	82.70	65.73	69.60	10.81
3: Coincidence	4.08	2.94	3.59	3.68	4.37	3.73	0.54
4: >20µm	0.00	0.00	0.00	0.00	0.00	0.00	0.00

1.12 **Table 45:** APS versus HPLC correlation data for **Figure** 22

Experimental Ref	Time (min)	APS Concentration (µg/L)	HPLC Concentration (µg/L)	Adjusted HPLC Concentration (µg/L)
EE397370	5.5	13.42	4.98	24.88
EE397370	15	4.77	2.51	12.53
EE397370	30	6.92	1.68	8.41
EE397370	45	6.54	1.33	6.63
EE398882	5	16.58	5.18	25.90
EE398882	15	7.80	2.56	12.80
EE398882	30	6.29	1.79	8.97
EE398882	45	4.25	1.33	6.67
EE398882	5	22.41	7.03	35.17
EE398882	15	7.53	3.20	15.98
EE398882	30	6.91	1.95	9.76
EE398882	45	4.85	1.45	7.26
EE398882	5	19.19	6.29	31.47
EE398882	15	10.57	3.03	15.16
EE398882	30	8.11	1.77	8.85
EE398882	45	6.79	1.53	7.66

Note: Aerosol concentration for HPLC filters multiplied by factor of 5 to match airflow of APS (5L/min)

1.13 **Table 46**: Marple Cascade Impactor data used for **Figure** 23 and **Figure** 24

Experiment Ref:	**EE551492**	**EE546938**	**EE554126**	**EE578568**	**EE579774**	**Mean %**	**%<ecd**	**ECD (mcm)**	**Log ECD**	**Probit**
Run No:	**1**	**2**	**3**	**4**	**5**					
	mcg/stage	**mcg/stage**	**mcg/stage**	**mcg/stage**	**mcg/stage**					
Stage 3	3.82	3.50	9.90	11.1	10.3	7.71	92.29	9.80	0.99	6.45
Stage 4	2.66	3.50	2.50	8.8	4.9	4.02	88.27	6.00	0.78	6.18
Stage 5	5.72	5.70	3.60	14.8	7.2	6.53	81.73	3.50	0.54	5.88
Stage 6	97.34	108.50	61.00	78.7	46.2	68.81	12.92	1.55	0.19	3.88
Stage 7	7.02	4.40	3.80	25.1	5	7.48	5.44	0.93	-0.03	3.37
Stage 8	1.31	1.10	0.00	2.9	2	1.29	4.15	0.52	-0.28	3.25
Filter	4.7	14.9	2.30	1.7	1.9	4.15		0.00		
Total	122.57	141.60	83.10	143.10	77.50	100.00			Slope :	2.935372

1.14 **Table 47**: APS data for **Figure** 24

Experiment Ref:	EE551492	EE546938	EE554126	EE578568	EE579774	Mean	STDEV
RUN	1	2	3	4	5		
Aerodynamic Diameter	Average %dM						
0.523	0.62	0.45	0.50	0.49	0.35	0.48	0.09
0.542	1.22	0.90	1.00	1.00	0.74	0.97	0.24
0.583	2.01	1.49	1.65	1.66	1.24	1.61	0.39
0.626	2.98	2.22	2.46	2.48	1.88	2.40	0.56
0.673	4.14	3.10	3.45	3.49	2.68	3.37	0.75
0.723	5.54	4.17	4.65	4.72	3.67	4.55	0.97
0.777	7.20	5.44	6.09	6.22	4.90	5.97	1.22
0.835	9.18	6.97	7.83	8.01	6.42	7.68	1.49
0.898	11.34	8.66	9.75	10.05	8.17	9.60	1.79
0.965	13.72	10.54	11.88	12.33	10.20	11.73	2.09
1.037	16.48	12.74	14.39	14.98	12.62	14.24	2.43
1.114	19.19	14.92	16.87	17.69	15.16	16.76	2.77
1.197	22.24	17.42	19.70	20.74	18.10	19.64	3.13
1.286	25.24	19.92	22.56	23.85	21.18	22.55	3.50
1.382	28.33	22.53	25.51	27.09	24.50	25.59	3.88
1.486	31.45	25.18	28.53	30.42	27.97	28.71	4.28
1.596	34.58	27.83	31.57	33.76	31.54	31.86	4.69
1.715	37.77	30.49	34.60	37.08	35.12	35.01	5.10
1.843	41.41	33.41	37.71	40.45	38.72	38.34	5.49
1.981	47.40	37.76	41.88	44.47	42.85	42.87	5.76
2.129	58.65	46.37	50.53	50.60	48.40	50.91	5.85
2.288	71.62	59.49	61.22	58.28	53.86	60.89	6.39
2.458	77.36	68.00	65.93	63.89	57.78	66.59	6.77
2.642	80.08	71.29	68.84	67.23	60.82	69.65	6.90
2.839	82.32	73.81	71.47	69.82	63.46	72.18	6.92
3.051	84.34	76.20	73.83	72.21	66.02	74.52	6.88
3.278	86.01	78.07	75.90	74.31	68.33	76.53	6.73
3.523	87.59	79.90	77.97	76.38	70.62	78.49	6.52
3.786	89.05	81.76	79.99	78.47	72.94	80.44	6.21
4.068	90.35	83.51	81.90	80.52	75.22	82.30	5.85
4.371	91.48	85.07	83.66	82.49	77.42	84.02	5.44
4.698	92.44	86.68	85.31	84.38	79.58	85.68	4.96
5.048	93.38	88.13	86.83	86.16	81.60	87.22	4.47
5.425	94.18	89.39	88.19	87.82	83.52	88.62	3.98
5.829	94.82	90.60	89.52	89.38	85.35	89.94	3.48
6.264	95.36	91.62	90.65	90.80	87.06	91.10	3.02
6.732	95.88	92.60	91.66	92.01	88.62	92.16	2.58
7.234	96.41	93.49	92.64	93.15	90.10	93.16	2.18
7.774	96.84	94.35	93.41	94.21	91.47	94.05	1.80
8.354	97.13	95.02	94.04	95.15	92.63	94.79	1.51
8.977	97.51	95.67	94.84	95.93	93.70	95.53	1.28

Table 47 Continued

Experiment Ref:	EE551492	EE546938	EE554126	EE578568	EE579774	Mean	STDEV
RUN	1	2	3	4	5		
Aerodynamic Diameter	Average %dM						
9.647	97.93	96.20	95.33	96.62	94.63	96.14	1.09
10.37	98.14	96.74	95.91	97.17	95.51	96.70	0.95
11.14	98.34	97.14	96.23	97.74	96.23	97.13	0.80
11.97	98.46	97.55	96.97	98.31	96.87	97.63	0.70
12.86	98.50	98.02	97.28	98.70	97.51	98.00	0.56
13.82	98.62	98.21	97.62	99.03	98.00	98.30	0.46
14.86	99.16	98.57	98.26	99.31	98.62	98.78	0.31
15.96	99.16	98.88	98.51	99.55	99.02	99.02	0.29
17.15	99.41	99.20	98.68	99.69	99.55	99.31	0.15
18.43	99.60	99.81	99.63	99.84	99.88	99.75	0.10
19.81	100.00	100.00	100.00	100.00	100.00	100.00	0.10

2 Validation of Nose-only Exposure System for Rodents

2.1

Table 48: Comparison of the aerosol concentration of the FMS-Lactose blends before and after application of charge neutralisation (see **Figure** 28).

Time (min)	Aerosol concentration (mg/m^3)	
	Before charge neutralisation	After charge neutralisation
5	6.83 ± 2.14	25.99 ± 8.74
10	0.79 ± 0.27	7.97 ± 0.62
15	0.45 ± 0.21	5.15 ± 0.29
20	0.01 ± 0.00	0.46 ± 0.25
25	0.35 ± 0.06	4.88 ± 0.76
30	0.29 ± 0.02	3.64 ± 0.30
35	0.22 ± 0.01	3.13 ± 0.42
40	0.23 ± 0.07	2.97 ± 0.31
45	0.18 ± 0.04	2.91 ± 0.27
50	0.20 ± 0.07	2.97 ± 0.17
55	0.20 ± 0.07	3.08 ± 0.05
60	0.22 ± 0.07	2.98 ± 0.47
65	0.26 ± 0.09	3.37 ± 0.27

2.2 **Table 49:** Assessing the variability of total particulate matter (TPM) in the exposure chamber (see **Figure** 29)

Tables below details the Total Particulate Matter (TPM) of aerosol powder collected on sampling filters for exposure chamber characterisation experiments. Sampling flow rate was set at 0.86 L/min per sampling port.

Run	Port (Mass of powder collected; µg)					Mean	STDEV	CV
	1	3	5	8	11			
1	4.2	3.0	2.4	2.5	2.7	3.0	0.7	24.7
2	4.1	2.5	1.9	3.6	2.3	2.9	0.9	32.2
3	2.7	3.3	3.3	2.9	3.2	3.1	0.3	8.7
4	3.1	2.9	2.8	2.2	2.6	2.7	0.3	12.6
5	3.5	3.7	3	2.8	2.9	3.2	0.4	12.5
6	4.2	3.3	3.6	3.5	3.5	3.3	0.3	10.4

Note: exposure time interval: 0-15 min. Exposure setup experiment: EE455550, HPLC experiment: EE457144.

Run	Port (Mass of powder collected; µg)					Mean	STDEV	CV
	1	3	5	8	11			
1	2.3	1.6	1.5	1.6	1.3	1.7	0.4	22.8
2	3.3	2.8	2	1.9	2.5	2.5	0.6	23.2
3	3.2	3.3	2	2.8	2.2	2.7	0.6	21.6
4	1.5	1.9	1.8	1.9	1.9	1.8	0.2	9.6
5	2.9	2.5	2.9	2.7	3.1	2.8	0.2	8.1
6	1.7	2.0	1.7	1.7	1.9	1.8	0.1	7.9

Note: exposure time interval: 20-65 min. Exposure setup experiment: EE455550, HPLC experiment: EE457144.

Run	Port (Mass of powder collected; µg)					Mean	STDEV	CV
	1	3	5	8	11			
1	6.5	4.6	3.9	4.1	4.0	4.6	1.1	23.5
2	7.4	5.3	3.9	5.5	4.8	5.4	1.3	23.9
3	5.9	6.6	5.3	5.7	5.4	5.8	0.5	8.9
4	4.6	4.8	4.6	4.1	4.5	4.5	0.3	5.7
5	6.4	6.2	5.9	5.5	6.0	6.0	0.3	5.7
6	5.9	5.3	5.3	5.2	5.4	5.4	0.3	5.1

Note: exposure time interval: 0-65 min. Exposure setup experiment: EE455550, HPLC experiment: EE457144.

2.3 **Table 50:** Assessing the variability of active test material in the exposure chamber (see **Table 7**)

Tables below details the mass of FMS particles assayed using HPLC technique and collected on sampling filters for exposure chamber characterisation experiments. Sampling flow rate was set at 0.86 L/min per sampling port. In addition to Table 6, the data below was used in Figure 30 and Figure 31 (Section 2.4, B– Results and Discussion).

	Port (Mass of powder collected; µg)							
Run	**1**	**3**	**5**	**8**	**11**	**Mean**	**STDEV**	**CV**
1	82.88	67.10	57.89	69.20	69.06	69.2	8.9	12.9
2	92.36	94.21	87.98	104.52	97.01	95.2	6.2	6.5
3	72.55	65.71	70.38	77.31	68.47	70.9	4.4	6.2
4	76.63	82.78	91.69	79.39	68.33	79.8	8.5	10.7
5	81.23	67.79	76.15	75.69	77.33	75.6	4.9	6.5
6	75.16	76.37	75.62	75.66	70.80	74.7	2.2	3.0

Note: exposure time interval: 0-15 min. Exposure setup experiment: EE455550, HPLC experiment: EE457144.

	Port (Mass of powder collected; µg)							
Run	**1**	**3**	**5**	**8**	**11**	**Mean**	**STDEV**	**CV**
1	84.65	80.51	-	81.59	78.08	81.2	2.7	3.4
2	96.66	82.27	94.10	90.99	81.6	89.1	6.9	7.7
3	83.5	64.23	66.45	68.57	58.76	68.3	9.2	13.5
4	78.01	99.46	81.02	100.3	74.86	86.7	12.2	14.1
5	61.65	73.82	67.73	64.34	57.28	65.0	6.3	9.6
6	68.87	67.53	70.71	73.86	67.34	69.7	2.7	3.9

Note: exposure time interval: 20-65 min. Exposure setup experiment: EE455550, HPLC experiment: EE457144.

	Port (Mass of powder collected; µg)							
Run	**1**	**3**	**5**	**8**	**11**	**Mean**	**STDEV**	**CV**
1	167.53	147.61	-	150.79	147.14	153.3	9.6	6.3
2	189.02	176.48	182.08	195.51	178.61	184.3	7.8	4.3
3	156.05	129.94	136.83	145.88	127.23	139.2	11.9	8.5
4	154.64	182.24	172.71	179.69	143.19	166.5	16.9	10.2
5	142.88	141.61	143.88	140.03	134.61	140.6	3.6	2.6
6	144.03	143.9	146.33	149.52	138.14	144.4	4.2	2.9

Note: exposure time interval: 0-65 min. Exposure setup experiment: EE455550, HPLC experiment: EE457144.

2.4 **Table 51:** Environmental conditions within exposure chamber

Table below details the environmental conditions recoded during exposure chamber characterisation experiments. Data presented was used to generate Figure 32 and Figure 33 (Section 2.5, B– Results and Discussion)

RUN	TIME (MIN)	Relative Humidity (% RH)	TEMP (°c)
1	5	12.8	23.9
1	15	13	24
1	30	13.7	24.5
1	45	13.6	24.7
1	65	13.5	24.7
2	5	13.6	25.1
2	10	13.6	25.1
2	35	13.8	25.3
2	45	14	25.2
3	5	13.2	23.8
3	20	13.8	24.4
3	45	13.9	24.8
3	55	14.1	24.9
3	60	14.3	25.1
3	65	14.3	25.2
4	5	14	24.9
4	10	13	24.9
4	15	13.3	24.9
4	20	14.5	25.1
4	30	13.4	25.2
4	35	13.4	25.6
4	40	13.9	25.3
4	45	13.7	25.4
4	50	13.6	25.3
4	55	14	25.3
4	60	14.5	25.5
4	65	14.5	25.5
5	5	15.4	24.4
5	10	14.6	24.5
5	15	14.6	24.5
5	20	14.3	24.7
5	30	14.5	25
5	35	14.2	25.1
5	45	14.4	25.1
5	50	14.6	25.2
5	55	14.3	25.3
5	60	14.2	25.2
6	5	13.8	25.5
6	10	13.4	25.5
6	30	13.4	25.7
6	45	14.3	25.8
6	55	13.9	25.9

2.5 **Table 52:** Characterisation of exposure atmosphere

Table below details the aerosol exposure data (concentration and particle size) collected using the APS instrument for replicate runs of the exposure chamber characterisation experiments. Sampling flow rate using APS probe was set at 5 L/min. Data presented was used to generate Figure 34 and Figure 35 (Section 2.6, B– Results and Discussion).

RUN	Time (min)	Total Concentration(µg/L)	MMAD (µm)	GSD
1	5	30.04	2.52	1.77
1	10	15.95	2.18	1.77
1	15	13.20	2.10	1.77
1	20	0.75	1.92	1.72
1	25	12.05	2.18	1.84
1	30	9.10	2.11	1.73
1	35	7.91	2.22	1.72
1	40	6.86	2.30	1.69
1	45	6.11	2.40	1.77
1	52	5.43	2.49	1.64
1	57	4.85	2.55	1.62
1	62	4.13	2.56	1.59
2	5	42.44	2.44	1.80
2	10	22.02	2.18	1.75
2	15	16.32	2.11	1.75
2	30	10.85	2.15	1.78
2	35	8.95	2.24	1.74
2	40	7.29	2.35	1.73
2	45	6.02	2.43	1.69
2	50	4.70	2.48	1.68
2	55	3.65	2.52	1.80
2	60	2.48	2.48	1.62
2	65	1.60	2.43	1.59
3	5	36.77	2.75	1.88
3	10	17.48	2.30	1.80
3	15	13.72	2.23	1.80
3	20	0.74	2.10	1.77
3	25	12.44	2.27	1.87
3	30	9.09	2.17	1.78
3	35	7.56	2.23	1.78
3	40	6.39	2.32	1.79
3	45	5.20	2.41	1.79
3	50	4.24	2.45	1.76
3	55	3.50	2.48	1.76
3	60	2.80	2.48	1.75
3	65	2.37	2.51	1.76
4	5	33.40	2.94	1.85
4	10	16.63	2.43	1.85
4	15	11.70	2.32	1.82

Table 52 Continued

RUN	Time (min)	Total Concentration(µg/L)	MMAD (µm)	GSD
4	20	0.65	2.31	2.01
4	25	10.16	2.33	1.87
4	30	7.83	2.29	1.81
4	35	6.52	2.34	1.78
4	40	5.94	2.42	1.82
4	45	5.49	2.48	1.73
4	50	4.99	2.52	1.72
4	55	4.98	2.55	1.68
4	60	4.65	2.56	1.70
5	5	24.05	2.82	1.77
5	10	11.99	2.48	1.81
5	15	10.21	2.46	1.82
5	20	0.53	2.36	1.81
5	25	9.37	2.47	1.81
5	30	7.29	2.42	1.77
5	35	6.81	2.46	1.78
5	40	6.35	2.50	1.76
5	45	5.67	2.52	1.74
5	50	5.21	2.56	1.72
5	55	4.54	2.56	1.70
5	60	3.77	2.56	1.67
5	65	3.19	2.55	1.65
6	5	24.06	2.35	1.83
6	10	12.98	2.18	1.81
6	15	11.27	2.23	1.80
6	20	1.30	4.41	2.18
6	25	10.74	2.37	1.80
6	30	8.38	2.34	1.77
6	35	6.71	2.38	1.75
6	40	5.66	2.42	1.73
6	45	4.67	2.46	1.70
6	50	3.87	2.50	1.69
6	55	3.18	2.52	1.66
6	60	2.47	2.52	1.65
6	65	2.13	2.52	1.62
6	35	6.71	2.38	1.75
6	40	5.66	2.42	1.73
6	45	4.67	2.46	1.70

3 Assessing the effect of aerosol characteristics on deposition in the rat model

3.1 Characterisation of exposure atmosphere for Table 8 and 9

Table below details the aerosol exposure concentration data (µg/L) collected on sampling filters and analysed using HPLC method. Data detailed below is listed in Table 8 (Section 4.1, B– Results and Discussion).

Table 53: Experimental results obtained with the *in vitro* rat model (IVR) using 2 and 4 µm FMS-Lactose inhalation blends.

Experimental Reference	Description	Mass on Filter (µg)	Flow Rate (L/min)	Time (min)	Aerosol Concentration (µg/L)
EE562850	4µm blend Replicate 1	289.3	3.0	45	2.1
EE572958	4µm blend Replicate 2	808.9	3.0	45	6.0
EE577542	4µm blend Replicate 3	320.3	3.0	45	2.4
EE551492	2µm blend Replicate 1	224.8	3.0	45	1.7
EE553046	2µm blend Replicate 2	276.6	3.0	45	2.1
EE554126	2µm blend Replicate 3	179.9	3.0	45	1.3

Table below details the aerosol exposure particle size data (MMAD) collected using the APS instrument for replicate blends containing 4 and 2µm-sized FMS active particles. Data detailed below is listed in Table 8 (Section 4.1, B– Results and Discussion).

Table 54: Experimental results obtained with the *in vitro* rat model (IVR) using 2 and 4 µm FMS-Lactose inhalation blends.

Experimental Reference	EE562850	EE572958	EE577542
Description	4µm blend Replicate 1	4µm blend Replicate 2	4µm blend Replicate 3
Time (min)	Mass Median Aerodynamic Diameter (µm)		
5	4.71	6.37	5.45
10	4.55	6.32	4.69
15	4.72	6.47	4.29
20	4.35	6.21	4.15
25	4.73	5.58	4.00
30	4.80	5.52	3.88
35	4.90	5.09	4.05
40	4.75	4.85	3.96
45	4.83	4.90	3.91
MEAN	**4.78**	**5.65**	**4.34**
STDEV	**0.19**	**0.60**	**0.45**

Table 54 Continued

Experimental Reference	EE551492	EE553046	EE554126
Description	**2µm blend Replicate 1**	**2µm blend Replicate 2**	**2µm blend Replicate 3**
Time (min)	**Mass Median Aerodynamic Diameter (µm)**		
5	2.13	2.86	2.78
10	2.15	2.30	2.30
15	2.16	2.29	2.29
20	2.15	2.27	2.23
25	2.11	2.22	2.15
30	2.08	2.20	2.10
35	2.00	2.15	1.95
40	1.92	2.09	1.90
45	1.78	2.04	1.82
MEAN	**2.05**	**2.27**	**2.17**
STDEV	**0.13**	**0.24**	**0.29**

3.2 IVR data for Table 8, Figure 42 and 43

Table below details the mass FMS particles (µg) collected in the sections of the IVR model. Data detailed below is listed in Table 8, Figure 42 and Figure 43 (Section 4.1, B– Results and Discussion).

Table 55: Experimental results obtained with the *in vitro* rat model (IVR) using 2 and 4 µm FMS-Lactose inhalation blends

Experimental Reference	**EE562850**	**EE572958**	**EE577542**	**EE551492**	**EE553046**	**EE554126**
Description	**4µm blend Replicate 1**	**4µm blend Replicate 2**	**4µm blend Replicate 3**	**2µm blend Replicate 1**	**2µm blend Replicate 2**	**2µm blend Replicate 3**
Section	**Mass of FMS deposited (µg)**					
S1	21.6	47.8	19.8	7.7	8.5	6.9
S2	1.8	3	1	1.1	1.4	1.1
S3	0.7	1	0.5	0.3	0.3	0.1
S4	0.5	0.2	0.3	0.1	0.1	
S5	0.9	0.8	0.6	0.7	1.7	0.4
S6	0.8	0.7	1.3	0.3	0.8	0.1
Total	21.6	53.5	23.5	10.2	12.8	8.6
Head (S1 + S2)	23.4	50.8	20.8	8.8	9.9	8.0
TB (S3 + S4 + S5)	2.10	2.0	1.40	1.1	2.1	0.5
Post-TB (S6)	0.80	0.70	1.30	0.3	0.8	0.1
Head (% of Total)	89.0	95.0	88.5	86.3	77.3	93.0
TB (% of Total)	8.0	3.7	6.0	10.8	16.4	5.8
Post-TB (% of Total)	3.0	1.3	5.5	2.8	6.3	1.2

3.3 MPPD data for Figure 43

Table below details the predicted fractions of FMS particles to be deposited in the rat lung model according to the MPPD model. Data detailed below was used to construct Figure 43 (Section 4.1, B– Results and Discussion).

Table 56: Comparison of particle deposition of FMS particles in the MPPD model for 2 and 4 µm containing inhalation blends

Experimental Reference	**EE562850**	**EE572958**	**EE577542**	**EE551492**	**EE553046**	**EE554126**
Description	**4µm blend Replicate 1**	**4µm blend Replicate 2**	**4µm blend Replicate 3**	**2µm blend Replicate 1**	**2µm blend Replicate 2**	**2µm blend Replicate 3**
Region	**Deposition fraction**					
Head	0.954	0.569	0.928	0.629	0.60	0.568
TB	4.83E-03	3.05E-03	7.82E-03	0.013	0.012	0.012
Pulmonary	7.95E-03	5.29E-03	0.014	0.025	0.024	0.024
Total	0.967	0.577	0.95	0.667	0.636	0.603
Head (% of Total)	98.66	98.97	97.68	94.30	94.34	94.20
TB (% of Total)	0.50	3.82E-01	0.82	1.95	1.89	1.99
Pulmonary (% of Total)	0.82	6.51E-01	1.47	3.75	3.77	3.98

3.4 Aerosol concentration data for Table 10

Table below details the aerosol exposure concentration data (µg/L) collected on sampling filters and analysed using HPLC method for blends containing magnesium stearate (MgSt). Data detailed below is listed in Table 10 (Section 4.2, B– Results and Discussion).

Table 57: Aerosol exposure concentration data for Table 10

Experimental Reference	Description	Mass on Filter (µg)	Flow Rate (L/min)	Time (min)	Aerosol Concentration (µg/L)
EE597868	0.8% FMS-MgSt Rep 1	635.2	3.0	45	4.7
EE599230	0.8% FMS-MgSt Rep 2	636.3	3.0	45	4.7
EE600542	0.8% FMS-MgSt Rep 3	718.9	3.0	45	5.3
EE602420	0.8% FMS-MgSt Rep 4	204.4	3.0	20	3.4
EE606604	3% FMS-MgSt Rep 1	606.4	2.0	15	20.2
EE608142	3% FMS-MgSt Rep 2	472.0	2.0	15	15.7
EE609652	3% FMS-MgSt Rep 3	557.0	2.0	15	18.6

3.5 IVR deposition data for Table 10 and Figure 45

Table below details the mass FMS particles (µg) collected in the sections of the IVR model for blends containing magnesium stearate (MgSt). Data detailed below is listed in Table 10 and Figure 45 (Section 4.2, B– Results and Discussion).

Table 58: Deposition data for IVR model for Table 10 and Figure 45

Experimental Reference	EE597868	EE599230	EE600542	EE602420	EE606604	EE608142	EE609652
Description	**0.8% FMS-MgSt Rep 1**	**0.8% FMS-MgSt Rep 2**	**0.8% FMS-MgSt Rep 3**	**0.8% FMS-MgSt Rep 4**	**3.0% FMS-MgSt Rep 1**	**3.0% FMS-MgSt Rep 2**	**3.0% FMS-MgSt Rep 3**
Section	**Mass of FMS deposited (µg)**						
S1	39	52.5	37.6	25.6	62.7	43.8	51.4
S2	12.8	12.0	15.4	6.1	14.6	13.4	14.8
S3	4.2	6.2	9.8	3.8	8.8	7.2	1.4
S4	2.0	1.0	1.6	0.5	0.8	0.9	1.3
S5	3.0	2.8	3.9	3.0	2.6	2.1	6.2
S6	1.0	0.9	0.9	0.5	1.5	1.1	2
Total	62	75.4	69.2	39.4	91	68.5	77.1
Head (S1 + S2)	51.8	64.5	53.0	31.7	77.3	57.2	66.2
TB (S3 + S4 + S5)	9.2	10.0	15.3	7.3	12.2	10.2	8.9
Post-TB (S6)	1.0	0.9	0.9	0.5	1.5	1.1	2
Head (% of Total)	83.6	85.5	76.5	80.4	84.9	83.5	85.9
TB (% of Total)	14.8	13.3	22.2	18.4	13.4	14.9	11.5
Post-TB (% of Total)	1.6	1.2	1.3	1.2	1.6	1.6	2.6

3.6 Marple particle size data for Table 10 and Figure 44

Table below details the mass and percentage amount of FMS particles collected in the Marple cascade Impactor for blends containing magnesium stearate (MgSt). The mass median aerodynamic diameter (MMAD) and geometric standard deviation (GSD) were determined from the probit-transformed cumulative particle mass frequency distribution and the logarithmic effective cut-off diameters (ECDs) by linear regression. Data detailed below was used to construct Table 10 and Figure 44 (Section 4.2, B– Results and Discussion).

Table 59: MCI data for Table 10 and Figure 44

Experimental Reference	**EE597868**		**EE599230**		**EE600542**		**EE602420**	
Description	**0.8% FMS- MgSt Rep 1**		**0.8% FMS- MgSt Rep 2**		**0.8% FMS- MgSt Rep 3**		**0.8% FMS- MgSt Rep 4**	
Marple Cascade Stages	**µg/stage**	**%**	**µg/stage**	**%**	**µg/stage**	**%**	**µg/stage**	**%**
Stage 3	0.8	11.27	0.3	9.09	1.17	25.49	1.11	21.43
Stage 4	0.0	0.00	0.0	0.00	0.0	0.00	0.19	3.67
Stage 5	1.1	15.49	0.5	15.15	0.44	9.59	0.6	11.58
Stage 6	3.2	45.07	1.5	45.45	1.79	39.00	2.38	45.95
Stage 7	1	14.08	0.6	18.18	0.41	8.93	0.9	17.37
Stage 8	0.6	8.45	0.4	12.12	0.42	9.15	0.0	0.00
Filter	0.4	5.63	0.0	0.00	0.36	7.84	0.0	0.00
MMAD (µm)	**2.40**		**2.48**		**3.06**		**3.81**	
GSD	**2.57**		**2.20**		**3.60**		**2.31**	

Table 59 Continued

Experimental Reference	**EE606604**		**EE608142**		**EE609652**	
Description	**3.0% FMS- MgSt Rep 1**		**3.0% FMS- MgSt Rep 2**		**3.0% FMS- MgSt Rep 3**	
Marple Cascade Stages	**µg/stage**	**%**	**µg/stage**	**%**	**µg/stage**	**%**
Stage 3	2.7	10.67	1.3	6.91	1.7	9.39
Stage 4	1.9	7.51	1.4	7.45	1.2	6.63
Stage 5	3.6	14.23	1.6	8.51	2.6	14.36
Stage 6	10.7	42.29	9.7	51.60	8.5	46.96
Stage 7	3.3	13.04	2.2	11.70	2.1	11.60
Stage 8	2	7.91	1.6	8.51	0.9	4.97
Filter	1.1	4.35	1.0	5.32	1.1	6.08
MMAD (µm)	**2.69**		**2.34**		**2.59**	
GSD	**2.58**		**2.44**		**2.55**	

Table below details the mass and percentage amount of FMS particles collected in the Marple cascade Impactor for binary blends of fluorescent microspheres and lactose. The mass median aerodynamic diameter (MMAD) and geometric standard deviation (GSD) were determined from the probit-transformed cumulative particle mass frequency distribution and the logarithmic effective cut-off diameters (ECDs) by linear regression. Data detailed below was used to construct Table 10 and Figure 44 (Section 4.2, B– Results and Discussion).

Table 60: MCI data for Table 10 and Figure 44

Experimental Reference	**EE551492**		**EE553046**		**EE554126**		**EE587866**	
Description	**2µm blend Replicate 1**		**2µm blend Replicate 2**		**2µm blend Replicate 3**		**2µm blend Replicate 4**	
Marple Cascade Stages	**µg/stage**	**%**	**µg/stage**	**%**	**µg/stage**	**%**	**µg/stage**	**%**
Stage 3	3.82	3.24	3.5	2.76	9.9	11.91	5.5	12.61
Stage 4	2.66	2.26	3.5	2.76	2.5	3.01	3.3	7.50
Stage 5	5.72	4.85	5.7	4.50	3.6	4.33	7.7	17.70
Stage 6	97.34	82.58	108.5	85.64	61	73.41	23.1	52.90
Stage 7	7.02	5.96	4.4	3.47	3.8	4.57	2.4	5.43
Stage 8	1.31	1.11	1.1	0.87	0	0.00	1.2	2.68
Filter	0	0.00	0	0.00	2.3	2.77	0.5	1.17
MMAD (µm)	**2.58**		**2.63**		**3.09**		**3.44**	
GSD	**1.83**		**1.81**		**2.18**		**2.26**	

4 Assessing the effect of ventilation parameters on deposition in the rat model

4.1 IVR deposition data for Table 11

Table below details the mass FMS particles (µg) collected in the sections of the in vitro rat lung model for Run 1-13. Data detailed below is listed in Table 11 (Section 5.2, B– Results and Discussion).

Table 61: IVR data for Table 11

Experimental Reference	EE551492	EE553046	EE554126	EE578568	EE579774	EE580808	EE582304	EE582304
Run No	**1**	**2**	**3**	**4**	**5**	**6**	**7**	**8**
Section	**Mass of FMS deposited (µg)**							
S1	7.7	8.5	6.9	21.6	7.8	102.5	3.7	14.7
S2	1.1	1.4	1.1	1.8	0.9	4.3	0.8	1.9
S3	0.3	0.3	0.1	0.4	0.4	0.6	0.1	0.4
S4	0.1	0.1		0.2	0.3	0.7	0.1	0.3
S5	0.7	1.7	0.4	1.6	1.8	0.9	0.4	0.5
S6	0.3	0.8	0.1	1	1.2	0.3	0.5	0.3
Total	10.2	12.8	8.6	26.6	12.4	109.3	5.6	18.1
Head (S1 + S2)	8.8	9.9	8.0	23.4	8.7	106.8	4.5	16.6
TB (S3 + S4 + S5)	1.1	2.1	0.5	2.2	2.5	2.2	0.6	1.2
Post-TB (S6)	0.3	0.8	0.1	1.0	1.2	0.3	0.5	0.3
Head (% of Total)	86.3	77.3	93.0	88.0	70.2	97.7	80.4	91.7
TB (% of Total)	10.8	16.4	5.8	8.3	20.2	2.0	10.7	6.6
Post-TB (% of Total)	2.9	6.3	1.2	3.8	9.7	0.3	8.9	1.7

Table 61 Continued

Experimental Reference	EE545394	EE584992	EE586574	EE587866	EE588636
Run No	**9**	**10**	**11**	**12**	**13**
Section	**Mass of FMS deposited (µg)**				
S1	5.6	6.9	66.3	13.3	8.3
S2	1.3	2.7	6.1	3.7	3.7
S3	0.2	0.4	0.4	0.4	0.4
S4	0.5	0.1	0.2	0.2	0.1
S5	0.6	1.9	0.6	0.4	0.3
S6	1.1	0.5	0.3	0.2	0.4
Total	9.2	12.5	73.9	18.3	13.2
Head (S1 + S2)	6.9	9.6	72.4	17.0	12.0
TB (S3 + S4 + S5)	1.2	2.4	1.2	1.0	0.8
Post-TB (S6)	1.1	0.5	0.3	0.2	0.4
Head (% of Total)	75.1	76.8	98.0	93.1	90.9
TB (% of Total)	13.3	19.2	1.6	5.6	6.1
Post-TB (% of Total)	11.6	4.0	0.4	1.3	3.0

4.2 MPPD deposition data for Table 12

Table below details the predicted fractions of FMS particles to be deposited in the rat lung model according to the MPPD model for Run 1-13. Data detailed below is listed in Table 12 (Section 5.5, B– Results and Discussion).

Table 62: MPPD data for Table 12

Experimental Reference	EE551492	EE553046	EE554126	EE578568	EE579774	EE580808	EE582304	EE582304
Run No	**1**	**2**	**3**	**4**	**5**	**6**	**7**	**8**
Region	**Deposition fraction**							
Head	0.629	0.60	0.568	0.596	0.476	0.706	0.316	0.586
TB	0.013	0.012	0.012	9.35E-03	0.015	3.88E-03	0.025	8.03E-03
Pulmonary	0.025	0.024	0.024	0.012	0.064	5.46E-03	0.061	8.24E-03
Total	0.667	0.636	0.603	0.617	0.555	0.72	4.02E-01	0.603
Head (% of Total)	94.30	94.34	94.20	96.60	85.77	98.74	78.61	97.18
TB (% of Total)	1.95	1.89	1.99	1.51	2.70	0.54	6.22	1.33
Pulmonary (% of Total)	3.75	3.77	3.98	1.94	11.53	0.76	15.17	1.37

Table 62 Continued

Experimental Reference	EE545394	EE584992	EE586574	EE587866	EE588636
Run No	**9**	**10**	**11**	**12**	**13**
Region	**Deposition fraction**				
Head	0.526	0.379	0.658	0.596	0.576
TB	0.012	0.015	3.02E-03	0.01	0.011
Pulmonary	0.043	0.045	4.70E-03	0.021	0.022
Total	0.581	0.44	0.67	0.63	0.61
Head (% of Total)	90.53	86.3	98.9	95.1	94.6
TB (% of Total)	2.07	3.4	0.5	1.6	1.8
Pulmonary (% of Total)	7.40	10.3	0.7	3.3	3.6

4.3 Statistical analysis for assessing the effect of ventilation parameters on deposition in the rat model

4.3.1 Head region deposition (% of Total)

Table 63: ANOVA Table assessing the effect of ventilation parameters on Head deposition (% of Total) in the IVR model

Response	Factor	Degree of Freedom (DF)	F Value	P-Value	Significant?
Head Deposition (% of Total)	Model	3	8.46	0.0055	Yes
	A-Tidal Volume	1	0.01	0.9134	No
	B-Breaths Per Minute	1	18.5	0.0020	Yes
	AB	1	3.59	0.0905	No
	Lack of Fit	8	4.56	0.3479	No

Table 63 shows breathing frequency (Factor B) had a statistically significant effect on head deposition levels. The Model F-value of 8.46 implies the model is significant. There is only a 0.55% chance that a "Model F-Value" this large could occur due to noise. The "Lack of Fit F-value" of 4.56 implies the Lack of Fit is not significant relative to the pure error. There is a 34.79% chance that a "Lack of Fit F-value" this large could occur due to noise. Therefore, the model selected is appropriate for performing the chosen analysis.

4.3.2 TB region deposition (% of Total)

Table 64: ANOVA Table assessing the effect of ventilation parameters on TB deposition (% of Total) in the IVR model

Response	Factor	Degree of Freedom (DF)	F Value	P-Value	Significant?
TB Deposition (% of Total)	Model	3	5.00	0.0260	Yes
	A-Tidal Volume	1	0.35	0.5645	No
	B-Breaths Per Minute	1	11.39	0.0082	Yes
	AB	1	1.69	0.2248	No
	Lack of Fit	8	15.23	0.1957	No

Table 64 shows breathing frequency (Factor B) had a statistically significant effect on TB deposition. The Model F-value of 5.00 implies the model is significant. There is only a 0.26% chance that a "Model F-Value" this large could occur due to noise. The "Lack of Fit F-value" of 15.23 implies the Lack of Fit is not significant relative to the pure error. There is a 19.57% chance that a "Lack of Fit F-value" this large could occur due to noise. Therefore, the model selected is appropriate for performing the chosen analysis.

4.3.3 Post-TB region deposition (% of Total)

Table 65: ANOVA Table assessing the effect of ventilation parameters on Post-TB deposition (% of Total) in the IVR model

Response	Factor	Degree of Freedom (DF)	F Value	P-Value	Significant?
Post TB Deposition (% of Total)	Model	3	7.62	0.0077	Yes
	A-Tidal Volume	1	0.72	0.4170	No
	B-Breaths Per Minute	1	14.58	0.0041	Yes
	AB	1	7.62	0.0077	No
	Lack of Fit	8	2.57	0.4492	No

Table 65 shows breathing frequency (Factor B) had a statistically significant effect on post-TB deposition. The Model F-value of 7.62 implies the model is significant. There is only a 0.77% chance that a "Model F-Value" this large could occur due to noise.

The "Lack of Fit F-value" of 2.57 implies the Lack of Fit is not significant relative to the pure error. There is a 44.92% chance that a "Lack of Fit F-value" this large could occur due to noise. Therefore, the model selected is appropriate for performing the chosen analysis.

4.3.4 Head region deposition (mcg)

Table 66: ANOVA Table assessing the effect of ventilation parameters on Post-TB deposition (mcg) in the IVR model

Response	Factor	Degree of Freedom (DF)	F Value	P-Value	Significant ?
Post TB Deposition (mcg)	Model	3	45.00	< 0.0001	Yes
	A-Tidal Volume	1	45.27	< 0.0001	Yes
	B-Breaths Per Minute	1	49.45	< 0.0001	Yes
	AB	1	45.00	< 0.0001	Yes
	Lack of Fit	8	3.67	0.3840	No

Table 66 shows tidal volume (A), breathing frequency (Factor B) and a combination of tidal volume and breathing frequency parameters had a statistically significant effect on post-TB deposition. The Model F-value of 45.00 implies the model is significant. There is only a 0.01% chance that a "Model F-Value" this large could occur due to noise.

The "Lack of Fit F-value" of 3.67 implies the Lack of Fit is not significant relative to the pure error. There is a 38.40% chance that a "Lack of Fit F-value" this large could occur due to noise. Therefore, the model selected is appropriate for performing the chosen analysis

5 Comparative deposition of inhaled aerosols in experimental rats and IVR rat lung model

5.1 **Table 67:** *in vivo* lung homogenate data of total deposition for compound Y, compound X and fluticasone propionate, data list was used to construct Figure 53 and Figure 54.

Test compound	Estimated achieved dose on day (µg/kg)	Lung Concentration (µg/g)	Tracheal Concentration (µg/g)	Total Concentration (µg/g)	Weight			Lung dose (µg)	Tracheal dose (µg)	Total dose (µg)	Total inhaled dose (µg)	Lung dose (%)
					Rat (kg)	Lung (g)	Tracheal (g)					
Compound Y, micronised form	1000	99.0	27.36	126.4	0.542	1.4800	0.13	146.52	3.56	150.1	542	27.7
		70.8	9.18	80.0	0.472	1.4000	0.14	99.12	1.24	100.4	472	21.3
		37.8	5.886	43.7	0.511	1.2420	0.16	46.95	0.92	47.9	511	12.4
Compound X, micronised form	600	13.9	6.12	20.0	0.394	1.068	0.10	14.85	0.61	15.5	236.40	6.5
		30.0	4.51	34.5	0.394	1.454	0.10	43.68	0.45	44.1	236.40	18.7
		11.3	1.63	13.0	0.394	1.122	0.10	12.73	0.16	12.9	236.40	5.5
Compound X, spray-dried Type 1	600	24.09	11.3	35.4	0.372	1.052	0.10	25.35	1.13	26.5	222.9	11.9
		10.49	9.58	20.1	0.372	1.086	0.10	11.39	0.96	12.3	222.9	5.5
		14.91	6.46	21.4	0.372	1.129	0.10	16.84	0.65	17.5	222.9	7.8
Compound X, spray-dried Type 2	600	19.8	3.18	23.0	0.409	1.197	0.10	23.70	0.32	24.0	245.34	9.8
		23.1	4.94	28.0	0.409	1.308	0.10	30.20	0.49	30.7	245.34	12.5
		24.7	5.34	30.0	0.409	1.234	0.10	30.44	0.53	31.0	245.34	12.6

Table 67 continued

Test compound	Estimated achieved dose on day (µg/kg)	Lung Concentration (µg/g)	Tracheal Concentration (µg/g)	Total Concentration (µg/g)	Weight			Lung dose (µg)	Tracheal dose (µg)	Total dose (µg)	Total inhaled dose (µg)	Lung dose (%)
					Rat (kg)	Lung (g)	Tracheal (g)					
FP (MMAD > 4.0 µm)	100	2.4	NT	2.4	0.282	0.687	NT	1.68	NT	1.7	28.2	5.9
		1.8	NT	1.8	0.282	0.797	NT	1.44	NT	1.4	28.2	5.1
FP (MMAD > 4.0 µm)	1000	20.1	NT	20.1	0.302	0.766	NT	15.38	NT	15.4	302.00	5.1
		12.9	NT	12.9	0.302	0.850	NT	10.99	NT	11.0	302.00	3.6
FP (MMAD < 2.0 µm)	100	4.537	NT	4.537	0.2915	1.391	NT	6.31	NT	6.31	29.15	21.6
		1.208	NT	1.208	0.2915	1.101	NT	1.33	NT	1.33	29.15	4.6
		1.107	NT	1.107	0.2915	1.527	NT	1.69	NT	1.69	29.15	5.8
	1000	24.332	NT	24.332	0.2915	1.118	NT	27.20	NT	27.20	291.50	9.3
		6.894	NT	6.894	0.2915	1.255	NT	8.65	NT	8.65	291.50	3.0
		8.922	NT	8.922	0.2915	1.311	NT	11.70	NT	11.70	291.50	4.0
	100	1.770	NT	1.770	0.2799	1.232	NT	2.18	NT	2.18	27.99	7.8
		2.695	NT	2.695	0.2799	1.280	NT	3.45	NT	3.45	27.99	12.3
		1.336	NT	1.336	0.2799	1.407	NT	1.88	NT	1.88	27.99	6.7
	1000	9.573	NT	9.573	0.2799	1.180	NT	11.30	NT	11.30	279.90	4.0
		9.847	NT	9.847	0.2799	1.148	NT	11.30	NT	11.30	279.90	4.0
		10.314	NT	10.314	0.2799	2.065	NT	21.30	NT	21.30	279.90	7.6

NT: Not Taken

5.2 IVR data for compound Y test material

Table below details the mass of GSK258899 test material collected in the sections of the IVR model. Data detailed below is listed in Table 13, Figure 53, Figure 54, Figure 55, Figure 56, Figure 57 and Figure 58 (Section 6, B– Results and Discussion).

Table 68: IVR data for Compound Y

RUN No	**1**	**2**	**3**	**4**	**5**	**6**
Target Dose (µg/kg/day)	**1000**	**1000**	**1000**	**1000**	**1000**	**1000**
Date of Dosing	**18.11.10**	**18.11.10**	**17.12.10**	**17.12.10**	**20.12.10**	**20.12.10**
Section	**Mass of Compound Y deposited (µg)**					
S1	78.4	85.2	71.4	46.2	27.6	50.0
S2	21.4	21.4	16.6	13.6	6.2	10.9
S3	4.7	8.5	1.7	<LOQ	<LOQ	3.0
S4	7.5	1.6	1.7	<LOQ	<LOQ	4.7
S5	10.1	6.9	10.4	4.2	6.0	4.7
S6	3.4	<LOQ	4.4	<LOQ	<LOQ	1.4
Total	125.5	123.7	106.1	64.1	39.8	74.8
Head (S1 + S2)	99.8	106.6	88	59.8	33.8	60.9
TB (S3 + S4 + S5)	22.3	17	13.8	4.2	6	12.4
Post-TB (S6)	3.4	0	4.4	0	0	1.4
Head (% of Total)	79.5	86.2	82.9	93.3	84.9	81.4
TB (% of Total)	17.8	13.7	13.0	6.6	15.1	16.6
Post-TB (% of Total)	2.7	0.0	4.1	0.0	0.0	1.9

5.3 IVR data for Compound X test material

Table below details the mass of GSK258899 test material collected in the sections of the IVR model. Data detailed below is listed in Table 13, Figure 53, Figure 54, Figure 55, Figure 56, Figure 57 and Figure 58 (Section 6, B– Results and Discussion).

Table 69: IVR data for Compound X test material

Material Description	**Micronised**		**Spray-dried. Type 1**		**Spray-dried. Type 2**	
Run Number	**RUN 1**	**RUN 2**	**RUN 3**	**RUN 4**	**RUN 5**	**RUN 6**
Target Dose (µg/kg/day)	**600**	**600**	**600**	**600**	**600**	**600**
Date of Dosing	**20.02.12**	**21.02.12**	**22.02.12**	**23.02.12**	**24.02.12**	**27.02.12**
Section	**Mass of Compound X deposited (µg)**					
S1	122.3	195.0	105.0	144.0	77.5	80.9
S2	37.3	28.6	57.0	83.7	33.7	42.2
S3	<LOQ	2.0	2.0	3.9	4.1	5.9
S4	<LOQ		6.5	2.1	3.0	2.4
S5	<LOQ	1.9	6.3	8.6	7.6	6.1
S6	<LOQ	1.9	10.0	8.5	6.1	3.6
Total	159.5	229.3	186.7	250.8	131.9	141.1
Head (S1 + S2)	159.6	223.6	162.0	227.7	111.2	123.1
TB (S3 + S4 + S5)	0.0	3.9	14.8	14.6	14.7	14.4
Post-TB (S6)	0.0	1.9	10.0	8.5	6.1	3.6
Head (% of Total)	100.0	97.5	86.8	90.8	84.3	87.2
TB (% of Total)	0.0	1.7	7.9	5.8	11.1	10.2
Post-TB (% of Total)	0.0	0.8	5.4	3.4	4.6	2.6

5.4 IVR data for fluticasone propionate

Table below details the mass of GSK258899 test material collected in the sections of the IVR model. Data detailed below is listed in Table 13, Figure 53, Figure 54, Figure 55, Figure 56, Figure 57 and Figure 58 (Section 6, B– Results and Discussion).

Table 70: IVR for fluticasone propionate

Run Number	**RUN 1**	**RUN 2**	**RUN 3**	**RUN 4**	**RUN 5**	**RUN 6**	**RUN 7**	**RUN 8**
Target Dose (mcg/kg/day)	**1000**	**100**	**1000**	**100**	**1000**	**100**	**1000**	**100**
MMAD (µm)	**5.10**	**4.90**	**3.90**	**1.78**	**1.92**	**1.88**	**1.84**	**1.82**
Date of Dosing	**08.12.11**	**15.12.11**	**15.12.11**	**20.06.13**	**20.06.13**	**27.06.13**	**27.06.13**	**12.07.13**
Section								
S1	132.9	13.9	145.9	32.7	89.1	17.3	49.3	25.9
S2	61.3	5.7	65.3	4.4	12.4	4.7	16.2	4.1
S3	9.4	0.5	7.9	0.5	2.3	0.3	0.7	0.3
S4	1.8	0.2	0.8	0.3	2.2	1.0	0.2	<LOQ
S5	4.7	1.0	3.9	0.5	2.3	0.5	0.2	<LOQ
S6	0.3	<LOQ	0.2	0.4	1.7	0.3	0.2	<LOQ
Total	210.3	21.3	223.9	38.8	110.0	24.1	66.8	30.3
Head (S1 + S2)	194.2	19.6	211.2	37.0	101.5	22.0	65.5	30.0
TB (S3 + S4 + S5)	15.9	1.7	12.6	1.3	6.8	1.8	1.1	0.3
Post-TB (S6)	0.3	0.0	0.2	0.4	1.7	0.3	0.2	0.0
Head (% of Total)	92.3	92.0	94.3	95.4	92.3	91.3	98.1	99.0
TB (% of Total)	2.2	4.7	1.7	3.5	6.2	7.5	1.6	1.0
Post-TB (% of Total)	0.1	0.0	0.1	1.1	1.5	1.2	0.3	0.0

5.5 Pooled lung deposition data for Figure 58

Table 71: Lung deposition data (% of total) used to construct Figure 58

Compound	Particle size (MMAD; µm)	Lung deposition (% of Total)		
		In Vivo	IVR	MPPD
Compound Y, micronised	2.2	27.7	20.5	8.5
	2.2	21.3	13.7	
	2.2	9.4	17.1	
	2.2		6.6	
	2.2		15.0	
	2.2		18.6	
Fluticasone propionate (MMAD < 2.0 µm)	1.9	21.6	4.6	6.2
	1.9	4.6	7.7	5.5
	1.9	5.8	8.7	5.8
	1.9	9.3	1.9	6.0
	1.9	3.0	1.0	6.0
	1.9	4.0		
	1.9	7.8		
	1.9	12.3		
	1.9	6.7		
	1.9	4.0		
Fluticasone propionate (MMAD > 4.0 µm)	4.6	5.9	8.4	2.8
	4.6	5.1	8.0	3.6
	4.6	5.1	5.9	10.5
	4.6	3.6		
compound X, micronised	5.28	6.5	0.0	2.7
	5.28	18.7	2.5	
	5.28	5.5		
compound X, Sprayed-Dried Type 1	2.46	11.9	13.2	9.5
	2.46	5.5	9.2	
	2.46	7.8		
compound X, Sprayed-Dried Type 2	1.77	9.8	15.7	10.6
	1.77	12.5	12.7	
	1.77	12.6		
FP (in vitro experiments)	2.41	NT	14.5	8.87
	2.76	NT	5.3	8.94
	2.34	NT	6.7	8.37
	2.72	NT	9.4	8.94

Table 71 continued

Compound	Particle size (MMAD; µm)	Lung deposition (% of Total)		
		In Vivo	IVR	MPPD
0.8 % FMS-MgSt Rep 1	2.40	NT	16.4	8.7
0.8 % FMS-MgSt Rep 2	2.48	NT	14.5	8.0
0.8 % FMS-MgSt Rep 3	3.06	NT	23.5	10.5
0.8 % FMS-MgSt Rep 4	3.81	NT	19.6	4.7
0.8 % FMS-Lactose Rep 1	2.58	NT	13.6	5.7
0.8 % FMS-Lactose Rep 2	2.63	NT	22.7	5.7
0.8 % FMS-Lactose Rep 3	3.09	NT	7	6.0
0.8 % FMS-Lactose Rep 4	3.44	NT	6.9	5.4
3.0 % FMS-MgSt Rep 1	2.69	NT	15	8.2
3.0 % FMS-MgSt Rep 2	2.34	NT	16.5	8.4
3.0 % FMS-MgSt Rep 3	2.59	NT	14.1	8.3
	MEAN	9.3	11.3	7.1
	STDEV	6.2	6.2	2.3
	RSD	67.1	54.6	31.9
	number	28	35	26
	Min	3.0	0.0	2.7
	Max	27.7	20.5	10.6

NT: Not Taken

6 Assessing the relationship between efficacy of inhaled Fluticasone in an allergen-induced rodent model with regional lung deposition

6.1 Summary table of data used in section 7, B- Results and Discussion

Table 72: Summary table of data used in section 7, B- Results and Discussion

Study Number	1	1	2	2	2
Target Dose (µg/kg)	100	1000	10	100	1000
Estimated Achieved Dose (µg/kg)	73.3	997	37.86	57.01	1183
Particle size (MMAD: µm)	4.9	4.5	NT	1.8	1.9
In vivo lung concentration (ng/lung)	1556.7	13184.5	409.3	3110	15850
In vivo lung concentration (ng/g of lung)	2120.9	16501.3	322	2284	13382.6
% of targeted dose in lung	5.5	4.4	14	10.7	5.4
IVR lung dose (% of total)	8	7.2	NT	4.8	4.8
IVR post-TB dose (% of total)	0	0.1	NT	0.8	0.9
MPPD Pulmonary fraction (% of total)	2.3	4.6	TBC	6	5.7
Neutrophils (MEAN ± SEM)	1.09 ± 0.32	0.80 ± 0.55	2.23 ± 0.24	0.83 ± 0.13	0.18 ± 0.06

E. Summary

1. Summary

The aim of this thesis was to develop an *in vitro* model (IVR) of the rat lung for the purpose of investigating the deposition of drug particles in the rat airways. The model attempted to account for the affect of drug product characteristics and physiological parameters on deposition in the lungs. In addition, the model outputs were compared with *in vivo* lung deposition results from live rats and *in silico* predictions using published computer model of lung deposition in pre-clinical species.

Initial work focussed on developing an aerosol exposure system capable of dosing small rodent to a range of airborne test materials. The system consists of two main parts; a fluidised bed aerosol generator and connection of the generator output to a nose only exposure chamber capable of accommodating 12 small animals in a single layer. In addition, an aerodynamic particle spectrometer (APS) was installed for continuously measuring the size distribution and airborne concentration of aerosol particles generated in the exposure chamber. System validation showed acceptable degree of variation of the test material tested, Fluorescent Microspheres (FMS) throughout the exposure chamber (CV < 15.0%). Particle size (MMAD ± GSD) using the APS was shown to be stable throughout the exposure periods.

The IVR model developed in this project was based on a number of euthanased (n=7), female Sprague-Dawley rats (weight: 372 ± 56 g), which underwent high-resolution micro-CT scans. The physical model consisted of five sub sections; Extra-Thoracic region containing the snout and nasophyarynx, trachea-bronchial region containing the trachea, bronchi, and bronchioles. All sections of the model were attached to one another in numerical order and housed within a containment unit. At the rear end of the cast, a flexible diaphragm was attached in order to collect the fraction of inhaled particles exiting the TB section and possibly reaching the lung, referred to as the Post-TB section.

A study was conducted to assess the influence of inhalation parameters such as the breathing frequency and tidal volume on total and regional dose distribution using FMS as test material. The major finding of this study was the demonstration of the model sensitivity to changes in breathing parameters especially respiratory frequency, where the data showed increased deposition in the peripheral regions of the model with decreased respiratory frequency. Other studies assessed the effect of particle characteristics on deposition on the IVR model, such as particle size, dose increase and formulation changes.

The results assessing particle size effect showed a slightly higher deposition levels for the 4µm sized particles versus 2µm sized particles in the head region; 90.8 ± 3.6% and 88.2 ± 6.6%. However, this difference did not reach statistical significance (P> 0.05) probably due to the polydispersity of aerosolised FMS particles. In addition, the regional deposition analysis showed an increased lung peripheral deposition with the smaller particles. In addition, the model was shown to be sensitive to changes in formulation composition mediated by inclusion of MgSt.

The next stage of work was to validate the model in terms of comparison with lung deposition for *in vivo* rats. For lung deposition comparison, the absolute amount deposited in the IVR lung model (expressed as µg/kg) was shown to have a reasonably strong correlation with *in vivo* lung concentration measures (µg/kg); R^2= 0.66, P < 0.05. Compounds were predicted well and within 2-folds of the measured lung deposition values. However, knowing the variability in biological systems and the multiple components required to estimate lung doses, predictions within 2-fold of the measured values would seem reasonable

In terms of comparison with *in silico* model predictions using MPPD, similar deposition levels were noted between the two models, particularly when the data was expressed as percentage of total particles inhaled. The data showed the highest deposition levels were noted in the head region (> 80%) and less than 5.0% deposition for the peripheral lung fractions.

With regards to using the IVR model to assess the relationship between dose, particle size and efficacy, an *in vivo* study using FP with different particle sizes (2.0 and 4.0 µm) but same doses (100 and 1000 µg/kg). This study demonstrated that exposure of rat to FP powder resulted in a dose-dependent inhibition of neutrophils in BAL fluids. However, a clear difference in neutrophils suppression was demonstrated for equivalent doses but different particle sizes of FP, where the smaller FP particles (2.0 µm) induced a greater level of neutrophils suppression in comparison with larger FP particles (4.0 µm). In addition, a reasonably good correlation for the relationship between lung deposition in the IVR model and a neutrophils suppression level was demonstrated. Furthermore this data support the hypothesis that regional deposition is an important determinant in efficacy. Therefore, this suggests that the IVR model may be a useful as a tool to describe *in vivo* efficacy with *in vitro* data. However, further studies should be conducted to evaluate the validity of this model and relationship.

The IVR model has a number of important limitations. First, the model is based on scans up to generation four of the rat respiratory tract as this represented the limits of the micro-CT scanning technology at the time of this study. Therefore deposition in the deeper region of the lung may not be reflected precisely in the IVR model. Second, the regional deposition data

generated using the model tended to show an overestimation of deposition in head region and an underestimation of deposition in the peripheral regions of the lung, in comparison with *in vivo* lung deposition data. Third, the current model does not take into account lung clearance. However, the amount of the drug present in the *in vivo* lungs is dependent on numerous physiological processes such as dissolution, passive or active absorption into the systemic circulation, binding to lung tissue and mucociliary clearance. Consequently, the results generated using this IVR model for drug molecules with high lung clearance rate should be treated with some caution.

Future work extending this research could go in a number of directions. In this research, a representative model of the rat respiratory tract was constructed from analysis of imaging data from a number of euthanised Sprague-Dawley rats. This model represented the “average respiratory tract” in terms of dimensions of Sprague-Dawley rats. However, there is considerable variability in the airway dimensions between rats. This variability encompasses a number of factors such as the strains of rats, sex and age, and disease state. Thus, it may be possible to produce a small number of airway models to represent small and large rats and scaled to represent the extrathoracic and peripheral regions based on literature reports of their dimensions in different rat populations. This approach will then enable the effect of intersubject airway dimensions for different rat populations on aerosol deposition to be thoroughly examined.

In addition, due to the limitation of the micro-CT technology used to construct the physical IVR model, detailed morphology only up to generation 4 were captured. However, recent advances in MRI technology, such as the use of *in situ*-MRI based scanning technology have enabled rat airway morphometry to be extended to 16 airway generation. This coupled with improvements in the resolutions of rapid-prototyping process means it may be possible to construct a rat model that reflects the *in vivo* lung morphology more accurately, and thus enable greater understanding of the link between aerosol deposition and airway geometry.

In conclusion, a model cast of the rat lung was developed and validated to allow the deposition of inhaled particles in the rat lung to be investigated. The model may be used to estimate the lung concentration *in vivo* rats in preference to exposure concentration measurements based on filter samples which have been shown to be a poor indicator of the lung concentration immediately after exposure. In addition, the model has the potential to be used along with live rats in an inhalation rig in pulmonary pharmaceutics research and may facilitate in development of inhaled formulations to target specific regions within the lung as well as screening of inhaled drugs in preclinical setting.

2. Zusammenfassung

Das Ziel dieser Arbeit war es, ein *in vitro* Modell (IVR) der Rattenlunge für die Untersuchung der Deposition von Wirkstoffpartikeln in den Atemwegen der Ratte zu entwickeln. Das Modell sollte dabei den Einfluss der Arzneistoffeigenschaften und physiologischer Parameter auf die pulmonale Deposition berücksichtigen. Darüber hinaus wurden die Modellergebnisse mit *in vivo* Daten aus Versuchen mit Ratten und *in silico* Vorhersagen eines etablierten Computermodells der Partikeldeposition in präklinischen Spezies verglichen.

Erste Arbeiten konzentrierten sich auf die Entwicklung eines Aerosol-Expositionssystems, das in der Lage war, kleine Nagetiere einer Reihe von inhalativ verabreichten Testmaterialien auszusetzen. Das System bestand aus zwei Hauptteilen, einem Wirbelbett-Aerosolgenerator und einer Verabreichungskammer, die eine nasale Partikelexposition und –inhalation („*Nose only* Inhalation“) bei 12 Kleintieren auf einer Etage ermöglichte. Darüber hinaus wurde ein aerodynamisches Partikelspektrometer (APS) zur kontinuierlichen Messung der Größenverteilung und Konzentration der erzeugten Aerosolpartikel eingebaut. Die Systemvalidierung zeigte einen akzeptablen Grad der Variabilität des Testmaterials, Fluoreszenz-Mikrosphären (FMS), in der gesamten Expositionskammer (VK < 15,0%). Es konnte gezeigt werden, dass die aerodynamische Partikelgröße (MMAD ± GSD) der APS über die Expositionszeiten konstant blieb.

Das IVR-Modell, das in diesem Projekt entwickelt wurde, basierte auf einer Anzahl euthanasierter, weiblicher Sprague-Dawley-Ratten (Gewicht: 372 ± 56 g), die hochauflösenden Mikro-CT-Scans unterzogen wurden. Das physikalische Modell gliederte sich in fünf Teilabschnitte, dem extrathorakalen Bereich bestehend aus der Schnauze und dem Nasopharynx, und dem tracheo-bronchialen Bereich (TB), der die Luftröhre, Bronchien und Bronchiolen umfasste. Alle Abschnitte des Modells wurden miteinander in numerische Reihenfolge gebracht und innerhalb einer Behältereinheit untergebracht. Am hinteren Ende des Gusses wurde eine flexible Membran angebracht, um den Anteil der inhalierten Partikel, der den TB-Abschnitt verlässt und möglicherweise die Lunge erreicht, zu sammeln. Dieses wurde als Post-TB-Anteil bezeichnet.

Eine Untersuchung sollte zeigen, welchen Einfluss Inhalationsparameter wie die Atemfrequenz und –volumen auf die gesamte und regionale Dosisverteilung der FMS als Testmaterial hatten. Das wichtigste Ergebnis dieser Studie war der Nachweis, dass das Modell empfindlich gegenüber Änderungen in der Respirationsparameter, vor allem der Atemfrequenz, war.

Die Daten zeigten, dass es unter verminderter Atemfrequenz zu einer verstärkten Partikeldeposition in den peripheren Modellbereichen kam. In weiteren Versuchsansätzen wurden die Wirkung von Partikeleigenschaften, wie Partikelgröße, Dosiserhöhung und Formulierungsänderungen auf die Deposition in dem IVR-Modell ermittelt.

Die Ergebnisse der Untersuchung des Partikelgrößeneffektes zeigten eine etwas höhere Deposition der 4 µm großen Partikel, verglichen mit den 2 µm Partikeln, im Kopfbereich, 90,8 ± 3,6% bzw. 88,2 ± 6,6%. Allerdings war dieser Unterschied statistisch nicht signifikant ($P > 0,05$), wahrscheinlich aufgrund der Polydispersität der FMS-Aerosolpartikel. Darüber hinaus zeigte die Analyse der regionalen Verteilung eine erhöhte periphere Lungendeposition bei kleineren Partikeln. Zudem war das Modell empfindlich gegenüber Veränderungen in der Formulierungszusammensetzung durch Zugabe von Magnesiumstearat.

In nächsten Schritt sollte das Modell in Bezug auf den Vergleich mit der Lungendeposition bei Ratten *in vivo* validiert werden. Es zeigte sich, dass die absolut im IVR-Lungenmodell deponierte Menge (ausgedrückt in µg/kg) eine annehmbar starke Korrelation mit *in vivo* Daten (µg/kg) aufwies; $R^2 = 0,66$, $p < 0,05$. Substanzen konnten gut innerhalb des 2-fachen Bereiches der gemessenen Lungendepositionsrate vorhergesagt werden. Angesichts der bekannt hohen Variabilität in biologischen Systemen und der Komplexität der Schätzung der Lungendeposition erscheinen Schwankungen der Vorhersagen innerhalb des 2-fachen Bereiches der tatsächlichen Werte akzeptabel.

Der Vergleich der *in silico* Vorhersagen mit den IVR-Resultaten zeigte ähnliche Depositionsraten in beiden Modellen, insbesondere dann, wenn die Daten als Prozentsatz der insgesamt inhalierten Partikel ausgedrückt wurden. Die höchste Deposition fand im Kopfbereich (> 80%) statt und weniger als 5,0 % der Partikel erreichte den peripheren Lungenbereich.

Das IVR-Modell wurde nachfolgend auch in einer *in vivo* Studie mit Fluticasonpropionat (FP) eingesetzt, um die Beziehung zwischen der Dosis, Partikelgröße und Wirksamkeit unterschiedlicher Teilchengrößen (2,0 und 4,0 µm) bei gleichen Dosen (100 und 1000 µg/kg) zu beurteilen. Diese Studie zeigte eine dosisabhängige Hemmung der Neutrophilen in der bronchoalveolären Lavage. Es wurde jedoch ein deutlicher Unterschied in der Neutrophilensuppression unter äquivalenten Dosen unterschiedlicher Partikelgrößen beobachtet. Kleinere Partikel (2,0 µm) von FP hemmten die Neutrophilen stärker als die größeren FP-Partikel (4,0 µm). Darüber hinaus konnte eine recht gute Korrelation zwischen der Lungendepositionsrate im IVR-Modell und der Neutrophilensuppression gezeigt werden.

Diese Daten unterstützen die Hypothese, dass die regionale Deposition eine wichtige Determinante der Wirksamkeit ist. Die Ergebnisse legen die mögliche Eignung des IVR-Modells als Hilfsmittel zur Beschreibung der *in vivo* Effektivität, ausgehend von *in vitro* Daten, nahe. Allerdings sollten weitere Studien durchgeführt werden, um die Valididtät dieses Modells und der gefundenen Beziehung zu bestätigen. Das IVR-Modell hat eine Reihe von wichtigen Einschränkungen. Erstens basiert das Modell auf Scans lediglich bis zu vierten Generation der Atemwege, was zum Zeitpunkt dieser Studie die Grenze der Mikro-CT-Scan-Technik darstellte. Daher wird in dem IVR-Modell eine Deposition in tieferen Bereichen der Lunge nicht präzise beschrieben. Zweitens zeigten die regionalen Depositionsdaten, die unter Verwendung des Modells ermittelt wurden, im Vergleich zu *in vivo* Ergebnissen eine Überschätzung der Deposition im Kopfbereich und eine Unterschätzung der Deposition in den peripheren Regionen der Lunge. Drittens berücksichtigt das Modell nicht die Clearance des Arzneistoffes.

Die Arzneistoffkonzentration in der Lunge hängt *in vivo* von zahlreichen physiologischen Prozessen ab, wie Auflösung, aktive und passive Absorption in den systemischen Kreislauf, die Bindung an das Lungengewebe und mukoziliäre Clearance. Daher sollten die Ergebnisse, die unter Verwendung dieses IVR-Modells gewonnen werden, für Wirkstoffmoleküle mit hoher Clearance-Rate mit einer gewissen Vorsicht behandelt werden.

Zukünftige weiterführende Arbeiten könnten in eine Reihe von Richtungen gehen. In der vorliegenden Untersuchung wurde ein repräsentatives Modell des Rattenrespirationstraktes aus der Analyse der Bilddaten mehrerer anästhesierter Sprague-Dawley-Ratten erstellt. Dieses Modell repräsentiert die "durchschnittlichen Atemwege " in Bezug auf Abmessungen der Sprague-Dawley-Ratten. Es gibt jedoch eine beträchtliche Variabilität basierend auf einer Reihe von Faktoren wie den Rattenstamm, Geschlecht, Alter und Krankheitszustand. Es wäre möglich, mehrere verschiedene Atemwegsmodelle zu erstellen, um kleine und große Ratten zu repräsentieren. Es könnten, basierend auf Literaturangaben, die extrathorakalen und peripheren Regionen in ihren Abmessungen skaliert werden, um verschiedenen Rattenpopulationen zu repräsentieren. Dieser Ansatz würde dann die detaillierte Untersuchung des Einflusses interindividueller Unterschiede der Atemwegsdimensionen verschiedener Rattenpopulationen auf die Aerosoldeposition ermöglichen.

Aufgrund der Beschränkung der Mikro-CT-Technologie, die eingesetzt wurde, um das IVR-Modell zu erstellen, konnte eine detaillierte Morphologie nur bis zur vierten Atemwegsgeneration abgebildet werden. Jüngste Fortschritte in der MRI-Technologie, wie die *in situ* MRI-Scan-Technologie, ermöglichen die Erfassung der Atemwegsmorphometrie bis zu 16 Atemwegsgenerationen. Dieser Ansatz, in Verbindung mit Verbesserungen in den räumlichen Auflösungen der „Rapid-Prototyping"-Verfahren, könnte die Konstruktion eines Rattenmodells ermöglichen, das die *in vivo* Lungenmorphologie genauer widerspiegelt, und so zu einem besseren Verständnis für den Zusammenhang zwischen Aerosoldeposition und Atemwegsgeometrie führen.

Zusammenfassend lässt sich sagen, dass in der vorliegenden Arbeit ein Modellguss der Rattenlunge entwickelt und validiert wurde, um die Untersuchung der Deposition von inhalierten Partikel in der Rattenlunge zu ermöglichen. Das Modell kann verwendet werden, um die *in vivo* Lungenkonzentrationen von Arzneistoffen in Ratten abzuschätzen. Es bietet Vorteile gegenüber der Expositionsabschätzung auf der Basis von Filterproben, die ein schlechter Indikator der Lungenkonzentrationen unmittelbar nach der Exposition sind. Darüber hinaus hat das Modell das Potenzial, zusammen mit lebenden Ratten in einer Inhalationskammer in der Forschung verwendet zu werden und könnte in der Entwicklung von inhalativen Formulierungen erleichtern, die in bestimmten Regionen innerhalb der Lunge deponiert werden sollen. Darüber hinaus ermöglicht das Modell ein Screening inhalativ verabreichter Arzneistoffe in der präklinischen Phase.

F. Abbreviations

ACGH	American Conference of Government Hygienist
AIT	Association of Inhalation Toxicologist
ANOVA	Analysis of Variance
APS	Aerodynamic Particle Sizer
APSD	Aerodynamic Particle Size Distribution
ANOVA	Analysis of Variance
AUC	Area Under Curve
BALF	Bronchial Alveolar Lavage Fluid
BW	Body Weight
CAD	Computer Aided Design
CBAG	Capsule Based Aerosol Generator
CFD	Computational Fluid Dynamic
COPD	Chronic Obstructive Pulmonary Disease
CT	Computer Topography
DF	Deposition Fraction
DOE	Design Of Experiment
ECD	Effective Cut off Diameter
FBAG	Fluidised Bed Aerosol Generator
FFD	Friesland Food Domo
FMS	Fluorescent Micro Spheres
GSK	GlaxoSmithKline
HPLC	High Performance Liquid Chromatography
IAD	Immediately After Dosing
ICH	International Conference of Harmonisation
ICRP	International Commission of Radiological Protection
IF	Inhaled Fraction
ISO	International Standard Organisation
IVR	In Vitro Rat
LOQ	Limit of Quantification
LPS	LipoPolySaccharide
MCI	Marple Cascade Impactor
MPPD	Multiple Particle Path Dosimetry

OECD	Organisation for European Cooperation and Development
OVAT	One Variable at A Time
PD	Pharmacodynamic
PET	Position Emission Tomography
PK	Pharmacokinetic
RH	Relative Humidity
RMV	Respiratory Minute Volume
RP	Rapid Prototyping
SPECT	Single Photon Emission Computed Tomography
STL	Stereo Lithography
TPM	Total Particulate Matter

G. References

Abdelrahim ME, Assi KH, and Chrystyn H (2011). Relative bioavailability of terbutaline to the lung following inhalation, using urinary excretion. Br 71:608-610.

Adams WP, Ahrens RC, Chen ML, Christopher D, Chowdhury BA, Conner DP, Dalby R, Fitzgerald K, Hendeles L, Hickey AJ, Hochhaus G, Laube BL, Lucas P, Lee SL, Lyapustina S, Li B, O'Connor D, Parikh N, Parkins DA, Peri P, Pitcairn GR, Riebe M, Roy P, Shah T, Singh GJP, Sharp SS, Suman JD, Weda M, Woodcock J, and Yu L (2010). Demonstrating bioequivalence of locally acting orally inhaled drug products (OIPs): Workshop summary report. J Aerosol Med Pulm Drug Deliv 23:1-29.

Ahmed A, Prime D, Burnell PKP, and Hogger P (2012). Development of an in vitro model to assess deposition of aerosol particles in a representative replica of the rat's respiratory tract. J Aerosol Med Pulm Drug Deliv 25:169-178.

Al-Amoud AI, Clark BJ, Assi KA, and Chrystyn H (2005). Determination of the bioavailability of gentamicin to the lungs following inhalation from two jet nebulizers. Br 59:542-545.

Alexander DJ, Collins CJ, Coombs DW, Gilkison IS, Hardy CJ, Healey G, Karantabias G, Johnson N, Karlsson A, Kilgour JD, and McDonald P (2008). Association of Inhalation Toxicologists (AIT) working party recommendation for standard delivered dose calculation and expression in non-clinical aerosol inhalation toxicology studies with pharmaceuticals. Inhal 20:1179-1189.

Ali M, Reddy RN, and Mazumder MK (2008). Electrostatic charge effect on respirable aerosol particle deposition in a cadaver based throat cast replica. Journal of Electrostatics 66:401-406.

Amani A, Amini MA, Ali HS, and York P (2011). Alternatives to conventional suspensions for pulmonary drug delivery by nebulisers: A review. Journal of Pharmaceutical Sciences 100:4563-4570.

Annapragada A and Mishchiy N (2007). In silico modeling of aerosol deposition in lungs. Drug Discov Today Dis Models 4:155-161.

Asgharain B, Kelly JT, and Tewksbury EW (2003). Respiratory deposition and inhalability of monodisperse aerosols in Long-Evans rats. Toxicol Sci 71:104-111.

Asgharian B and Anjilvel S (1998). A multiple-path model of fiber deposition in the rat lung. Toxicol Sci 44:80-86.

Batycky R, Nice J, Chen D, Sung J, Lipp M, Mintzes J, Dunbar C, Niven R, and Edwards D (1999). Production and characterization of large porous particles for pulmonary drug delivery. Materials Research Society Symposium - Proceedings 550:95-100.

Benson JM, Barr EB, Bechtold WE, Cheng YS, Dunnick JK, Eastin WE, Hobbs CH, Kennedy CH, and Maples KR (1994). Fate of inhaled nickel oxide and nickel subsulfide in F344/N rats. Inhal 6:167-183.

Berg EJ, Weisman JL, Oldham MJ, and Robinson RJ (2010). Flow field analysis in a compliant acinus replica model using particle image velocimetry (PIV). Journal of Biomechanics 43:1039-1047.

Bernstein DM, Mast R, Anderson R, Hesterberg TW, Musselman R, Kamstrup O, and Hadley J (1994). An experimental approach to the evaluation of the biopersistence of respirable synthetic fibers and minerals. Environ Health Perspect 102:15-18.

Bide RW, Armour SJ, Yee E, Authors FN, Armour SJ, and Yee E (2000). Allometric respiration/body mass data for animals to be used for estimates of inhalation toxicity to young adult humans. J Appl Toxicol 20:273-290.

Blyth DI, Pedrick MS, Savage TJ, Hessel EM, and Fattah D (1996). Lung Inflammation and Epithelial Changes in a Murine Model of Atopic Asthma. American journal of respiratory cell and molecular biology 14:425-438.

Borgstrom L and Nilsson M (1990). A method for determination of the absolute pulmonary bioavailability of inhaled drugs: Terbutaline. Pharm Res 7:1068-1070.

Brown JS, Wilson WE, Grant LD, Authors FN, Wilson WE, and Grant LD (2005). Dosimetric comparisons of particle deposition and retention in rats and humans. Inhal 17:355-385.

Byron PR, Hindle M, Lange CF, Longest PW, McRobbie D, Oldham MJ, Olsson B, Thiel CG, Wachtel H, and Finlay WH (2010). In vivo-in vitro correlations: Predicting pulmonary drug deposition from pharmaceutical aerosols. J Aerosol Med Pulm Drug Deliv 23.

Byron PR, Roberts NSR, and Clark AR (1986). An isolated perfused rat lung preparation for the study of aerosolized drug deposition and absorption. Journal of Pharmaceutical Sciences 75:168-171.

Cannon WC, Blanton EF, and McDonald KE (1983). The flow-past chamber: An improved nose-only exposure system for rodents. Am Ind Hyg Assoc J 44:923-928.

Carpenter RL, Yerkes K, Authors FN, and Yerkes K (1980). Relationship between fluid bed aerosol generator operation and the aerosol produced. Am Ind Hyg Assoc J 41:888-894.

Cassee FR, Muijser H, Duistermaat E, Freijer JJ, Geerse KB, Marijnissen JC, Arts JH, Authors FN, Muijser H, Duistermaat E, Freijer JJ, Geerse KB, Marijnissen Jan CM, and rts Josje HE (2002). Particle size-dependent total mass deposition in lungs determines inhalation toxicity of cadmium chloride aerosols in rats. Application of a multiple path dosimetry model. Arch Toxicol 76:277-286.

Chan HK and Gonda I (1989). Aerodynamic properties of elongated particles of cromoglycic acid. J Aerosol Sci 20:157-168.

Chen BT, Yeh HC, and Fan BJ (1995). Evaluation of the TSI small-scale powder disperser. J Aerosol Sci 26:1303-1313.

Cheng KH, Cheng YS, Yeh HC, and Swift DL (1995). Deposition of ultrafine aerosols in the head airways during natural breathing and during simulated breath holding using replicate human upper airway casts. Aerosol Sci Technol 23:465-474.

Cheng YS, Barr EB, Benson JM, Damon EG, Medinsky MA, Hobbs CH, Goehl TJ, Authors FN, Barr EB, Benson JM, Damon EG, Medinsky MA, Hobbs CH, and Goehl TJ (1988). Evaluation of a real-time aerosol monitor (RAM-S) for inhalation studies. Fundam Appl Toxicol 10:321-328.

Cheng YS, Hansen GK, Su YF, Yeh HC, and Morgan KT (1990). Deposition of ultrafine aerosols in rat nasal molds. Toxicology and Applied Pharmacology 106:222-233.

Cheng YS, Zhou Y, and Chen BT (1999). Particle deposition in a cast of human oral airways. Aerosol Sci Technol 31:286-300.

Cheng Y-SYS (1995). Inhalation exposure systems. Concepts in Inhalation Toxicology25-66.

Chiang PC, Hu Y, Blom JD, and Thompson DC (2010). Evaluating the suitability of using rat models for preclinical efficacy and side effects with inhaled corticosteroids nanosuspension formulations. Nanoscale Research Letters 5:1010-1019.

Chiang PC, Hu Y, Thurston A, Sommers CD, Guzova JA, Kahn LE, Lai Y, and Blom JD (2009). Pharmacokinetic and pharmacodynamic evaluation of the suitability of using fluticasone and an acute rat lung inflammation model to differentiate lung versus systemic efficacy. Journal of Pharmaceutical Sciences 98:4354-4364.

Christopher JD, Dey M, Lyapustina S, Mitchell JP, Tougas TP, Van Oort M, Strickland H, Wyka B, and Zaidi K (2010). Generalized simplified approaches for mass median aerodynamic determination. Pharmacopeial Forum 36.

Chrystyn H (2001). Methods to identify drug deposition in the lungs following inhalation. Br 51:289-299.

Coates MS, Chan HK, Fletcher DF, and Chiou H (2007). Influence of mouthpiece geometry on the aerosol delivery performance of a dry powder inhaler. Pharm Res 24:1450-1456.

Cohen BS and Briant JK (1989). Flow distribution in human and canine tracheobronchial airway casts. Health Physics 57:21-27.

Cohen BS, Sussman RG, and Lippmann M (1993). Factors affecting distribution of airflow in a human tracheobronchial cast. Respiration Physiology 93:261-278.

Cohen J, Douma WR, Ten Hacken NHT, Vonk JM, Oudkerk M, and Postma DS (2008). Ciclesonide improves measures of small airway involvement in asthma. European Respiratory Journal 31:1213-1220.

Conway J (2012). Lung imaging - Two dimensional gamma scintigraphy, SPECT, CT and PET. Advanced Drug Delivery Reviews 64:357-368.

Cooper AE, Ferguson D, and Grime K (2012). Optimisation of DMPK by the inhaled route: Challenges and approaches. Current Drug Metabolism 13:457-473.

Creton S, Dewhurst IC, Earl LK, Gehen SC, Guest RL, Hotchkiss JA, Indans I, Woolhiser MR, and Billington R (2010). Acute toxicity testing of chemicals - Opportunities to avoid redundant testing and use alternative approaches. Critical Reviews in Toxicology 40:50-83.

Crowder TM, Rosati JA, Schroeter JD, Hickey AJ, Martonen TB, and Author e-mail Address (2002). Fundamental effects of particle morphology on lung delivery: Predictions of Stokes' law and the particular relevance to dry powder inhaler formulation and development [Review]. Pharm Res 19:239-245.

D.Behera (2010). Textbook of Pulmonary Medicine. JP Medical Ltd.

Dahlback M, Eirefelt S, Karlberg IB, and Nerbrink O (1989). Total deposition of evans blue in aerosol exposed rats and guinea pigs. J Aerosol Sci 20:1325-1327.

Darquenne C (2012). Aerosol deposition in health and disease. J Aerosol Med Pulm Drug Deliv 25:140-147.

De Backer JW, Vos WG, Burnell P, Verhulst SL, Salmon P, De Clerck N, and De Backer W (2009). Study of the variability in upper and lower airway morphology in Sprague-Dawley rats using modern micro-CT scan-based segmentation techniques. Anatomical Record 292:720-727.

Delvadia RR, Longest PW, and Byron PR (2012). In vitro tests for aerosol deposition. i: Scaling a physical model of the upper airways to predict drug deposition variation in normal humans. J Aerosol Med Pulm Drug Deliv 25:32-40.

Derendorf H, Hochhaus G, and Mollmann H (2001). Evaluation of pulmonary absorption using pharmacokinetic methods. Journal of Aerosol Medicine: Deposition, Clearance, and Effects in the Lung 14:S9-S17.

Derom E, Borgstrom L, Van Schoor J, Lofroos A, and Pauwels R (2001). Lung deposition and protective effect of terbutaline delivered from pressurized metered-dose inhalers and the Turbuhaler in asthmatic individuals. American Journal of Respiratory and Critical Care Medicine 164:1398-1402.

Eberl S, Chan HK, Daviskas E, Constable C, and Young I (2001). Aerosol deposition and clearance measurement: A novel technique using dynamic SPET. European Journal of Nuclear Medicine 28:1365-1372.

Fabbri LM, Romagnoli M, Corbetta L, Casoni G, Busljetic K, Turato G, Ligabue G, Ciaccia A, Saetta M, and Papi A (2003). Differences in airway inflammation in patients with fixed airflow obstruction due to asthma or chronic obstructive pulmonary disease. American Journal of Respiratory and Critical Care Medicine 167:418-424.

Ferron GA, Upadhyay S, Zimmermann R, and Karg E (2013). Model of the deposition of aerosol particles in the respiratory tract of the rat. II. hygroscopic particle deposition. J Aerosol Med Pulm Drug Deliv 26:101-119.

Ferziger JHPM (2002). Computational Methods for Fluid Dynamics.

Finlay WH, Stapleton KW, and Zuberbuhler P (1998). Variations in predicted regional lung deposition of salbutamol sulphate between 19 nebulizer types. Journal of Aerosol Medicine: Deposition, Clearance, and Effects in the Lung 11:65-80.

Forbes B, Asgharian B, Dailey LA, Ferguson D, Gerde P, Gumbleton M, Gustavsson L, Hardy C, Hassall D, Jones R, Lock R, Maas J, McGovern T, Pitcairn GR, Somers G, and Wolff RK (2011). Challenges in inhaled product development and opportunities for open innovation. Advanced Drug Delivery Reviews 63:69-87.

Geldart D (1973). Types of gas fluidization. Powder Technology 7:285-292.

Gentile DA and Skoner DP (2010). New asthma drugs: Small molecule inhaled corticosteroids. Current Opinion in Pharmacology 10:260-265.

Gerde P, Cheng YS, and Medinsky MA (1991). In vivo deposition of ultrafine aerosols in the nasal airway of the rat. Fundamental and Applied Toxicology 16:330-336.

Green GM, Jakab GJ, Low RB, and Davis GS (1977). Defense mechanisms of the respiratory membranes. American Review of Respiratory Disease 115:479-514.

Griffis LC, Wolff RK, Beethe RL, Hobbs CH, McClellan RO, Authors FN, Wolff RK, Beethe RL, Hobbs CH, and McClellan RO (1981). Evaluation of a multitiered inhalation exposure chamber. Fundam Appl Toxicol 1:8-12.

Guchardi R, Frei M, John E, and Kaerger JS (2008). Influence of fine lactose and magnesium stearate on low dose dry powder inhaler formulations. Int J Pharm 348:10-17.

Harris J and Fraser DA (1976). A model for deposition of fibers in the human respiratory system. Am Ind Hyg Assoc J 37:73-89.

Hindle M and Chrystyn H (1992). Determination of the relative bioavailability of salbutamol to the lung following inhalation. Br 34:311-315.

Hindle M and Longest PW (2010). Evaluation of Enhanced Condensational Growth (ECG) for controlled respiratory drug delivery in a mouth-throat and upper tracheobronchial model. Pharm Res 27:1800-1811.

Hinds WCW (1999). Aerosol technology: properties, behaviour, and measurement of airborne particles. Aerosol Technology.

Hofmann W (2011). Modelling inhaled particle deposition in the human lung-A review. J Aerosol Sci 42:693-724.

Hofmann W and Asgharian B (2003). The effect of lung structure on mucociliary clearance and particle retention in human and rat lungs. Toxicol Sci 73:448-456.

Hofmann W, Bergmann R, and Koblinger L (1999). Characterization of local particle deposition patterns in human and rat lungs by different morphometric parameters. J Aerosol Sci 30:651-667.

ICRP (1994). Human respiratory tract model for radiological protection. A report of a Task Group of the International Commission on Radiological Protection. Annals of the ICRP 24:1-482.

Jarvis NS and Birchall A (1994). LUDEP 1.0, a personal computer program to implement the new ICRP respiratory tract model. Radiation Protection Dosimetry 53:191-193.

Karrasch S, Eder G, Bolle I, Tsuda A, and Schulz H (2009). Breath-by-breath measurement of particle deposition in the lung of spontaneously breathing rats. Journal of Applied Physiology 107:1293-1299.

Kelly JT, Kimbell JS, and Asgharian B (2001). Deposition of fine and coarse aerosols in a rat nasal mold. Inhal 13:577-588.

Kleinstreuer C, Shi H, and Zhe Z (2007). Computational analyses of a pressurized metered dose inhaler and a new drug-aerosol targeting methodology. Journal of Aerosol Medicine: Deposition, Clearance, and Effects in the Lung 20:294-309.

Koblinger L and Hofmann W (1995). Aerosol inhalation in the rat lung. Part II: Theoretical predictions of particle deposition patterns. Journal of Aerosol Medicine: Deposition, Clearance, and Effects in the Lung 8:21-32.

Kuehl PJ, Anderson TL, Candelaria G, Gershman B, Harlin K, Hesterman JY, Holmes T, Hoppin J, Lackas C, Norenberg JP, Yu H, and McDonald JD (2012). Regional particle size dependent deposition of inhaled aerosols in rats and mice. Inhal 24:27-35.

Lange CF and Finlay WH (2006). Liquid atomizing: Nebulizing and other methods of producing aerosols. Journal of Aerosol Medicine: Deposition, Clearance, and Effects in the Lung 19:28-35.

Larhrib H, Martin GP, Marriott C, and Prime D (2003). The influence of carrier and drug morphology on drug delivery from dry powder formulations. Int J Pharm 257:283-296.

Le Brun PPH, De Boer AH, Frijlink HW, and Heijerman HGM (2000). A review of the technical aspects of drug nebulization. Pharmacy World and Science 22:75-81.

Leach CL, Davidson PJ, and Boudreau RJ (1998). Improved airway targeting with the CFC-free HFA-beclomethasone metered- dose inhaler compared with CFC-beclomethasone. European Respiratory Journal 12:1346-1353.

Lee SL, Adams WP, Li BV, Conner DP, Chowdhury BA, and Yu LX (2009). In vitro considerations to support bioequivalence of locally acting drugs in dry powder inhalers for lung diseases. AAPS Journal 11:414-423.

Lee Z, Ljungberg M, Muzic RF, and Berridge MS (2001). Usefulness and pitfalls of planar gamma-scintigraphy for measuring aerosol deposition in the lungs: A Monte Carlo investigation. J Nucl Med 42:1077-1083.

Liden C, Lundgren L, Skare L, LidÃ©n G, Tornling G, and Krantz S (1998). A new whole-body exposure chamber for human skin and lung challenge experiments - The generation of wheat flour aerosols. Ann Occup Hyg 42:541-547.

Lind T, Danner S, and Guentay S (2010). Monodisperse fine aerosol generation using fluidized bed. Powder Technology 199:232-237.

Liu BYH, Pui DYH, and Lin BY (1986). AEROSOL CHARGE NEUTRALIZATION BY A RADIOACTIVE ALPHA SOURCE. Particle Characterization 3:111-116.

Londahl J, Massling A, Pagels J, Swietlicki E, Vaclavik E, and Loft S (2007). Size-resolved respiratory-tract deposition of fine and ultrafine hydrophobic and hygroscopic aerosol particles during rest and exercise. Inhal 19:109-116.

Longest PW and Holbrook LT (2012). In silico models of aerosol delivery to the respiratory tract - Development and applications. Advanced Drug Delivery Reviews 64:296-311.

Lundgren L, Skare L, Lidén C, and Tornling G (2006). Large organic aerosols in a dynamic and continuous whole-body exposure chamber tested on humans and on a heated mannequin. Ann Occup Hyg 50:705-715.

MacLoughlin RJ, Higgins BD, Laffey JG, and O'Brien T (2009). Optimized aerosol delivery to a mechanically ventilated rodent. J Aerosol Med Pulm Drug Deliv 22:323-332.

Marple VA, Liu BY, Rubow KL, Authors FN, Liu BY, and Rubow KL (1978). A dust generator for laboratory use. Am Ind Hyg Assoc J 39:26-32.

Martin RJ (2002). Therapeutic significance of distal airway inflammation in asthma. Journal of Allergy and Clinical Immunology 109:S447-S460.

Martonen TB and Yang Y (1993). Simulation of aerosol deposition in extrathoracic and laryngeal passages of the laboratory rat. J Aerosol Sci 24:103-113.

Martonen TB, Zhang Z, Yue G, and Musante CJ (2003). Fine particle deposition within human nasal airways. Inhal 15:283-303.

McCallion ONM, Taylor KMG, Thomas M, and Taylor AJ (1995). Nebulization of fluids of different physicochemical properties with air-jet and ultrasonic nebulizers. Pharm Res 12:1682-1688.

McRobbie DW, Pritchard S, and Quest RA (2003). Studies of the Human Oropharyngeal Airspaces Using Magnetic Resonance Imaging. I. Validation of A Three-Dimensional MRI Method for Producing Ex Vivo Virtual and Physical Casts of the Oropharyngeal Airways during Inspiration. Journal of Aerosol Medicine: Deposition, Clearance, and Effects in the Lung 16:401-415.

Menache MG, Raabe OG, and Miller FJ (1996). An empirical dosimetry model of aerodynamic particle deposition in the rat respiratory tract. Inhal 8:539-578.

Menzies D, Nair A, Hopkinson P, McFarlane L, and Lipworth BJ (2007). Differential anti-inflammatory effects of large and small particle size inhaled corticosteroids in asthma. Allergy: European Journal of Allergy and Clinical Immunology 62:661-667.

Mercer RR, Russell ML, and Crapo JD (1994). Alveolar septal structure in different species. Journal of Applied Physiology 77:1060-1066.

Miller FJ (2000). Dosimetry of particles: Critical factors having risk assessment implications. Inhal 12:389-395.

Miller NC, Ross DL, and Nas MM (1998). Effect of formulation factors on the observed bounce in cascade impactors used to measure the spray particle size of metered dose inhalers. Int J Pharm 173:93-102.

Minard K, Einstein D, Jacob R, Kabilan S, Kuprat A, Timchalk C, Trease L, and Corley R (2006). Application of magnetic resonance (MR) imaging for the development and validation of computational fluid dynamic (CFD) models of the rat respiratory system. Inhal 18:787-794.

Mitchell JP and Authors FN (2008). Appropriate face models for evaluating drug delivery in the laboratory: the current situation and prospects for future advances. [Review] [63 refs]. J Aerosol Med Pulm Drug Deliv 21:97-112.

Mitchell JP and Nagel MW (2003). Cascade Impactors for the Size Characterization of Aerosols from Medical Inhalers: Their Uses and Limitations. Journal of Aerosol Medicine: Deposition, Clearance, and Effects in the Lung 16:341-377.

Mitchell JP, Nagel MW, Nichols S, and Nerbrink O (2006). Laser diffractometry as a technique for the rapid assessment of aerosol particle size from inhalers. Journal of Aerosol Medicine: Deposition, Clearance, and Effects in the Lung 19:409-433.

Mollmann H, Wagner M, Meibohm B, Hochhaus G, Barth J, Stockmann R, Krieg M, Weisser H, Falcoz C, and Derendorf H (1998). Pharmacokinetic and pharmacodynamic evaluation of fluticasone propionate after inhaled administration. European Journal of Clinical Pharmacology 53:459-467.

Morgan K, Monticello T, Patra A, and Fleishman A (1989). Preparation of rat nasal airway casts and their application to studies of nasal airflow. In: Crapo JD, Smolko ED, Miller FJ, Graham JA, and Hayes AW, editors. Extrapolation of dosimetric relationships for inhaled particles and gases. New York, NY: Academic Press, Inc.

Moss OR, James RA, and Asgharian B (2006). Influence of exhaled air on inhalation exposure delivered through a directed-flow nose-only exposure system. Inhal 18:45-51.

Nadarassan DK, Chrystyn H, Clark BJ, and Assi KH (2007). Validation of high-performance liquid chromatography assay for quantification of formoterol in urine samples after inhalation using UV detection technique. Journal of Chromatography B: Analytical Technologies in the Biomedical and Life Sciences 850:31-37.

Natiello M, Kelly G, Lamca J, Zelmanovic D, Chapman RW, and Phillips JE (2009). Manual and automated leukocyte differentiation in bronchoalveolar lavage fluids from rodent models of pulmonary inflammation. Comparative Clinical Pathology 18:101-111.

Nerbrink O, Dahlback M, Smaldone GC, and Matthys H (1994). Basic nebulizer function. Journal of Aerosol Medicine: Deposition, Clearance, and Effects in the Lung 7:S7-S11.

Newman SP (2000). Can lung deposition data act as a surrogate for the clinical response to inhaled asthma drugs? Br 49:529-537.

Newman SP, Pellow PGD, and Clarke SW (1987). Dropsizes from medical atomisers (nebulisers) for drug solutions with different viscosities and surface tensions. Atomization Spray Tech 3:1-11.

O'Callaghan C and Barry PW (1997). The science of nebulised drug delivery. Thorax 52:S31-S44.

O'Shaughnessy PT, Achutan C, O'Neill ME, and Thorne PS (2003). A small whole-body exposure chamber for laboratory use. Inhal 15:251-263.

Oakes JM, Scadeng M, Breen EC, Marsden AL, and Darquenne C (2012). Rat airway morphometry measured from in situ MRI-based geometric models. Journal of Applied Physiology 112:1921-1931.

OECD (2004). Organisation for Economic Cooperation and Development (OECD), *subchronic inhalation toxicity: 90 day study*, OECD guidelines for testing of Chemicals. OECD guidelines for testing of Chemicals 413.

Oldham M (2006). Challenges in validating CFD-derived inhaled aerosol deposition predictions. Inhal 18:781-786.

Owen K (2013). Regulatory toxicology considerations for the development of inhaled pharmaceuticals. Drug and Chemical Toxicology 36:109-118.

Pagels J, Gudmundsson A, Gustavsson E, Asking L, and Bohgard M (2005). Evaluation of aerodynamic particle sizer and electrical low-pressure impactor for unimodal and bimodal mass-weighted size distributions. Aerosol Sci Technol 39:871-887.

Parent RA (1992). Treatise on Pulmonary Toxicology, Volume I: Comparative Biology of the Normal Lung. Informa Healthcare.

Paul G. The Capsule Based Aerosol Generator -Conserving Test Article in SmallScale Inhalation Exposures. Respiratory Drug Delivery 2012 . 2012.
Ref Type: Conference Proceeding

Pauluhn J (2005). Overview of inhalation exposure techniques: Strengths and weaknesses. Experimental and Toxicologic Pathology 57:111-128.

Peart J. Multicomponent particle interactions in dry powder aerosol. Pharmaceutical Research 14 (11 Suppliment)[S-142]. 1997.
Ref Type: Abstract

Peters TM (2006). Use of the aerodynamic particle sizer to measure ambient PM 10-2.5: The coarse fraction of PM10. Journal of the Air and Waste Management Association 56:411-416.

Peters TM and Leith D (2003). Concentration measurement and counting efficiency of the aerodynamic particle sizer 3321. J Aerosol Sci 34:627-634.

Phalen RF (1984). Inhalation Expsure Methodology. Environ Health Perspect 56:23-34.

Phalen RF, Mendez LB, and Oldham MJ (2010). New developments in aerosol dosimetry. Inhal 22:6-14.

Phalen RF, Oldham MJ, Wolff RK, Authors FN, Oldham MJ, and Wolff RK (2008). The relevance of animal models for aerosol studies. [Review] [118 refs]. J Aerosol Med Pulm Drug Deliv 21:113-124.

Pickrell JA, Snipes MB, Benson JM, Hanson RL, Jones RK, Carpenter RL, Thompson JJ, Hobbs CH, and Brown SC (1989). Talc deposition and effects after 20 days of repeated inhalation exposure of rats and mice to talc. Environmental Research 49:233-245.

Pinkerton KE, Gallen JT, Mercer RR, Wong VC, Plopper CG, and Tarkington BK (1993). Aerosolized fluorescent microspheres detected in the lung using confocal scanning laser microscopy. Microscopy Research and Technique 26:437-443.

Raab OG, Yeh HC, Newton GJ, Phalen RF, and Velasquez DJ (1975). Deposition of inhaled monodisperse aerosols in small rodents. Inhaled particles 4 Pt 1:3-21.

Raabe OG, Al-Bayati MA, Teague SV, and Rasolt A (1988). Regional deposition of inhaled monodisperse coarse and fine aerosol particles in small laboratory animals. Ann Occup Hyg 32:53-63.

Raeburn D, Underwood SL, and Villamil ME (1992). Techniques for drug delivery to the airways, and the assessment of lung function in animal models. Journal of Pharmacological and Toxicological Methods 27:143-159.

Robinson RJ, Snyder P, and Oldham MJ (2008). Comparison of analytical and numerical particle deposition using commercial CFD packages: Impaction and sedimentation. Inhal 20:485-497.

Rohatagi S, Appajosyula S, Derendorf H, Szefler S, Nave B, Zech K, and Banerji D (2004). Risk-Benefit Value of Inhaled Glucocorticoids: A Pharmacokinetic/Pharmacodynamic Perspective. Journal of Clinical Pharmacology 44:37-47.

Rostami AA (2009). Computational modeling of aerosol deposition in respiratory tract: A review. Inhal 21:262-290.

Rudolf G, Kalbrich R, and Stahlhofen W (1990). Modelling and algebraic formulation of regional aerosol deposition in man. J Aerosol Sci 21:S403-S406.

Rudolf JGJHGSaWS (1988). Mass Deposition from Inspired Polydisperse Aerosols. The Annals of Occupational Hygiene 32:919-938.

Sakagami M (2006). In vivo, in vitro and ex vivo models to assess pulmonary absorption and disposition of inhaled therapeutics for systemic delivery. Advanced Drug Delivery Reviews 58:1030-1060.

Scarpelli EM (1998). The alveolar surface network: A new anatomy and its physiological significance. Anatomical Record 251:491-527.

Schachtner W (2011). Product Development: Case study of an inhaled biologic. Inhalation.

Scheuch G, Bennett W, Borgstrom L, Clark A, Dalby R, Dolovich M, Fleming J, Gehr P, Gonda I, O'Callaghan C, Taylor G, and Newman S (2010). Deposition, imaging, and clearance: What remains to be done? J Aerosol Med Pulm Drug Deliv 23:S39-S57.

Schlesinger RB (1985). Comparative deposition of inhaled aerosols in experimental animals and humans: A review. Journal of Toxicology and Environmental Health 15:197-214.

Schmid O, Bolle I, Harder V, Karg E, Takenaka S, Schulz H, and Ferron GA (2008). Model for the deposition of aerosol particles in the respiratory tract of the rat. I. Nonhygroscopic particle deposition. J Aerosol Med Pulm Drug Deliv 21:291-307.

Schmoll LH, Elzey S, Grassian VH, and O'Shaughnessy PT (2009). Nanoparticle aerosol generation methods from bulk powders for inhalation exposure studies. Nanotoxicology 3:265-275.

Schroeter JD, Kimbell JS, Asgharian B, Tewksbury EW, and Singal M (2012). Computational fluid dynamics simulations of submicrometer and micrometer particle deposition in the nasal passages of a Sprague-Dawley rat. J Aerosol Sci 43:31-44.

Schulz H (1998). Mechanisms and factors affecting intrapulmonary particle deposition: Implications for efficient inhalation therapies. Pharmaceutical Science and Technology Today 1:336-344.

Sheth P, Sandhu H, Singhal D, Malick W, Shah N, and Kislalioglu MS (2012). Nanoparticles in the pharmaceutical industry and the use of supercritical fluid technologies for nanoparticle production. Current Drug Delivery 9:269-284.

Shin YS, Takeda K, and Gelfand EW (2009). Understanding asthma using animal models. Allergy, Asthma and Immunology Research 1:10-18.

Silver SD (1949). Constant flow gassing chambers: Principles influencing design and operation. The Journal of Laboratory and Clinical Medicine 31:1153-1161.

Smith DMD (1981). A method for chronic nose-only exposures of laboratory animals to inhaled fibrous aerosols. Inhalation Toxicology and Technology89-105.

Snipes MB, McClellan RO, Mauderly JL, and Wolff RK (1989). Retention patterns for inhaled particles in the lung: comparisons between laboratory animals and humans for chronic exposures. Health Physics 57:69-78.

Sorkness RL, Remus JL, and Rosenthal LA (2004). Systemic and pulmonary effects of fluticasone administered through a metered-dose inhaler in rats. Journal of Allergy and Clinical Immunology 114:1027-1032.

Stein SW, Myrdal PB, Gabrio BJ, Obereit D, and Beck TJ (2003). Evaluation of a new Aerodynamic Particle Sizer spectrometer for size distribution measurements of solution metered dose inhalers. Journal of Aerosol Medicine: Deposition, Clearance, and Effects in the Lung 16:107-119.

Stone KC, Mercer RR, Gehr P, Stockstill B, and Crapo JD (1992). Allometric relationships of cell numbers and size in the mammalian lung. American journal of respiratory cell and molecular biology 6:235-243.

Sturm R and Hofmann W (2009). A theoretical approach to the deposition and clearance of fibers with variable size in the human respiratory tract. Journal of Hazardous Materials 170:210-218.

Svartengren K, Philipson K, Svartengren M, Andersen M, and Camner P (1996). Tracheobronchial deposition and clearance in small airways in asthmatic subjects. European Respiratory Journal 9:1123-1129.

Swift DL and Proctor DF (1988). A dosimetric model for particles in the respiratory tract above the trachea. Ann Occup Hyg 32:1035-1044.

Tang P, Fletcher DF, Chan HK, and Raper JA (2008). Simple and cost-effective powder disperser for aerosol particle size measurement. Powder Technology 187:27-36.

Tayab ZR and Hochhaus G (2005). Pharmacokinetic/pharmacodynamic evaluation of inhalation drugs: Appllication to targeted pulmonary delivery systems. Expert Opinion on Drug Delivery 2:519-532.

Taylor L, Reist PC, Boehlecke BA, and Jacobs RR (2000). Characterization of an aerosol chamber for human exposures to endotoxin. Applied Occupational and Environmental Hygiene 15:303-312.

Telko MJ and Hickey AJ (2005). Dry powder inhaler formulation. Respiratory Care 50:1209-1227.

Timsina MP, Martin GP, Marriott C, Ganderton D, and Yianneskis M (1994). Drug delivery to the respiratory tract using dry powder inhalers. Int J Pharm 101:1-13.

Tougas TP, Christopher D, Mitchell JP, Strickland H, Wyka B, Van Oort M, and Lyapustina S (2009). Improved quality control metrics for cascade impaction measurements of orally inhaled drug products (OIPs). AAPS PharmSciTech 10:1276-1285.

Tuli RA, Dargaville TR, George GA, and Islam N (2012). Polycaprolactone microspheres as carriers for dry powder inhalers: Effect of surface coating on aerosolization of salbutamol sulfate. Journal of Pharmaceutical Sciences 101:733-745.

Usmani OS, Biddiscombe MF, and Barnes PJ (2005). Regional lung deposition and bronchodilator response as a function of β2-agonist particle size. American Journal of Respiratory and Critical Care Medicine 172:1497-1504.

Usmani OS, Biddiscombe MF, Nightingale JA, Underwood SR, Barnes PJ, Authors FN, Biddiscombe MF, Nightingale JA, Underwood S Richard, and Barnes PJ (2003). Effects of bronchodilator particle size in asthmatic patients using monodisperse aerosols. Journal of Applied Physiology 95:2106-2112.

Wakasugi Y, Tohara H, Nakane A, Murata S, Mikushi S, Susa C, Takashima M, Umeda Y, Suzuki R, and Uematsu H (2014). Usefulness of a handheld nebulizer in cough test to screen for silent aspiration. Odontology 102:76-80.

Weibel ER (1963). Principles and methods for the morphometric study of the lung and other organs. Laboratory investigation; a journal of technical methods and pathology 12:131-155.

Wichers LB, Rowan III WH, Nolan JP, Ledbetter AD, McGee JK, Costa DL, and Watkinson WP (2006). Particle deposition in spontaneously hypertensive rats exposed via whole-body inhalation: Measured and estimated dose. Toxicol Sci 93:400-410.

Willeke K, Lo CSK, and Whitby KT (1974). Dispersion characteristics of a fluidized bed. J Aerosol Sci 5:449-455.

Wolff RK and Dorato MA (1993). Toxicologic testing of inhaled pharmaceutical aerosols. Critical Reviews in Toxicology 23:343-369.

Wong BA (2007). Inhalation exposure systems: Design, methods and operation. Toxicologic Pathology 35:3-14.

Wright BM (1950). A new dust-feed mechanism. Journal of Scientific Instruments 27:12-15.

Wu K, Blomgren AL, Ekholm K, Weber B, Edsbaecker S, and Hochhaus G (2009). Budesonide and ciclesonide: Effect of tissue binding on pulmonary receptor binding. Drug Metabolism and Disposition 37:1421-1426.

Wu Y, Kotzer CJ, Makrogiannis S, Logan GA, Haley H, Barnette MS, and Sarkar SK (2011). A noninvasive [99mTc]DTPA SPECT/CT imaging methodology as a measure of lung permeability in a guinea pig model of COPD. Molecular Imaging and Biology 13:923-929.

Y.S.Cheng and O.R.Moss (1989). Inhalation exposure systems. Concepts in inhalation Toxicology,49.

Yang JZ, Young AL, Chiang PC, Thurston A, and Pretzer DK (2008). Fluticasone and budesonide nanosuspensions for pulmonary delivery: Preparation, characterization, and pharmacokinetic studies. Journal of Pharmaceutical Sciences 97:4869-4878.

Yeh HC, Newton GJ, and Barr EB (1986). Studies of the temporal and spatial distribution of aerosols in multi-tiered inhalation exposure chambers. Am Ind Hyg Assoc J 47:540-545.

Yeh HC, Snipes MB, and Brodbeck RD (1987). Nose-only exposure system for inhalation exposures of rodents to large particles. Am Ind Hyg Assoc J 48:247-251.

Young PM, Cocconi D, Colombo P, Bettini R, Price R, Steele DF, and Tobyn MJ (2002). Characterization of a surface modified dry powder inhalation carrier prepared by "particle smoothing". Journal of Pharmacy and Pharmacology 54:1339-1344.

Zanen P, Go LT, and Lammers JWJ (1996). Optimal particle size for β2 agonist and anticholinergic aerosols in patients with severe airflow obstruction. Thorax 51:977-980.

Zhang Y, Chia TL, and Finlay WH (2006). Experimental measurement and numerical study of particle deposition in highly idealized mouth-throat models. Aerosol Sci Technol 40:361-372.

Zhou Y and Cheng YS (2005). Particle deposition in a cast of human tracheobronchial airways. Aerosol Sci Technol 39:492-500.